Heinrich Heine Universität Düsseldorf

Immune cell infiltration triggers heart failure after induction of pressure overload in cardiac p38 MAPKα-deficient mice

Inaugural dissertation

presented to the Faculty of Mathematics and Natural Sciences at the

Heinrich Heine University Düsseldorf for the degree of

Doctor of Natural Sciences

by

Anne Hemmers

Düsseldorf, March 2024

from the Institute of Cardiovascular Physiology

Heinrich Heine University, Düsseldorf

Printed by permission of the

Faculty of Mathematics and Natural Sciences at

Heinrich Heine University, Düsseldorf

Supervisors:

1. Prof. Dr. Axel Gödecke
2. Prof. Dr. Joachim Altschmied

Date of the oral examination: 06. Juni 2024

Content

Abstract

Heart failure (HF) is associated with systemic, sterile inflammation of the myocardium, characterized by the infiltration of immune cells. Although chronic inflammation is recognized as a major factor in the pathophysiology of HF, the current treatment for HF-patients does not specifically target immune cells. This thesis should advance our knowledge of how immune cells impair cardiac function in HF conditions and pave the way for potential therapeutics targeting immune cell infiltration.

To study the infiltration of immune cells in cardiac tissue and the progression of fibrosis, a mouse model was used. In mice with a cardiomyocyte-specific deletion of the p38 MAPKα gene (iCM-p38 KO), the induction of pressure overload (PO) via angiotensin II (AngII) results in energy depletion and strongly impaired heart function just within 48h, characterized by a low ejection fraction (EF) (KO 25.8 ± 10.1% vs. control 51.9 ± 14.2%). Interestingly, the HF condition was reversible, since cardiac function recovered after the end of the 48h AngII treatment. A prolongation of the AngII treatment to 7d, however, resulted in a sustained deterioration of cardiac function for at least 14d beyond AngII administration in iCM-p38 KO mice.

The course of immune cell infiltration demonstrated a particularly strong infiltration after 48h of AngII treatment and an almost complete disappearance of immune cells at later times, despite continuous AngII administration. Interestingly, neutrophils and pro-inflammatory monocytes massively infiltrated the cardiac tissue of iCM-p38 KO mice after 48h of AngII treatment. In contrast, dendritic cells mainly infiltrated the hearts of control mice. Furthermore, cardiac fibrosis was observed in iCM-p38 KO hearts 3 weeks after the induction of PO. This is indicated by increased extracellular matrix accumulation and an increased expression of fibrosis-related genes.

Two attempts have been made to save the iCM-p38 KO phenotype. The first attempt targeted the increased sympathetic stimulation under HF conditions via β-blocker administration. However, an improvement of cardiac function did not occur. In a second attempt, neutrophils were targeted since a particularly strong infiltration was measured in iCM-p38 KO hearts. A depletion of early infiltrating neutrophils by injection of a α-Ly6G antibody resulted in a significantly improved cardiac function (EF increased up to 41.4%). Additionally, these hearts showed reduced signs of cardiac fibrosis.

In conclusion, this thesis demonstrates the importance of early neutrophil infiltration in the progression of chronic heart failure and shows that a treatment targeting this infiltration represents possibilities for therapy of HF patients.

Zusammenfassung

Bei einer Herzinsuffizienz kann eine starke Infiltration von Immunzellen in das Myokard beobachtet werden. Obwohl chronische Entzündungen als wichtiger Faktor in der Pathophysiologie der Herzinsuffizienz anerkannt sind, zielt die derzeitige Behandlung von Patienten mit Herzinsuffizienz nicht auf Immunzellen ab. Diese Arbeit soll das Wissen darüber erweitern, wie Immunzellen die Funktion und Morphologie des Herzens bei Herzinsuffizienz beeinflussen, und den Weg für potenzielle Therapeutika ebnen, die gezielt die Immunzellinfiltration modifizieren.

Um die Immunzellinfiltration in das Herzgewebe und das Fortschreiten kardialer Fibrose zu untersuchen, wurde ein spezifisches Mausmodell verwendet. Bei Mäusen mit einer kardiomyozyten-spezifischen Deletion des p38 MAPKα-Gens (iCM-p38 KO) führt eine Drucküberlastung durch Angiotensin II (AngII) schnell zu einem Energiemangel des Myokards und innerhalb von 48h zu einer stark beeinträchtigten Herzfunktion, die durch eine niedrige Ejektionsfraktion (EF) gekennzeichnet ist (KO 25,8 ± 10,1% vs control 51,9 ± 14,2%). Interessanterweise war der Herzinsuffizienz-Zustand reversibel, da sich die Herzfunktion nach dem Ende der 48-stündigen AngII Behandlung erholte. Eine Verlängerung der AngII-Behandlung auf 7 Tage führte jedoch in iCM-p38-KO-Mäusen zu einer anhaltenden Beeinträchtigung der Herzfunktion für mindestens 14 Tage über die AngII Behandlung hinaus.

Untersuchungen zum Verlauf der Immunzellinfiltration zeigten eine besonders starke Infiltration nach 48h AngII-Behandlung und ein fast vollständiges Verschwinden der Immunzellen zu späteren Zeitpunkten trotz kontinuierlicher AngII-Verabreichung. Interessanterweise infiltrierten Neutrophile und pro-inflammatorische Monozyten nach 48-stündiger AngII-Behandlung massiv das Herzgewebe von iCM-p38-KO-Mäusen. Im Gegensatz dazu infiltrierten dendritische Zellen hauptsächlich die Herzen von Kontrollmäusen. Darüber hinaus wurde 3 Wochen nach Start der AngII-Behandlung Fibrose in iCM-p38-KO-Herzen beobachtet. Dies wurde durch eine erhöhte Akkumulation von extrazellulärer Matrix und einer erhöhten Expression Fibrose-assoziierter Gene angezeigt.

Zusätzlich habe ich versucht den iCM-p38-KO-Phänotyp zu retten. Dazu wurden zwei verschiedene Ansätze verfolg. Der erste Versuch zielte auf die Hemmung der verstärkten sympathischen Stimulation unter Herzinsuffizienz-Bedingungen mittels β-Blocker-Gabe ab. Eine signifikante Verbesserung der Herzfunktion trat jedoch nicht ein. In einem zweiten Versuch wurden früh, infiltrierende Neutrophile mittels spezifischer Antikörper eliminiert, da eine besonders starke Infiltration in iCM-p38-KO-Herzen

gemessen wurde. Eine Depletion dieser Neutrophile durch eine Injektion von α-Ly6G-Antikörpern führte zu einer deutlich verbesserten Herzfunktion (EF verbesserte sich auf bis zu 41,4%). Darüber hinaus waren die Anzeichen einer kardialen Fibrose vermindert.

Zusammenfassend unterstreicht diese Arbeit die Bedeutung der Neutrophilen-Infiltration für das Fortschreiten einer chronischen Herzinsuffizienz und zeigt, dass eine Behandlung, die auf diese Infiltration abzielt, Möglichkeiten für die Therapie von HF-Patienten darstellen kann.

1. Introduction

1.1 Varieties of heart failure

Heart failure (HF) is defined as a chronic and progressive disease in which the heart is not able to pump blood sufficiently through the body. With a prevalence of 64 million patients globally [1], HF belongs to the most common cardiovascular diseases (CVD), which are generally the leading cause of death, particularly in industrialized countries [2]. Causes of HF are diverse and range from arrhythmia, cardiomyopathy, and hypertension to heart valve disease. HF can also be a consequence of an acute cardiovascular event, for example, following a myocardial infarction. Smoking, obesity, and diabetes mellitus even increase the risks of CVD and HF. The symptoms of HF are diverse and have serious impacts on patients' everyday lives. They include, but are not limited to, dyspnea, edema, and fatigue. The prognosis of patients with heart failure continues to be poor. The 5-year survival rate is still < 57% [3]. Several types of heart failure exist. The two main forms of left-sided heart failure are:

- Systolic heart failure is the most common type of heart failure. In this condition, the left ventricle (LV) does not pump blood efficiently, which leads to an undersupply of oxygen in the organs of the body, and the blood accumulates in the lungs, which causes i.a. edema and therefore shortness of breath. Restriction of LV function is characterized by an increase in end-diastolic volume (EDV) relative to stroke volume (SV), indicating a dilation of the LV. Because the heart is not able to pump blood efficiently, the ejection fraction (EF) is reduced as well and reaches values < 40% [4], hence this condition is also referred to as heart failure with reduced ejection fraction (HFrEF).

- Diastolic heart failure occurs when the myocardium of the LV stiffens and is therefore not able to relax normally after contraction. Consequently, the heart cannot fill properly during diastole. The systolic phase, i.e., the ejection of blood during the contraction of the heart, is hardly affected, so the EF is often in a normal or slightly reduced range > 50%. Hence, the condition is also referred to as heart failure with preserved ejection fraction (HFpEF).

Right-sided heart failure, on the other hand, is often triggered by left-sided heart failure since the accumulation of blood in the lungs caused by left-sided heart failure increases the right ventricular workload. The increased overload of the right ventricle leads to its failure. Right-sided heart failure can also occur due to valve or lung disease. Right heart failure is marked by swelling of the lower extremities and abdomen due to fluid accumulation in these areas.

Heart failure usually develops over a period of time and involves various stages. The healthy heart generates 70% of the energy it needs by utilizing fatty acids (FA) [5]. The residual part of the energy is obtained from the oxidation of carbohydrates, primarily glucose but also lactate and ketones [6, 7]. Under stress conditions, e.g., increase in blood pressure, the healthy heart works in a compensatory stage, in which the walls of the ventricles develop hypertrophy to ensure that the body is adequately supplied with oxygen and nutrients. Cardiac function in general is preserved in this phase, but metabolic remodeling and changes in substrate preferences may occur (Figure 1). Several studies demonstrate a switch in substrate utilization in this stage, in that FA oxidation declines [8-10] and the use of carbohydrates increases [11-13] reflecting the high metabolic flexibility of the heart. While physiological hypertrophy of the heart (occurring primarily during pregnancy and in professional athletes) is usually reversible, pathological hypertrophy is not. In this case, the heart gradually dilates, symptoms of cardiac dysfunction occur, and ultimately the heart develops failure. Due to insufficient substrate utilization, a significant reduction in ATP level in the failing myocardium is present. There is a consensus that FA metabolism remains reduced in heart failure, as it is already the case in the compensatory phase [10]. However, until the advanced stages of heart failure, ATP level in the myocardium remains stable, whereby the contraction force of the heart remains initially unaffected. Instead, phosphocreatine and total creatine levels decrease. Over time, this reduction results in a severe decline of ATP transfer and a reduction in energy delivery to myofibrils. Therefore, a hallmark of changes in metabolism of the failing heart is a reduced phospocreatin:ATP ratio [14].

Although metabolic remodeling in HF has been shown in many studies, the underlying mechanism is still under debate, and more research is needed to unsettle remaining questions.

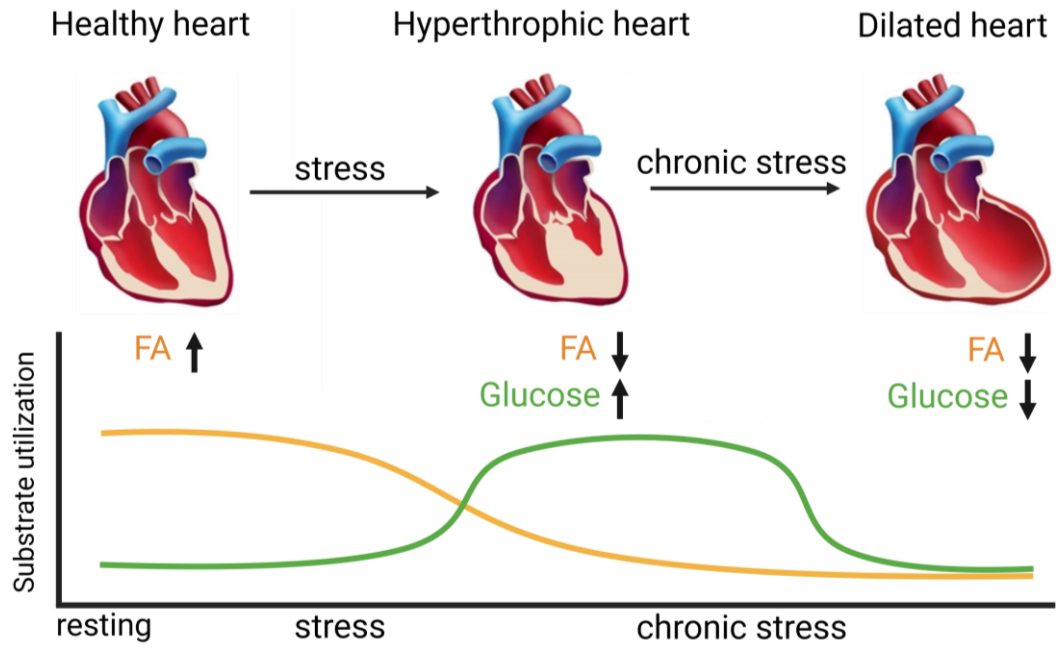

Figure 1: Characteristics of heart failure and associated changes in substrate metabolism. The development of heart failure involves various stages. The healthy heart generates most of the energy it needs by utilizing fatty acids (FA). The remaining energy required is obtained from the oxidation of carbohydrates. Under stress conditions, the healthy heart subject the compensatory stage, where the walls of the ventricles become hypertrophied to ensure the bodies adequate supply with oxygen and nutrients. A switch in substrate utilization in this stage indicates a decline in FA oxidation and an increased use of glucose. If the heart is exposed to persistent stress, it gradually dilates and thus becomes insufficient. Due to insufficient substrate utilization, a significant reduction in ATP levels in the failing myocardium is present. Created with BioRender.com.

1.1.1 The influence of the sympathetic nervous system on cardiac disease and cardio protective effect of β-adrenoceptor inhibition

Heart function, including heart rate and pressure development, is controlled by the sympathetic nervous system (SNS). The SNS, along with the parasympathetic nervous system (PNS), belongs to the two divisions of the autonomic nervous system (ANS). These systems are important for the regulation of many functions of the body. While the SNS increases heart rate, contractile force, and contraction velocity, the PNS exerts important opposite functions, e.g., reduction of heart rate and contraction velocity. In heart failure, an imbalance of the activity of the SNS and vagal activity occurs, which even worsens the prognosis of heart failure. Clinical and basic studies showed that increased SNS activation is caused by the enhancement of excitatory inputs and includes upregulation of the renin-angiotensin system. The inhibition of the activated SNS, e.g., by β-adrenoceptor antagonists (β-blockers), is still an essential part of the treatment of heart failure patients [15].

Various studies on mice and humans demonstrated that the diverse effects of β-adrenoceptor antagonists protect against cardiac dysfunction [16-18]. The blockade of the β_1-receptors leads to negative dromotropy, inotropy, and chronotropy. Thus, the

excitation conduction in the heart and the speed of the excitation formation, or the frequency of the action potentials in the sinus node, are slowed down, and the contraction force is diminished. This decreases oxygen consumption of cardiac tissue, and myocardial ischemia is reduced. A reduction in heart rate also prolongs diastole and increases coronary perfusion time. A simultaneous reduction in sympathetic tone causes a decrease of cardiac output. Non-selective β-adrenoceptor antagonists, like propranolol, inhibit not only β_1-receptors but also β_2-receptors. The additional blocking of β_2-receptors has, among other things, bronchoconstrictive, vasoconstrictive, and metabolic effects.

1.2 Complexity of the vertebrate immune system

The immune system is of central importance for the defense against exogenous organisms and thus infections in a body [19], but it also takes on important tasks in stressed and damaged tissue, in a process known as sterile inflammation, executed by white blood cells, also called leukocytes. In jawed vertebrates, the immune system comprises two parts.

The innate immune system, which can be found in nearly all forms of life, provides a non-specific but immediate response against pathogens [20]. For a long time, it was thought that this type of immune response does not have a memory and is therefore unable to recognize recurring microorganisms. However, recent studies indicate that this is not true. The concept of trained immunity describes the immunological process in which an immunological memory is also formed in innate immune cells [21, 22]. Several immune cell subtypes belong to the innate immune system. Granulocyte eosinophils, basophils, neutrophils, and monocytes, as well as dendritic cells (DCs) differentiate from myeloid stem cells. Monocytes themselves have an important role in the immune system, but they also differentiate further and thus form macrophages and also DCs (Figure 2). The main tasks of the innate immune response involve the recruitment of further immune cells to the site of infection/injury, the identification and removal of exogenous bacteria, viruses, apoptotic cells, and cell debris, as well as the activation of the adaptive immune system through antigen presentation [19, 23].

In cases where pathogens evade the innate immune system, vertebrates possess additional protection by the adaptive immune system. The immune response of this system is not as fast, but adapts its response to improve the recognition of a pathogen in cases of re-exposure [24, 25]. The adaptive immune system comprises lymphoid cells, which are separated into B-lymphocytes and T-lymphocytes, but also dendritic cells. Both originate from lymphoid stem cells [26]. B-lymphocytes are crucial for humoral immunity. They produce antibodies, present antigens, and secrete cytokines [23]. T-

lymphocytes can be divided into two major subgroups: $CD4^+$, also called T-helper cells, and cytotoxic $CD8^+$ cells (Figure 2). $CD8^+$ cells directly eliminate invading microorganisms and viruses, as well as cancer cells and apoptotic cells. By secreting small signaling proteins, $CD8^+$ T-lymphocytes recruit other immune cells, thereby enhancing the immune response even more [27]. $CD4^+$ T-lymphocytes are known to mount immune responses as well. They are activating cytotoxic $CD8^+$ T-lymphocytes and B-lymphocytes [28].

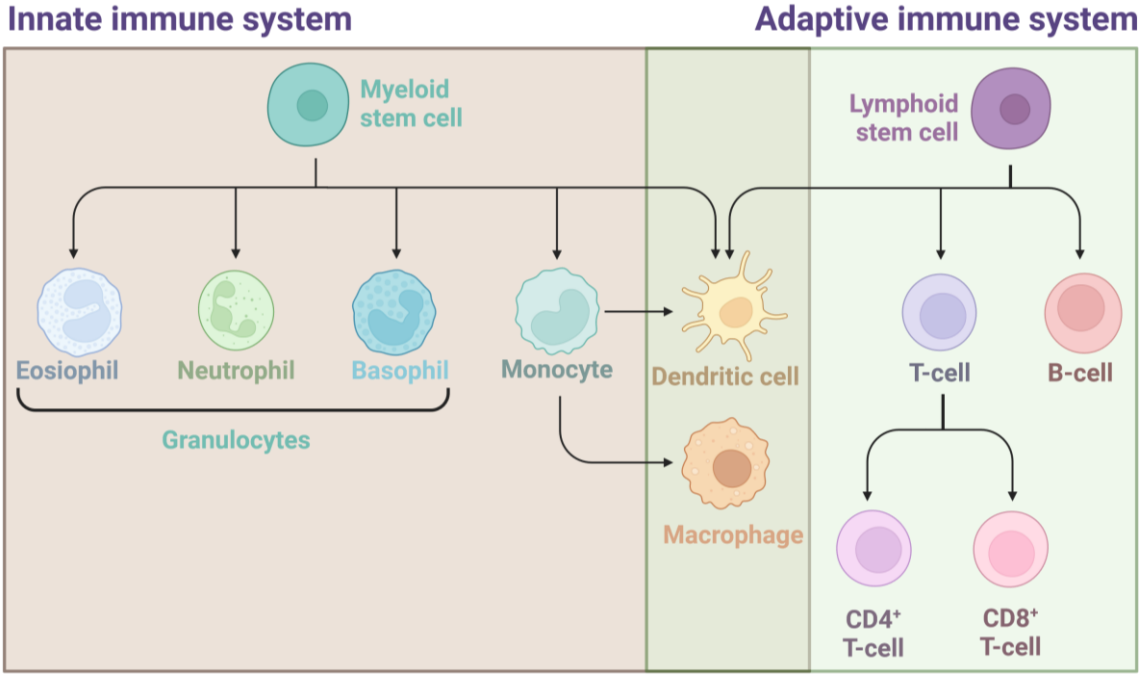

Figure 2: Composition of the vertebrate immune system. The vertebrate immune system consists of two layers: the innate and adaptive immune system. The innate immune system includes myeloid cells, which are formed from myeloid stem cells. Formed monocytes can further differentiate into macrophages and dendritic cells. The adaptive immune system includes lymphoid cells. Stem cells differentiate into B- or T-lymphocytes or dendritic cells. T-lymphocytes, in turn, be divided into $CD4^+$ helper cells and $CD8^+$ cytotoxic T-lymphocytes. Created with BioRender.com.

1.2.1 The impact of immune cells in pressure overload induced HF

In a healthy heart, resident immune cells only make up about 5% of all cells. However, this proportion increases drastically when the heart is exposed to stress or injury in terms of ischemia (MI) or pressure overload (PO), since immune cells start to infiltrate the myocardium. When cardiomyocytes are subject to stressors, they start to release damage-associated molecular patterns (DAMPs), such as heat shock protein (HSP) 60. DAMPs are ligands of Toll-like receptors (TLRs), which are expressed on the surface of intact cardiomyocytes [29]. Signaling of these receptors stimulates the transcription factor nuclear factor-κB (NF-κB), resulting in the expression and subsequent release of pro-inflammatory cytokines and chemokines like TNF-α, IL-1, and CXCL10. The release of cytokines and chemokines attracts immune cells, which consequently infiltrate the myocardium. But innate immune cells themselves can detect DAMPs via pattern-

recognition receptors (PRRs), resulting in an activation of the immune cell and, therefore, an increased cytokine release [30].

Inflammation is a crucial process for the clearance of tissue damage. However, prolonged or excessive inflammation may result in, e.g., rupture of the myocardium caused by disproportionate degradation of collagens or expansion in infarct size due to phagocytosis of healthy cardiomyocytes. Therefore, the right balance of immune cell infiltration plays a decisive role in myocardial injury. A better understanding of the role of certain immune cells in cardiac injury holds great potential for novel therapies. First of all, a closer look at the individual immune cell populations should be taken, and their various roles in regard to myocardial injury should be described in more detail.

In contrast to MI-related heart damage, monocytes are the first cells to infiltrate the injured cardiac tissue in pressure overload (PO)-induced heart failure. They serve three main functions within the innate immune system: **1**. Production of cytokines, **2.** Antigen presentation, and **3.** Elimination of apoptotic cells and debris via phagocytosis. Additionally, monocytes can have pro- or anti-inflammatory characteristics that are associated with the expression of the surface marker Ly6C. Ly6C^{high} monocytes are pro-inflammatory cells. In MI injury, these cells accumulate, along with macrophages, at the site of injury, providing a pro-inflammatory environment [31, 32], thus inhibiting myocardial healing [33]. Ly6C^{low} monocytes, however, are considered to have anti-inflammatory properties. These cells are involved in the post-MI healing process by activating fibroblasts [34], enhancing angiogenesis [35], and increasing the formation of collagen [36]. However, the actions of monocytes in PO-induced heart failure remain elusive. Nevertheless, an early increase in Ly6C^{high} monocytes was found in the hearts of PO-induced mice, which may provide clues to the importance of monocytes in this model [37]. As described before, under certain stimuli, monocytes differentiate into macrophages or dendritic cells.

Neutrophils make up the largest population of circulating leukocytes. The short-lived cells are often the first cells to arrive at the site of injury after MI and also early infiltrate damaged tissue in PO-induced heart failure. It is still debated whether neutrophil infiltration improves or worsens cardiac function. In mice, it could be shown that depletion of neutrophils following MI does not affect scar size but causes extended fibrosis and thus decreases cardiac function, indicating a cardio-protective role of neutrophils after MI. The beneficial effect of neutrophils comes from promoting macrophage polarization to a reparative phenotype [38]. The role of neutrophils in chronic PO, in turn, has not yet been clarified. On the one hand, an increase in cardiac neutrophils after PO induction was reported [39]. On the other hand, no change in neutrophil infiltration due to PO was observed in another study [37], indicating that neutrophil infiltration is rather a hallmark

of ischemic heart disease than of PO-induced heart failure. However, this study has recently been questioned as a neutrophil-dependent deterioration in cardiac function was observed. Depletion of neutrophils in a mouse model of PO-induced heart failure decreases mRNA levels of pro-inflammatory cytokines *IL-6* and *IL-1β*. This was accompanied by a reduced monocyte and macrophage infiltration, indicating an important role of neutrophils in the recruitment of other immune cell types. Neutrophil depletion also reduced LV hypertrophy and improved fractional shortening (FS), although the development of fibrosis remained unaltered [40]. Bottermann et al. observed a massive infiltration of neutrophils in the cardiac tissue of iCM-p38 KO mice in response to PO, resulting in severely reduced cardiac function. Depletion of early neutrophils caused a significant improvement of cardiac function, proving the destructive role of neutrophils in PO-induced heart failure [41].

Immature resident dendritic cells (DCs) are shown to be present also in healthy cardiac tissue, where they are responsible for maintaining vascular homeostasis by recognizing self- and non–self-antigens [42]. DCs bridge the innate and adaptive immune system. *In vitro* and *in vivo* experiments demonstrated, that DCs present antigens to $CD8^+$ T-lymphocytes, indicating their function to elicit T-lymphocyte responses [43]. However, the exact role of DCs in PO-induced heart failure remains unsettled so far. Zhang et al. demonstrated already in 1993 a rapid accumulation of DCs in the border zone of rat hearts after MI. DCs clustered together with $CD4^+$ T-lymphocytes, although these clusters disappeared 21 days after MI [44]. Through stimulation of TLR4 on the surface of DCs, they presumably, participate in a short-term cyto-protective response [45]. On the other hand, deletion of TLR/MyD88 downstream kinase interleukin-1 receptor-associated kinase-4 in mice had beneficial effects on cardiac function and survival after MI through diminution of DC infiltration in cardiac tissue [46]. These results rather suggest detrimental properties of DCs.

Macrophages are often attracted by the release of cytokines and chemokines from monocytes and neutrophils. Therefore, macrophages infiltrate cardiac tissue later in the progression of PO-induced heart failure. Brenes-Castro et al. summarized that macrophages can be found around a week after PO-induction in the myocardium [37]. Macrophages are considered to be especially sensitive to their environment and can adjust their physiology depending on the stimuli. They play important roles in the homeostasis, tissue repair, regeneration, and remodeling of cardiac tissue [47]. Overall, the resident macrophage population within the healthy heart is the largest immune cell population. They are greatly heterogeneous, and macrophages can be divided into subgroups by means of the expression of various markers, like CCR2, CD206, or MHCII. If macrophages act cardio-protectively or rather destructively in injured myocardium, is

often related to their phenotype, origin, and accumulation in the respective tissue. In acute HF, mainly pro-inflammatory M1 ($CD206^+$) macrophages are found in the cardiac tissue. Beyond that, increased pro-inflammatory cytokines, like TNF-α and IL-1β, accumulate in HF patients, which has been shown to worsen heart function even more [48, 49]. Additionally, pro-inflammatory macrophages are primary drivers for fibrosis [50] since it was shown that depletion of macrophages reduces levels of αSMA^+ myofibroblasts and decreases collagen content in a PO mouse model [51]. Over time, pro-inflammatory macrophages decrease and anti-inflammatory M2 ($CD206^-$) macrophages infiltrate the myocardium. Through the secretion of cytokines like IL-10 and chemokines such as CCL17 and CCL22, they mainly help to resolve the inflammation and promote tissue repair and angiogenesis [52]. Through the secretion of cytokines and chemokines, macrophages also recruit other immune cells to the site of injury. [53]. The secretion of the chemokines CXCL9 and CXCL10, for example, attracts $CD4^+$ T-lymphocytes [54].

B- and T-lymphocytes infiltrate the damaged myocardium later in the process of inflammation (2-6 weeks after the induction of PO) [37]. These cells modulate the progression of heart failure in various ways. Mice lacking PD-1, a key factor for B-lymphocyte differentiation, develop spontaneously severe cardiac dilation [55], suggesting a cardio-protective role of B-lymphocytes in the progression of heart failure. In other studies, however, it was shown that activated B-lymphocytes trigger apoptosis in myocytes via complement-mediated cytotoxicity [56]. In addition, memory B-lymphocytes cause persistent inflammation in the damaged myocardium, which induces cardiac cell death and injury [57, 58]. Although very little is known about the importance of B-lymphocytes in heart failure, T-lymphocytes were examined more closely. The T-lymphocyte-mediated immune response was shown to be primarily detrimental in the progression of heart failure. T-lymphocytes play a crucial role in the transition from hypertrophy to heart failure since it could be shown that mice lacking functional B- and T-lymphocytes are protected from PO-induced heart failure [59]. A depletion of T-lymphocytes by anti-CD3 antibodies showed similar results, as cardiac function was preserved after transverse aortic constriction (TAC) [60]. $CD4^+$ T-lymphocytes are known to be involved in scar formation by stimulating collagen matrix formation, thus reducing the risk of myocardial rupture [59], which, on the other hand, stiffens the myocardium. The role of $CD8^+$ T-lymphocytes in cardiac disease is also controversially discussed. It was shown that $CD8^+$ T-lymphocytes 7 days after MI produced more IL-10 and less IL-2 and INF-γ, resulting in a reduction of cardiac injury [61]. On the other hand, in *in vitro* experiments, $CD8^+$ T-lymphocytes had detrimental effects on healthy cardiomyocytes through increased cytotoxic activity [62].

In summary, it is undisputed that immune cells are of great importance in the context of PO-induced heart failure. They are involved in the removal of apoptotic cells, the resolution of inflammation, and the progression of fibrosis. However, the influence of the multitude of immune cells varies and can have a positive or negative effect on the course of disease. The effect of the different immune cells depends primarily on the subpopulation of the individual immune cells but also on the time of infiltration. Therapies for cardiac disease may be able to target immune cells, but more research and understanding are required to fully comprehend the complex relationships between these cells.

1.3 Mechanisms of myocardial interstitial fibrosis (MIF)

Cardiac fibrosis is a pathological healing process of damaged tissue in which an excess of extracellular matrix (ECM) deposition predominantly by cardiac fibroblasts (CFs) occurs. This leads to considerable tissue remodeling and can subsequently cause cardiac dysfunction and heart failure. Fibrosis appears mainly in two forms: **1.** Replacement fibrosis, which indicates scar formation after myocardial infarction (MI). The scar is important to stabilize damaged cardiac tissue and to prevent rupture of the tissue. In this case, fibrosis can be considered a reparative process. **2.** Myocardial interstitial fibrosis (MIF) occurs in hypertension-induced heart failure but develops during aging as well [63]. MIF is a hallmark of cardiac disease, and alters myocardial architecture and function, and is associated with the progression of heart failure. Fibrosis increases myocardial stiffness, thereby impeding diastolic filling. Thus, leading to HFpEF, characterized by compromised diastolic function. Unlike MI-induced focal fibrosis, MIF is a diffuse and irregular process in which interstitial microscars, excessive collagen accumulation, and an extended thickness of collagen strands appear. Substantial changes occur in HF due to the imbalance of the formation and deposition of collagen I and III fibers, leading to changes in the quality, quantity, and conformation of the collagen network [64, 65].

But also, non-fibrillar extracellular matrix components, like fibronectin, are subject to change. The main effector cells in cardiac fibrosis are activated fibroblasts (myofibroblasts), but several other cell types, like cardiomyocytes, endothelial cells, and immune cells, such as macrophages and lymphocytes, contribute to the progression of fibrosis. Myofibroblasts are characterized by the expression of alpha smooth muscle actin (αSMA) and the production of the matricellular protein periostin. Secreted cytokines and growth factors also play a distinct role in the fibrotic response. These cytokines include, but are not limited to, several interleukins (IL-1, IL-10, IL-11), tumor necrosis factor alpha (TNF-α), and members of the transforming growth factor-β (TGF-β) family.

They are secreted by macrophages, mast cells, and other immune cells and promote the activation of fibroblasts. Furthermore, fibroblast proliferation and subsequent ECM synthesis in damaged myocardium are triggered by the activation of the renin-angiotensin-aldosterone system (RAAS) via mineralocorticoid receptor signaling or activation of the angiotensin type 1 receptor (AT1) [66, 67]. In 2004, it was shown that AT1 blockade in patients with hypertensive cardiac disease had significantly fewer indicators of cardiac fibrosis [68]. Moreover, the administration of an aldosterone antagonist caused reduced levels of circulating markers of collagen synthesis in various patients suffering from myocardial infarction [69] or heart failure (HFrEF or HFpEF) [70, 71].

Activated fibroblasts ultimately undergo different fates. Myofibroblasts lose αSMA expression over time (e.g., in the case of MI after 10 days). Consecutively, the fibroblasts develop in different ways. A part of the fibroblasts undergo apoptosis, whereas others remain in the tissue as resting or senescent fibroblasts. Other fibroblasts may further differentiate into matrifibrocytes (see Figure 3). A hallmark of these cells is the expression of genes usually expressed in bone and cartilage; these mainly include cartilage oligomeric matrix protein (*Comp*), cartilage intermediate layer protein 2 (*Cilp2*), and TNF Receptor Superfamily Member 11b (*Tnfrsf11b*). In experiments with mice, matrifibrocytes were eliminated from the mature scar by cryoinjury, resulting in significantly reduced cardiac function compared to sham controls, suggesting that matrifibrocytes contribute to maintaining the integrity of the mature scar [72].

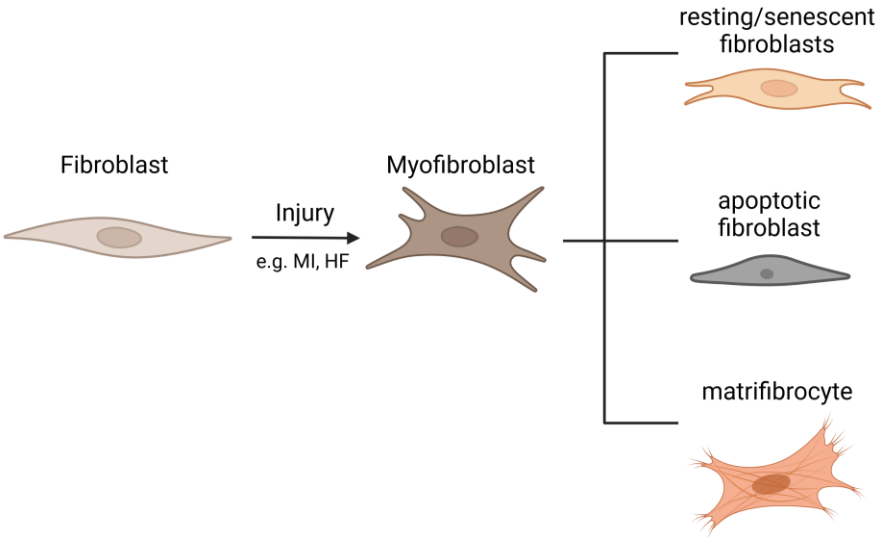

Figure 3: Schematic presentation of fibroblast differentiation in response to cardiac injury (e.g., MI, HF). Tissue fibroblasts get activated after injury, including MI and HF. Activated fibroblasts are called myofibroblasts and are characterized by high αSMA expression. Around 10 days after the injury, αSMA expression decreases and myofibroblasts differentiate differently. They either remain in the tissue as resting or senescent fibroblasts or undergo apoptosis. However, fibroblasts can also become so-called matrifibrocytes; this special type of fibroblast shows increased expression of genes that are normally found in bone and cartilage. The scheme is based on Kurose et al. 2021 [73]. Created with BioRender.com.

1.3.1 The role of immune cells in the onset of fibrosis

Immune cells infiltrating the damaged cardiac tissue actively enhance cardiac fibrosis via comprehensive communication with cardiomyocytes, endothelial cells, and fibroblasts. Since neutrophils are mainly associated with acute inflammatory responses within the myocardium and are cleared rapidly from the site of injury, their role may be limited to the early phase of fibroblast activation. Nevertheless, activation of neutrophils via reactive oxygen species (ROS) induces the formation of neutrophil extracellular traps (NETosis), which is suggested to contribute to interstitial fibrotic modifications in cardiac tissue [74-76]. T-lymphocytes and macrophages infiltrate the cardiac tissue at later time points and therefore probably have a greater influence on the development of fibrosis. Subpopulations of T-lymphocytes may directly induce fibroblast activation through the secretion of pro-fibrotic cytokines IL-4 and IL-13. Both are known to promote fibroblast-derived collagen synthesis [77-79]. Furthermore, Ly6C^{high} macrophages derived from Ly6C^{high} monocytes secrete IL-10 [80] and TGF-β [81], which act as fibrogenic signals. In mice with cardiac-specific TNF-α overexpression, Bryant et al. observed a progression of heart failure accompanied by extensive collagen synthesis [82], again indicating the importance of cytokine-producing macrophages and lymphocytes in the progression of fibrosis. However, considering the diverse phenotypes of macrophages, other subsets may also contribute to the resolution of fibrotic tissue. In hepatic fibrosis, for example, matrix metalloproteinases expressed by Ly6C^{low} macrophages suppressed the fibrotic response [83, 84]. Additionally, the anti-fibrotic effect of specific macrophages also involves the suppression of fibroblast activation, possibly through the secretion of mediators that deactivate fibroblasts. Although the exact role of the various immune cell types is not conclusively characterized, a close link between the development of cardiac fibrosis and the infiltration of immune cells into the heart is certain.

1.4 The structure of the skeletal muscle and mechanisms mediating cardiac cachexia

The skeletal muscle is made up of three distinct fiber types: type I fibers, type IIa fibers, and type IIb/x fibers. The composition of the different fiber types within a muscle determines its properties. Type I fibers are described as slow-twitch fibers. They use aerobic metabolic pathways and depend on oxygen supply. Therefore, they are rich in mitochondria and myoglobin. Myoglobin is an oxygen-binding protein in muscle cells; it has a higher affinity for oxygen compared to hemoglobin and is responsible for oxygen transport within the muscle. Type I fibers do not contract forcefully, therefore they need

less energy. They are important for less-explosive, sustained movements like long-distance running because they do not fatigue as quickly as other fiber types. Type IIa fibers are considered as fast-twitch fibers. They are able to use both, aerobic and anaerobic metabolic pathways. Because they have a higher myosin ATPase activity than type I fibers, they have a faster contraction time. These fibers are important for activities involving speed, strength, and power. Type IIb/x fibers have a very fast contraction time and a very high force production; therefore, they also fatigue quickly. They operate independent of oxygen availability and generate force through glycolytic metabolism. Thus, they are not as high in mitochondria and myoglobin as the other fibers (Figure 4). However, it must be mentioned that in large mammals, including humans, no type IIb fibers exists, but only type IIx fibers. Type IIb fibers are found in small mammals, such as mice. In adult mice, type IIb fibers make up most muscle fibers (70-80%) in healthy conditions. However, the distribution of muscle fibers depends on the corresponding muscles and is dependent on their oxidative or glycolytic profiles, respectively [85].

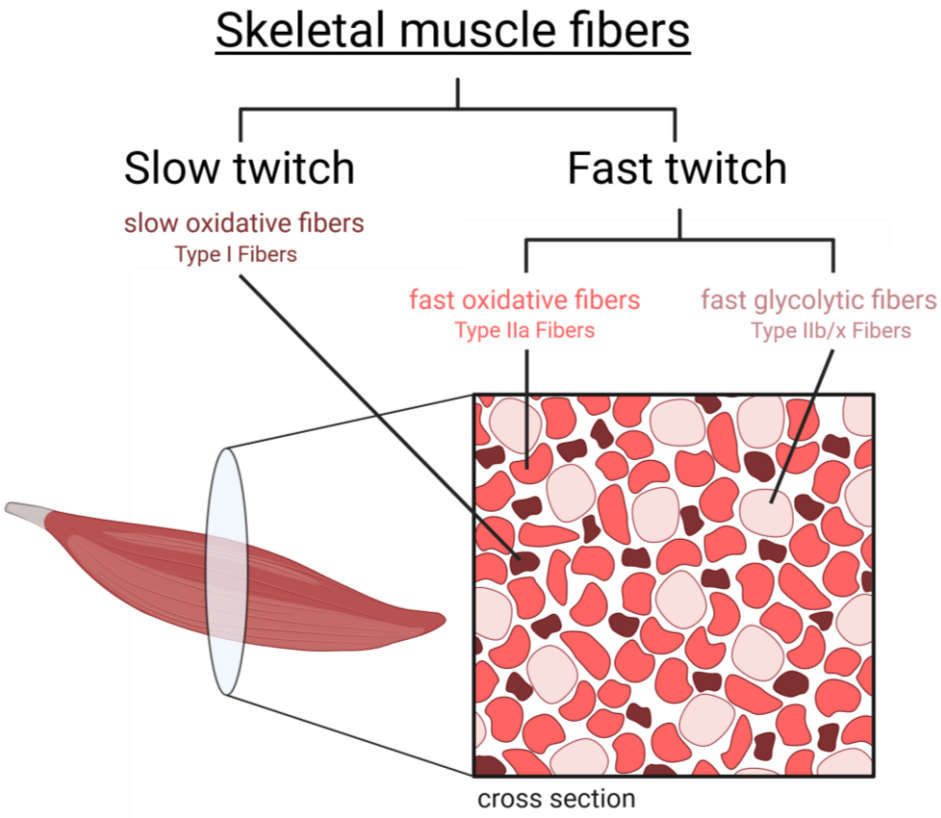

Figure 4: Structure of the skeletal muscle and the different fiber types. The skeletal muscle consists of various fiber types. They are divided into slow-twitch and fast-twitch fibers. Slow-twitch fibers are type I muscle fibers. They are rich in myoglobin and depend on oxygen supply. Fast-twitch fibers can be further subdivided into fast oxidative fibers and fast glycolytic fibers. Fast oxidative fibers are type IIa fibers and are able to use both aerobic and anaerobic metabolic pathways to generate energy. Type IIb/x fibers, on the other hand, use glycolytic metabolism to generate energy and are independent of oxygen supply. Due to their lower myoglobin content, these fibers appear brighter in color than the others. Created with BioRender.com.

Cardiac cachexia is a common comorbidity in heart failure

Cachexia (chronic disease-associated weight loss) describes a multifactorial syndrome that causes progressive loss of body fat and skeletal muscle mass exceeding at least 5% of the body weight within 12 months or less without trying to lose weight and in the presence of a known disease. Often, the term is mistaken for anorexia, which is defined as weight loss due to insufficient food intake. Remarkably, the process of cachexia is not reversible by nutritional supplementation or targeted training of the affected muscle groups. Further treatment approaches using anabolic or anti-catabolic therapies are under development. Numerous diseases like cancer, chronic heart failure (CHF), chronic obstructive pulmonary disease (COPD), chronic kidney disease (CKD), and acquired immunodeficiency syndrome (AIDS) may lead to cachexia. Cachexia is known to be associated with high mortality and poor symptom status, which drastically diminishes quality of life. Up to 15% of CHF patients suffer from cachexia [86], and the mortality rates of patients with cachexia have a high variability, ranging from 10 – 15% in COPD patients to 20 – 30% per year in patients with CHF or CKD. The treatment of cachexia is challenging and targets mainly the underlying chronic disease. So far, there is no treatment that targets cachexia specifically or reverses the process. As already mentioned, a variety of chronic diseases can cause cachexia, but some general pathomechanisms trigger cachexia [87]. First, elevated levels of pro-inflammatory cytokines were found in cachexia patients. These include TNF-α, interferon-γ (IFN-γ), and several interleukins (IL-1, 2, 6). These cytokines stimulate the release of cortisol and catecholamines [88, 89], induce lipolysis [90], and adversely affect protein synthesis in skeletal muscle tissue [91]. In combination, this leads to a negative energy balance and ultimately to a loss of body weight. Furthermore, elevated levels of myostatin, a suppressor of muscle growth [92], and declined levels of testosterone [93] and insulin-like growth factor 1 (IGF-1) [94] contribute to the progression of cachexia. Leitner et al. summarized the importance of ROS in cachectic muscles, since elevated ROS levels induce E3-ubiquitin ligases. The E3-ubiquitin ligase Muscle RING Finger 1 (MuRF1) is, together with muscle atrophy F-box (MAFbx or Atrogin1), the most prominent player in the progression of skeletal muscle atrophy, and their activity is highly upregulated in cachectic patients. ROS production in skeletal muscle is increased, among others, by AngII. Simultaneously, AngII enhances muscle wasting by antagonizing the action of growth factors like IGF-1 and reducing insulin sensitivity. Therefore, anabolic actions are impaired, which even amplifies the progression of muscle wasting [85].

Early publications by Mendell and Engel indicated that the distinct fiber types within a skeletal muscle react differently to stimuli such as cytokines and ROS. Glycolytic type II muscle fibers are particularly susceptible to atrophy, while oxidative type I muscle fibers

appear to be more resistant [95]. These results were confirmed by later work that demonstrated a fiber-type-specific atrophy in glycolytic but not oxidative fibers in a mouse model for heart failure [96-98]. On the other hand, contradictory results were obtained in a study with CHF patients. Here, a shift from oxidative type I fibers to glycolytic type II fibers was observed [99].

1.5 Mouse models of heart failure

To study the mechanisms of cardiac dysfunction, various *in vitro*, *in vivo,* and *ex vivo* methods are available. Heart failure is a multifactorial syndrome that includes not only the heart tissue itself but rather arises through the interaction of many different influences from various organs. Thus, the use of animal models, e.g., mice, to study cardiac dysfunction is widespread and long-established. Heart failure can be triggered by the induction of pressure overload. Constriction of the transverse aorta (TAC) is a widely used model for this. Initially, TAC causes hypertrophy of the LV as a compensatory mechanism. However, over time, pressure overload induced hypertrophy becomes maladaptive, ultimately dilation of the LV and heart failure are observed [100]. On the other hand, many genetically modified mouse lines are available to study heart failure. Either the KO of a certain gene leads directly to heart failure or an additional stimulus must be used. This can be, for example, a pressure overload induced by angiotensin II. This thesis uses two different heart failure mouse models. The iCM-p38 MAPKα KO mouse model and the iCM-AKT1/2 mouse model. Details about each are provided below.

1.5.1 Cardiac-specific deletion of p38 MAPKα as a mouse model of pressure overload-induced heart failure

To investigate the role of p38 MAPKα in the heart, our group generated a cardiomyocyte-specific knockout mouse line. The iCM-p38 MAPKα KO (referred to in this work as iCM-p38 KO) mouse model is described in detail in Bottermann,… Hemmers,… et al. 2022 [41]. The deletion of the *p38 MAPKα* gene specifically in cardiomyocytes via OH-tamoxifen injection does not affect cardiac function under baseline conditions. However, induction of pressure overload (PO) via angiotensin II (AngII) results in a pronounced cardiac insufficiency, characterized by a significant increase in end-diastolic (EDV) and end-systolic volumes (ESV) just within 2 days (see Figure 10 (section 4.1)). Since the left ventricle is severely affected, HFrEF is present in this model, as described in 1.1. Remarkably, the heart does not undergo a hypertrophic state, as it is usually observed in models for LV dilation. The rapid development of cardiac dysfunction suggests a protective role of p38 MAPKα in cardiomyocytes.

Analysis of cardiac tissue after induction of heart failure reveals an accumulation of lipid droplets and a massive infiltration of neutrophils in close proximity to the lipids. Figure 5 schematically illustrates the processes in iCM-p38 KO hearts after AngII treatment. Analysis targeting the interorgan communication between the failing heart and the skeletal muscle [101], adipose tissue [102], and pancreas [103] indicates metabolic dysfunction in iCM-p38 KO mice and systemic organ crosstalk.

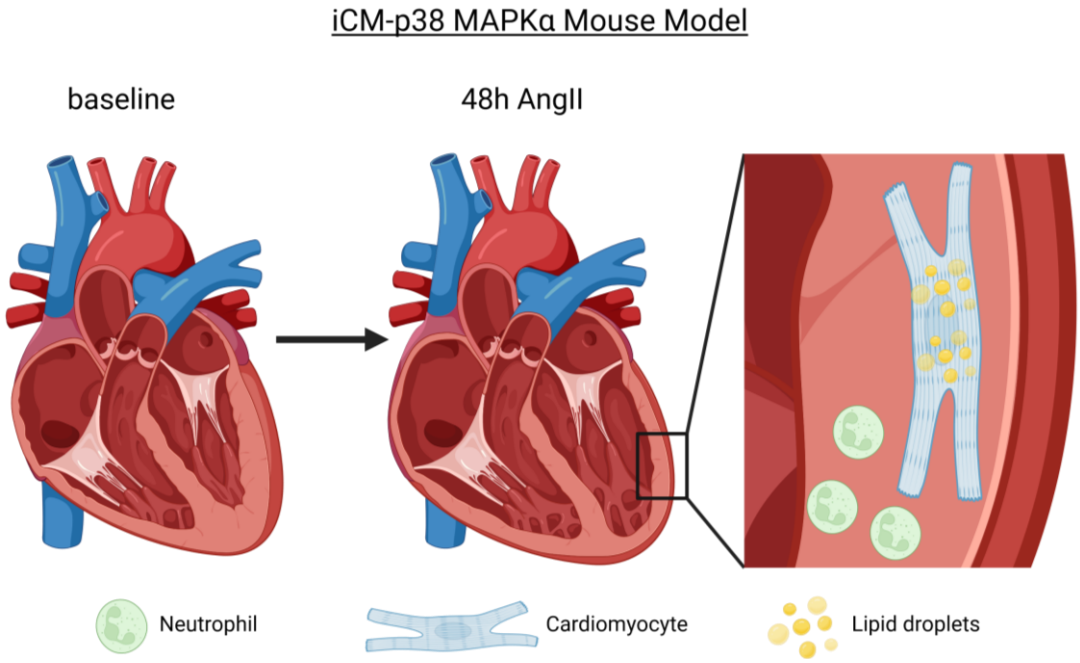

Figure 5: Schematic illustration of the processes in iCM-p38 KO hearts after induction of PO via AngII treatment. The induction of iCM-p38 KO via tamoxifen does not affect cardiac function under baseline conditions. However, 48h after induction of PO via AngII, the hearts severely dilate and cardiac function is restricted. This is characterized by a reduced EF due to an increase in EDV and ESV. Additionally, lipid droplets accumulate in cardiomyocytes, and neutrophils infiltrate cardiac tissue. Created with BioRender.com.

p38 mitogen-activated protein kinases (MAPK) in cardiac tissue

Mitogen-activated protein kinase (MAPK) cascades comprise at least three kinases connected in series: a MAP kinase kinase kinase (MKKK), a MAP kinase kinase (MKK), and a MAP kinase (MAPK), which are phosphorylated in this order [26]. They are activated by a variety of extracellular stimuli, e.g., UV light, heat shock, or osmotic shock [104, 105], but also by ligand binding to G-protein-coupled receptors [106]. Within the MAP Kinase family, four subgroups are distinguished [107]:

1. c-jun N-terminal or stress-activated protein kinases (JNK/SAPK)
2. ERK/ big MAP kinase 1 (BMK1)
3. extracellular signal-regulated kinases (ERKs)
4. p38 group of protein kinases

p38 MAPK was first isolated in 1993 as a 38-kDa protein that is rapidly tyrosine-phosphorylated in response to LPS stimulation [108]. So far, 4 different splice variants

of the p38 MAPK could be identified, which share ~60% identity. Homologues of the conserved protein have been identified in yeast (Hog1 & Spc/Sty1), worm (pmk-2), fly (p38), and frog (p38) [109-112]. While p38 MAPKα (MAPK14) is ubiquitously expressed [104], the other three isoforms, MAPKβ (MAPK11), MAPKγ (MAPK12), and MAPKδ (MAPK13), are differentially expressed depending on tissue type. In brain and lung tissue, mainly p38 MAPKβ can be detected. p38 MAPKγ is primarily expressed in skeletal muscle and the nervous system, and p38 MAPKδ in the uterus and pancreatic tissue [105]. P38 kinases are, like all MAP kinases, activated by a conserved dual phosphorylation at threonine 180/tyrosine 182 residues by distinct MAP kinase kinases (MKKs), such as MKK3, MKK4, and MKK6 [113, 114]. The specific activator of the p38 MAPK isoform is stimulus-dependent [115]. The phosphorylation of p38 MAPKs triggers a translocation into the nucleus. This results in the activation of transcription factors and, therefore, a modified expression of target genes. Numerous genes regulated by the p38 MAPK pathway could be identified using inactive and constitutively active mutants of MKK3 and 6, as well as the p38 inhibitor SB 203580. Additionally, p38 MAPKα phosphorylates MAP kinase-activated protein kinase 2 (MK2), which is shown to activate small heat shock protein 27 (HSP27) [116], lymphocyte-specific protein 1 (LSP1) [117], cAMP response element-binding protein (CREB) [118], and various transcription factors such as ATF1 [118] and serum response factor (SRF) [119]. Later, it was demonstrated that p38 MAPK phosphorylates tristetraprolin (TTP), which results in destabilization of mRNA, hinting towards a potential role of p38 MAPK in mRNA stability [120] (Figure 6). p38 MAPKs are dephosphorylated by phosphatases of the protein phosphatase (PP) family, protein tyrosine phosphatase (PTP) family, and dual-specificity phosphatase (DUSP) family [117]. The dephosphorylation of p38 MAPKs causes their inactivation and subsequent export to the cytoplasm [107].

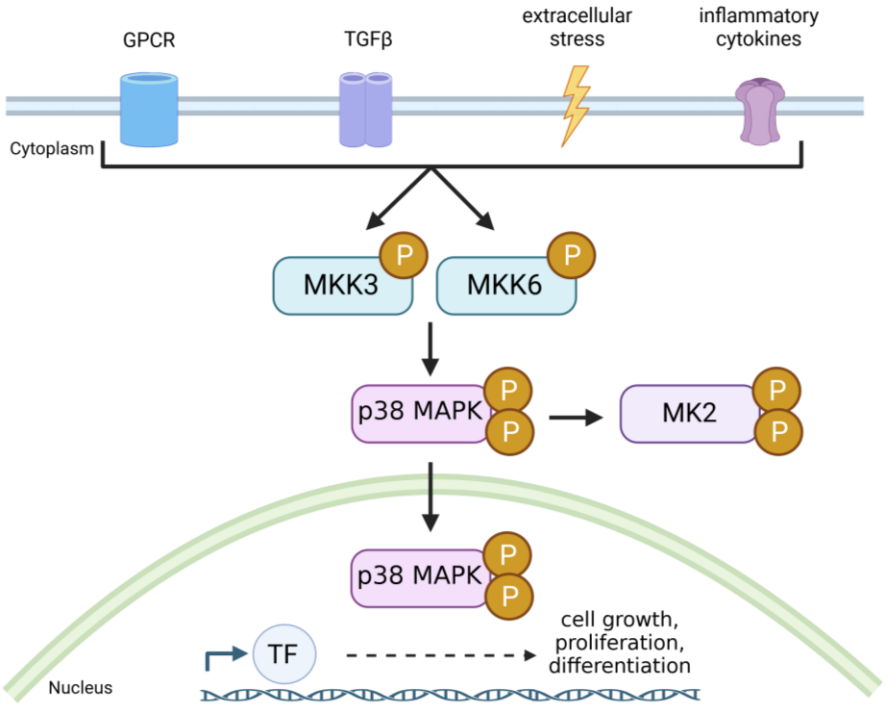

Figure 6: Signaling cascade of p38 MAPK in cardiomyocytes. p38 mitogen-activated protein kinases (MAPK) are activated via phosphorylation triggered by a variety of signals, such as molecules binding G protein-coupled receptors (GPCR), transforming growth factor-β (TGF-β), extracellular stress, or inflammatory cytokines. As an initial step, the distinct MAP kinase kinases (MKKs), MKK3 and MKK6, get phosphorylated. These in turn phosphorylate p38 MAPK at the phosphorylation sites threonine 180/tyrosine 182. P38 MAPK either gets translocated into the nucleus, where the protein activates transcription factors (TF), which modulate gene expression of target genes and affect cell growth, proliferation, and differentiation, or p38 MAPK phosphorylates the downstream target MAP kinase-activated protein kinase 2 (MK2). Created with BioRender.com.

A strong link between the p38 MAPK pathway and inflammation has been established as well. Inflammatory diseases, such as Alzheimer's disease, rheumatoid arthritis, and inflammatory bowel disease, are postulated to be regulated in part by the p38 MAPK pathway [121-123]. p38 MAPK pathway activation is implicated in the production of inflammatory cytokines such as IL-1β, TNF-α, and IL-6 [124]. p38 MAPK is also involved in cardiovascular disease. In HF, the p38 pathway is activated and especially participating in the regulation of pathological cardiac remodeling [125, 126].

However, *in vitro* and *in vivo* experiments investigating the role of p38 MAPK led to contradictory results, and its role is by far not clear. It is known that deficiency of the p38 MAPKα isoform is embryonic lethal due to impaired placental development [127, 128]. Several studies report that inhibition of p38 MAPK through specific inhibitors, SB203580 and SB202190, has a cardioprotective effect after myocardial infarction by improving post-ischemic functional recovery [129] and restraining myocardial cell death [130]. On the other hand, inhibition of p38 MAPK or expression of dominant negative mutant p38 MAPK *in vitro* restricts cardiomyocyte growth after hypertrophic stimuli [128]. Further, studies in cultured rat cardiomyocytes showed that p38 MAPKα activation is sufficient to

induce a hypertrophic response [131]. In our group, a cardioprotective effect of p38 MAPKα was demonstrated as well, since the deletion of p38 MAPKα in cardiomyocytes results in severe dilation of the heart after induction of pressure overload [41].

1.5.2 Cardiomyocyte-specific AKT1/2 KO as a mouse model for cardiac atrophy and differences to the iCM-p38 MAPKα KO mouse model

Although the iCM-AKT1/2 mouse model is also a model for heart failure, it differs substantially from the iCM-p38 KO model. The *Akt* gene encodes for protein kinase B (PKB), a serine/threonine-specific protein kinase. There are three different isoforms of the gene, namely *Akt1*, *Akt2*, and *Akt3*, and all are key players in cellular processes like glucose metabolism, cell migration, and cell cycle regulation, including apoptosis and proliferation. The mammalian heart expresses mainly *Akt1* and *Akt2*. A specific mouse line holding a cardiomyocyte-specific deletion of *Akt1* and *Akt2* (referred to in this work as iCM-AKT1/2 KO) after OH-tamoxifen injection turned out to be suitable as a model to study the mechanisms of heart failure. Heart function of AKT1/2 KO mice started to worsen 14 days after the start of tamoxifen injection, as indicated by a reduced ejection fraction (EF), a progressive increase in end-systolic volume (ESV), and reduced cardiac output (CO) (Figure 7a–d). Survival studies show that after about 21 days, deterioration of cardiac function is so severe that animals gradually die (Figure 7f). In contrast, mice with single KO of *Akt1* or *Akt2*, respectively, do not show a reduction in cardiac function [132].

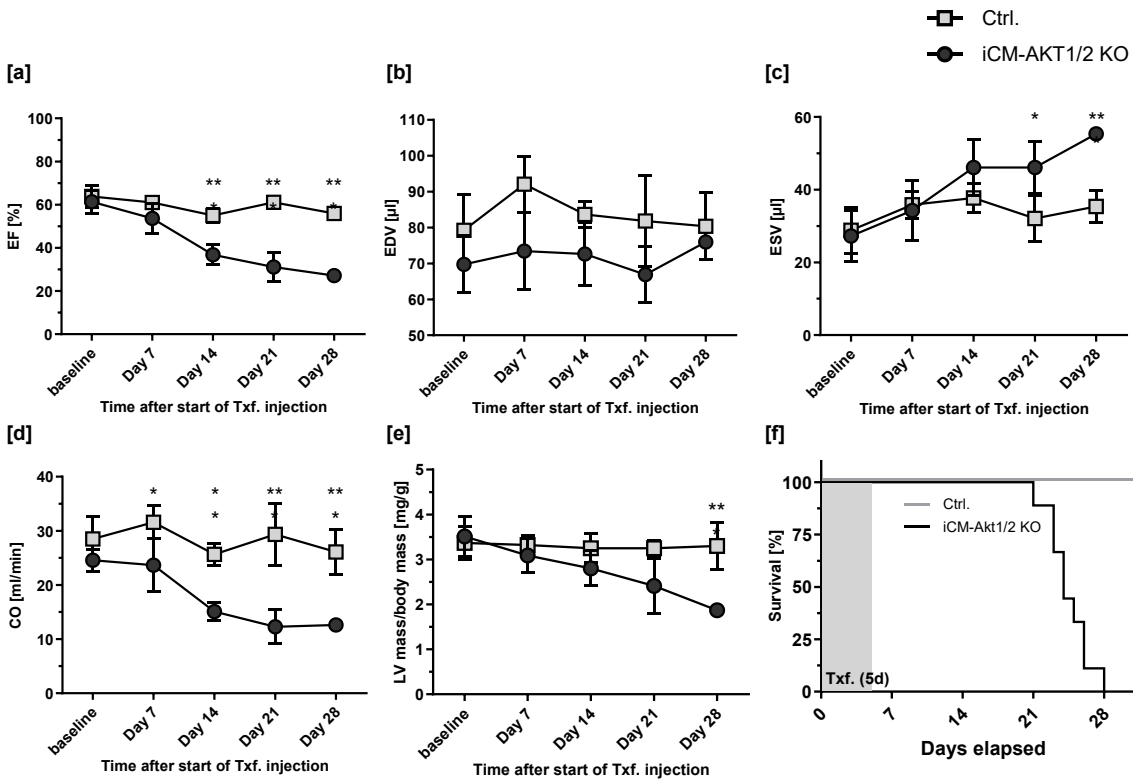

Figure 7: Cardiac function and lifespan of iCM-AKT1/2 KO and control mice over time after KO induction through tamoxifen (Txf.) injection. Cardiac dysfunction in iCM-AKT1/2 KO mice (dark) started to deteriorate around 14 days after the start of tamoxifen injection. **[a]** A decrease in ejection fraction (EF) caused by **[c]** an increased end-systolic volume (ESV) was found in KO mice compared to the controls (bright). **[b]** End-diastolic volume (EDV) was not altered over time, but was lower in iCM-Akt1/2 KO mice compared to controls. **[d]** Cardiac output (CO) drastically decreased in KO mice as well, while CO in controls stayed unchanged over time. **[e]** Left ventricular mass (LV) decreased in KO animals as well. **[f]** Survival rate in %. Data are presented as mean ±SD, n = 5-15. Statistical significance was calculated using Two-way ANOVA (repeated measures) with Bonferroni's multiple comparisons test (*** p <0.001). Data are obtained from Dr. rer. nat. Stefanie Gödecke and Prof. Dr. Dr. med. André Heinen; Institute of Cardiovascular Physiology, University Hospital Düsseldorf.

The iCM-AKT1/2 double KO model differs in various points from the previously described iCM-p38 KO model. No additional pharmacological treatment is required to induce cardiac dysfunction in iCM-AKT1/2 KO mice; merely the elimination of the two AKT isoforms is sufficient. In addition, this model does not show a dilation of the heart, which is primarily characterized by an increase in EDV. However, a pronounced atrophy of the heart is observed. This is determined primarily by a precise examination of cardiomyocytes, which are reduced in size and undergo apoptosis. Both mouse models are therefore completely different, but both offer the opportunity to get a better understanding of severe cardiac disease and furthermore enable the investigation of potential interorgan communication between the failing heart and peripheral organs.

1.6 Aim of the project

Heart failure is a complex clinical syndrome, and the underlying mechanisms are not fully understood yet. The inducible cardiomyocyte-specific p38 MAPKα KO mouse model develops severe left ventricular (LV) dilation rapidly after induction of pressure overload via AngII. This makes the model useful to study underlying mechanisms involving the immune system as well as the effect on peripheral organs to investigate the interorgan communication between the failing heart and, e.g., adipose tissue, pancreatic tissue, and skeletal muscle. The primary aims of this thesis are:

1. Analysis of early transcriptomic alterations in iCM-p38 KO hearts:
   Up to this point, the AngII-induced metabolic alterations in the iCM-p38 KO mouse model were investigated mainly after 48h of AngII administration. However, at this time point, the massive reduction in cardiac function has already been established. Analysis of cardiac tissue at an earlier time point (12h) should reveal which metabolic alterations occur first and therefore supposedly have the greatest influence on the development of heart failure in those mice.

2. Investigation of the influence of sympathetic nervous system activity on the development of cardiac dysfunction:
   As it is known, sympathetic overstimulation can exacerbate cardiac function in heart failure conditions. To investigate the influence of SNS over-activation on the development of cardiac dysfunction in iCM-p38 KO mice, the effect of blockade of β-adrenergic stimulation on cardiac function and immune cell infiltration should be addressed as a possible pharmacological intervention.

3. Establishment of a long-term heart failure model excluding pharmacological intervention:
   The iCM-p38 KO mouse model is an exceptional model to analyze heart failure. Just within 2 days of AngII treatment, healthy mice develop severe cardiac dysfunction characterized by strong dilation of the heart. However, it remains unknown to what extent this fast dilation is transient or already reflects long-lasting LV remodeling. Therefore, the long-term functional alterations in the heart induced by 2d and 7d AngII treatment should be addressed with the aim to establish a chronic HF model for studying the interorgan communication in HF conditions.

4. Analysis of the influence of infiltrating immune cells in cardiac tissue of the failing heart:
   A hallmark of cardiac tissue in iCM-p38 KO mice after AngII treatment is the massive infiltration of immune cells, in particular neutrophils. Since histological analysis of

cardiac tissue revealed a close proximity of accumulating lipid droplets and neutrophils, and FACS analysis of cardiac tissue revealed a massive infiltration of neutrophils, it stands to reason that, in particular, the initial infiltration of neutrophils may contribute to the deterioration of cardiac function in iCM-p38 KO mice.

Therefore, the role of neutrophils on long-term outcomes after AngII-mediated LV dilation should be investigated.

5. Characterization of the interorgan communication between the failing heart and skeletal muscle:

   Since HF is a systemic disease, a possible interorgan communication between the heart and skeletal muscle should be examined in the iCM-p38 KO model of heart failure and compared with the effects of cardiac atrophy on skeletal muscle as observed in inducible cardiomyocyte-specific AKT1/2 double KO mice.

2. Materials

In the following lists, general laboratory equipment, technical devices, chemicals, and kits, as well as used software, are listed.

2.1 General laboratory equipment and technical devices

Table 1: Laboratory equipment

Material	**Manufacturer (*Product name*)**
1 ml syringe	Braun AG, Melsungen, Germany
10 cm cell culture plates	Greiner Bio-One, Germany
15/50 ml Falcon tubes	Greiner Bio-One, Germany
5/10/25 ml stripettes	Corning Costar®, Germany
EASYstrainer™ 40/100 µm cell filter	Greiner Bio-One, Germany
Echocardiography gel	Aquasonic 100, Parker Laboratories, USA
Electrode cream	Gello GmbH, Germany
Eppendorf tubes	Eppendorf AG, Germany
FACS tubes	Falcon, Germany
Gilson Pipetman classic pipet	Fisher Scientific, UK
Improved Neubauer chamber	Laboroptik, Germany
Microscope slides	Marienfeld Superior™, Germany
Sterile disposable gloves	Ansell, Brussels, Belgium
Surgical tools	Fine Science Tools GmbH, Germany

Table 1 lists all materials applied during the experiments.

Table 2: Technical devices

Product name	Manufacturer
-20 °C Freezer Premium NoFrost	Liebherr, Germany
-80 °CFreezer	Thermo Fisher Scientific, USA
Autoclave maschine	Systec, Germany
Centrifuges	Eppendorf (5415R), Eppendorf (5402), VWR (Mega Star 1.6R), Labnet (Spectrafuge Mini Centrifuge), Roth (Rotilabo)
Cryostat microtome Rotation CM1860	Leica Biosystems, GErmany
Electrical shaver	Contura, Germany
FACS Canto II	BD Bioscience, USA
Fluoresence microscope BZ 9000	Keyence, Japan
Fridge	Liebherr, Germany
Homogenizer TissueRuptor II	Qiagen, Germany
Ice Maschine	Ziegra, Germany
iMark Microplate Absorbance Reader	Bio-Rad Laboratories, Inc., USA
Incubator	Heraeus (B6120), Infors HAT (Ecotron)
Isoflurane vaporizer	Vet Equipment Inc., USA
Light microscope M60	Leica, Germany
Liquid nitrogen tanks Apollo	Cryothem, Germany
Magnetic stirrer MR3001	Heidolph, Germany
McIlwain tissue chopper	Cavey Laboratory Engineering Co. Ltd., UK
Nitrocellulose Blotter PierceTM G2 Fast Blotter	Thermo Fisher Scientific, USA
PCR plate centrifuge 521-1648E	VWR, USA
Real Time PCR System QuantStudio	Applied Biosystems, USA
SDS-Page flow chamber, SE400-SE600	Hoefer Instruments, USA
Spectralphotometer ND-1000	PEQLAB Biotechnologie GmbH, USA
Vevo 2100 High Frequency Ultrasound System	Visualsonics, Toronto, Canada

Table 2 lists all technical devices used for the experiments.

2.2 Chemicals and Kits

Table 3: Chemicals

Chemicals	Manufacturer
Acrylamid-Bisacrylamid-Stock solution (40%)	Carl Roth GmbH + Co. KG; Germany
Angiotensin II	Sigma-Aldrich, USA
APS	Carl Roth GmbH + Co. KG; Germany
BETAISODONA® solution	Mundipharma, Germany
BSA Fraction V	PanReac AppliChem, Germany
Buprenorphin (Temgesic) 0.3 mg/ml	Indivior Europe Limited, Ireland
Collagenase type I	Worthington Biochemical Corp., USA
Dobutamine Liquid (500 mg/50 ml)	Fresenius Kabi GmbH, Germany
DTT	Carl Roth GmbH + Co. KG; Germany
Eye ointment	Bayer AG, Germany
Fab-Fragment	Jackson Immunoresearch, USA
FBS/HS	Biochrom, Germany
Hair removal creme - Veet sensitive	Reckitt Benckiser Group, UK
HBSS	Gibco, Thermo Fisher Scientific,USA
Isoflurane	Piramal Critical Care, USA
Isopentane	Carl Roth GmbH + Co. KG; Germany
Normal goat serum	Jackson Immunoresearch, USA
PageRuler™ prestained proteinladder, 10 – 180 kDa	Thermo Fisher Scientific, USA
Propranolol	Sigma-Aldrich, USA
Proteinase K	Qiagen, Germany
Rat IgG2a Isotype control LEIN-I—1177	LeincoTechnologies, USA
Rimadyl (Carprofen)	Zoetis, Inc., USA
RNase-Free DNase	Qiagen, Germany
Saponin	Carl Roth GmbH + Co. KG; Germany
SDS	Sigma-Aldrich, USA
Tamoxifen	Sigma-Aldrich, USA
TEMED	Carl Roth GmbH + Co. KG; Germany
Tris	Carl Roth GmbH + Co. KG; Germany
Triton-X100	Sigma-Aldrich, USA
Trypan blue	Invitrogen, USA
Trypsin	LifeTechnologies, USA
Tween 20	Sigma-Aldrich, USA
α-Ly6G-antibody, clone 1A8 LEIN-L280	LeincoTechnologies, USA
β-Mecaptoethanol	Carl Roth GmbH + Co. KG; Germany

Table 3 lists all chemicals used during the experiments.

Table 4: Kits and master mixes

Product name	Manufacturer
Halt Protease & Phosphatase Inhibitor Single-Use Cocktail (78443)	Thermo Fisher Scientific, USA
Maxima SYBR green/ROX qPCR master mix (K0221)	Thermo Fisher Scientific, USA
NEFA-HR(2) Assay	FUJIFILM Wako Chemicals, Japan
Odyssey Blocking Buffer in TBS (927-40000)	LI-COR Bioscience, USA
Page Ruler Prestained Protein Ladder (26616)	Thermo Fisher Scientific, USA
Pierce BCA Protein Assay Kit (23225)	Thermo Fisher Scientific, USA
Quantitect Reverse Transcription kit (205311)	Qiagen, Germany
Revert 700 Total Protein Stain (926-11011)	LI-COR Bioscience, USA
RNeasy Fibrous Tissue Mini Kit	Qiagen, Germany

Table 4 lists all Kits applied during the experiments.

2.3 Software

Table 5: Applied softwares

Software	Manufacturer
BD FacsDiva Software v.8.0.2	BD Biosciences
Empiria Studio™ Software	LI-COR Biosciences
Endnote X7	Clarivate Analytics, Philadelphia, USA
GraphPad Prism 10	GraphPad Software, Inc., La Jolla, USA
Image Studio Lite Ver 5.2	LI-COR Biosciences
Microsoft Excel	Microsoft Corporation, Redmond, USA
Microsoft Word	Microsoft Corporation, Redmond, USA
QuantStudio™ Design & Analysis Software	Applied Biosystems, USA
Vevo LAB 1.7.1	FUJIFILM Visualsonics, Japan

Table 5 lists all software used during this work.

3. Methods

3.1 Mouse strains: inducible cardiomyocyte-specific gene knockouts

All animal experiments were performed in accordance with the national guidelines of the National Institutes of Health (NIH) and approved by the local animal care and use committee (LANUV, Recklinghausen, License No. AZ.: 81-02.04.2020.A190 and AZ.: 81-02.04.2019.A244). Mice (*Mus musculus*) were kept at 20-22 °C in a 12h light-dark cycle with water and a standard mouse diet ad libitum.

In all experiments, male mice of an inbred C57BL/6J mouse line background were used. By crossbreeding mice expressing tamoxifen-inducible Cre-recombinase (merCremer), specifically in cardiomyocytes, under the control of αMHC (murine alpha myosin-heavy chain) promotor [133, 134] with mice homozygously expressing a loxP-flanked target gene, knockout mouse lines were generated.

The Cre-Lox system is widespread for decades and is frequently used to delete, insert, translocate, or inverse specific genes in the DNA of cells or animals. By coupling Cre-recombinase to tissue-specific promoters, genes can be targeted in individual organs (e.g., αMHC promotor to target cardiomyocytes). In order to avoid the issue of fetal lethality, the localization into the nucleus of Cre-recombinase can also be controlled pharmacologically. Therefore, a fusion protein of the Cre-recombinase and a mutant of the human estrogen receptor ligand binding domain (merCremer) [135] is expressed in transgenic mice. By injection of 4-hydroxytamoxifen (OH-Tx), which functions as a ligand of the merCremer, the Cre-recombinase is translocated into the nucleus, where it recognizes and deletes the loxP-flanked gene subsequently [136-138].

3.1.1 iCM-p38 MAPKα KO mouse line

iCM-p38 KO mice were generated by crossing *p38 MAPKα*$^{flox/flox}$ (exon 2 and 3) mice with heterozygous merCremer mice [133, 134] under the control of a α-MHC promotor. In heterozygous (control) and homozygous (iCM-p38 KO) merCremer mice, the Cre-recombinase was induced via injection of 500 µg of 4OH-Tamoxifen (5 mg/ml in peanut oil) intraperitoneally (i.p.) for 10 consecutive days when mice were 6-8 weeks old. Afterwards, they recovered for 2-4 weeks. Because the α-MHC promotor is cardiomyocyte-specific, the p38 MAPK KO occurs exclusively in the heart. In heterozygous (control) merCremer mice, no effect of tamoxifen injections was observed.

3.1.2 iCM-AKT1/2 KO mouse line

iCM-AKT1/2 KO mice were generated by crossing *Akt1*$^{flox/flox}$/*Akt2*$^{flox/flox}$ (*Akt1* exon 6 and 7, *Akt2* exon 5 and 6) mice with heterozygous merCremer mice [133, 134] under the control of a α-MHC promotor. In heterozygous (control) and homozygous (iCM-AKT1/2 KO) merCremer mice, the Cre-recombinase was induced via injection of 500 µg of 4OH-Tamoxifen (5 mg/ml in peanut oil) i.p. for 5 consecutive days when mice were 12 weeks old. Since the α-MHC promotor is used, the AKT1/2 KO occurs exclusively in cardiomyocytes. In heterozygous (control) merCremer mice, no effect of tamoxifen injections was observed.

3.2 *In vivo* methods

For all in *vivo* experiments, mice were anesthetized using isoflurane inhalation at a flow rate of 1-3% (v/w) and placed on a warm pad (temperature set to 40-42 °C) to keep the core temperature at 37 °C. A rectal thermometer was inserted to monitor the temperature of the animals. Mice were prepared for surgery using a shaver and hair remover lotion to access the surgery spot. To avoid eye injury during the procedures, eye ointment was used.

3.2.1 Echocardiography

To investigate the influence of genetic modifications and treatments on cardiac performance, left ventricular echocardiography was performed using the Vevo 2100 High Frequency Ultrasound System. Mice were anesthetized and placed with their backs on a warm pad, as described in 3.2. To monitor heart and breathing frequency, all four limbs were taped to a metal ECG (electrocardiogram). The heart rate was maintained at 400-500 beats per minute (BPM). The chest hair of the mice was first removed by shaving. A hair removal cream was then applied to the area to be examined to completely remove

all hair. Imaging of the mouse heart first requires the application of pre-warmed echo gel to the mouse's chest, and was performed using an echo transducer MS400 (18-38 mHz). To visualize the two-dimensional left ventricular parasternal long-axis, the transducer was placed along the long-axis. By rotating the transducer clockwise by 90°, the short-axis of the left ventricle was obtained, and m-mode and b-mode were imaged, respectively. After the recordings were completed, the echo gel was removed from the mice, and the mice were placed in a recovery cage. The recordings were analyzed using the Vevo Lab 1.7.1 software. At least four cardiac cycles were analyzed and averaged for the interpretation of any given measurement. Ejection fraction (EF), left ventricular end-diastolic, and end-systolic volume (EDV; ESV) were calculated via Simpson's protocol from parasternal short and long axis B-Mode images. Left ventricular anterior wall thickness in diastole and systole (LVAW,d; LVAW,s) were calculated from short-axis m-mode images.

3.2.2 Implantation of osmotic mini pumps

The implantation of osmotic pumps allows the continuous administration of active ingredients for a defined period. According to the manufacturer, pumps were filled 12-16 hours before implanting and stored overnight in PBS at 37 °C. For pump implantation, mice were anesthetized and placed ventral on a warm pad, as described in 3.2. For subcutaneous insertion of the pump, the neck of the mouse was shaved to remove the hair, and a small incision was made. After insertion of the osmotic pump, the opening of the skin was sewn up with 3-4 stitches, and the scar was treated with an antiseptic (Betaisodona). Animals were injected with an analgesic (Carprofen 5 mg/kg s.c.) while they were still under anesthesia. The analgesic was injected repeatedly 24 hours after the pump had been implanted.

Angiotensin II treatment via osmotic mini pumps

To increase cardiac workload and consequently induce hypertension, angiotensin II (AngII) was used as a potent vasoconstrictor. AngII was solved in sterile phosphate buffered saline (pH 5). Continuous AngII application from 24 hours up to 7 days was implemented using osmotic mini pumps (Alzet models 1003D or 1007D). Pumps were filled and implanted, as described in 3.2.2. Pumps reach a constant pump performance of 1.5 mg/kg/day.

Combinational treatment with propranolol and angiotensin II via osmotic mini pumps

Propranolol specifically inhibits the activity of the sympathetic nervous system by blocking the β-receptors on the nerves of the sympathetic system without activating them (no intrinsic activity). Propranolol is a non-cardiac-selective blocker that binds to both β_1- and β_2-adrenoceptors. Propranolol treatment was based on a publication from King et al. 2013 [139]. Propranolol was solved in sterile phosphate buffered saline (pH 5) and administered via drinking water (10 mg/kg/day) for 24h and afterwards for 48h together with AngII via osmotic mini pumps (10 mg/kg/day). Filling and implantation of the pumps were performed as described in 3.2.2.

Depletion of the infiltrating neutrophils prior to the induction of pressure overload

Neutrophil depletion was performed as described in Bottermann et al. 2022 [41]. Briefly, neutrophils were depleted once by an injection (i.p.) of 500 µg α-Ly6G-antibody, clone 1A8, or with a corresponding isotype control. Injection was performed 12-16h prior to the implantation of osmotic mini pumps filled with AngII.

3.2.3 Invasive Blood pressure measurements

Blood pressure measurements were performed to ensure propranolol treatment was effectively administered via osmotic mini pumps. Therefore, mice's blood pressure measurements were performed under anesthesia as part of terminal experiments and were carried out as followed: Anesthesia was induced with isoflurane (2.5%). Buprenorphin (Temgesic; 0.1 mg/kg, s.c.) was administered for perioperative analgesia. The anesthetized animal was positioned on its back on a pre-warmed plate, and all extremities were fixed using tape. An eye ointment was applied. Anesthesia was maintained with isoflurane (2%) mixed with respiratory gas. Next, the common carotid artery was exposed through a skin incision (approx. 1.5 cm) on the left ventral side of the neck. This was followed by a ligature and the subsequent opening of the vessel. A 1.4 F millar pressure volume catheter was inserted, and the vessel around the catheter was closed with a permanent knot. After the blood pressure had stabilized (approx. 10-15 minutes), dobutamine was injected (s.c., 1 µg/g). Dobutamine shows a β_1-agonistic effect, thus increasing heart rate. With previous propranolol treatment, the effect of dobutamine should be reduced. After completing the functional measurements, the catheter was removed, and the animals were killed by cervical dislocation.

3.3 Non-esterified fatty acid (NEFA) measurements

A sign of increased lipolysis of adipose tissue is the elevation of non-esterified fatty acid (NEFA) levels in blood serum. To prepare samples, blood was taken directly from the hearts of sacrificed mice. The blood was then incubated on ice for 30 minutes to allow coagulation factors to take effect and thus remove them from the serum. Samples were centrifuged for 5 min at 4 °C (2800xg). The supernatant was collected and again centrifuged under the same conditions. Afterwards, NEFA levels were measured using the NEFA-HR(2) Assay Kit (Fujifilm) according to the manufacturer's instructions. Precisely, a standard series composed of 0, 0.125, 0.25, 0.5, and 1 mM NEFA standard was prepared. 4 µl of each standard or sample were mixed with 200 µl of FUJIFILM NEFA (HR)1 solution and incubated for 5 minutes at room temperature. In order to prevent background in the photometric measurement, all samples and standards are then first measured by using a SYNERGY microplate at a wavelength of 550 nm. Afterwards, 100 µl NEFA (HR) 2 solution was added, and samples and standard were again incubated for 5 min at room temperature, followed by a second photometric measurement at a wavelength of 550 nm.

3.4 Protein analysis

3.4.1 Protein extraction from tissue

Tissue samples were collected from euthanized mice and snap-frozen in liquid nitrogen. They were stored at -80 °C until use. To homogenize the tissue (using tissue rupture), the tissues were placed in lysis buffer (10 mM Tris-Cl, 150 mM NaCl, 0.1% IGEPAL, pH 7.4) containing protease- and phosphatase inhibitors. Afterwards, the samples were centrifuged for 5 minutes at full speed at 4 °C. The supernatant was transferred into a new 1.5 ml tube and centrifuged again as described. The supernatant was again transferred into a fresh tube, and protein concentrations were determined before samples were used.

3.4.2 BCA assay

Protein concentrations were determined using the bicinchoninic acid (BCA) assay, based on Smith, Krohn, et al. 1985 [140]. Therefore, a standard series was prepared using ascending BSA concentrations in lysis buffer (25-2000 µg/ml). 25 µl of the standards and the samples were mixed with 200 µl of BCA reagent and pipetted as doublets onto a 96-well plate. After an incubation time of 30 minutes at 37 °C, the absorption was measured at 577 nm with an Elisa-Reader SpectraCount (Packard) and analyzed with the computer

program Plate Reader V3.0. Based on the standard curve, the protein concentration of the samples could be determined. Afterwards, samples were adjusted to a concentration of 0.5-2 µg/µl.

3.4.3 Polyacrylamidelectrophoresis with SDS

Electrophoretic separation of proteins according to their size via polyacrylamide electrophoresis (PAGE) was performed according to Laemmli et al. [141]. Therefore, samples with a concentration of 0.5-2 µg/µl were mixed 1:4 with Laemmli-buffer (4x concentrated, composition see below) and incubated for 5 minutes at 95 °C to denature proteins. The SDS-PAGE consists of two gels to achieve a uniform transition of the proteins. First, the resolving-gel was prepared. After polymerization of the gel, the stacking-gel was added. The composition of the SDS-PAGE is shown in Table 6. The stacking gel allows a smooth transition of the proteins into the resolving gel, where the proteins are finally separated according to their molecular weight. The concentration of the resolving gel was determined based on the estimated size of the protein of interest.

Table 6: Composition SDS-PAGE consisting of resolving- and stacking gel (two small gels).

	Resolving Gel 7.5%	**Resolving Gel 10%**	**Resolving Gel 12.5%**	**Stacking Gel 2.5%**
Millipore H_2O	5.625 ml	5 ml	4.375 ml	3.7 ml
Acrylamide 40%	1.875 ml	2.5 ml	3.125 ml	625 µl
1.5 M Tris pH 8.8	2.5 ml	2.5 ml	2.5 ml	-
1.0 M Tris pH 6.8	-	-	-	625 µl
SDS 10%	100 µl	100 µl	100 µl	50 µl
TEMED	20 µl	20 µl	20 µl	10 µl
APS 10%	25 µl	25 µl	25 µl	15 µl

20 µl of each sample (in total 10-40 µg) and 4 µl of the ladder (PageRuler, Prestained Protein Ladder, ThermoSientific) were loaded. The ladder was important to estimate the protein size. Proteins were separated in a Hoefer-electrophoresis tank in SDS running buffer at 50-200 V for ~ 1 h.

Laemmli-buffer:

- 0.25 M Tris (pH 6.8)
- 8% (w/v) SDS
- 100 mM DTT
- 20% (v/v) Glycerol
- 0.02% (w/v) Bromphenol blue

SDS running buffer:

- 25 mM Tris
- 250 mM Glycin (pH 8.3)
- 0.1% (w/v) SDS

3.4.4 Western blot

For western blot analysis, SDS-PAGE separated proteins are visualized via specific antibodies. Therefore, the proteins were transferred from the gel to a nitrocellulose membrane using the Pierce™ G2 Faster Blotter with the pre-programmed method for mixed molecular weight (25 V, 1.3 mA, 7 minutes). Therefore, two papers were placed in anode buffer, and two papers and the nitrocellulose membrane were placed in cathode buffer (for the composition of the buffers, see below). On the cathode of the blotter, two papers with cathode buffer were placed, followed by the SDS-Gel and the membrane. At last, two papers with anode buffer were placed on the membrane, and the anode was placed on top of the preparation. After the transfer, the membrane was blocked for 30-60 minutes by using a blocking solution (TBS 1:1 LI-COR Odyssey solution). The protein of interest is detected by binding of a specific primary antibody to a peptide sequence of the protein. The membrane was incubated with the primary antibody (1:1000 in TBS-T + 5% albumin) over night at 4 °C. Afterwards, the membrane was washed 3x 10 minutes with TBS-T before the secondary antibody (1:10,000 in TBS-T) was added and incubated at RT for 1 hour in the dark. The secondary antibody was designed to bind the primary antibody and allow the visualization of specific proteins. The used antibodies are shown in Table 7. After incubation, the membrane was again washed 2x 10 minutes with TBST and 1x with TBS. Afterwards, the fluorescence of the secondary antibody could be detected by using the computer program LI-COR Image Studio of the LI-COR Odyssey imaging systems.

Table 7: Primary and secondary antibodies used for western blot analysis.

Primary Antibody	**Company**
p38α MAPK Antibody #9218	Cell signaling, USA
Phospho-MAPKAPK-2 (Thr334) (27B7) Rabbit mAb #3007	Cell signaling, USA
Secondary antibody	
IRDye® 680RD Goat anti-Rabbit IgG	LI-COR Biosciences GmbH, USA

Table 7 lists all antibodies used for western blot analysis.

Anode buffer

- 300 mM Tris
- 100 mM Tricin
- pH 8.8

Cathode buffer

- 300 mM Aminocapronsäure
- 30 mM Tris
- pH 8.7

TBS (10x)/ TBST

- 200 mM Tris
- 1.4 M NaCl
- Ad 1 l ddH_2O
- pH 7.5

TBST: + 0.1% Tween20

3.5 Analysis of messenger RNA

3.5.1 RNA isolation from tissue

After the removal of the relevant organs, tissues were immediately snap-frozen in liquid nitrogen. Storage at -80 °C is possible until use. To isolate the mRNA, the RNeasy Fibrous Tissue Mini Kit from Qiagen was used. Up to 30 mg of tissue was lysed in a specific amount of lysis buffer (according to the manufacturer's instructions) containing β-mercaptoethanol. Afterwards, a treatment with proteinkinase K was performed, and the samples were centrifuged at 1000xg for 3 minutes. The supernatant was mixed with 98% EtOH and transferred to an attached RNA-specific column. The genomic DNA was then digested via several washing steps (only needed for RNA sequencing analysis). The purified mRNA was eluted in 20-30 µl of Rnase-free TE (TrisEDTA), and the concentration was determined with the Nanodrop ND-1000. The purity of the samples was indicated by the 260/280 ratio, which should be higher than 1.9.

3.5.2 RNA Sequencing Transcript Expression Analysis

To identify the RNA transcript profile of cardiac tissue, RNA sequencing transcript expression analysis (RNAseq) was performed. The method is based on the analysis of the synthesis of millions of different DNA fragments in parallel by one sequencing run. The RNA was isolated as described in 3.5.1. It was particularly important to remove the genomic DNA through digestion on a column. The RNA concentration was determined by Nanodrop ND-1000, and samples were diluted, if required, to a final concentration of 100 ng/µl. Further analysis was performed by the “Biologisch-Medizinisches Forschungszentrum” (BMFZ by P. Petzsch) of the Heinrich-Heine-University. Before measuring the RNA transcript, a quality control of the mRNA samples was done by defining the RNA quality number (RQN), which indicates the integrity of the RNA. For this purpose, the ribosomal RNA subunits 18S and 28S were examined more closely. A decrease in the 18S to 28S ribosomal band ratio indicated the degradation of RNA. RQN values were given in numbers 1-10, where 10 indicates intact RNA and 1 represents severely degraded RNA [142]. RNA expression analysis requires RNA samples of high quality with an RNA value > 8. The samples that passed the quality control were then further analyzed by the BMFZ. As a first step, DNA libraries were created by DNA fragmentation and the subsequent ligation of adapters to both ends of the DNA fragments. The adapters contained sequence motifs serving as binding sites for the flow cell and additional PCR primers, which are essential for the following steps using the ‘VAHTS™ Stranded mRNA-Seq Library Prep Kit for Illumina®’. A purification of the libraries was performed via beads. As a last step, libraries were normalized and then

sequenced on the HiSeq 3000/4000 system (Illumina Inc., San Diego, USA) with a read setup of SR 1x150 bp. The bcl2fastq tool was used for adapter trimming and demultiplexing, which required a conversion of bcl files into fastq files.

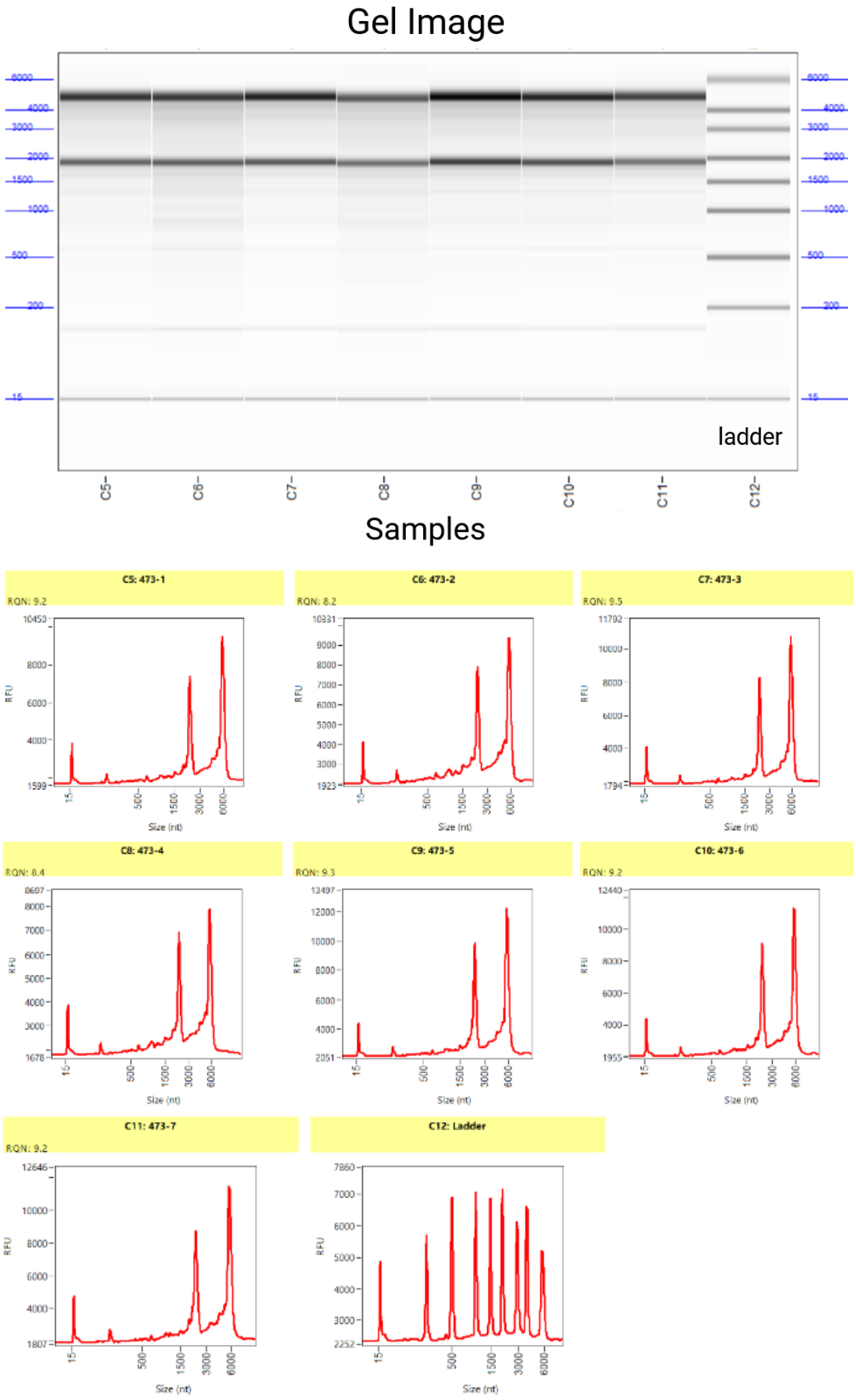

Figure 8: Quality control results of mRNA isolates from heart tissue from iCM-p38 KO and control mice. The length of 18S and 28S mRNA is displayed in nucleotides [nt]. The 18S subunit is about 2000nt in size and the 28S subunit is about 4000nt. The amount of both ribosomes is calculated based on their fluorescence [RFU].

3.5.3 Real-time Quantitative Polymerase Chain Reaction (qPCR)

The real-time quantitative polymerase chain reaction (qPCR) is a molecular biological method to quantify the mRNA amount in a specified sample. The method is based on conventional PCR. Using a fluorescent signal, the amount of DNA can be detected. During each PCR cycle, the amount of DNA will be doubled, and therefore the fluorescence will increase proportionally to the amount of DNA. The quantification of mRNA occurs at the start of the exponential phase of the PCR.

cDNA Transcription

To transcribe mRNA into complementary DNA (cDNA), the QuantiTect Reverse Transcription Kit from Qiagen was used. Therefore, 1 µg of mRNA was diluted in RNase-free water to a reaction volume of 20 µl. In the first step, genomic DNA was degraded using gDNA buffer, and then mRNA was transcribed into cDNA by reverse transcriptase in a reaction for 15 minutes at 42 °C. To inactivate this process, the reverse transcriptase was heated to 95 °C for 3 minutes. The synthesized cDNA could be used immediately or stored at -20 °C until use.

Polymerase Chain Reaction and cDNA detection via SybrGreen

The cDNA expression was detected using Maxima SYRB Green/ROX qPCR Master Mix from Thermo Scientific. The master mix consists of an optimized PCR buffer containing Maxima Hot Start Taq DNA Polymerase and desoxyribonucleosidtriphosphates (dNTPs). Specific primers and cDNA were added, as indicated in Table 8.

Table 8: Composition of the cDNA reaction medium.

SybrGreen MM (2x)	10 µl
RNase-free H_2O	7.2 µl
cDNA (25-40 ng/µl)	1 µl
Fwd. Primer	1 µM
Rev. Primer	1 µM
Total	20 µl

The cDNA was adjusted to a concentration of 25-40 ng/µl (depending on the tissue). The primers were specifically designed to ensure that only cDNA and no genomic DNA (gDNA) could be amplified. Therefore, at least one primer (forward or reverse) has to be exon spanning.

All quantitative PCR experiments were performed using the 'StepOne Plus Real-Time PCR Detection System' (Applied Biosystems). The reaction was started by the activation of the tag-polymerase. Therefore, the samples were heated for 10 min at 95 °C. This

was followed by 40 cycles at 95 °C for 15 secs and 60 °C for 60 secs. During the last period, the specificity of amplicons was verified by a melting curve analysis. This was started with 15 secs at 95 °C, then 60 sec 60 °C. The temperature was then increased every 15 sec 0.3 °C until a final temperature of 95 °C was reached.

Table 9: Primer pairs used for qPCR.

Gene name	Sequence 5'-3'	Manufacturer
Acta2	Fwd: CATCTTTCATTGGGATGGAG Rev: TTAGCATAGAGATCCTTCCTG	Sigma-Aldrich, USA
Col1a1	Fwd: CGTATCACCAAACTCAGAAG Rev: GAAGCAAAGTTTCCTCCAAG	Sigma-Aldrich, USA
Col3a1	Fwd: CTGTAACATGGAAACTGGGGAAA Rev: CCATAGCTGAACTGAAAACCACC	Sigma-Aldrich, USA
Csnk2b	Fwd: GATCTTAGACCTGGAACCTG Rev: CAACCCATAAAGCATCTCAG	Sigma-Aldrich, USA
Fbxo32	Fwd: CTGAAAGTTCTTGAAGACCAG Rev: GTGTGCATAAGGATGTGTAG	Sigma-Aldrich, USA
Gabarapl1	Fwd: CCAGTTCTACTTCTTAATCCG Rev: CTGCCTCATTTTCCATAGAC	Sigma-Aldrich, USA
Has1	Fwd: CCTGGTACAACCAAAAGTTC Rev: CTCGGAAGTAAGATTTGGAC	Sigma-Aldrich, USA
Has2	Fwd: GATTATGTACAGGTGTGTGAC Rev: CCTCTAAGACCTTCACCATC	Sigma-Aldrich, USA
Hprt1	Fwd: AGGGATTTGAATCACGTTTG Rev: TTTACTGGCAACATCAACAG	Sigma-Aldrich, USA
Nudc	Fwd: AGAACTCCAAGCTATCAGAC Rev: CTTCAGGATTTCCTGTTTCTTC	Sigma-Aldrich, USA
Postn	Fwd: CCATTAACGGAATCAAGATGG Rev: AACTTGTTTGGCAGAATCAG	Sigma-Aldrich, USA
Trim63	Fwd: ACATGGACTACTTTACTCTGG Rev: CATTGGTGTTCTTCTTTACCC	Sigma-Aldrich, USA
Comp	Fwd: AAAGATAACCCAGACCAGAG Rev: GTCATTGTCATCATCGTCATC	Sigma-Aldrich, USA
Tnsf11b	Fwd: GAAGATCACCAAGACATTGAC Rev: TCCTCCATAAACTGAGTAGC	Sigma-Aldrich, USA

Table 9 lists all qPCR-Primer used during the experiments.

Analysis of qPCR experiments

Quantification of genes of interest was performed using the X_0 method based on Sasse et al. 2003 [143], which requires an endogenous reference gene to compare different conditions. The following general equation for PCR amplification was used:

$$X_n = X_0(1 + E_{amp})^n$$

X_0 = amount of transcript in the sample at cycle 0
X_n = amount of transcript after n-cycles (defined by Ct-value)
E_{amp} = efficiency of amplification (usually 1)
n = number of cycles to reach X_n

In the case where E_{amp} equals 1, which indicates a 100% qPCR efficiency, the equation can be solved for X_0 and therefore simplified:

$$X_0 = \frac{X_n}{2^n}$$

Samples from different conditions were normalized by dividing the X_0 value of a gene of interest by the X_0 value of a reference gene. Normalized X_0 values were used in the graphical representation of the results.

3.6 Cell culture

In this work, three hybridoma cell lines (BA-F8, BF-F3, and SC-71) were used. All cell lines were cultivated according to the distributor's recommendations at 37 °C and 5% CO_2. The cells were maintained at 0.1-0.5 x 10^6 cells/ml, and the growth media were changed every 2-3 days.

3.6.1 Culture Media

The culture and freezing media differ between the cell lines. Table 10 shows the composition of the growth media, and Table 11 shows the composition of the freezing media for the different cell lines.

Table 10: Composition growth media for cell lines BA-F8, SC-71, and BF-F3.

	BA-F8, SC-71,	**BF-F3**
DMEM	89%	89%
Serum	10% FBS	10% HS
Penicillin/Streptomycin	1%	1%
L-glutamine	2 mM	2 mM

HS = Donor Equine Serum, FBS = Fetal Bovine Serum.

Table 11: Composition freezing media for cell lines BA-F8, SC-71, and BF-F3.

	BA-F8, SC-71,	BF-F3
DMEM	60%	60%
Serum	20% FBS	20% HS
DMSO	20%	20%

HS = Donor Equine Serum, FBS = Fetal Bovine Serum.

3.6.2 Hybridoma cell lines

The hybridoma cell lines are achieved by fusion of an immortalized cancer cell line (here: NSO myeloma cells) and an antibody-producing cell line (here: spleen cells from BALB/c mice). Secreted antibodies can be harvested from the supernatant; they can be used directly for immunohistochemical staining or purified for western blotting. The three cell lines were purchased from the DSMZ-German Collection of Microorganisms and Cell Cultures GmbH.

All three cell lines, BA-F8, BF-F3, and SC-71, are hybridoma cell lines, which were derived from mice that had been immunized and purified myosin from bovine atrium. The BA-F8 cells secrete a monoclonal IgG2b antibody that reacts with rat type I (slow-twitch oxidative) muscle fibers [144]. BF-F3 cells secrete a murine monoclonal antibody (IgM) reacting with rat type IIb (fast-twitch glycolytic) muscle fibers, and SC-71 cells secrete a murine monoclonal antibody (IgG1) against rat type IIa (fast-twitch oxidative) muscle fibers [145].

3.6.3 Thawing and splitting hybridoma cells

All cell lines were stored in 2 ml cryotubes in liquid nitrogen at -196 °C. After removal from the liquid nitrogen, the cells were thawed as fast as possible in a 37 °C water bath. The cells were transferred into a 50 ml tube, and 8 ml of pre-warmed growth medium was slowly added to the cells. The cells were then centrifuged for 5 min at 2000xg. The supernatant was discarded, and the pellet was suspended in 10 ml of fresh growth medium. The cells were then plated onto a 10 cm cell culture dish. Cells were cultivated at 37 °C and 5% CO_2.

All media used for splitting the cells were pre-warmed at 37 °C. Cells were split when they reached a confluence of about 80% (1 x 10^6 cells/ml). Hybridoma cells, which are suspension cells, were directly transferred into a 50 ml tube. The cells were centrifuged for 5 min at 220xg. Afterwards, the supernatant was discarded, and the cells were suspended in 1 ml of fresh growth medium. The number of living cells was then calculated using trypan blue staining and a Neubauer chamber cell counter. Therefore, the cell suspension was incubated with trypan blue (1:10) for 5 min. Dead cells will be

stained blue due to the disrupted membrane. All living cells remained unstained. 0.1-0.5 x 10^6 cells were then plated into 10 ml of fresh growth medium.

3.6.4 Freezing hybridoma cells

Before freezing, the cell number was counted using the Neubauer chamber. Afterwards, the cell number was adjusted to 1-2 x 10^6 cells/ml. Freshly prepared freezing medium (see Table 11) was slowly added to the cell suspension to a final concentration of 0.5-1 x 10^6 cells/ml (cell suspension and freezing medium 1:1). Cells were then aliquoted into 1 ml cryotubes. These were placed in a thick-walled Styrofoam container and stored at -80 °C for at least 48 hours. This enables a slow freezing of the cells to a maximum of -1 °C/min and ensures that the cells remain intact. Thereafter, the cryotubes were transferred into liquid nitrogen for long-term storage.

3.6.5 Antibody production and harvesting from Hybridoma cell lines

To increase antibody production, hybridoma cells were starved (no change of growth medium) for 2-3 days. This stress situation due to nutrient depletion causes the hybridoma cells to produce more antibodies, which can be identified by the growth medium turning from a pinkish to a yellow color. Afterwards, the antibodies can be harvested. Therefore, the cell suspension was transferred into a 15 ml tube and centrifuged for 10 min at full speed. The supernatant was transferred into a new tube and centrifuged again for 10 min at full speed. The supernatant, containing the antibodies, was then aliquoted into 1.5 ml tubes. The antibodies were stored at -80 °C until use. Previous studies from Leitner et al. [101] proved that all antibodies can be used as a cocktail; thus, a separate use of them is not necessary. These experiments also revealed that the antibodies are working best in a concentration range between 1:10 and 1:50 dilutions. The IgM antibody (BF-F3, anti-MyHC type IIb) should be used at a higher concentration (1:10) than the others.

3.7 Histological analysis

The skeletal muscles *Musculus gastrocnemius*, *Musculus plantaris,* and *Musculus soleus* were isolated from the murine hind limb. Immediately after isolation, the muscles were specifically oriented (*Musculus soleus* on the upside, and the tendon pointed to the pre-marked side of the mold) and immersed in an O.C.T. compound-filled mold. The molds were put in cold isopentane (-90 °C – -100 °C) until the block was completely frozen. To prevent the block from breaking, it should be ensured that the block is not entirely immersed in isopentane. For freezing skeletal muscles, the very low temperature,

compared to other organs, is of paramount importance; freezing at higher temperatures could lead to freezing artifacts in the tissue. Since muscle tissue is prone to damage, it is necessary that the tissue does not thaw at any point. The irreparable damage after even partially thawing makes immunohistological analysis impossible. Therefore, after freezing, the tissue has to be kept on dry ice, especially when tissue is harvested from more than one animal. For long-term storage, the tissue can be kept at -80 °C.

3.7.1 Cryosectioning

Before cutting the tissue, the block has to be relocated from -80 °C to -22 °C for at least 1 hour (or overnight). Also, the cryostat has to be pre-cooled at -22 °C. 8 µm thick sections were prepared, and two sections were put on one object slide. They were dried for 5 minutes using a hairdryer (not heated). Slides were stored in microscope slide boxes containing dry beads to avoid humidity. To keep the slides as long as possible dry, the boxes were additionally sealed with adhesive tape. Boxes were stored at -20 °C or -80 °C, respectively. Before opening the boxes, they have to slowly acclimate to room temperature. Therefore, the boxes will be stored at 4 °C over night and then at room temperature for 30 minutes. If necessary, the dry beads should be changed (color change from blue to pink). Thereby, it also has to be considered that multiple freezing and thawing cycles might impair enzyme-based staining's.

3.7.2 Immunofluorescence

Immunofluorescence staining was performed as described by Emde et al. [146]. Prepared tissue sections were fixed for 10 minutes with 4% paraformaldehyde (PFA) in 0.1 M phosphate buffered saline (PBS; pH 7.4). For permeabilization of the sections, they were incubated for 1 hour in 1% Triton-X in PBS. Afterwards, sections were blocked for 1 hour at room temperature using 10% NGS (normal goat serum) in PBS + 1% Triton-X. After blocking, the samples were washed again for 10 minutes in PBS/Tween20 (0.2%) and 10 minutes in PBS. In order to prevent background staining of endogenous immunoglobulins using indirect detection methods, it is possible to pre-incubate the sample tissue with Fab fragments of unconjugated anti-mouse antibodies. The sections were incubated with a goat Fab-Fragment for 3 hours at room temperature. Before adding the primary antibody, the samples were washed again two times for 10 minutes in PBS/Tween20 (0.2%). The primary antibody was diluted in PBS/Tween20 + 2% NGS, and the samples were incubated over night at 4 °C. Samples were washed again two times in PBS/Tween20 (0.2%) before the secondary antibody was added. The secondary antibody was as well diluted in PBS/Tween20 + 2% NGS. The samples were incubated for 3 h at room temperature. Thereby, it has to be ensured that the samples were stored

in the dark to avoid a decrease of immunofluorescence of the secondary antibodies. The samples were washed in a final washing step two times for 15 minutes in PBS; these washing steps also had to take place in the dark. Afterwards, the sections could be stocked with fluoromount. The samples were microscoped using the fluorescence microscope Keyence BZ 9000 (Keyence).

3.7.3 Wheat Germ Agglutinin staining

Wheat germ agglutinin (WGA) belongs to the group of lectins, which are proteins that bind to carbohydrates. WGA is derived from wheat and binds to the carbohydrates N-acetylglucosamin and sialic acid [147, 148] which are present on the cells surfaces. Therefore, WGA histologically labeled with fluorescent dyes or horseradish peroxidase is a qualified marker to visualize cell surfaces [149-151]. It was further reported that WGA binds to the extracellular matrix and connective tissue [152-154]. Since fibrotic tissue is defined as an excessive accumulation of extracellular matrix [155], WGA serves as a suitable marker for the development of fibrosis in damaged cardiac tissue [146].

Immunofluorescence staining was performed as described by Emde et al. [146]. Prepared tissue sections were stored over night at 4 °C; one hour before the start of the staining, they were kept at room temperature. Sections were fixed for 10 minutes with 4% paraformaldehyde (PFA) in 0.1 M phosphate buffered saline (PBS; pH 7.4), followed by three washing steps on a shaker for 10 minutes in PBS. The WGA-Alexa488 antibody was added to the samples in a dilution of 1:300 in PBS. Sections must be kept in the dark for 1 hour. Afterwards, samples were washed again 3x for 15 minutes with PBS and kept dark as well. To cover the sections, Fluoromount G with DAPI (Southen Biotech, 0100-20) was used. Samples were dried at 4 °C.

Specimens were microscopically examined at a magnification of 4x and 20x and an exposure time of 2.5 seconds. The quantification of fibrotic tissue was analyzed by measuring the signal area using ImageJ software. Briefly, ImageJ was opened using the ImageJ program. Select: Image → Type → RGB stack. Adjust the area of interest. Set the threshold by selecting Image → Adjust → Threshold (20-220). The signal was quantified by selecting Analyze → Set measurement (turn on “Limit to threshold” and “Area”), then select Analyze → Measure. The results are displayed in a separate window as an area (pixel^2). This means that the signal occupies an area within the set threshold value.

Table 12: Table lists all primary and secondary antibodies used for immunohistochemistry.

Primary Antibodies	**Company Art. No. #**
WGA Alexa Fluor 488	Invitrogen, USA #W11261
Murine monoclonal IgG2b antibody - reacts with rat type I (slow-twitch oxidative) fibers	produced using the hybridoma cell line BA-F8 purchased from Leibniz Institute DSMZ-German Collection of Microorganisms and Cell Cultures GmbH
Murine monoclonal antibody (IgM) – reacts with rat type IIb (fast-twitch glycolytic) fibers	produced using the hybridoma cell line BF-F3 purchased from Leibniz Institute DSMZ-German Collection of Microorganisms and Cell Cultures GmbH
Murine monoclonal antibody (IgG1) - reacts with rat type IIa (fast-twitch oxidative) fibers	produced using the hybridoma cell line SC-71 purchased from Leibniz Institute DSMZ-German Collection of Microorganisms and Cell Cultures GmbH
Secondary antibodies	
Rhodamine Red™-X (RRX) AffiniPure Goat Anti-Mouse IgG, Fcγ subclass 2b specific	Jackson ImmunoResearch Laboratories, Inc. #115-295-207
AMCA AffiniPure Goat Anti-Mouse IgM, μ chain specific	Jackson ImmunoResearch Laboratories, Inc. #115-155-075
Fluorescein (FITC) AffiniPure Goat Anti-Mouse IgG, Fcγ subclass 1 specific	Jackson ImmunoResearch Laboratories, Inc. #115-095-205

Table 12 lists all antibodies used for histological stainings.

3.8 Flow cytometric analysis

Flow cytometry is a powerful tool for the detailed analysis of complex cell populations within a sample. It provides rapid multi-parametric analysis of single cells, which allows a comprehensive description of the individual samples. Cells can simultaneously be differentiated due to their different physical and chemical properties as they are in suspension and flow through the measuring device. Depending on the light scattering features of the cells, they can be clustered due to their size and granularity. Using fluorescence-labeled monoclonal antibodies, additional features on the cell surface or even inside the cell can be recognized, which enables an even more precise specification of the individual cell types. By exciting the fluorescent dyes with different wavelengths, a large number of different cell types within one single sample can be precisely identified and analyzed.

3.8.1 Preparation of heart tissue

Heart tissue was prepared using an adapted protocol from Heinen et al. and Pinto et al. [156, 157]. Mice were sacrificed by an isoflurane overdose. Hearts were isolated and hung on a needle. Then they were flushed with 5 ml of PBS/heparin to remove the

remaining blood. Afterwards, hearts were flushed with 5 ml of collagenase (450 U/ml) to start the digestion process. Atria and valves were removed, and the heart was weighted. Hearts were then cut into ~ 1 mm pieces using a tissue chopper. Tissue pieces were placed in 5 ml of collagenase and incubated at 37 °C for 45 minutes. Every 15 minutes, the mixture was pipetted through a 10 ml serological pipette to support the digestion mechanically. By the end of the incubation period, final trituration was performed by pipetting 30 times with a 1 ml pipette. Digested heart tissue was then poured through a 100 µm filter to remove larger tissue pieces. Cells were centrifuged for 1 minute at 500 rpm (60xg) in order to pellet the cardiomyocytes, which were discarded. The supernatant was filtered through a 40 µm filter. Cells were again centrifuged for 10 minutes at 1400 rpm (450xg). This time, the supernatant was discarded, and the pellet, containing cardiac immune cells, was dissolved in 2 ml PEB (see Table 13). 100 µl of each sample was transferred to a FACS tube, and the cells were incubated for 30 minutes with Fc-block to avoid unspecific binding and, when applicable, Fixable viability dye eFluor 780 was added. After a washing step (add 2 ml PEB and centrifuge for 7 minutes at 1400 rpm (450xg), remove the supernatant, and resolve the pellet in 100 µl PEB), cells were stained with antibodies listed in Table 14. Intracellular staining required a fixation of the cells and permeabilization of the cell membrane to allow the antibodies to bind to the antigens. Therefore, the Fix & PERM™ Cell Permeabilization Kit (Invitrogen™) was used. Briefly, 100 µl of Fixation Medium was added to each sample after the end of the Fc-block incubation time, and cells were incubated for another 15 minutes at RT. Samples were washed once (add 2 ml PEB and centrifuged for 7 minutes at 1400 rpm (450xg)). The supernatant was discarded, and the cell pellet was dissolved in 100 µl permeabilization medium and incubated for 20 minutes at RT. A final washing step was accomplished as described above, and cells were dissolved in 100 µl PEB. Finally, cells were measured using BD FACSCanto II. Data were analyzed using the associated software, BD FACSDiva version 8.0.2.

Table 13: Composition of PEB

Compounds
0.2 g KCl (potassium chloride)
0.2 g KH_2PO_4 (potassium dihydrogen phosphate)
8 g NaCl (sodium chloride)
1.17 g Na_2HPO_4 (disodium hydrogen phosphate)
1 l ddH_2O
4 ml EDTA (500 mM)
5 g BSA
pH 7.5

Table 14: Antibodies used for FACS analysis of heart tissue.

Antibody	Clone	Dilution	Format	Manufacturer
αSMA	1A4	1:100	AF488 (Alexa Fluor 488)	eBioscience, Inc, USA
CCR2	SA203G11	1:50	BV421 (Brilliant Violet 421)	BioLegend, USA
CD11b	M1/70	1:100	AF488 (Alexa Fluor 488)	BioLegend, USA
CD19	1D3	1:100	PE (Phycoerythrin)	BD Bioscience, USA
CD206	C068C2	1:100	BV421 (Brilliant Violet 421)	BioLegend, USA
CD3	145-2C11	1:100	APC (Allophycocyanin)	BioLegend, USA
CD31	390	1:100	PerCP (Peridinin-chlorophyll-Protein Complex)	BioLegend, USA
CD4	RM4-5	1:100	Pacific Blue	BD Bioscience, USA
CD45	30-F11	1:100	BV510 (Brilliant Violet 510)	BD Bioscience, USA
CD64	X54-5/7.1	1:100	PE (Phycoerythrin)	BioLegend, USA
CD8	53-6.7	1:100	APC/Fire	BD Bioscience, USA
Ly6C	AL-21	1:100	APC (Allophycocyanin)	BD Bioscience, USA
Ly6G (127654)	1A8	1:100	PerCP/Cy5.5 (Cyanine5.5)	BioLegend, USA
Anti-Feeder cells	mEF-SK4	1:100	APC (Allophycocyanin)	Miltenyi Biotec, Germany
MHCII	M5/114.15.2	1:100	BV510 (Brilliant Violet 510)	BioLegend, USA
7-AAD (420404)		1:100	7-Aminoactinomycin D	BioLegend, USA
Fixable viability Dye (65086514)		1:100	eFluor 780	BD Bioscience, USA
Fc-block (CD16/32) (B264872)		1:20		BioLegend, USA

Table 14 lists all antibodies and fluorophores applied during FACS experiments of heart tissue.

FACS Panel for heart tissue

Five panels with different antibodies were used in order to differentiate individual cell populations within one sample. One panel was created to identify myofibroblasts. One panel was used to identify lymphocyte distribution, and the other panels should characterize different macrophage/monocyte populations and neutrophils. The following antibody panels were used to differentiate the existing cell populations:

<u>Lymphocytes</u>

- CD45 - BV510
- CD3 - APC
- CD19 – PE
- CD4 – Pacific Blue
- CD8 – APC/Fire
- L/D – 7AAD

<u>Classical/ non-classical monocytes</u>

- CD11b – AF488
- Ly6G – PerCP/Cy5.5
- CD64 – PE
- Ly6C – APC
- MCHII – BV510
- L/D - Fixable Viability Stain (FVS)

Resident/ infiltrating macrophages
- CD11b – AF488
- Ly6G – PerCP/Cy5.5
- CD64 – PE
- CCR2 – BV421
- L/D - Fixable Viability Stain (FVS)

Pro-/anti-inflammatory macrophages
- CD11b – AF488
- Ly6G – PerCP/Cy5.5
- CD64 – PE
- CD206 – BV421
- L/D - Fixable Viability Stain (FVS

Myofibroblasts
- CD45 - BV510
- CD31 - PerCP
- MEFSK (anti-feeder) – APC
- αSMA – AF488 (intracellular)
- L/D - Fixable Viability Stain (FVS)

3.8.2 FACS gating strategy and definition of cell populations

In order to differentiate the numerous cells measured in a single sample, the cells are classified according to size, granularity, and the presence or absence of specific markers. These markers are often, but not exclusively, CD (clusters of differentiation) surface molecules. This process is referred to as gating.

All hematopoietic cells (except erythrocytes) are defined by the expression of CD45 [158]. Additional expression of CD19 indicates B-lymphocytes [159], whereas CD3 expression can be found in T-lymphocytes [160]. The separation of T-lymphocytes in T-helper cells and cytotoxic T-lymphocytes occurs through the markers CD4 and CD8a. $CD4^+$ T-lymphocytes are T-helper cells, and $CD8a^+$ T-lymphocytes are cytotoxic cells [161].

$CD11b^+$ cells can be defined as monocyte/macrophages, granulocytes, and natural killer cells [162-164]. For further subdivision of these cell populations, additional markers are needed. The cells that are only positive for CD11b are considered monocytes. A differentiation of monocytes into pro- and anti-inflammatory monocytes is enabled by additional Ly6C expression [31, 32]. Neutrophils are $CD11b^+$ cells, which are also positive for Ly6G [165]. To distinguish macrophages from the $CD11b^+$ population, the cell surface marker CD64 can be used. Cells that are positive for both CD11b and CD64 are therefore defined as macrophages [166]. The macrophage population can be further subdivided using the makers CD206, CCR2, and MHCII (see 1.2 for a detailed description). Cells that are negative for all markers mentioned, except MHCII are antigen-presenting cells, here defined as dendritic cells [167]. Non-immune cells with the absence of CD45 and CD31 (markers for endothelial cells) but positive for MEFSK are considered to be fibroblasts. Activated fibroblasts, so-called myofibroblasts, are additionally positive for αSMA [168]. Table 15 summarizes all immune cell populations that were investigated and how they were defined.

Table 15: Definition of cell populations analyzed in cardiac tissue and blood via FACS.

Cell type	Antibodies used for detection
Leukocytes	$CD45^+$
B-Lymphocytes	$CD45^+/CD19^+$
T-Lymphocytes	$CD45^+/CD3^+$
$CD4^+$ T-Lymphocytes	$CD45^+/CD3^+/CD4^+$
$CD8a^+$ T-Lymphocytes	$CD45^+/CD3^+/CD8a^+$
Monocytes	$CD11b^+/CD64^-/Ly6G^-/MHCII^-$
$Ly6C^{high}$ Monocytes	$CD11b^+/CD64^-/Ly6G^-/MHCII^-/Ly6C^+$
$Ly6C^{low}$ Monocytes	$CD11b^+/CD64^-/Ly6G^-/MHCII^-/Ly6C^-$
Neutrophils	$CD11b^+/Ly6G^+$
Dendritic cells	$CD11b^-/CD64^-/Ly6G^-/MHCII^+$
Macrophages	$CD11b^+/CD64^+$
CCR^+ Macrophages	$CD11b^+/CD64^+/CCR^+$
CCR^- Macrophages	$CD11b^+/CD64^+/CCR^-$
M1 Macrophages	$CD11b^+/CD64^+/CD206^-$
M2 Macrophages	$CD11b^+/CD64^+/CD206^+$
$Ly6C^{high}$ Macrophages	$CD11b^+/CD64^+/Ly6C^+$
$Ly6C^{low}$ Macrophages	$CD11b^+/CD64^+/Ly6C^-$
$MHCII^{high}$ Macrophages	$CD11b^+/CD64^+/MHCII^+$
$MHCII^{low}$ Macrophages	$CD11b^+/CD64^+/MHCII^-$
$MEFSK^+$ cells (Fibroblasts)	$CD31^-/CD45^-/MEFSK^+$
αSMA^+ Fibroblasts	$CD31^-/CD45^-/MEFSK^+/\alpha SMA^+$

Table 15 lists all cell populations analyzed during FACS experiments of cardiac tissue.

3.9 Statistics

All data are presented as mean ± standard deviation (SD). Statistical analysis was performed using GraphPad Prism 10. Repeated measurements were analyzed by Two-way ANOVA, followed by Bonferroni post-test. Two groups were compared with Student's t-test when a normal distribution was present. Otherwise, the Mann-Whitney U test was performed. Normal distribution was analyzed by the Shapiro-Wilk test. For comparison of more than two groups, One-way ANOVA followed by Tukey post-test was used. Differences of $p < 0.05$ were considered statistically significant (* $p < 0.05$*, ** $p < 0.01$, *** $p < 0.001$).

4. Results

4.1 Cardiac-specific deletion of the *p38 MAPKα* gene caused impaired heart function just within two days after the induction of pressure overload

After the induction of the cardiomyocyte-specific deletion of the *p38 MAPKα* gene via tamoxifen injection for 10 consecutive days, the effectiveness of the deletion was analyzed on protein level using western blot analysis. The p38 MAPKα protein amount in iCM-p38 KO hearts was reduced by 70% compared to controls (Figure 9a). Additionally, phospho-MK2 protein levels were analyzed since this protein is a known downstream target of p38 MAPKα. After AngII treatment of the mice, p38 MAPKα gets activated through phosphorylation, which in turn acts as a kinase and phosphorylates MK2. Under baseline conditions, the phosphorylation level of MK2 is low. In control animals, a significant increase in phosphorylated MK2 protein was observed (233%) as a result of the AngII treatment, while in iCM-p38 KO hearts, an increase of MK2 phosphorylation was minor (43%) (Figure 9b).

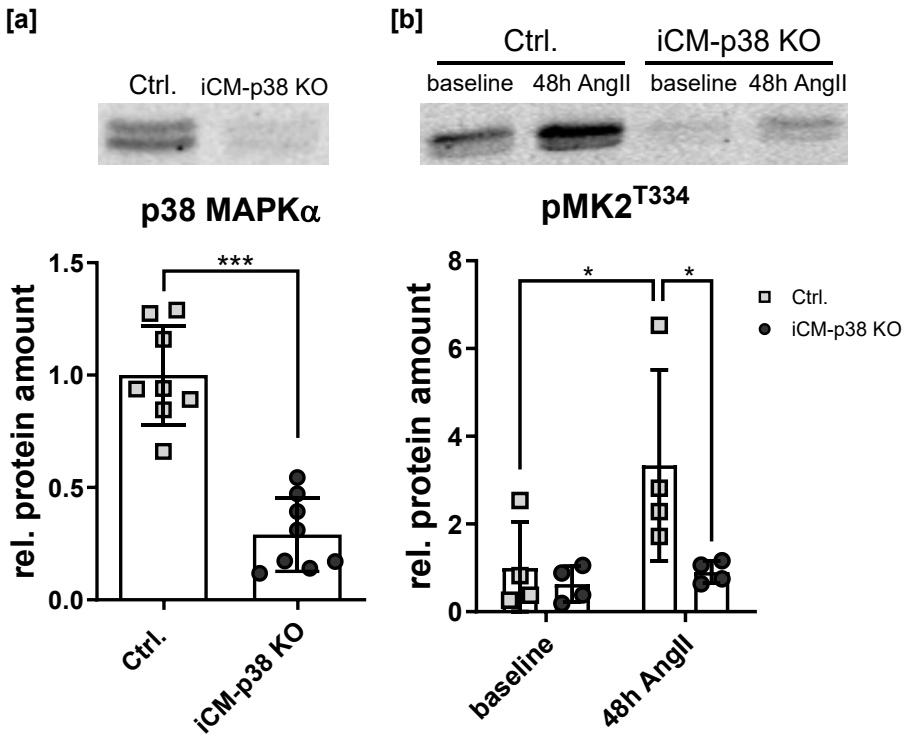

Figure 9: Verification of the cardiomyocyte-specific p38 MAPKα KO on protein level. [a] Western blot analysis of heart tissue showed significantly reduced amounts of p38 MAPKα protein in iCM-p38 KO hearts compared to controls. **[b**] Downstream targets of p38 MAPKα were affected as well, since phosphorylation of MK2 was absent in iCM-p38 KO mice after AngII treatment. The relative protein amount was normalized to the total protein amount. Data are presented as mean ± SD, n = 4-8. Statistical significance was calculated using unpaired two-tailed students t-test (** p <0.01) or Two-way ANOVA with Bonferroni's multiple comparisons test (* p <0.05).

Moreover, the cardiac function of iCM-p38 KO and control mice was analyzed after induction of the KO via tamoxifen injection. The deletion of the *p38 MAPKα* gene specifically in cardiomyocytes did not have any effect on heart function under baseline conditions. A pronounced LV failure, characterized by a significant increase in end-diastolic (EDV) and end-systolic volume (ESV), develops just 2 days after the induction of pressure overload (PO) through AngII. The ejection fraction (EF) decreased in iCM-p38 KO mice by 60%, from 64.1% to 25.8%, while in control animals the reduction of EF was only 22.9% and not statistically significant (Figure 10a). The EDV increased by 33% (from 85.4 µl to 114.1 µl after 48h AngII) in iCM-p38 KO mice, and no elevation in EDV was measured in control animals (Figure 10b). The increase in ESV was even more pronounced. In control mice, a small increase from 24.3 µl to 39.9 µl due to the AngII treatment could be observed. In iCM-p38 KO mice, an increase of 188% (30.2 µl to 87.0 µl) after 48h of AngII was measured (Figure 10c). Since the left ventricle is severely affected, HFrEF is present in this model, as described in 1.1. Remarkably, the heart did not undergo a hypertrophic state as it would be expected during the development of heart failure. The rapid development of cardiac dysfunction in response to pressure overload

suggests a protective role of p38 MAPKα in cardiomyocytes. Thus, the data obtained here are in line with earlier findings by Bottermann et al. [41].

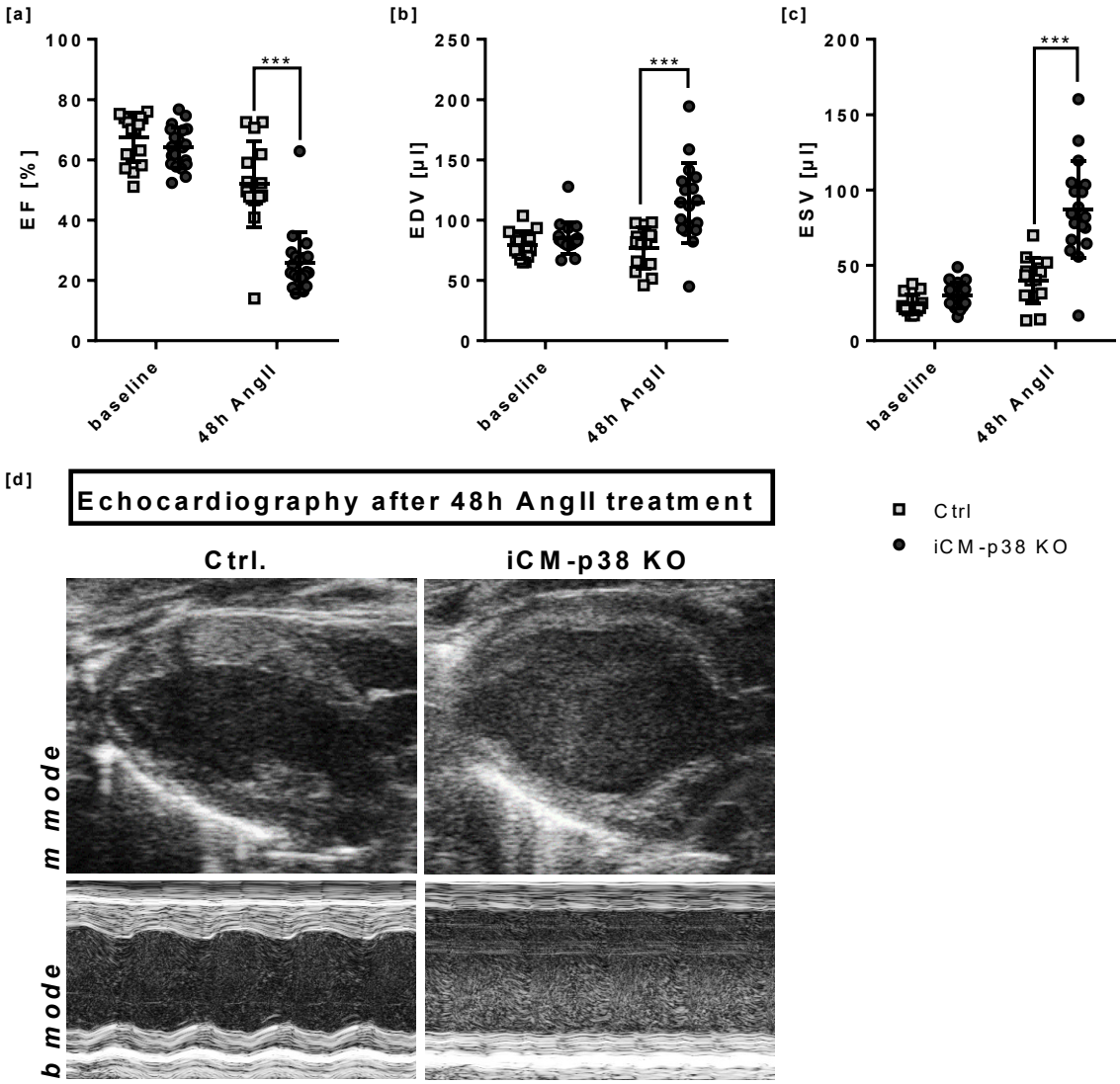

Figure 10: Characterization of pressure overload-induced cardiac dysfunction in the iCM-p38 KO mouse model. Cardiac dysfunction of iCM-p38 KO mice (dark) after 48h of AngII treatment was defined by **[a]** a decrease in ejection fraction (EF) caused by **[b]** an increased end-diastolic volume (EDV) and **[c]** an increased end-systolic volume (ESV) compared to controls (bright). Data are presented as mean ± SD, n = 16-20. Statistical significance was calculated by using Two-way ANOVA (repeated measures) with Bonferroni's multiple comparisons test (*** p <0.001). **[d]** Representative high-resolution ultrasound images of control (left panels) and iCM-p38 KO (right panels) hearts after 48h of AngII administration exhibit left ventricular dilation in iCM-p38 KO hearts.

Up to this point, analyses of cardiac tissue were mainly made after 48h of AngII treatment. However, cardiac dysfunction was already established at this time. To identify molecular mechanisms that occur even before the development of heart failure, cardiac tissue was analyzed on an expressional level after 12h of AngII treatment. Using a significance level of $p < 0.05$ and an absolute fold change of > 1.3, 239 differentially expressed transcripts were identified by RNA sequencing analysis. Hierarchical clustering allowed a clear separation of the control and iCM-p38 KO transcriptomes (Figure 11). Using Ingenuity

Pathway Analysis (IPA), two altered pathways with an activation Z-score < 2|-2 were identified via pathway analysis. These pathways are “Oxidative Phosphorylation” and “Superpathway of Inositol Phosphate Compounds”/“3-phospho-inositide Biosynthesis”. Those pathways also belong to the most prominent pathways altered after 48h of AngII treatment, as described in Bottermann et al. 2022 [41]. Altered genes of the “Oxidative Phosphorylation” pathway are downregulated (Z-score < -2) in iCM-p38 KO hearts compared to controls, while altered genes of the other two pathways are upregulated (Z-score < 2) in iCM-p38 KO hearts compared to controls (Table 16). These results demonstrate that alterations in gene expression, especially of genes that are involved in cardiac metabolism, occurred already at a very early stage. This suggests that metabolic depression is one of the main factors contributing to the decrease in cardiac function of iCM-p38 KO mice.

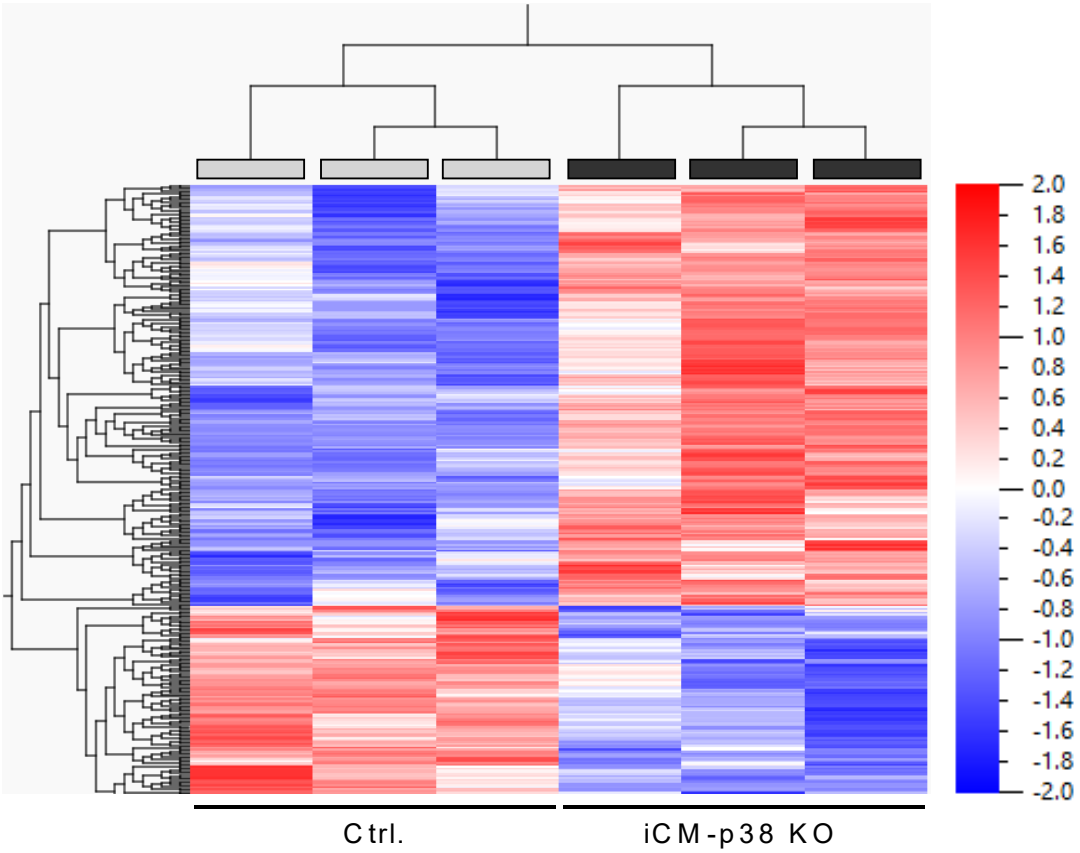

Figure 11: RNA sequencing analysis of iCM-p38 KO and control hearts after 12h of AngII treatment. Hierarchical clustering of differentially expressed genes ($p < 0.05$, fold change > 1.3). Red indicates an upregulation of genes while blue indicates a downregulation of genes.

Table 16: Results of pathway analysis using Ingenuity Pathway Analysis software (IPA®, Qiagen Inc.). Only pathways with an absolute Z-Score > 2 and –logP-value < 1.3 (0.05) were considered to be affected. The analysis revealed that only a small number of genes were differentially expressed. The genes were grouped under the respective terms.

Pathway	-log P-value	Z-Score	Down-regulated	No change	Up-regulated	No overlap with dataset	Molecules
Oxidative Phosphory-lation	8.4	-3.32	11/110 (10%)	0/110 (0%)	0/110 (0%)	99/110 (90%)	ATP5F1D, COX6A1, COX8A, NDUFA11, NDUFA2, NDUFA5, NDUFB10, NDUFB7. NDUFS8, NDUFV3, UQCRQ
Superpath-way of Inositol Phosphate Compounds	1.75	2.45	0/232 (0%)	0/232 (0%)	6/232 (3%)	226/232 (97%)	IP6K3, MTMR9, PAWR, PIK3R1, PPIP5K1, PTPN11
3-phospho-inositide Biosynthesis	1.46	2.24	0/202 (0%)	0/202 (0%)	5/202 (2%)	197/202 (98%)	MTMR9, PAWR, PIK3R1, PPIP5K1, PTPN11

4.2 Inhibition of sympathetic activity slightly improves cardiac function and has no effect on immune cell infiltration in iCM-p38 KO hearts

An overstimulation of sympathetic activity is associated with deterioration of cardiac function in heart failure. Therefore, treatment with β-blockers is widely used to overcome this overstimulation in heart failure patients. Indications of overstimulation in the iCM-p38 KO mouse model already exist since Bottermann et al. [41] demonstrated the presence of elevated plasma glycerol levels and the accumulation of lipids in cardiac tissue. Both are clear signs of increased sympathetic activity, as this promotes the release of catecholamines by the adrenal medulla and the postganglionic fibers of the sympathetic nervous system, which in turn induces lipolysis in adipocytes, causing elevated plasma glycerol levels. To investigate if increased sympathetic activity is crucial for the severe phenotype of iCM-p38 KO mice, animals were treated with propranolol (PR) prior to and during the AngII administration. PR belongs to the group of non-selective β-adrenoceptor

antagonists, which inhibit β_1- and β_2-receptors and are used to treat various cardiovascular conditions like high blood pressure, irregular heart rate, and heart failure.

In first experiments, it was evaluated if the application of propranolol (10 mg/kg/day) was effective to block β-adrenergic stimulation. Therefore, wild-type mice were treated with PR or vehicle (PBS) as described in 3.2.2. Afterwards, heart rate and blood pressure were measured in a terminal experiment (3.2.3). During the measurement, dobutamine was administered to the animals. In vehicle-treated animals, dobutamine administration increases heart rate by 20% (from 465.2 ± 50.7 BPM to 564.9 ± 28.8 BPM), while no change in heart rate could be observed in PR-treated animals (422.9 ± 23.2 BPM and 425.3 ± 19.5 BPM) (Figure 12a). The mean arterial pressure was not affected by PR treatment or dobutamine administration. In all groups, the mean pressure was between 64 and 70 mmHg (Figure 12b).

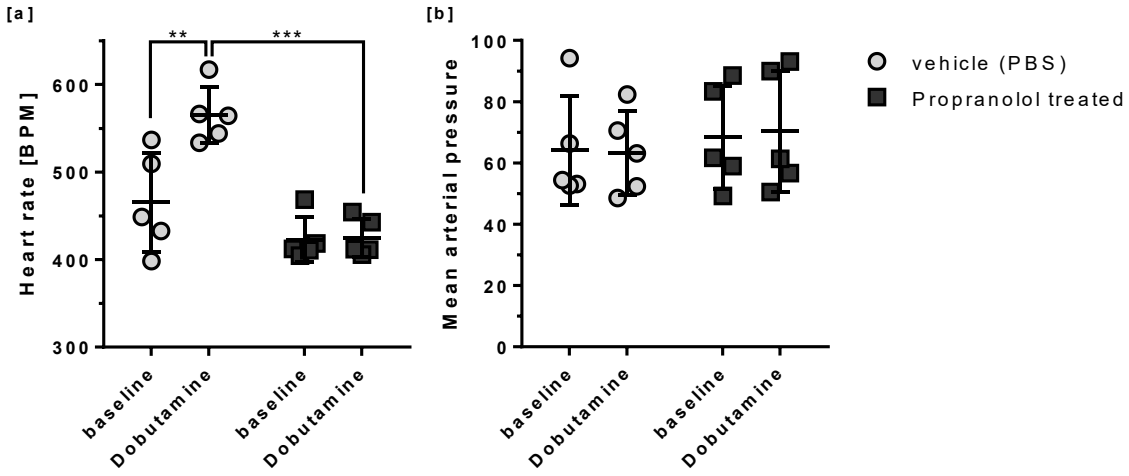

Figure 12: Heart rate [a] and mean arterial pressure [b] in wild-type mice treated with propranolol or vehicle (PBS). Measurements were performed before and after s.c. administration of dobutamine (1 µg/g body weight). Propranolol treatment prevented dobutamine-induced increases in heart rate but had no effect on blood pressure. Data are presented as mean ±SD, n = 5. Statistical significance was calculated by using Two-way ANOVA (repeated measures) with Bonferroni's multiple comparisons test (** p <0.01; *** p <0.001).

Since in PR-treated animals no increase in heart rate due to dobutamine administration was observed, the experiment proved that the chosen treatment effectively blocked β_1- and β_2-adrenoceptors.

In the next set of experiments, it was investigated if β-adrenergic stimulation contributed to the heart failure development in iCM-p38 KO mice. To address this, PR was administered together with AngII, as described in 3.2.2. Briefly, mice received PR (10 mg/kg/day) for 24h before the start of the AngII treatment via drinking water. Afterwards, osmotic mini pumps filled with either AngII alone or AngII + PR were implanted, and the PR treatment via drinking water ended (Figure 13). Additional control groups received no PR but only AngII.

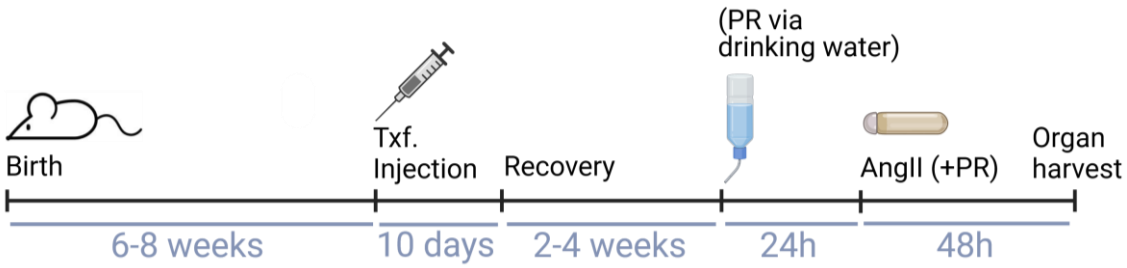

Figure 13: Experimental procedure for combinational AngII and propranolol (PR) treatment in iCM-p38 KO and control mice. The iCM-p38 KO was induced by a tamoxifen (Txf.) injection for 10 consecutive days when mice were 6-8 weeks old. After a recovery time of 2-4 weeks, mice received propranolol (PR) via drinking water. 24h later, osmotic mini pumps filled with AngII and PR were implanted, and the PR treatment via drinking water was stopped. Organs were harvested 48h after pump implantation. The treatment was performed as described on iCMp38 KO and control mice. Additional controls were accomplished, in which iCMp38 KO and control mice did not receive PR but only AngII. Created with BioRender.com.

The activation of β-adrenergic receptors in adipose tissue leads to increased lipolysis. This process can be detected by measuring fatty acids in the blood [169]. Non-esterified fatty acids (NEFA) were analyzed in blood samples of AngII and AngII/PR-treated mice. Measurements of blood serum samples indicated an increase in NEFA levels by around 30% in AngII-treated iCM-p38 KO mice compared to AngII-treated controls. Additional PR administration reduced NEFA levels in both groups. The reduction was about 15% in control animals and even 45% in iCM-p38 KO mice (Figure 14). These results suggest as well an elevated sympathetic activation in iCM-p38 KO mice and show an effective inhibition of this activity by additional PR treatment.

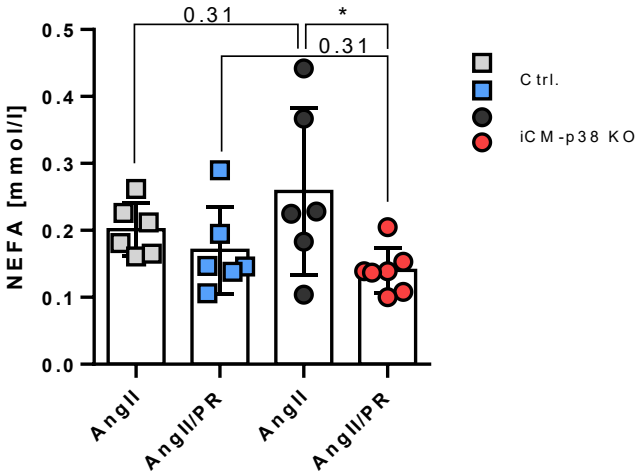

Figure 14: Non-esterified fatty acid (NEFA) levels in blood serum of iCM-p38 control (square) and KO (round) mice after 48h of AngII or AngII/PR treatment. Elevated NEFA levels were observed in AngII-treated iCM-p38 KO mice compared to controls. Additional PR administration in turn reduced NEFA level in both groups. Data are presented as mean ±SD, n = 6-7. Statistical significance was calculated by using One-way ANOVA with Tukey's multiple comparisons test (* $p < 0.05$). In collaboration with Heba Zabri, Institute for Pharmacology, University Hospital Düsseldorf.

Echocardiographic analysis of heart function after 48h confirmed that AngII compromised cardiac function in iCM-p38 KO mice. The ejection fraction (EF) was

strongly reduced in iCM-p38 KO mice compared to controls (45% reduction) (Figure 15a). A significant increase in EDV (42%) and ESV (97%) in iCM-p38 KO mice treated with AngII compared to AngII-treated controls was measured (Figure 15b+c). Accordingly, SV and CO were decreased in iCM-p38 KO mice. The SV was reduced by 20% in AngII-treated iCM-p38 KO mice, and the CO even by 26% compared to AngII-treated control mice (Figure 15d+e). When looking at LV wall thickness during systole, it was observed that AngII treatment caused a reduction of 28.7% in iCM-p38 KO hearts compared to AngII-treated control hearts (Figure 15h). However, the LV wall thickness during diastole did not differ between iCM-p38 KO and control mice. The same applies to FS (Figure 15g+i).

When treating control mice not only with AngII but additionally with PR, no changes were observed regarding cardiac function. All measured parameters were the same in control mice treated with AngII and AngII/PR. The only exception was the heart rate, which was significantly reduced by 14% in control mice treated with AngII/PR compared to only AngII-treated controls (Figure 15f).

Interestingly, additional PR treatment did affect the cardiac function of iCM-p38 KO mice. EF was slightly improved (increase of 27%) in AngII/PR-treated iCM-p38 KO mice compared to AngII-treated iCM-p38 KO mice (Figure 15a). However, this increase in EF did not reach statistical significance. Because EDV did not differ between AngII and AngII/PR-treated iCM-p38 KO mice, a slight reduction of ESV was responsible for the measured increase in EF. AngII/PR treatment caused an ESV reduction of 11% in iCM-p38 KO mice compared to only AngII-treated iCM-p38 KO mice (Figure 15c). SV and CO were increased in iCM-p38 KO mice when treated with AngII/PR compared to only AngII treatment. The elevation of SV reached statistical significance with an increase of 18% due to additional PR administration (Figure 15d). The increase in CO was 12% in iCM-p38 KO mice treated with AngII/PR compared to AngII-treated iCM-p38 KO mice (Figure 15e). However, AngII/PR treatment reduced heart rate in iCM-p38 KO mice compared to only AngII treatment, as observed for control mice as well (Figure 15f). LV wall thickness during diastole and systole, as well as FS, were not altered in iCM-p38 KO hearts when treated with AngII/PR compared to only AngII-treated hearts (Figure 15g-i).

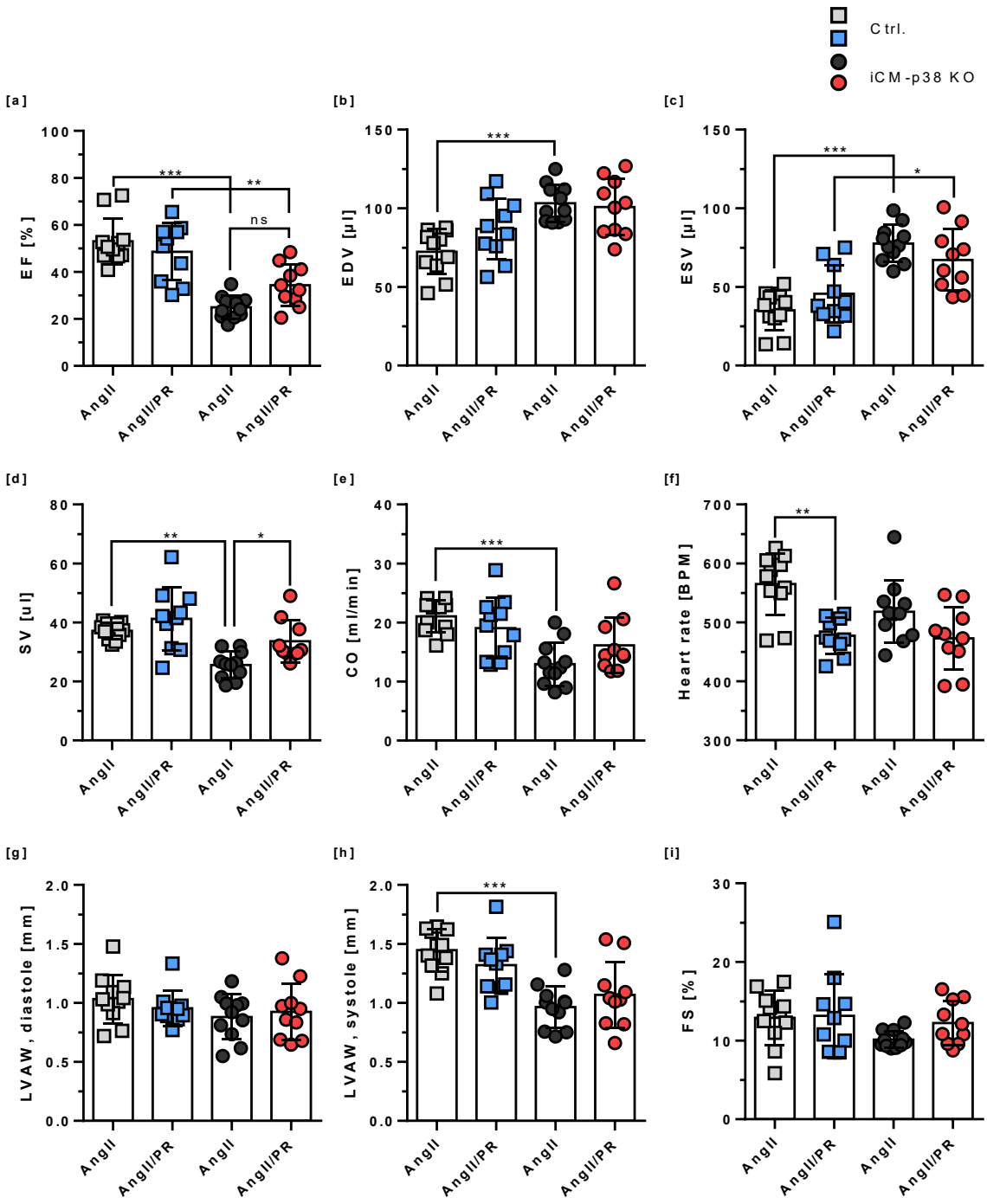

Figure 15: Cardiac function of iCM-p38 control (square) and KO (round) mice treated with AngII and propranolol (PR) or vehicle (PBS) for 48h. [a] Ejection fraction (EF) decreased in iCM-p38 KO mice due to AngII treatment. In PR-treated iCM-p38 KO mice, EF trended to be improved. **[b]** End-diastolic volume (EDV) was elevated in iCM-p38 KO mice and did not change with additional PR administration, while **[c]** end-systolic volume (ESV) increased in iCM-p38 KO mice with only AngII treatment and slightly decreased in PR-treated animals. While both parameters were distinctly lower in control mice, **[d]** stroke volume (SV) and **[e]** cardiac output (CO) were decreased in iCM-p38 KO mice of both groups compared to control. SV increased again in iCM-p38 KO mice due to additional PR treatment. **[f]** Heart rate dropped in control and iCM-p38 KO mice treated with AngII/PR compared to solely AngII, but no differences between control and iCM-p38 KO were observed. **[g]** Left ventricular anterior wall, diastole (LVAW, diastole) was not altered in all groups. **[h]** Left ventricular anterior wall, systole (LVAW, systole) was significantly reduced in iCM-p38 KO mice compared to controls. **[i]** Fractional shortening (FS) was unaltered through the groups. Data are presented as mean ±SD, n = 7-10. Statistical significance was calculated by using One-way ANOVA with Tukey's multiple comparisons test (* p <0.05; ** p <0.01; *** p <0.001).

In conclusion, additional PR administration caused moderate improvement in cardiac function in AngII-treated iCM-p38 KO mice. EF, ESV, and SV were mainly affected in PR-treated iCM-p38 KO mice compared to only AngII-treated mice; however, most of them were not statistically significant.

In addition to heart function, immune cell infiltration into cardiac tissue was analyzed in iCM-p38 KO and control mice after 48h AngII(PR) treatment in more detail. Therefore, FACS analysis was performed on cardiac tissue to quantify different immune cell populations infiltrating the heart during the treatment.

To begin with, the total number of infiltrating leukocytes ($CD45^+$) was analyzed. The number of infiltrating leukocytes was the same in AngII-treated iCM-p38 KO and control mice. Additional PR treatment also did not affect leukocyte infiltration in control hearts, while a slight increase of 30% was measured in AngII/PR-treated iCM-p38 KO hearts compared to AngII-treated iCM-p38 KO hearts (Figure 16a). However, this increase did not reach statistical significance.

Next, infiltrating neutrophils ($CD11b^+/Ly6G^+$) were examined in more detail. Early stages of acute inflammation are characterized by the infiltration of neutrophils, which are involved in paving the way for macrophages to repair tissue damage. As previously described by us [41], it was found here that neutrophils ($CD11b^+/Ly6G^+$) invaded the hearts of AngII-treated iCM-p38 KO, while this massive infiltration was absent in AngII-treated control hearts. The number of neutrophils increased by almost 250% in iCM-p38 KO hearts compared to controls. Additional PR treatment did not affect neutrophil infiltration in control hearts, while in AngII/PR-treated iCM-p38 KO hearts, a reduction of 22% was measured compared to AngII-treated iCM-p38 KO hearts. However, this reduction was not statistically significant (Figure 16b).

Following that, dendritic cells (DCs) were investigated. Their main task in inflammatory processes is to present MHCII antigens to other cells of the immune system, as for example to T-lymphocytes, in order to activate them. Remarkably, infiltration of DCs ($CD11b^-/CD64^-/Ly6G^-/MHCII^+$) showed the opposite effect than it was observed for neutrophils. A reduction of 55% of infiltrating DCs was measured in AngII-treated iCM-p38 KO hearts compared to AngII-treated controls. Again, additional PR treatment did not affect DC infiltration in controls but led to a significant increase of 225% in iCM-p38 KO hearts compared to only AngII-treated iCM-p38 KO hearts (Figure 16c).

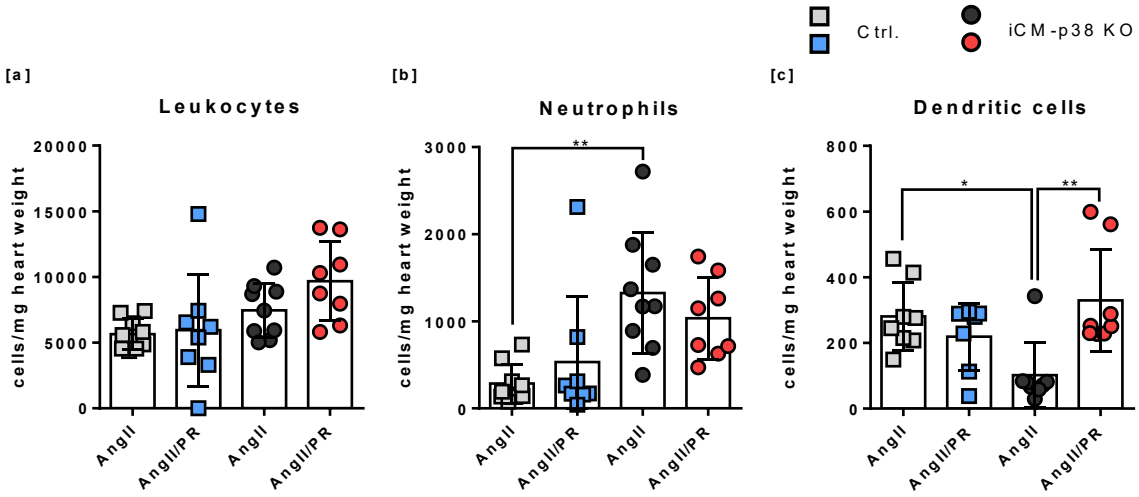

Figure 16: Leukocyte infiltration in cardiac tissue of AngII and AngII/Propranolol (PR)-treated iCM-p38 KO (round) and control (square) hearts after 48h. [a] Total leukocyte ($CD45^+$) number slightly increased in AngII/PR-treated iCM-p38 KO mice compared to only AngII-treated iCM-p38 KO mice and controls. **[b]** Neutrophils ($CD11b^+/Ly6G^+$) accumulated in iCM-p38 KO; however, accumulation was slightly reduced in AngII/PR-treated iCM-p38 KO hearts compared to only AngII-treated iCM-p38 KO hearts. **[c]** The number of dendritic cells ($CD11b^-/CD64^-/Ly6G^-/MHCII^+$) was decreased in AngII-treated iCM-p38 KO mice compared to controls. Additional PR treatment increased DCs again. Data are presented as mean ±SD, n = 7-9. Statistical significance was calculated by using One-way ANOVA with Tukey's multiple comparisons test (* $p < 0.05$; ** $p < 0.01$).

When focusing on monocyte infiltration, it could be observed that the total number of monocytes ($CD11b^+/CD64^-/Ly6G^-/MHCII^-$) was doubled in AngII-treated iCM-p38 KO mice compared to AngII-treated controls. Additional PR administration did not affect monocyte infiltration in control hearts but decreased monocyte infiltration in iCM-p38 KO hearts by 45% compared to only AngII-treated iCM-p38 KO hearts (Figure 17a).

The differentiation of monocytes revealed that most of the infiltrating monocytes were of the classical type, which means being positive for Ly6C ($CD11b^-/C64^-/Ly6G^-/MHCII^-/Ly6C^{+/high}$). The number of $Ly6C^{+/high}$ monocytes was elevated by 150% in AngII-treated iCM-p38 KO mice compared to AngII-treated controls. While between AngII-treated controls and AngII/PR-treated controls the number of infiltrating $Ly6C^{+/high}$ monocytes was unaltered, in AngII/PR-treated iCM-p38 KO hearts the number of infiltrating $Ly6C^{+/high}$ monocytes was reduced by 39% compared to AngII-treated iCM-p38 KO hearts (Figure 17b). Nevertheless, this difference was not statistically significant.

In contrast, the number of infiltrating $Ly6C^{low}$ monocytes ($CD11b^-/C64^-/Ly6G^-/MHCII^-/Ly6C^{-/low}$) did not differ, regardless of the analyzed genotype and treatment (Figure 17c). The same applies for monocytes, which are transitioning between the classical and non-classical phenotypes ($CD11b^-/C64^-/Ly6G^-/MHCII^-/Ly6C^{inter}$) (Figure 17d).

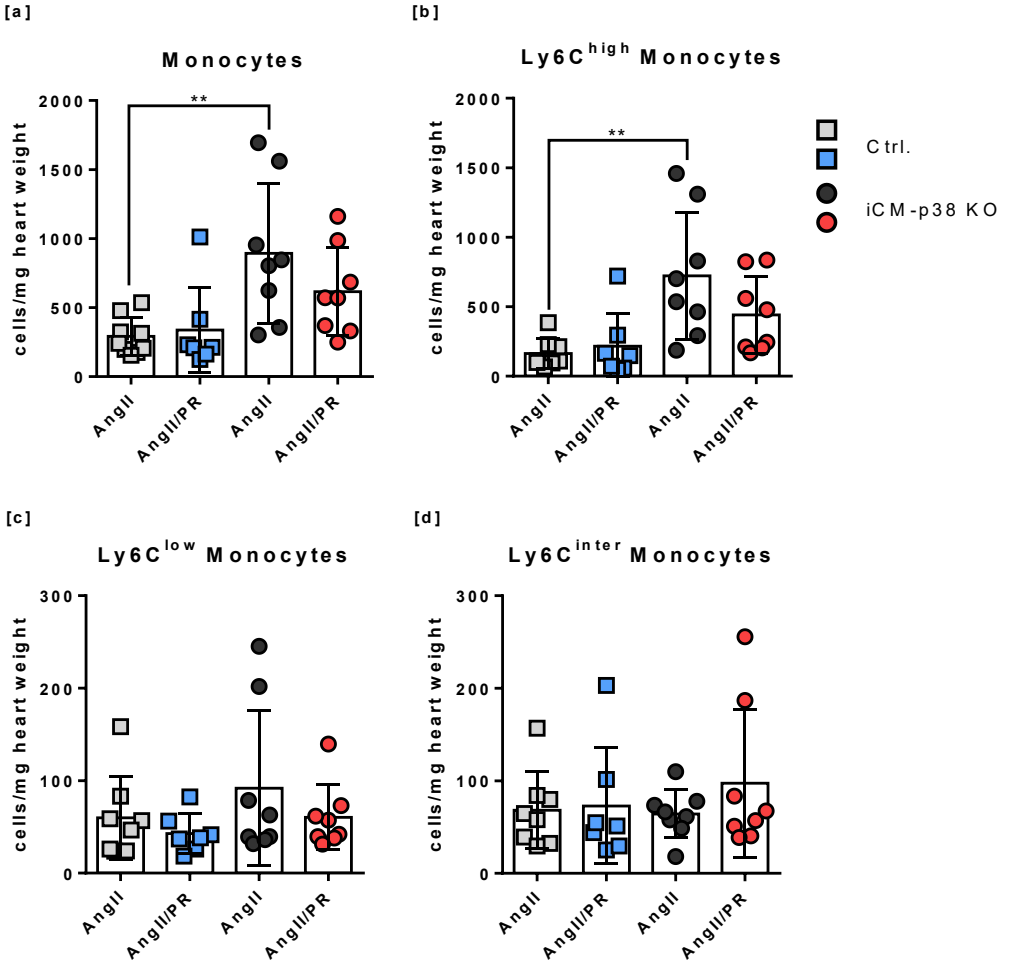

Figure 17: Monocyte infiltration and differentiation in cardiac tissue of AngII and AngII/Propranolol (PR)-treated iCM-p38 KO (round) and control (square) hearts after 48h. [a] Monocyte ($CD11b^+/CD64^-/Ly6G^-/MHCII^-$) infiltration was elevated in iCM-p38 KO mice treated with AngII compared to controls, while additional PR treatment decreased the number again. A differentiation of monocytes in **[b]** $Ly6C^{high}$ ($CD11b^+/CD64^-/Ly6G^-/MHCII^-/Ly6C^{+/high}$) and **[c]** $Ly6C^{low}$ ($CD11b^+/CD64^-/Ly6G^-/MHCII^-/Ly6C^{-/low}$) showed that most cells are $Ly6C^{high}$ monocytes. iCM-p38 KO mice showed elevated levels compared to controls, and additional PR treatment decreased the number of $Ly6C^{high}$ monocytes again in iCM-p38 KO mice. The number of $Ly6C^{low}$ monocytes and **[d]** $Ly6C^{inter}$ monocytes was unaltered between the analyzed groups. Data are presented as mean ±SD, n = 7-9. Statistical significance was calculated by using One-way ANOVA with Tukey's multiple comparisons test (** p <0.01).

Since monocytes can differentiate during their lifetime, e.g., into macrophages, these cells have also been given more attention. The number of macrophages ($CD11b^+/CD64^+$) in cardiac tissue did not differ between AngII-treated iCM-p38 KO and control mice. Additional PR treatment also had no effect on macrophage infiltration in control hearts, while in iCM-p38 KO mice, additional PR administration caused an increase in macrophage accumulation of 35% compared to only AngII-treated iCM-p38 KO mice (Figure 18a).

In general, the majority of macrophages expressed CCR2 (C-C chemokine receptor type 2) receptors (Figure 18b+d), which indicates these cells as infiltrating and non-resident macrophages. No differences were measured for the number of $CCR2^+$

macrophages (CD11b$^+$/CD64$^+$/CCR2$^+$) in AngII-treated iCM-p38 KO and control hearts. As for the total number of macrophages, AngII/PR treatment caused an elevation of 46% of the CCR2$^+$ macrophage number in iCM-p38 KO mice compared to only AngII-treated iCM-p38 KO mice. In control mice, there is no difference in the number of CCR2$^+$ macrophages, regardless of the treatment (Figure 18b). Also, the number of CCR2$^-$ macrophages (CD11b$^+$/CD64$^+$/CCR2$^-$) was unaltered within all analyzed groups (Figure 18c).

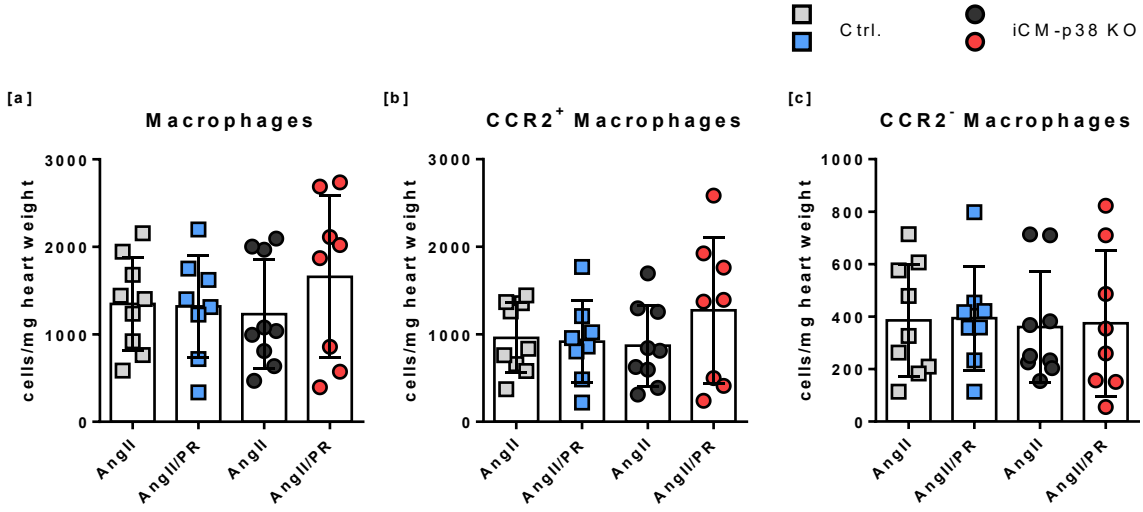

Figure 18: Macrophage infiltration in cardiac tissue of AngII and AngII/Propranolol (PR)-treated iCM-p38 KO (round) and control (square) hearts after 48h. [a] Macrophage (CD11b$^+$/CD64$^+$) infiltration trended to be higher in PR-treated iCM-p38 KO hearts compared to solely AngII-treated animals, while no differences could be observed in control mice. **[b]** The majority of macrophages expressed the CCR2-receptor (CD11b$^+$/CD64$^+$/CCR2$^+$). In iCM-p38 KO mice, the number was slightly increased when treated with AngII/PR. **[c]** The number of CCR2$^-$ macrophages (CD11b$^+$/CD64$^+$/CCR2$^-$) stayed unaltered within all analyzed groups. Data are presented as mean ± SD, n = 7-9. Statistical significance was calculated by using One-way ANOVA with Tukey's multiple comparisons test.

In addition, the macrophage population was even further differentiated to gain detailed insights into several subpopulations infiltrating the hearts. The presence or absence of certain markers on the surface of macrophages can help define macrophage populations. If macrophages express CD206, cells are considered to have anti-inflammatory properties (M2 macrophages), thus participating in the resolution of inflammatory processes, e.g., by the production of anti-inflammatory cytokines. These help to resolve inflammation and thereby contribute to tissue healing. On the other hand, macrophages not expressing CD206 are said to have pro-inflammatory (M1 macrophages) characteristics and produce pro-inflammatory cytokines [170].

This differentiation of the macrophage population demonstrated that most infiltrating macrophages do not express CD206 and therefore are most likely M1-like macrophages (CD11b$^+$/CD64$^+$/CD206$^-$). However, when considering the two genotypes, iCM-p38 KO and controls, as well as the two treatments, AngII and AngII/PR, no differences can be

found in the number of M1-like and M2-like macrophages (Figure 19a+b). These results indicate that the present macrophage population is predominantly M1-like and thus has pro-inflammatory characteristics.

The concept of subdividing macrophages into M1 and M2 subgroups is based on their ability to polarize *in vitro* under defined conditions. This classification is a simplification to describe the activation status of macrophages. During the recent decade, a classification based on the expression of Ly6C has become more and more relevant. $Ly6C^{high}$ macrophages derive from classical, circulating $Ly6C^{high}$ monocytes as an acute inflammatory response showing pro-inflammatory ability. $Ly6C^{low}$ macrophages, on the other hand, are supposedly derived from patrolling $Ly6C^{low}$ monocytes. $Ly6C^{low}$ macrophages possess anti-inflammatory and anti-fibrotic properties [83, 171]. When considering Ly6C expression on the surface of macrophages, the number of $Ly6C^{high}$ macrophages ($CD11b^{+}/CD64^{+}/Ly6C^{+/high}$) in general tended to be slightly decreased compared to the number of $Ly6C^{low}$ macrophages ($CD11b^{+}/CD64^{+}/Ly6C^{-/low}$). In AngII-treated iCM-p38 KO hearts, the number of $Ly6C^{high}$ macrophages is more than halved compared to AngII-treated controls. Additional PR administration did not alter the number of $Ly6C^{high}$ macrophages in iCM-p38 KO and control mice compared to only AngII-treated mice (Figure 19c). Furthermore, no differences between genotypes and treatments were found for the amount of $Ly6C^{low}$ macrophages in cardiac tissue (Figure 19d).

Macrophages can also express the major histocompatility complex class II ($MCHII^{high}$), therefore presenting the receptor on the cell surface. $MCHII^{high}$ macrophages are able to interact with receptors on the surface of $CD4^{+}$ T-lymphocytes, which is a crucial step for the activation of the adaptive immune response [172, 173]. Overall, the number of $MCHII^{high}$ macrophages ($CD11b^{+}/CD64^{+}/MHCII^{+/high}$) is lower than the number of $MCHII^{low}$ macrophages ($CD11b^{+}/CD64^{+}/MHCII^{-/low}$). AngII-treated iCM-p38 KO mice showed a reduced (75%) number of $MCHII^{high}$ macrophages compared to AngII-treated controls. AngII/PR treatment did not affect the number of $MCHII^{high}$ macrophages in controls, while AngII/PR treatment increased the number of $MCHII^{high}$ macrophages in iCM-p38 KO hearts by almost 70% compared to only AngII-treated iCM-p38 KO hearts (Figure 19e). The amount of $MCHII^{low}$ macrophages was unaltered between the four groups that were analyzed (Figure 19f).

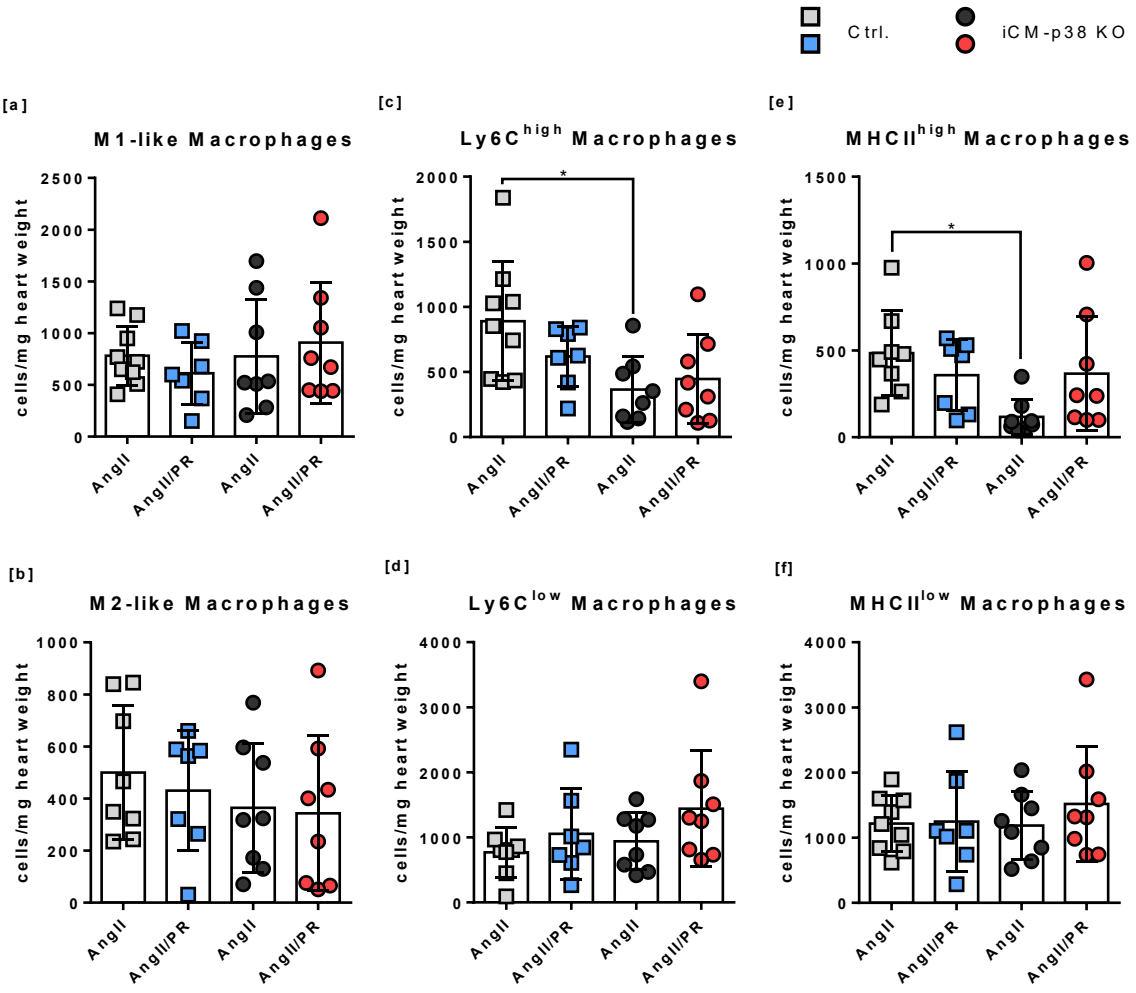

Figure 19: Differentiation of infiltrating macrophages in cardiac tissue of AngII and AngII/Propranolol (PR)-treated iCM-p38 KO (round) and control (square) mice after 48h. The macrophage ($CD11b^+/CD64^+$) population can be differentiated into different subgroups. One possibility is the subdivision into M1 and M2 macrophages based on the expression of CD206. **[a]** The amount of M1 ($CD11b^+/CD64^+/CD206^-$) and **[b]** M2 ($CD11b^+/CD64^+/CD206^+$) macrophages did not differ between the two genotypes and the two treatments. **[c]** The number of macrophages expressing Ly6C ($CD11b^+/CD64^+/Ly6C^{+/high}$) remains unchanged in control mice independent of their treatment, while the number was reduced in AngII-treated iCM-p38 KO mice. Additional PR administration did not alter the number of $Ly6C^{high}$ macrophages in iCM-p38 KO mice. **[d]** The number of macrophages that do not express Ly6C ($CD11b^+/CD64^+/Ly6C^{-/low}$) was mainly unaltered between the different groups. **[e]** The number of $MHCII^{high}$ ($CD11b^+/CD64^+/MHCII^{+/high}$) macrophages was significantly reduced in AngII-treated iCM-p38 KO mice compared to AngII-treated controls, while the number increased again after additional PR administration. In control animals, cell numbers did not differ due to additional PR treatment. **[f]** The number of $MCHII^{low}$ ($CD11b^+/CD64^+/MHCII^{-/low}$) macrophages was the same between all groups. Data are presented as mean ± SD, n = 7-9. Statistical significance was calculated by using One-way ANOVA with Tukey's multiple comparisons test (* $p < 0.05$).

Lastly, infiltrating lymphoid immune cells were examined more closely. They are part of the adaptive immune system and can be separated into B-lymphocytes and T-lymphocytes. B-lymphocytes function in humoral immunity and produce antibodies that are secreted or inserted into the plasma membrane. Additionally, B-lymphocytes present antigens and secrete cytokines.

Immature T-lymphocytes migrate to the thymus gland to mature and differentiate into $CD4^+$ or $CD8^+$ T-lymphocytes. $CD4^+$ T-lymphocytes, also called T-helper cells, carry the

CD4 protein on their cell surface. Their main task is to magnify the immune response by further activating B-lymphocytes and $CD8^+$ T-lymphocytes [28]. $CD8^+$ T-lymphocytes, or cytotoxic T-lymphocytes, however, present the CD8 protein on their surface. These cells are responsible for directly eliminating damaged and apoptotic cells. Through the secretion of cytokines, $CD8^+$ T-lymphocytes are able to recruit other cell types, therefore enhancing the immune response [27].

In all groups, T-lymphocyte ($CD45^+/CD3^+$) and B-lymphocyte ($CD45^+/CD19^+$) infiltration did not differ independent of genotype or treatment (Figure 20a+b). Further subdivision into $CD4^+$ and $CD8^+$ T-lymphocytes showed that the majority of T-lymphocytes generally carry $CD4^+$ markers, but differences between the individual groups were not observed in either $CD4^+$ nor $CD8^+$ cells (Figure 20c+d).

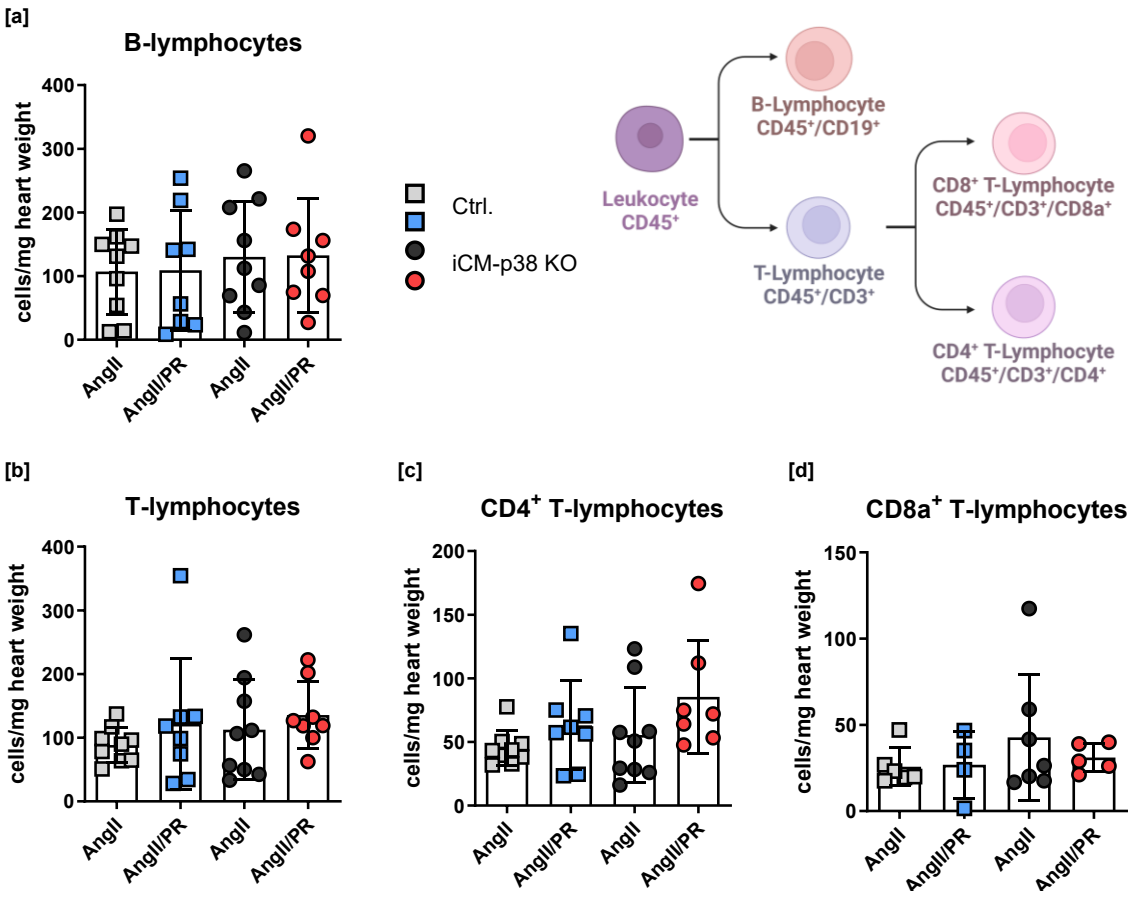

Figure 20: Lymphocyte infiltration in cardiac tissue of AngII and AngII/Propranolol (PR)-treated iCM-p38 KO (round) and control (square) hearts after 48h. [a] B-lymphocyte ($CD45^+/CD19^+$) and **[b]** T-lymphocyte ($CD45^+/CD3^+$) infiltration did not show any alterations between the four groups analyzed. T-lymphocytes were further differentiated into **[c]** $CD4^+$ T-lymphocytes ($CD45^+/CD3^+/CD4^+$) and **[d]** $CD8^+$ T-lymphocytes ($CD45^+/CD3^+/CD8^+$). There were no significant differences in these groups either. Data are presented as mean ±SD, n = 4-9. Statistical significance was calculated by using One-way ANOVA with Tukey's multiple comparisons test.

In conclusion, it was shown that PR is a potent $\beta_{1/2}$-adrenoceptor antagonist and effectively inhibits β-adrenergic stimulation in mice, as proven via invasive blood pressure measurements and NEFA levels in blood serum (Figures 12 + 14). PR treatment in combination with AngII in iCM-p38 KO and control mice trended to improve cardiac function in iCM-p38 KO mice, as indicated by an increase in EF and SV and a decrease in ESV (Figure 15a, c, d). However, immune cell infiltration in cardiac tissue was not significantly altered by additional PR treatment, indicating sympathetic overstimulation is not the main reason for the development of cardiac dysfunction in iCM-p38 KO mice.

4.3 iCM-p38 KO mice develop persistent cardiac dysfunction after 7 days of AngII treatment: Establishment of a long-term heart failure mouse model

By now, all work on iCM-p38 KO mice focused on the time window of 48h after the start of the AngII treatment, and already at this time, an extensive LV dilation was observed. However, so far, no information is available about whether the fast LV dilation results in persistent HF. The question of whether iCM-p38 KO mice recover from cardiac dysfunction following a 48h AngII treatment was investigated by stopping the treatment and continuing to monitor cardiac function for additional 14 days. The modified protocol is described in Figure 21.

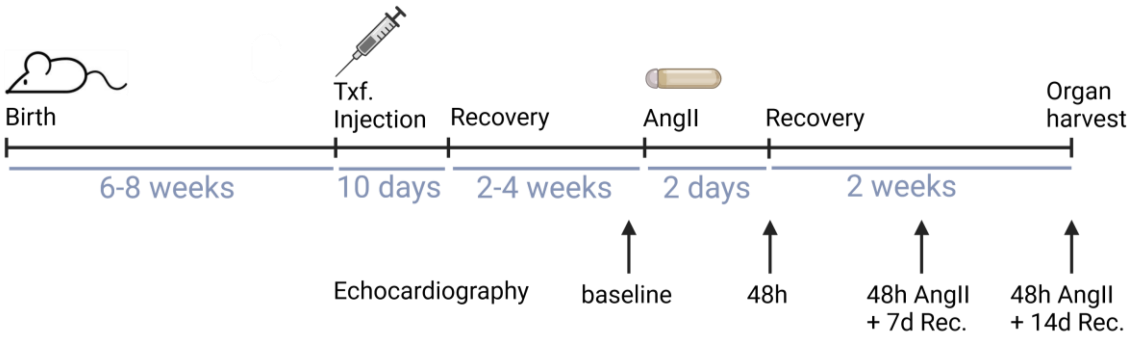

Figure 21: Modified experimental procedure to analyze the long-term effects of 48h AngII treatment in iCM-p38 KO and control mice. The iCM-p38 KO was induced by tamoxifen (Txf.) injection for 10 consecutive days when mice were 6-8 weeks old. After a recovery time of 2-4 weeks, mice received AngII via osmotic mini pumps for 48h. After the end of AngII administration, animals were monitored for additional 2 weeks. The cardiac function was analyzed at different time points, as indicated. Created with BioRender.com.

Echocardiographic monitoring showed that 48h AngII treatment results in a mildly reduced EF in iCM-p38 control mice. After the end of the AngII administration, the EF did not change in these animals (Figure 22a). This result is based on the fact that although the EDV remains unchanged over the entire measured time, a small increase

in the ESV could be measured (Figure 22b+c). In those control mice, AngII administration did not alter SV and CO over the course of the experiment (Figure 22d+e). The analysis of the wall thickness during diastole and systole revealed a reduction over time in control mice (Figure 22f+g). However, all measured alterations did not reach statistical significance in control mice.

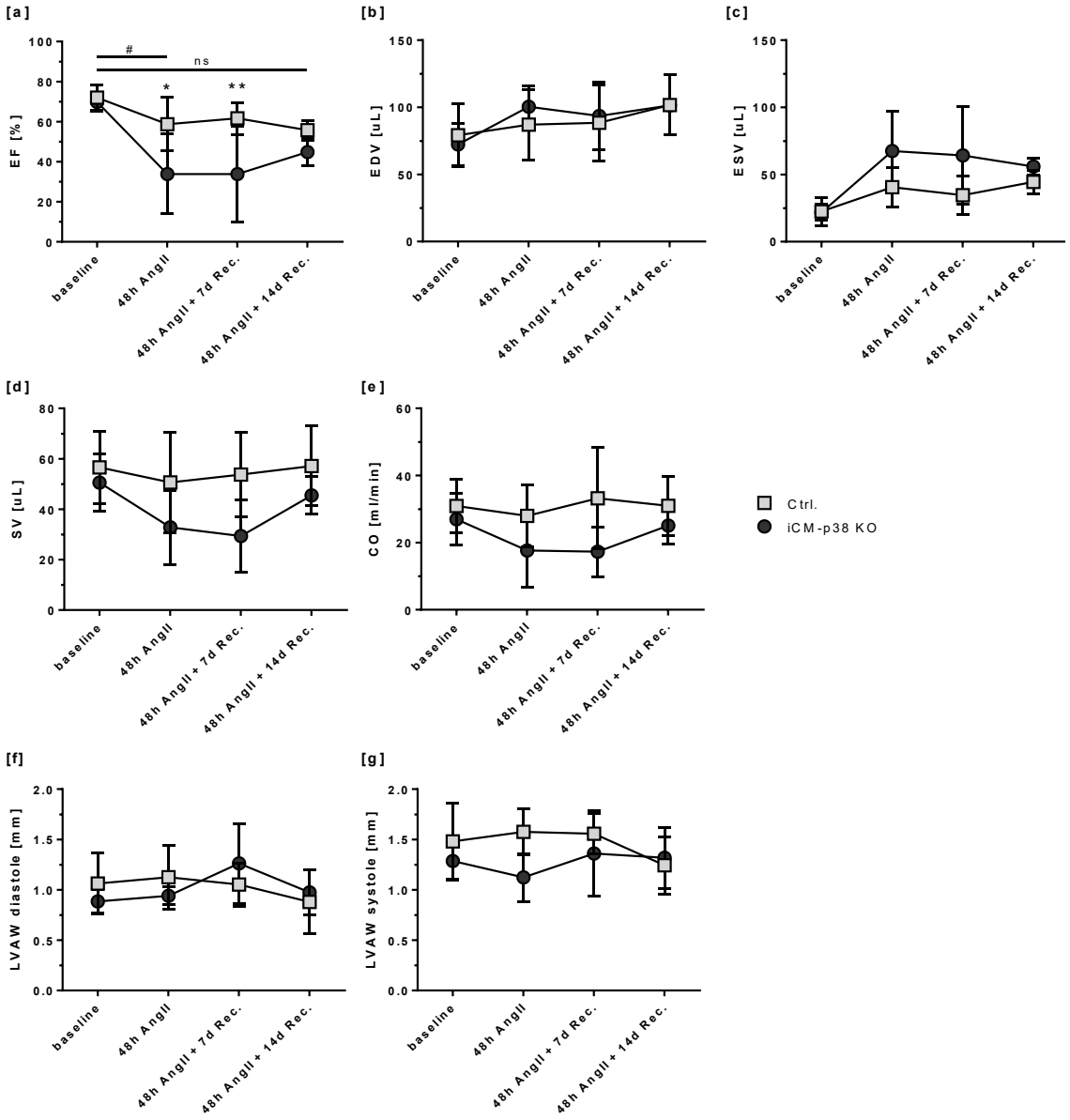

Figure 22: Cardiac function of iCM-p38 KO (round) and control (square) mice treated with AngII for 48h and a subsequent recovery period of additional 14 days. [a] Ejection fraction (EF) dropped initially in both groups due to AngII treatment within 48h and recovered after 14 days. **[b]** End-diastolic volume (EDV) and **[c]** end-systolic volume (ESV) were elevated after AngII administration, especially in iCM-p38 KO mice, but normalized over time. **[d]** Stroke volume (SV) and **[e]** cardiac output (CO) dropped initially but recovered as well after the end of AngII treatment. **[f]** Left ventricular anterior wall, diastole (LVAW, diastole), and **[g]** left ventricular anterior wall, systole (LVAW, systole) did not change over time. Data are presented as mean ±SD, n = 3-6. Statistical significance was calculated by using Two-way ANOVA (repeated measures) with Bonferroni's multiple comparisons test (* p <0.05; ** p <0.01 control vs. iCM-p38 KO; # p <0.05 iCM-p38 KO at different time points).

In contrast, 48h of AngII treatment initially had a more detrimental effect on the cardiac function of iCM-p38 KO mice. EF dropped within the first 48h by 50% compared to baseline measurements and was therefore significantly lower than the EF of controls. While the EF remained unchanged after 7 days of recovery without AngII, it increased again after 14 days (Figure 22a). Although the EDV increased slightly over time, a concomitant decline of the ESV after discontinuation of AngII treatment was observed (Figure 22b+c). In iCM-p38 KO mice, SV and CO changes followed a similar trajectory as EF. First, AngII treatment resulted in a notable decrease in SV and CO compared to baseline measurements. Even seven days after the treatment ended, SV and CO remained reduced. However, both parameters rise substantially again after a 14-day recovery period (Figure 22d+e). Changes in LV wall thickness were not observed throughout the entire experiment (Figure 22f+g).

In conclusion, these results indicate a non-persistent cardiac dysfunction in iCM-p38 KO mice. Although cardiac function was reduced in the first days after the end of the AngII treatment (48h AngII + 7d Rec.), mice recovered after 14d without AngII. Therefore, 48h of AngII treatment induces only a reversible HF in iCM-p38 KO mice, which makes this model unsuitable to investigate long-term heart failure without pharmacological intervention.

4.3.1 Long-term monitoring of cardiac function in iCM-p38 KO mice

Since the establishment of a mouse model with persistent cardiac dysfunction without any further pharmacological intervention is of great interest, AngII administration via osmotic mini pumps was prolonged to 7 days, and mice were allowed to recover again for 14 additional days. Echocardiographic analyses were performed at various time points to accurately assess heart function. Additionally, body weight was routinely measured. Figure 23 shows schematically the changes in the experimental procedure.

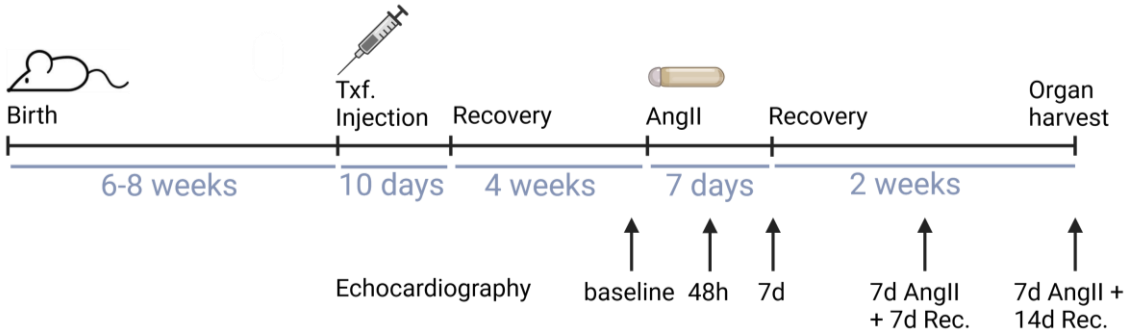

Figure 23: Modified experimental procedure to induce persistent HF in iCM-p38 KO and control mice. The iCM-p38 KO was induced by tamoxifen (Txf.) injection for 10 consecutive days, when mice were 6-8 weeks old. After a recovery time of 2-4 weeks, mice received AngII via osmotic mini pumps for 7 days. After the end of AngII administration, animals were monitored for additional 2 weeks. The cardiac function was analyzed at different time points, as indicated. Created with BioRender.com.

Repeated measurements of body weight in iCM-p38 KO mice and controls treated with AngII showed a body weight loss of around 7.7% in both groups after 24h of AngII administration. After 48h, control mice started to gain weight again, although administration of AngII continued for five more days. In iCM-p38 KO mice, body weight loss continued until 7 days of AngII administration, and mice lost around 15% of their baseline weight, while body weight in control mice was constantly increasing. Following the 7-day AngII treatment, iCM-p38 KO mice also regained weight. These animals even reached their initial weight after 14 days of recovery (Figure 24).

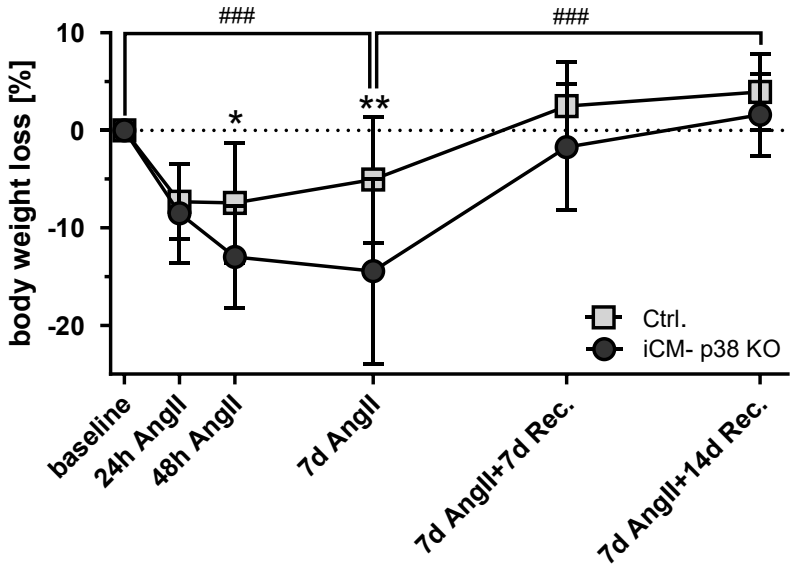

Figure 24: Body weight development of iCM-p38 KO (round) and control (square) mice during 7 days of AngII administration and subsequent recovery period of additional 14 days. Initially, mice in both groups lost body weight. Control animals gained weight again after 24h while iCM-p38 KO mice continuously lost weight. Only after the end of AngII treatment, iCM-p38 KO animals gained weight again and reached basal weight at the end of the experiment. Loss of body weight is given in %. Data are presented as mean ±SD, n = 9-16. Statistical significance was calculated by using Two-way ANOVA (repeated measures) with Bonferroni's multiple comparisons test (control vs. iCM-p38 KO: * $p < 0.05$; iCM-p38 KO comparison of time points: ### $p < 0.001$).

In this experimental series, cardiac parameters were also measured after 48h, resulting in a comparable phenotype as demonstrated before in control and iCM-p38 KO mice. However, the AngII treatment was prolonged to 7 days, and the heart function was closely monitored. Interestingly, after 7 days of AngII treatment, the EF was still at the same low level as it was after 48h (Figure 25a) in iCM-p38 KO mice. Also, EDV and ESV remained massively increased (Figure 25b+c). Of note, even after the AngII administration ended, EF, EDV, and ESV did not normalize but stayed at the same level as after 48h in iCM-p38 KO mice.

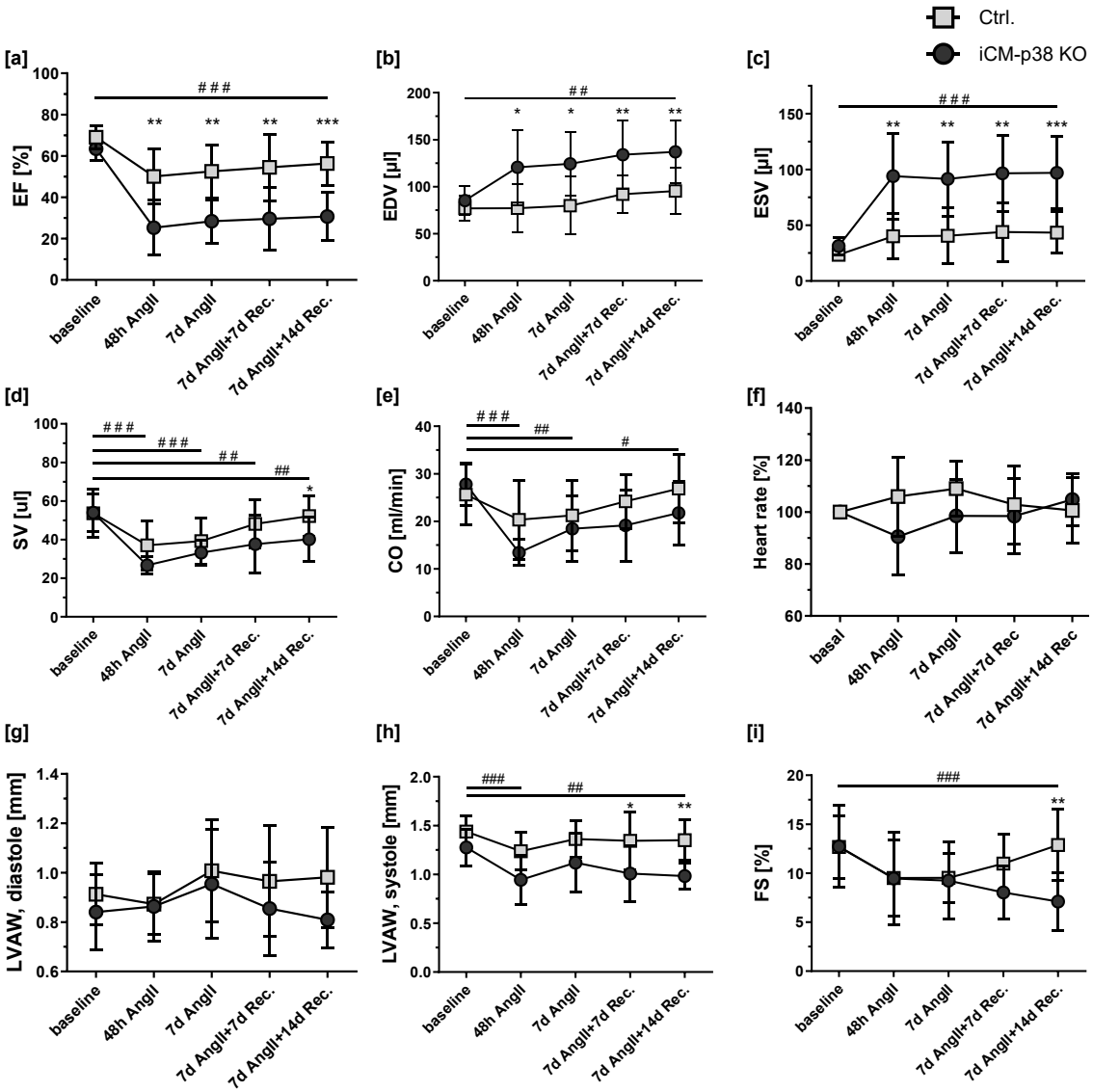

Figure 25: Cardiac function of iCM-p38 KO (round) and control (square) mice treated with AngII for 7 days and additional recovery from the treatment for 14 days. [a] Ejection fraction (EF) was reduced in iCM-p38 KO mice compared to controls and could not recover over time. **[b]** End-diastolic volume (EDV) and **[c]** end-systolic volume (ESV) were consistently increased over the duration of the entire experiment. **[d]** Stroke volume (SV) and **[e]** cardiac output (CO) were reduced after 48h of AngII treatment, particularly in iCM-p38 KO mice, and increased over time again. **[f]** Heart rate was not affected by AngII administration in iCM-p38 control mice and slightly increased in iCM-p38 KO mice over time. **[g]** Left ventricular anterior wall, diastole (LVAW, diastole) did not change over time. **[h]** Left ventricular anterior wall, systole (LVAW, systole) was slightly reduced in iCM-p38 KO mice compared to the baseline level. **[i]** Fractional shortening (FS) dropped severely in both groups. After the end of AngII administration, control animals recovered, while FS continued to decrease sharply in iCM-p38 KO mice. The heart function of p38 KO mice did not improve after stopping AngII treatment. Data are presented as mean ±SD, n = 7-11. Statistical significance was calculated by using Two-way ANOVA (repeated measures) with Bonferroni's multiple comparisons test (control vs. iCM-p38 KO: * p <0.05; ** p <0.01; *** p <0.001; iCM-p38 KO comparison of time points: # p <0.05; ## p <0.01; ### p <0.001).

SV and CO, on the other hand, improved over time, and after 7 days, an increase in both parameters was measured, although the AngII treatment had not yet been completed. During the 14-day recovery period, SV and CO continued to increase but were still significantly reduced in iCM-p38 KO mice compared to the baseline level. At the end of the experiment (7d AngII + 14d Rec.), the SV was still reduced by 25% and the CO by

21% compared to the basal values in iCM-p38 KO mice (Figure 25d+e). However, the increase of CO at the end of the experimental series was rather due to an increased heart rate (by around 10% compared to 48h of AngII) (Figure 25f) than an improved pump function. This view is supported by the progressive decline in fractional shorting, which is a surrogate parameter for contractile function. The FS was only 53% of the initial value in iCM-p38 KO hearts (Figure 25i) at the end of the experiment and was therefore significantly reduced compared to controls.

At the end of the recovery period, the LV wall thickness during systole was reduced by 10% in iCM-p38 KO mice (Figure 25h), whereas the LV wall thickness during diastole remained mainly unchanged throughout the experiment in iCM-p38 KO mice and controls (Figure 25g).

These results demonstrate that a prolonged AngII treatment only transiently affects the heart function of control mice. However, in iCM-p38 KO mice, 7d AngII treatment induced a sustained deterioration in cardiac function, also beyond AngII administration. This heart failure was independent of the continued pharmacological intervention with AngII, since the heart failure condition persisted even beyond AngII administration. This makes the iCM-p38 KO mouse model a useful tool to study the interorgan communication between the failing heart and peripheral organs and allows the investigation of immune cell infiltration into cardiac tissue during the development of cardiac malfunction.

4.3.2 Course of immune cell infiltration in the iCM-p38 KO mouse model of persistent cardiac dysfunction without pharmacologic intervention

The persistent cardiac dysfunction in iCM-p38 KO mice after 7d of AngII treatment raised the question, to what extent the cardiac inflammation was affected in the chronic model of HF. Therefore, the time course of immune cell infiltration in the heart was analyzed at different time points of AngII treatment as well as after a recovery period of an additional 14 days. This was accomplished by performing an FACS analysis, as described in 3.8.

First, the total number of leukocytes ($CD45^+$) in iCM-p38 KO and control hearts was analyzed over time. Under baseline conditions, the total number of leukocytes ($CD45^+$) was around 900 cells/mg heart weight and did not differ between iCM-p38 KO and control hearts. After 24h of AngII treatment, no accumulation of leukocytes was observed. However, 48h after the beginning of AngII administration, the number of infiltrating leukocytes was significantly elevated in both groups. An increase of 6.5-fold in controls and even 8-fold in iCM-p38 KO hearts was measured compared to baseline level. In the further time course, the number of leukocytes decreased, although AngII was continued to be administered. There were no further changes in the leukocyte infiltration during the subsequent recovery period either (Figure 26a).

Under baseline conditions, the number of neutrophils ($CD11b^+/Ly6G^+$) in cardiac tissue was minor in iCM-p38 KO and control mice. Interestingly, after 48h of AngII treatment, a strong infiltration of neutrophils was observed, but primarily in iCM-p38 KO hearts. An increase of almost 240-fold from baseline to 48h AngII was measured. However, this strong increase was not found in the hearts of control mice. This discrepancy in infiltration results in a 4.6-fold increase in iCM-p38 KO hearts compared to controls at 48h of AngII treatment. At later time points (7d AngII and 7d AngII + 14d Rec.), neutrophil numbers returned to baseline levels in both groups (Figure 26b).

Although under baseline conditions the number of dendritic cells (DCs) ($CD11b^-/C64^-/Ly6G^-/MHCII^+$) in iCM-p38 KO and control mice was minimal and did not differ between the two groups, a significant infiltration was measured after 48h. However, the effect that was seen was the reverse of the neutrophil infiltration. While in the hearts of control animals, the number of DCs increased massively after 48h of AngII treatment (15-fold increase compared to baseline), the number of DCs increased only slightly in iCM-p38 KO hearts (5-fold increase compared to baseline). Therefore, DC infiltration was 2.7-fold higher in control hearts than in iCM-p38 KO hearts after 48h of AngII treatment. After 7d of AngII treatment, the number of DCs decreased again, and no differences between iCM-p38 KO and control hearts were observed anymore. Over time, the number of DCs decreased further to the baseline level in both groups (Figure 26c).

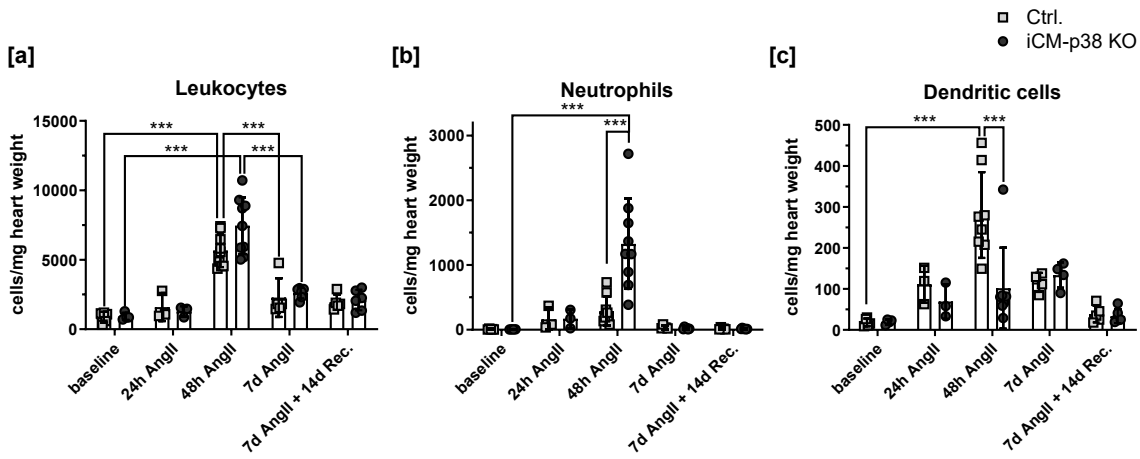

Figure 26: Course of total leukocyte, neutrophil, and dendritic cell infiltration in cardiac tissue of iCM-p38 KO (round) and control (square) mice in response to AngII treatment over time. [a] The number of total leukocytes ($CD45^+$) peaked in both groups at 48h of AngII treatment before returning to the baseline level. **[b]** Neutrophils ($CD11b^+/Ly6G^+$) were strongly infiltrating the cardiac tissue of iCM-p38 KO mice, but not of controls, after 48h of AngII treatment. At later time points, neutrophils were not found any more. **[c]** Dendritic cells (DCs) ($CD11b^-/CD64^-/Ly6G^-/MHCII^+$) also peaked at 48h after the start of AngII treatment but were mainly present in controls, while the number of DCs in iCM-p38 KO hearts did not increase. Over time, the number of CDs declined. Data are presented as mean ±SD, n = 3-9. Statistical significance was calculated by using Two-way ANOVA with Bonferroni's multiple comparisons test (* $p < 0.05$; ** $p < 0.01$; *** $p < 0.001$).

Brenes-Castro summarized that monocytes are one of the first cells infiltrating cardiac tissue in PO-induced heart failure [37]. Therefore, a closer look was taken at monocyte infiltration as well. The hearts of untreated iCM-p38 KO and control mice were devoid of monocytes. After 48h of AngII treatment, the number of monocytes ($CD11b^{+}/CD64^{-}/Ly6G^{-}/MHCII^{-}$) increased by 33-fold in iCM-p38 KO hearts compared to baseline conditions. Since in control mice this infiltration was absent, the number of monocytes was significantly higher in iCM-p38 KO hearts compared to controls after 48h AngII treatment (Figure 27a). Over the course of the experiment, the number of monocytes diminished in both groups, although AngII was still administered for five more days.

Further differentiation of the infiltrating monocytes revealed that infiltrating monocytes were mainly $Ly6C^{high}$ monocytes ($CD11b^{+}/CD64^{-}/Ly6G^{-}/MHCII^{-}/Ly6C^{+/high}$) and therefore are considered pro-inflammatory immune cells. In this subset of monocytes, the difference between iCM-p38 KO and control hearts was striking as well, since the number of $Ly6C^{high}$ monocytes was 4.4-fold higher in iCM-p38 KO hearts compared to controls at 48h of AngII treatment (Figure 27b). At later time points, the number of $Ly6C^{high}$ monocytes went back to baseline level.

Although the number of $Ly6C^{inter}$ and $Ly6C^{low}$ monocytes ($CD11b^{+}/CD64^{-}/Ly6G^{-}/MHCII^{-}/Ly6C^{-/low}$) was elevated after 48h AngII treatment compared to baseline conditions, no differences were observed between iCM-p38 KO mice and controls (Figure 27c+d). At later time points (7d AngII and 7d AngII + 14d Rec.), the number of $Ly6C^{inter}$ and $Ly6C^{low}$ monocytes decreased again and returned to the baseline level.

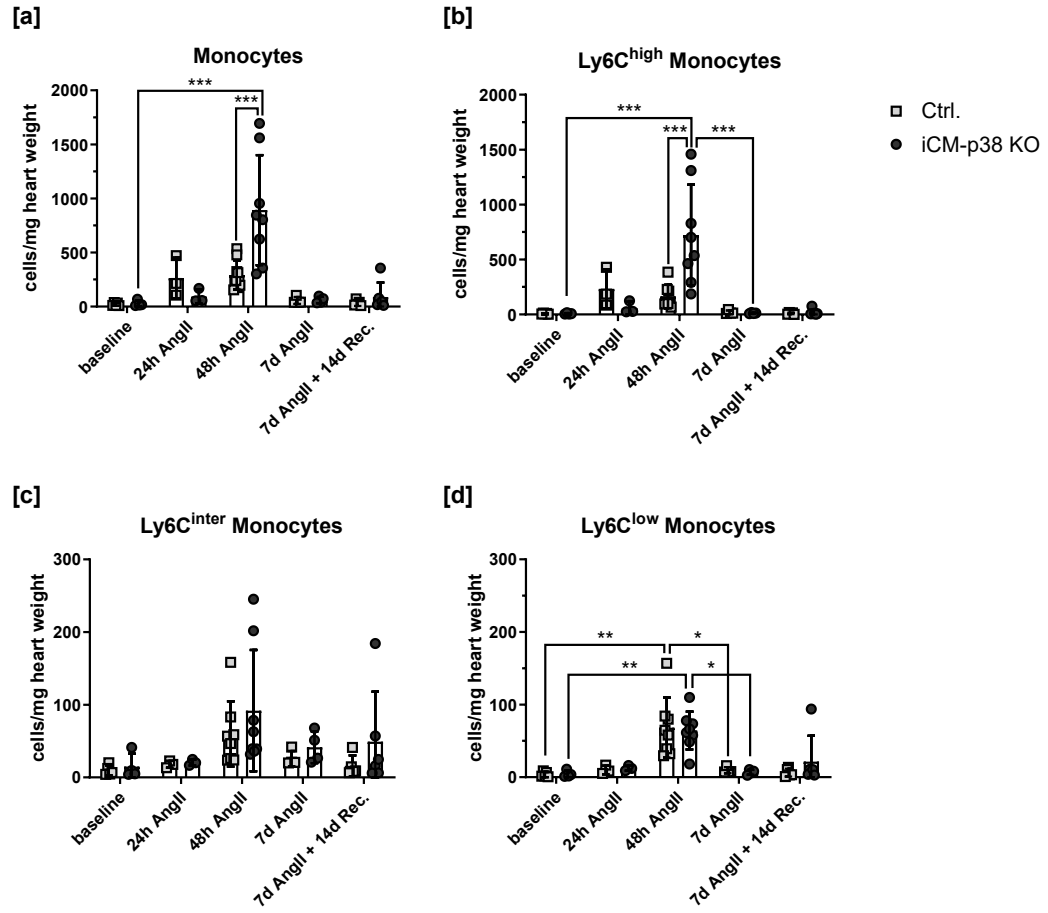

Figure 27: Monocyte infiltration in cardiac tissue of AngII-treated iCM-p38 KO (round) and control (square) mice over time. [a] The number of monocytes ($CD11b^+/CD64^-/Ly6G^-/MHCII^-$) was elevated after 48h of AngII administration, especially in iCM-p38 KO hearts, while the increase was less severe in controls. Differentiation of the monocyte population in **[b]** $Ly6C^{high}$ ($CD11b^+/CD64^-/Ly6G^-/MHCII^-/Ly6C^{+/high}$), **[c]** $Ly6C^{inter}$ and **[d]** $Ly6C^{low}$ ($CD11b^+/CD64^-/Ly6G^-/MHCII^-/Ly6C^{-/low}$) showed an elevation in all monocyte subtypes after 48h of AngII treatment, but the strongest effect was in $Ly6C^{high}$ monocytes. A significant elevation in iCM-p38 KO hearts was measured compared to controls. Data are presented as mean ±SD, n = 3-9. Statistical significance was calculated by using Two-way ANOVA with Bonferroni's multiple comparisons test (* p <0.05; ** p <0.01; *** p <0.001).

As described before in 1.2, monocytes have the ability to differentiate into other cell types, including macrophages. Consequently, a closer examination of macrophages and their various subtypes was conducted. So far, 48h of AngII treatment have resulted in the most extensive infiltration of immune cells into the heart tissue. The process appears to be different for macrophages. Compared to baseline conditions, no elevation in macrophage numbers ($CD11b^+/CD64^+$) was observed for 24h and 48h of AngII treatment. However, after 7d of AngII treatment, the number of macrophages was doubled in hearts of control mice and even tripled in iCM-p38 KO hearts. However, the differences between controls and iCM-p38 KO hearts did not reach statistical significance. During the recovery phase of 14 days, infiltrating macrophages vanished, and numbers reached almost baseline levels in both groups (Figure 28a).

Macrophages were further characterized and therefore differentiated into infiltrating CCR2$^+$ (CD11b$^+$/CD64$^+$/CCR2$^+$) and resident CCR2$^-$ macrophages (CD11b$^+$/CD64$^+$/CCR2$^-$). The number of infiltrating CCR2$^+$ macrophages was increased by 6-fold and 8.5-fold after 48h and 7d of AngII treatment in iCM-p38 KO hearts compared to baseline conditions but decreased with the recovery period of 14 days (Figure 28b). This was also observed in the control group, although the differences were less severe. The number of resident CCR2$^-$ macrophages decreased in both groups after 48h of AngII by 40% but increased afterwards (Figure 28c). Though the number of CCR2$^+$ macrophages slightly exceeded the number of CCR2$^-$ macrophages, this demonstrates that most macrophages were infiltrated macrophages.

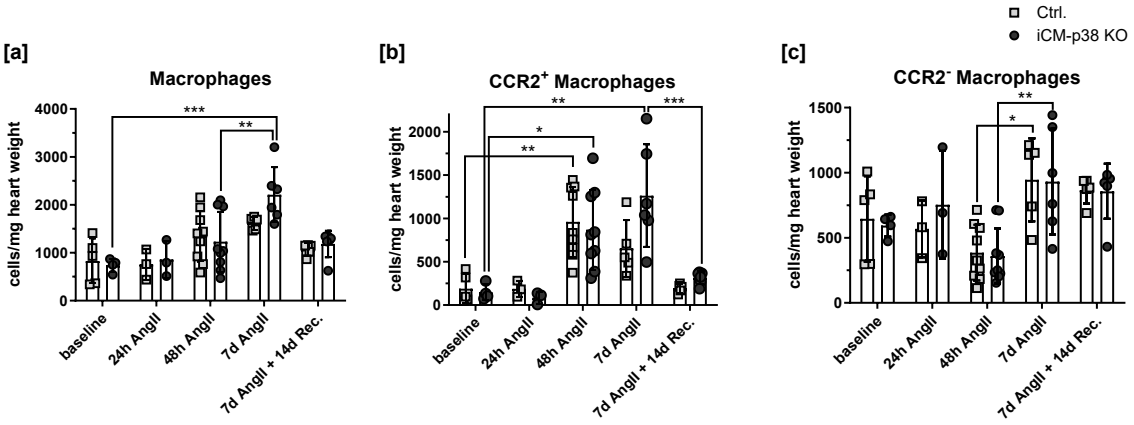

Figure 28: Macrophage infiltration in cardiac tissue of AngII-treated iCM-p38 KO (round) and control (square) mice over time. [a] The number of macrophages (CD11b$^+$/CD64$^+$) was elevated in both iCM-p38 KO and control hearts after 7d of AngII treatment but decreased after the recovery period again. A differentiation of macrophages in **[b]** infiltrating CCR2$^+$ (CD11b$^+$/CD64$^+$/CCR2$^+$) and **[c]** resident CCR2$^-$ macrophages (CD11b$^+$/CD64$^+$/CCR2$^-$) revealed that macrophages were infiltrating the cardiac tissue mainly between day 2 and 7 of AngII treatment. Data are presented as mean ±SD, n = 3-9. Statistical significance was calculated by using Two-way ANOVA with Bonferroni's multiple comparisons test (* p <0.05; ** p <0.01; *** p <0.001).

Macrophages diverse surface markers enable them to be classified according to their pro- and anti-inflammatory properties. The number of pro-inflammatory M1-like macrophages (CD11b$^+$/CD64$^+$/CD206$^-$) was minimal in iCM-p38 KO and control hearts under baseline conditions and after 24h of AngII treatment. Surprisingly, an increase of M1-like macrophages was observed after 48h of AngII treatment, although the total number of macrophages peaked on day 7 after the start of AngII administration, as described before. At 48h of AngII treatment, the number of M1-like macrophages was increased by 3.1-fold in control hearts and 3.6-fold in iCM-p38 KO hearts. The number decreased again on day 7 of AngII treatment and stayed at this level after the 14-day recovery period. Differences between control and iCM-p38 KO hearts could not be measured at any of the analyzed time points (Figure 29a).

Infiltration of M2-like macrophages, however, showed a different pattern. The number of anti-inflammatory M2-like macrophages ($CD11b^{+}/CD64^{+}/CD206^{+}$), stayed at the same level until 7d of AngII treatment. At this time point, the number of M2-like macrophages peaked, with a 2-fold increase in controls and a 3-fold increase in iCM-p38 KO hearts. After 14 days of recovery, the number of M2-like macrophages decreased in both groups, but the baseline level was not reached again (Figure 29b).

Another way to identify pro- and anti-inflammatory macrophages is by looking for the Ly6C marker. In both groups, controls and iCM-p38 KO mice, the number of pro-inflammatory $Ly6C^{high}$ macrophages ($CD11b^{+}/CD64^{+}/Ly6C^{+/high}$) was elevated after 7d AngII treatment (2.2-fold increase in controls and 3.3-fold increase in iCM-p38 KO mice compared to baseline level). Before, no alterations in the number of $Ly6C^{high}$ macrophages were measured. During the recovery phase of 14 days, the number of $Ly6C^{high}$ macrophages decreased again in both groups but was still 60% higher than the baseline level (Figure 29c).

$Ly6C^{low}$ macrophages ($CD11b^{+}/CD64^{+}/Ly6C^{-/low}$) were elevated earlier at 24h of AngII treatment (3.6-fold increase in controls and 3.6-fold increase in iCM-p38 KO hearts compared to baseline). After 48h, the number of $Ly6C^{low}$ macrophages was still elevated in both groups. On day 7 of the AngII treatment, the number of $Ly6C^{low}$ macrophages decreased again, went back to the baseline level, and stayed there even after the recovery period (Figure 29d). However, significant differences between controls and iCM-p38 KO hearts were not observed.

The number of $MCHII^{high}$ macrophages ($CD11b^{+}/CD64^{+}/MHCII^{+/high}$) was elevated on day 7 of the AngII treatment. In control hearts, an increase of 1.6-fold and in iCM-p38 KO hearts, an increase of 1.5-fold was measured. Before this point, there were no alterations in the infiltration of $MCHII^{high}$ macrophages (Figure 29e). After the recovery period, numbers were decreasing to the baseline level in both groups. The number of $MCHII^{low}$ macrophages ($CD11b^{+}/CD64^{+}/MHCII^{-/low}$) was highest after 48h of AngII treatment, although the increase was only 2.7-fold in iCM-p38 KO hearts and 3.4-fold in controls (Figure 29f) compared to baseline level.

In general, all differences between the hearts of control and iCM-p38 KO mice regarding macrophage infiltration were minor, and no significant differences between the two groups appeared.

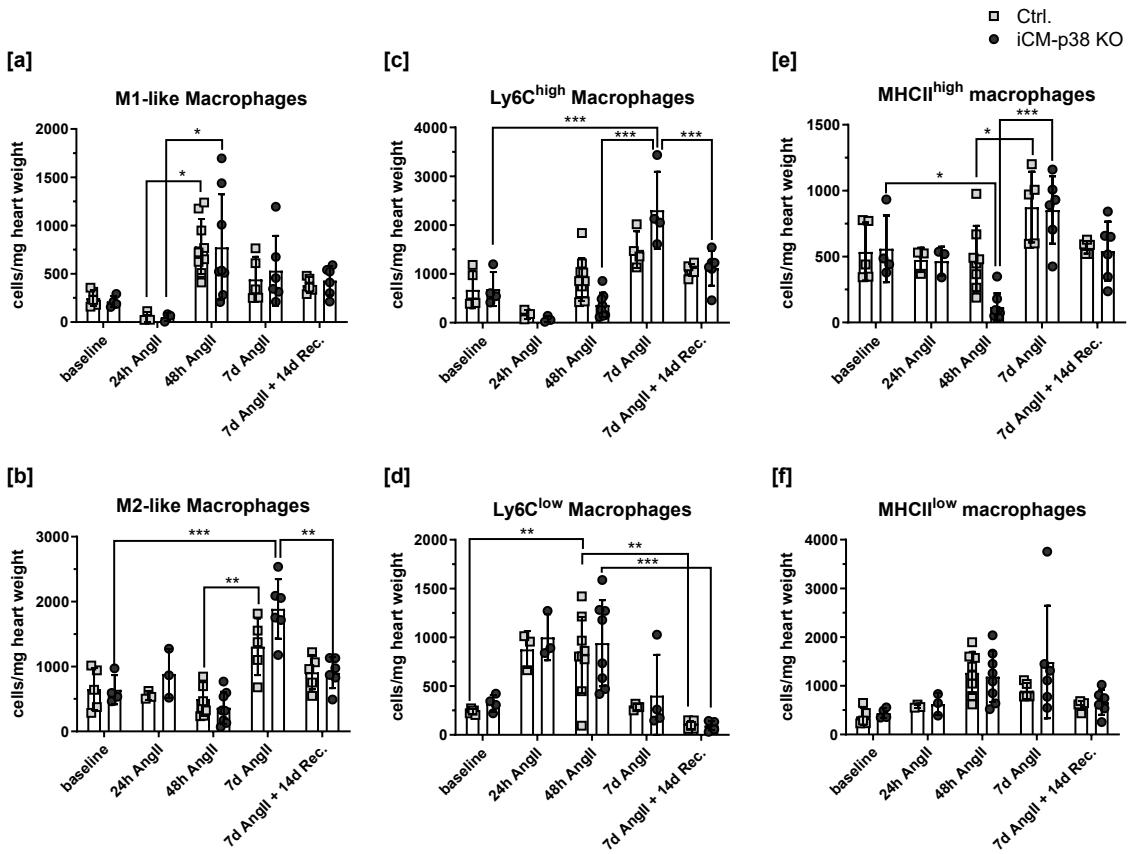

Figure 29: Differentiation of infiltrating macrophages in cardiac tissue of AngII-treated iCM-p38 KO (round) and control (square) mice over time. By using the marker CD206, macrophages were divided into **[a]** pro- ($CD11b^+/CD64^+/CD206^-$) and **[b]** anti-inflammatory macrophages ($CD11b^+/CD64^+/CD206^+$). After 48h of AngII treatment, the number of pro-inflammatory macrophages peaked, while at day 7, more anti-inflammatory macrophages were present in cardiac tissue. The marker Ly6C also gives information about the inflammatory state of macrophages. The number of **[c]** $Ly6C^{high}$ macrophages ($CD11b^+/CD64^+/Ly6C^{+/high}$) increased, especially in iCM-p38 KO mice, after 7d of AngII, while the number of **[d]** $Ly6C^{low}$ macrophages ($CD11b^+/CD64^+/Ly6C^{-/low}$) already strongly increased after 24h of AngII treatment and decreased at later time points. The ability of macrophages to present antigens to other immune cells is another type of differentiation of these cells. Macrophages especially presented **[e]** MCHII ($CD11b^+/CD64^+/MHCII^+$) at day 7 of the AngII treatment. The number of **[f]** $MHCII^{low}$ macrophages ($CD11b^+/CD64^+/MHCII^-$) was mainly unchanged over time. Data are presented as mean ±SD, n = 7-10. Statistical significance was calculated by using Two-way ANOVA with Bonferroni's multiple comparisons test (* p <0.05; ** p <0.01; *** p <0.001).

Until now, the primary focus has been on the investigation of myeloid immune cells, which are part of the innate immune system. The next step includes the examination of lymphoid immune cells, which belong to the adaptive immune system. Accordingly, B- and T-lymphocytes were taken into account, whereby T-lymphocytes were in turn subdivided into $CD4^+$, $CD8^+$, or $CD4^-/CD8^-$ cells.

The number of B-lymphocytes ($CD45^+/CD19^+$) was minimal under baseline conditions. AngII treatment increased the number of B-lymphocytes slightly after 24h in both groups, and after 48h, an even stronger accumulation of B-lymphocytes in iCM-p38 KO and control hearts was observed compared to baseline conditions. Over time, the accumulation of B-lymphocytes diminished but stayed above the baseline level. Differences between iCM-p38 KO and control mice were not observed (Figure 30a).

The number of T-lymphocytes ($CD45^+/CD3^+$) increased as well in iCM-p38 KO and control mice hearts in response to AngII treatment. A steady increase in cell numbers occurred for up to 48h and stayed high during the AngII treatment. After 7 days of AngII administration, a 9-fold increase in iCM-p38 KO and control hearts was measured compared to baseline conditions. During the recovery phase, the number of T-lymphocytes in cardiac tissue decreased in both groups; however, the baseline level was not reached again (Figure 30b).

A differentiation of T-lymphocytes in $CD4^+$ and $CD8^+$ T-lymphocytes showed similar patterns, since an increase in numbers of $CD4^+$ and $CD8^+$ T-lymphocytes was observed after 48h and 7d of AngII treatment, while cell numbers were decreasing again after the recovery time. This applied to control animals and iCM-p38 KO mice to the same extent (Figure 30c+d). Very few T-lymphocytes were negative for both markers, CD4 and CD8. The differences in the accumulation of these cells in cardiac tissue between the two groups were minor (Figure 30e).

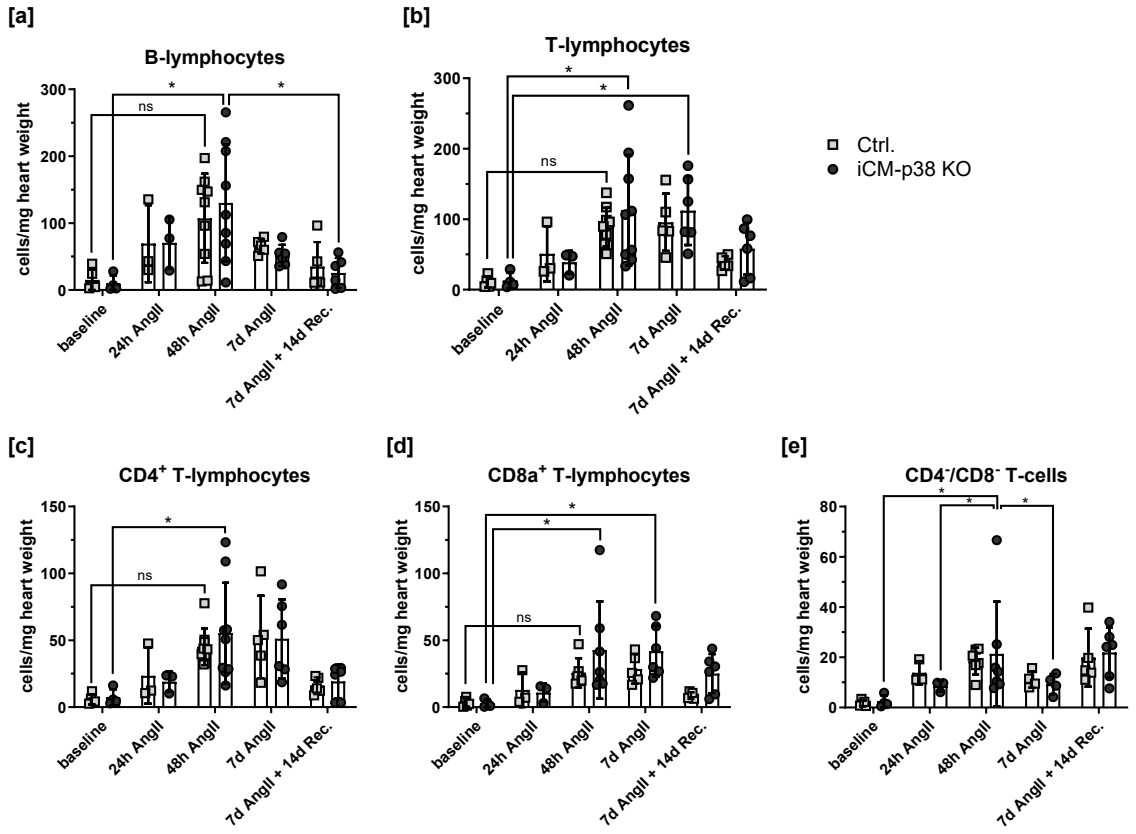

Figure 30: Infiltration of lymphoid immune cells into cardiac tissue of iCM-p38 KO (round) hearts and controls (square) after AngII treatment over time. [a] The number of B-lymphocytes ($CD45^+/CD19^+$) peaked in both analyzed groups at 48h of AngII treatment before returning to the baseline level. **[b]** The number of T-lymphocytes ($CD45^+/CD3^+$) stayed at an elevated level until the end of AngII administration after 7 days and decreased within the recovery period in both groups. A differentiation into **[c]** $CD4^+$, **[d]** $CD8a^+$ and **[e]** $CD4^-/CD8a^-$ T-lymphocytes revealed only minor alterations in the accumulation of these cells. Data are presented as mean ±SD, n = 3-9. Statistical significance was calculated by using Two-way ANOVA with Bonferroni's multiple comparisons test (* $p < 0.05$; *** $p < 0.001$).

In summary, FACS analysis showed that AngII treatment is associated with commendable infiltration of pro-inflammatory cells, in particular neutrophils and Ly6C^{high} monocytes and macrophages. The maximum immune cell response took place 48h after the start of the AngII administration, but even after 7 days of AngII treatment, some immune cells stayed elevated. These primarily include some subtypes of macrophages and T-lymphocytes. For most immune cells analyzed, no differences between control and iCM-p38 KO hearts were observed. Significant differences between the two groups were found in the infiltration of neutrophils, monocytes, and dendritic cells after 48h of AngII. The results indicate that especially the infiltration of neutrophils and monocytes contribute to the severely deteriorated cardiac function of iCM-p38 KO mice, while control animals show only a very slight impairment of cardiac function due to pressure overload.

4.3.3 iCM-p38 KO mice with persistent heart failure show signs of cardiac fibrosis

Heart failure is related to morphological, structural, and functional changes referred to as cardiac remodeling. Pathological remodeling is characterized by an excess of extracellular matrix (ECM) deposition, termed fibrosis. In the iCM-p38 mouse model, the progression of fibrosis was investigated using FACS analysis and immunohistological staining for wheat germ agglutinin (WGA).

Cardiac fibroblasts are the main driver of the progression of fibrosis. Pinto et al. 2016 [157] characterized these cells as MEFSK-positive cells and therefore allowed the identification of those cells via FACS analysis. The separation of αSMA$^+$ and αSMA$^-$ cells from all MEFSK$^+$ cells enables a statement to be made about the activation state of the fibroblasts, whereby αSMA$^+$ fibroblasts are considered activated and serve as a marker for fibrosis [174]. FACS analysis of heart tissue from iCM-p38 KO and control mice revealed a gradual increase in the number of fibroblasts (CD31$^-$/CD45$^-$/MEFSK$^+$) in control hearts of 1.3-fold and even 2.4-fold in iCM-p38 KO mice over time (baseline compared to 7d AngII + 14d Rec.) (Figure 31a). The number of αSMA$^+$ fibroblasts (CD31$^-$/CD45$^-$/MEFSK$^+$/αSMA$^+$) started to rise after 48h of AngII treatment and peaked after 7d of AngII treatment. Remarkably, the elevation is significantly higher in iCM-p38 KO hearts compared to controls. After 7d AngII treatment, a 36-fold increase in the number of αSMA$^+$ fibroblasts was measured in iCM-p38 KO hearts compared to baseline conditions. In contrast, the increase in controls was only 16-fold. During the recovery phase, αSMA$^+$ fibroblasts diminished immensely in both groups (Figure 31b).

WGA is a lectin that binds to N-acetyl-D-glucosamine, a part of the polysaccharide chain of hyaluronic acid. Thus, fibrotic scar tissue and cell membranes can be labeled with it. Quantification of the WGA$^+$ area (in % of the total area of the heart section) in cardiac

tissue was performed in iCM-p38 KO and control mice at two different time points: after 7d of AngII treatment and after 7d of AngII treatment followed by a recovery phase. A slight increase in WGA$^+$ area was measured in iCM-p38 hearts at 7d AngII compared to controls at the same time. This effect was increased after the recovery period, leading to a 5.1-fold increase in the WGA$^+$ area in iCM-p38 KO mice compared to the earlier time point. Since the increase was less in control hearts, the WGA$^+$ area in the hearts of iCM-p38 KO mice after 7d of AngII + 14d recovery was doubled when compared to controls (Figure 31c+d).

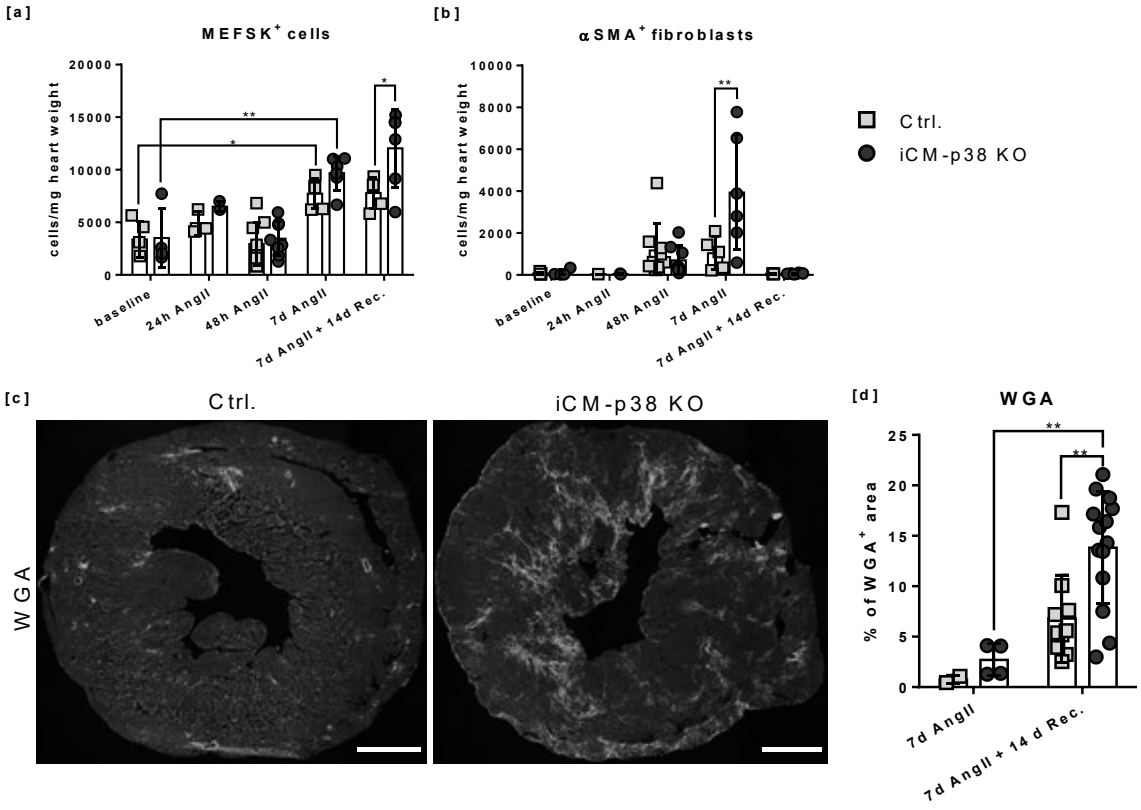

Figure 31: Incipient fibrosis in iCM-p38 KO hearts after 7 days of AngII treatment and 14 days of additional recovery. [a]FACS analysis of cardiac tissue showed a slight increase in MEFSK$^+$ cells (CD31$^-$/CD45$^-$/MEFSK$^+$), which are considered as fibroblasts, in both experimental groups over time. **[b]** In iCM-p38 KO hearts, an increase in αSMA$^+$ fibroblasts (CD31$^-$/CD45$^-$/MEFSK$^+$/αSMA$^+$) was observed after 7d of AngII treatment. **[c]** Representative pictures of iCM-p38 KO hearts and control hearts after 7d AngII and 14d of recovery period stained with WGA (wheat germ agglutinin staining) (exposure time: 2.5 sec. scale bar = 1000 µm). **[d]** Quantification of WGA positive area (in % of the total area of the heart section) in heart sections showed an increase in WGA positive area in iCM-p38 KO hearts compared to controls, especially after 14d of recovery period subsequent to the end of 7d of AngII administration. Data are presented as mean ±SD, n = 4-10. Statistical significance was calculated by using Two-way ANOVA with Bonferroni's multiple comparisons test (* p <0.05; ** p <0.01; *** p <0.001).

In summary, FACS analysis and histological staining of cardiac tissue from AngII-treated iCM-p38 KO and control mice showed elevated levels of activated fibroblasts and an expansion of the WGA$^+$ area, particularly in iCM-p38 KO hearts. These findings demonstrate that cardiac fibrosis, established just within 7d of AngII treatment and continued to spread over time.

To further investigate the degree of fibrosis, hearts that had received AngII treatment for 7 days and then underwent a 14d recovery period were subjected to quantitative expression analyses. Six genes known to be overexpressed in fibrotic tissue were examined: *collagen I* (*Col1a1*), *collagen III* (*Col3a1*), *periostin* (*Postn*), *actin alpha 2* (*Acta2*), *hyaluronan synthase 1* (*Has1*) and *hyaluronan synthase 2* (*Has2*).

The normalized expression of *Col1a1* was 3.8-fold higher in the hearts of iCM-p38 KO mice compared to controls (Figure 32a). In comparison to controls, iCM-p38 KO hearts showed a statistically significant increase in expression for *Col3a1* and *Postn*. *Col3a1* and *Postn* expression increased by 3.4-fold and 4.6-fold, respectively (Figure 32b+c). *Acta2* expression was increased by 1.6-fold in iCM-p38 KO hearts compared to controls (Figure 32d). Given that *Acta2* expression peaks 2-4 days after cardiac injury, it is possible that the expression is already downregulated at the time of analysis. In line with that, the αSMA expression in fibroblasts was downregulated after the recovery phase of 14d on the protein level as well (see Figure 31b). The expression of *Has1* and *Has2* was unaltered between iCM-p38 KO and control hearts (Figure 32e+f).

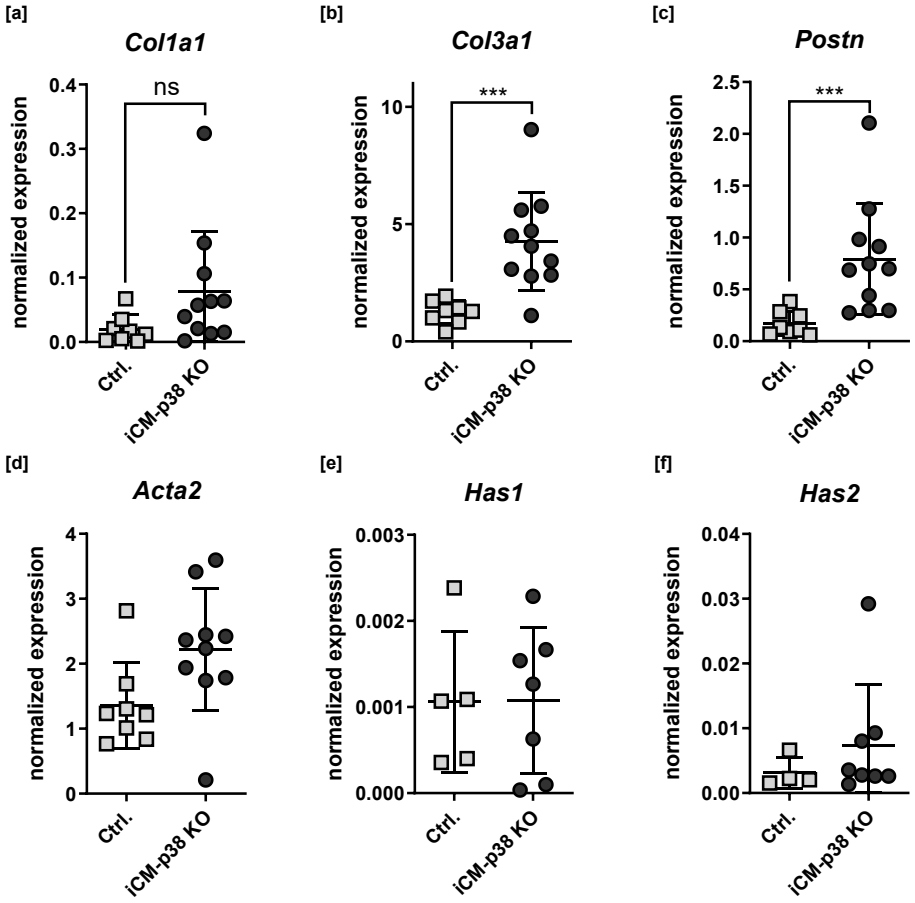

Figure 32: Expression of fibrosis-related genes in iCM-p38 KO (round) and control (square) hearts after 7 days of AngII treatment and 14 days of additional recovery. [a] *Col1a1* (*collagen1a1*), **[b]** *Col3a1* (collagen3a1), **[c]** *Postn* (*periostin*), and **[d]** *Acta2* (*actin alpha 2*) expression was increased in iCM-p38 KO hearts compared to controls. **[e]** *Has1* (*Hyaluronan synthase 1*) and **[f]** *Has2* (*Hyaluronan synthase 2*) expression did not differ between the two groups. Data are normalized to the reference gene *Csnk2b*. Data are presented as mean ±SD, n = 4-11. Statistical significance was calculated by using unpaired two-tailed students t-test or Mann-Whitney U test (*** p <0.001).

As already described in 1.3, myofibroblasts are able to differentiate further into matrifibrocytes. This process is suggested to contribute to the stabilization of the damaged myocardium and is characterized by an increased expression of *Comp* and *Tnfrsf11b*, as these genes are usually expressed in cartilage and bone tissue [72]. An increase of 6.7-fold was identified for *Comp* expression in iCM-p38 KO mice compared to controls (Figure 33a). *Tnfrsf11b* expression in iCM-p38 KO mice was significantly increased by 4-fold compared to controls (Figure 33b).

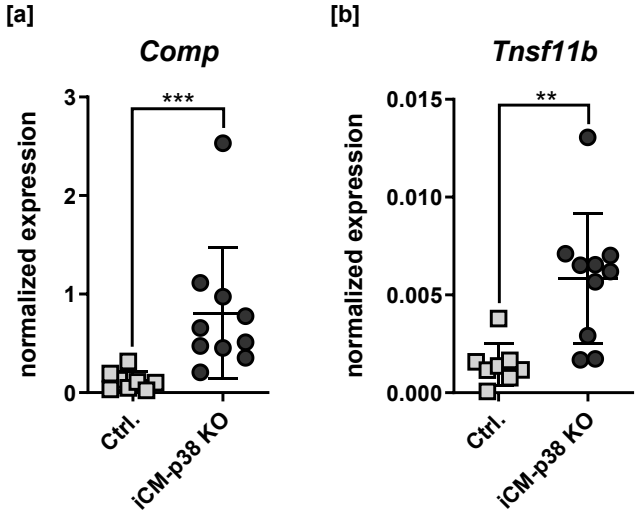

Figure 33: Expression of genes related to matrifibrocytes in iCM-p38 KO (round) and control (square) hearts after 7 days of AngII treatment and 14 days of additional recovery. [a] *Comp* (*cartilage oligomeric matrix protein*) expression was increased in iCM-p38 KO hearts. The same applies for **[b]** *Tnsf11b* (*TNF receptor superfamily member 11b)* expression. Data are normalized to the reference gene *Csnk2b*. Data are presented as mean ±SD, n = 8-10. Statistical significance was calculated by using unpaired two-tailed students t-test or Mann-Whitney U test (** p <0.01; *** p<0.001).

In conclusion, the quantitative expression data of cardiac tissue of iCM-p38 KO and control hearts after 7d AngII treatment and 14d of recovery period revealed an increase in 4 out of 8 genes (*Col3a1, Postn, Comp, Tnsf11b*) analyzed and a tendency in one additional gene (*Col1a1*). Together with the FACS analysis, where the number of αSMA$^+$ fibroblasts was analyzed, and histological staining for WGA, the presence of cardiac fibrosis in iCM-p38 KO mice was confirmed.

4.4 Neutrophil depletion prior to pressure overload induction significantly improved cardiac function in iCM-p38 KO mice in the long-term

FACS analysis of cardiac tissue from iCM-p38 KO and control mice revealed a particularly strong infiltration of neutrophils after 48h AngII treatment in iCM-p38 KO hearts (Figure 26b). Since it has already been shown that neutrophils can have

detrimental roles in cardiac injury [175], it can be speculated that the massive infiltration substantially contributes to the development of cardiac dysfunction in these animals. Hence, mice were injected either with α-Ly6G antibodies to prevent an increase in neutrophil accumulation or with corresponding isotype antibodies (IT) as a control. The antibody injection was performed 12-16h prior to the onset of AngII-induced pressure overload, as described in 3.2.2. Figure 34 shows a schematic representation of the modifications made to the experimental design.

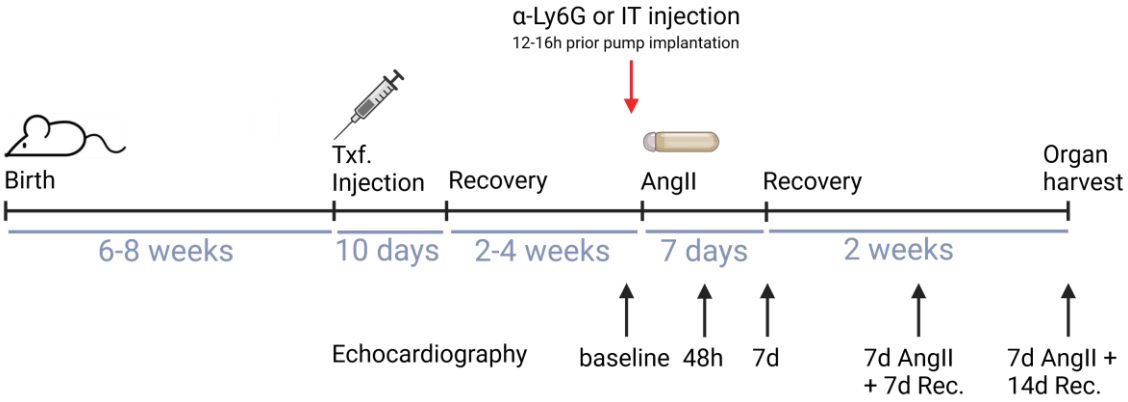

Figure 34: Modified experimental procedure to validate the role of infiltrating neutrophils in the progression of persistent heart failure in iCM-p38 KO mice. The iCM-p38 KO was induced by tamoxifen (Txf.) injection for 10 consecutive days, when mice were 6-8 weeks old. After a recovery time of 2-4 weeks, neutrophil depletion occurred by injection with α-Ly6G antibody (or isotype control (IT)). 12-16h after the neutrophil depletion, mice received AngII via osmotic mini pumps for 7 days. After the end of AngII administration, animals were monitored for additional 2 weeks. The cardiac function was analyzed at different time points, as indicated. Created with BioRender.com.

First of all, the body weight of the mice was closely monitored throughout the entire experiment. It was observed that all mice, regardless of genotype and treatment, initially lost weight. However, weight loss was most severe in iCM-p38 KO mice. After 48h of AngII treatment, α-Ly6G and IT-injected control mice started to gain weight again, although AngII administration continued. At the end of the experiment, they even exceeded the initial body weight by 8% and 7%, respectively.

Interestingly, the course of the body weight in α-Ly6G-treated iCM-p38 KO mice was almost the same as in the controls. These mice had already gained weight, although AngII administration was still ongoing. On the other hand, IT-injected iCM-p38 KO mice lost weight until the AngII treatment stopped. Only then, did the animals recover and start gaining weight (Figure 35). The development of body weight in IT-injected iCM-p38 KO and control mice behaves exactly like that of non-injected mice, which was presented before (see Figure 24). Accordingly, it can be assumed that the experiments are unaffected by the IT injection.

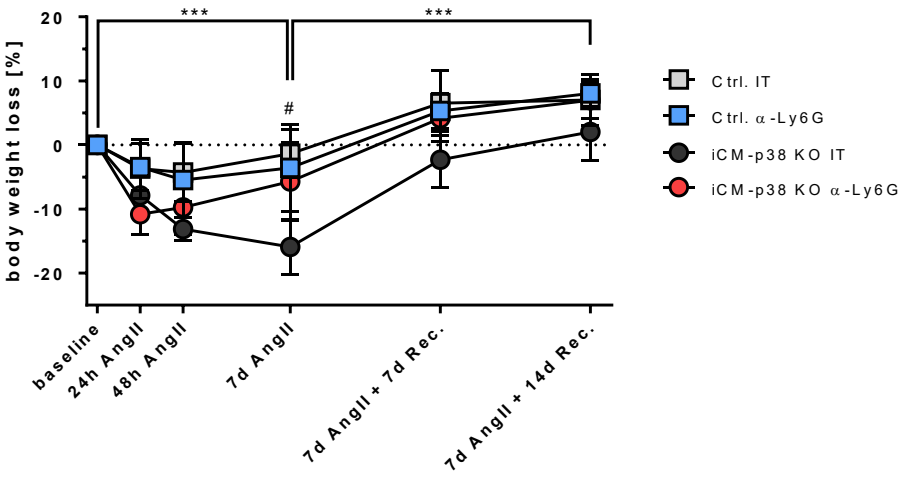

Figure 35: Body weight development of iCM-p38 KO (round) and control (square) mice during 7 days of AngII administration and subsequent recovery period of additional 14 days with (blue and red) and without (grey and black) neutrophil depletion prior to AngII administration. Initially, mice in all groups lose body weight. Control animals (injected either with isotype control (IT) or α-Ly6G) gained weight again after 48h, while iCM-p38 KO mice injected with IT continuously lost weight. iCM-p38 KO mice injected with α-Ly6G, on the other hand, behave like control animals and regain weight sooner. Only after the end of AngII treatment, iCM-p38 KO animals gained weight again and reached basal weight again at the end of the experiment. Loss of body weight is given in %. Data are presented as mean ±SD, n = 4-6. Statistical significance was calculated by using Two-way ANOVA (repeated measures) with Bonferroni's multiple comparisons test (iCM-p38 KO IT comparison between the time points: *** p <0.001; iCM-p38 KO IT vs. iCM-p38 KO α-Ly6G: # p <0.05).

Cardiac function was analyzed at various time points in the four groups via echocardiographic measurements.

The heart function of the IT-injected control and iCM-p38 KO mice was the same as it was in earlier studies when mice received no antibody injection (see 4.3.1). Briefly, in iCM-p38 KO mice, AngII administration resulted in a pronounced heart failure characterized by a strong reduction of the EF due to an increase in EDV and ESV. The SV and CO were decreased as well. The HF persisted also beyond the AngII administration. In control mice, however, AngII treatment did not affect cardiac function. The same was observed in control mice, which were injected with an α-Ly6G antibody prior to AngII administration. Conclusively, antibody injection did not affect the cardiac function of control mice, and IT-antibody injection had no influence on the manifestation of HF in iCM-p38 KO mice.

The α-Ly6G-injected iCM-p38 KO mouse group proved to be the most thrilling group in this experiment. In this group, a reduction in EF after 48h of AngII treatment of 50% compared to baseline conditions was observed. However, this means a 78% improvement in the EF compared to IT-injected iCM-p38 KO mice after 48h of AngII treatment. Over time, the EF in α-Ly6G-injected iCM-p30 KO mice increased to a final EF of 41%, whereas the EF in IT-injected iCM-p38 KO mice was 27% (Figure 36a). Similar results were found for EDV and ESV. In particular, ESV was significantly reduced

in α-Ly6G-injected iCM-p38 KO mice compared to IT-injected iCM-p38 KO mice (Figure 36b+c). This was evident at every time point. Notably, the SV, CO, and FS in α-Ly6G-injected iCM-p38 KO mice did not differ from α-Ly6G-injected or IT-injected control mice, although a strong reduction in IT-injected iCM-p38 KO mice was found (Figure 36d, e, i).

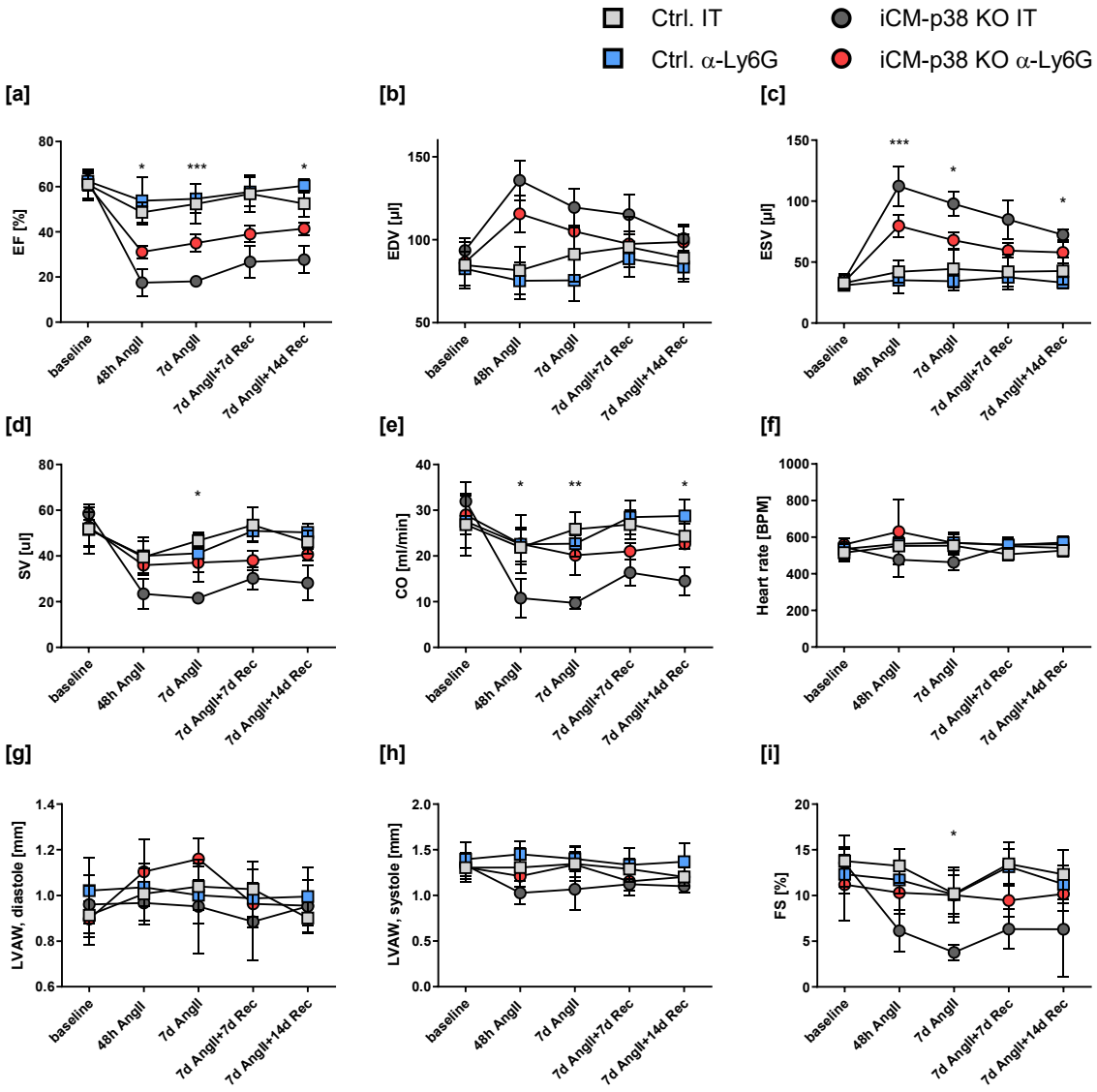

Figure 36: Cardiac function of iCM-p38 KO (round) and control (square) mice treated with AngII for 7 days and subsequent recovery period of additional 14 days with (blue and red) and without (grey and black) neutrophil depletion prior to AngII administration. [a] The ejection fraction (EF) was unchanged in control animals regardless of the treatment. In iCM-p38 KO mice, EF was reduced, while neutrophil depletion through α-Ly6G injection caused an increase in EF in iCM-p38 KO mice, which was consistent over time. **[b]** End-diastolic volume (EDV) and **[c]** end-systolic volume (ESV) were consistently increased over the course of the entire experiment in iCM-p38 KO mice compared to controls, although α-Ly6G injection reduced both in iCM-p38 KO mice. In control mice, no differences between isotype control (IT) and α-Ly6G injections were observed. **[d]** Stroke volume (SV) and **[e]** cardiac output (CO) were reduced after 48h of AngII treatment in iCM-p38 KO mice injected with IT compared to controls. iCM-p38 KO mice injected with α-Ly6G, on the other hand, showed no differences compared to controls. **[f]** Heart rate was mainly unchanged within all groups throughout the whole experiment. **[g]** Left ventricular anterior wall, diastole (LVAW,d) and **[h]** systole (LVAW,s) did not change over time. **[i]** Fractional shortening (FS) dropped severely in iCM-p38 KO mice injected with IT. Reductions in all other groups were less severe. Data are presented as mean ±SD, n = 4-6. Statistical significance was calculated by using Two-way ANOVA (repeated measures) with Bonferroni's multiple comparisons test (iCM-p38 KO IT vs. iCM-p38 KO α-Ly6G: * p <0.05; ** p <0.01; *** p <0.001).

The heart rate and LV wall thickness during diastole and systole were unaltered between the four groups and throughout the entire experiment (Figure 36f-h).

In conclusion, these results showed that depletion of infiltrating neutrophils significantly improved long-term cardiac function of iCM-p38 KO mice after induction of PO via AngII. This was observed throughout the experiment, even though the AngII treatment lasted for 7d and the depletion was only temporary, affecting only the early infiltrating neutrophils. Accordingly, the infiltrating neutrophils must be primarily responsible for the development of heart failure in iCM-p38 KO mice.

4.4.1 Functional improvement of neutrophil-depleted iCM-p38 KO hearts is accompanied by reduced cardiac fibrosis

The functional improvement in iCM-p38 KO mice due to neutrophil depletion raised the question to what extent long-term cardiac remodeling was affected.

Staining for WGA in the heart sections of these mice revealed an increase of 80% of the fibrotic area in iCM-p38 KO mice compared to controls when injected with the IT antibody. Neutrophil depletion by α-Ly6G antibody injection caused a reduction in the WGA^+ area in controls as well as in iCM-p38 KO hearts. In controls, a reduction of 2.6-fold was measured, whereas the reduction in iCM-p38 KO hearts was 1.6-fold (Figure 37).

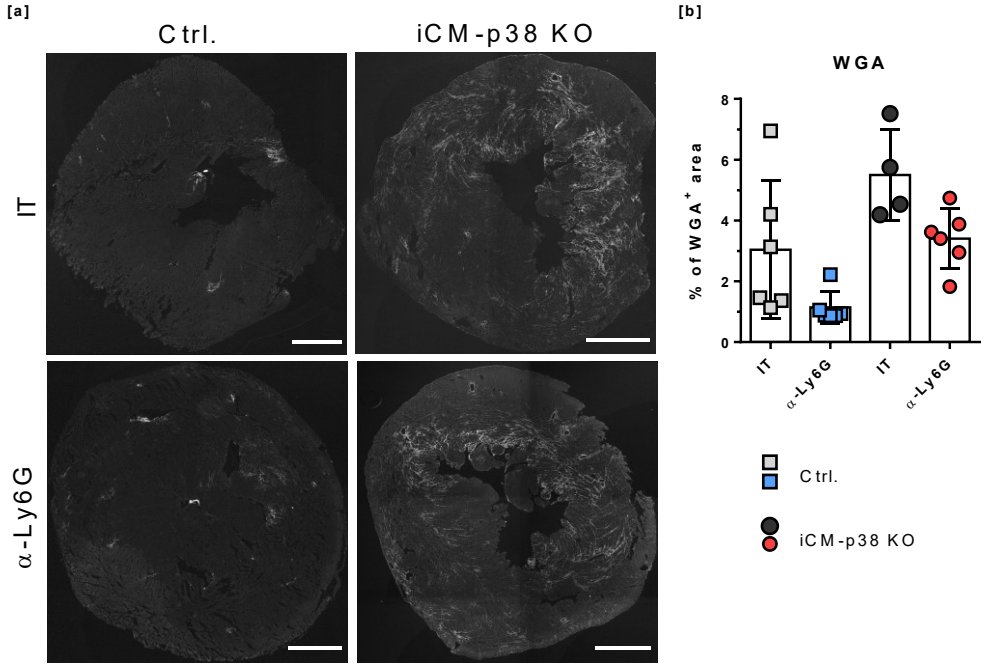

Figure 37: Progression of fibrosis in iCM-p38 KO (round) and control (square) hearts after 7 days of AngII treatment and 14 days of additional recovery with or without neutrophil depletion. [a] Representative pictures of iCM-p38 KO hearts and control hearts after 7d AngII and 14d of recovery period with or without neutrophil depletion via α-Ly6G injection, stained with WGA (wheat germ agglutinin staining) (exposure time: 2.5 sec. scale bar = 1000 µm). **[b]** Quantification of WGA^+ area in heart sections showed an increase in WGA^+ area in iCM-p38 KO hearts compared to controls, especially when not injected with α-Ly6G. In neutrophil-depleted mice, the WGA^+ area is reduced. Data are presented as mean ±SD, n = 4-6. Statistical significance was calculated by using One-way ANOVA with Tukey's multiple comparisons test.

The quantification of gene expression of several genes in iCM-p38 KO and control mice was performed with heart tissue after 7d AngII + 14d recovery, also in neutrophil-depleted mice. Measured genes (*Col1a1, Col3a1, Postn, Acta2,* and *Has2*) are related to fibrotic processes in cardiac tissue, as already described in 1.3 and 4.3.3.

A 2.5-fold increase in *Col1a1* expression was measured in iCM-p38 KO hearts injected with IT compared to IT-injected controls. Neutrophil depletion via α-Ly6G injection reduced *Col1a1* expression in iCM-p38 KO hearts by around 1.5-fold. However, expression was still higher than in IT or Ly6G-injected control hearts. In controls injected with α-Ly6G, a decrease of 3.1-fold was also measured compared to IT-injected controls (Figure 38a).

Similar results were obtained for *Col3a1* expression. In iCM-p38 KO (IT) hearts, a 1.8-fold increase in expression compared to controls (IT) was measured. α-Ly6G injection caused a 1.6-fold decrease in expression in iCM-p38 KO hearts compared to IT-injected iCM-p38 KO hearts. α-Ly6G injection also caused a slight reduction in *Col3a1* expression in control mice compared to IT-injected controls (Figure 38b).

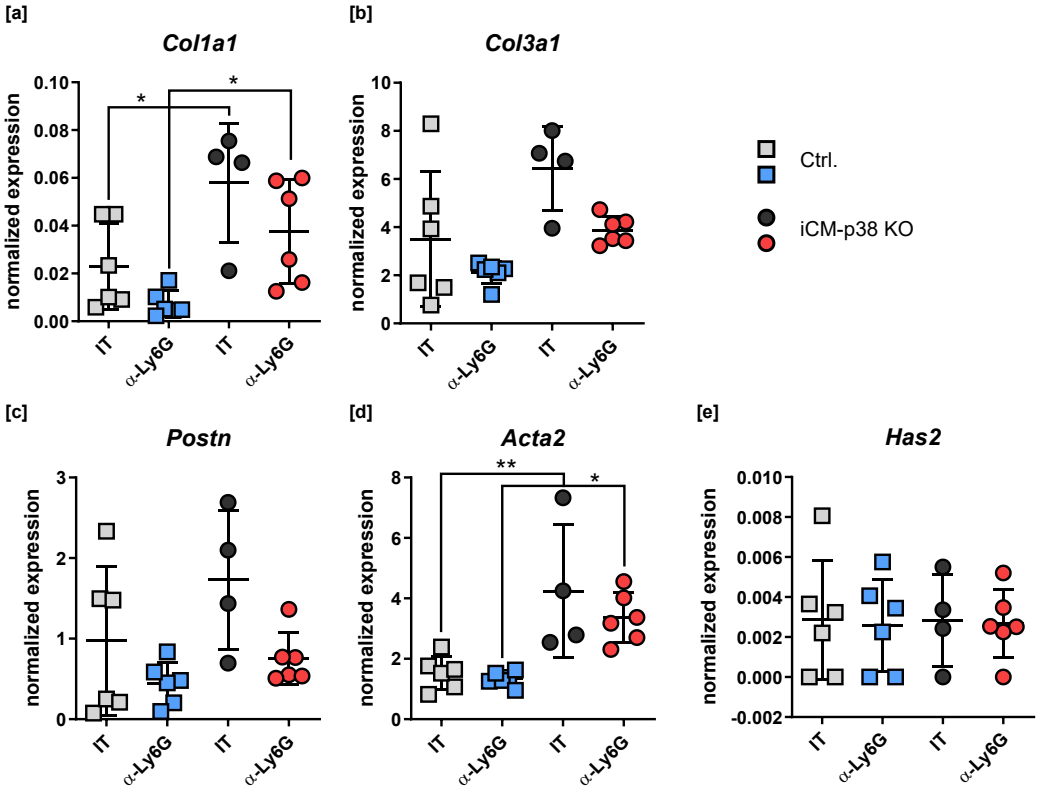

Figure 38: Expression of fibrosis-related genes in iCM-p38 KO (round) and control (square) mice treated with AngII for 7 days and 14 days of additional recovery with (blue and red) or without (gray and black) neutrophil depletion prior to AngII administration. [a] *Col1a1* (*collagen 1a1*) expression is increased in iCM-p38 KO hearts injected with isotype control (IT) compared to controls and is reduced again in iCM-p38 KO hearts injected with α-Ly6G. The same applies for **[b]** *Col3a1* (*collagen 3a1*), **[c]** *Postn* (*periostin*), and **[d]** *Acta2* (*actin alpha 2*) expression. **[e]** *Has2* (*Hyaluronan synthase 2*) expression did not differ between all groups analyzed. Data are normalized to the reference gene *Csnk2b*. Data are presented as mean ±SD, n = 4-6 Statistical significance was calculated by using One-way ANOVA with Tukey's multiple comparisons test (* p<0.05; **p<0.01).

Postn expression was increased by 1.7-fold in iCM-p38 KO (IT) mice compared to IT-injected controls. α-Ly6G injection reduced the expression by 2.3-fold in iCM-p38 KO hearts, and a minor reduction in expression was measured as well in controls when injected with α-Ly6G compared to IT-injected controls (Figure 38c).

The effect on *Acta2* expression was even stronger. A 2.8-fold increase was measured in iCM-p38 KO (IT) compared to controls (IT). α-Ly6G injection reduced the expression by 1.2-fold in iCM-p38 KO hearts. In this case, no differences in *Acta2* expression were observed between α-Ly6G-injected and IT-injected controls (Figure 38d). Also, *Has2* expression did not differ between all four groups analyzed (Figure 38e).

In addition, genes that are expressed in so-called matrifibrocyte were analyzed. A 2.4-fold increase was measured for *Comp* expression in iCM-p38 KO (IT) mice compared to controls (IT). α-Ly6G injection caused a 1.3-fold reduction in iCM-p38 KO hearts and even a 4.2-fold reduction in controls (Figure 39a).

Tnsf11b expression was increased 2.6-fold in iCM-p38 KO (IT) mice compared to the respective controls. In the hearts of mice injected with α-Ly6G, a reduction of 3.2-fold in iCM-p38 KO hearts and 1.8-fold in control hearts was measured (Figure 39b). Although the reduction in gene expression due to the α-Ly6G injection in iCM-p38 KO mice did not reach statistical significance, a trend was observed, leading to the assumption that an initial neutrophil depletion leads to an approximation to the conditions of control mice.

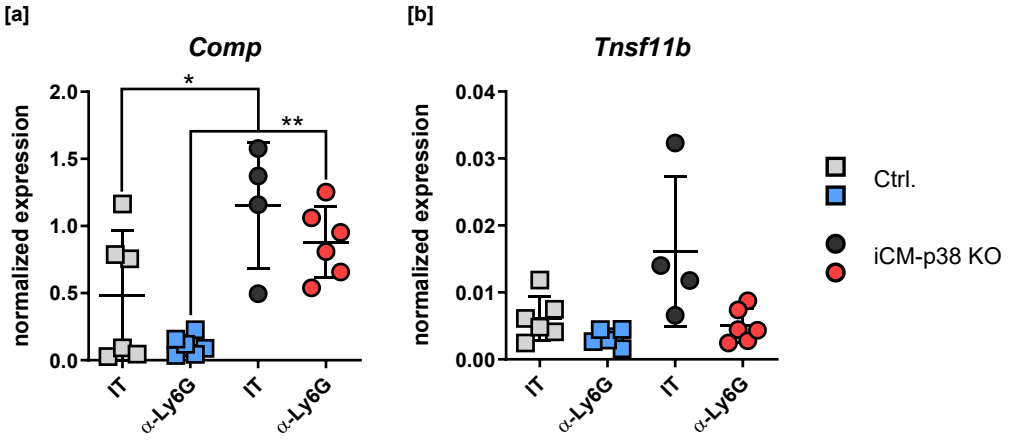

Figure 39: Expression of genes related to matrifibrocyte in iCM-p38 KO (round) and control (square) mice treated with AngII for 7 days and 14 days of additional recovery with (blue and red) or without (gray and black) neutrophil depletion prior to AngII administration. [a] *Comp* (*cartilage oligomeric matrix protein*) expression was increased in iCM-p38 KO hearts injected with isotype control (IT) compared to controls and decreased in iCM-p38 KO hearts injected with α-Ly6G. The same applies for **[b]** *Tnsf11b* (*TNF receptor superfamily member 11b*) expression. Data are normalized to the reference gene *Csnk2b*. Data are presented as mean ±SD, n = 4-6. Statistical significance was calculated by using One-way ANOVA with Tukey's multiple comparisons test (* $p<0.05$; ** $p<0.01$).

In conclusion, an increased fibrotic area indicated by WGA^+ staining in heart sections as well as an increased expression of genes related to the onset of fibrosis and maker genes for matrifibrocytes were observed in IT-injected iCM-p38 KO hearts after 7d AngII + 14d

of recovery. These results confirm the findings described in 4.3.3. Furthermore, the depletion of neutrophils prior to the start of the AngII administration caused a trend towards decreased ECM deposition in cardiac tissue. Additionally, gene expression of genes related to fibrosis was reduced due to neutrophil depletion. These results indicate that the process of fibrosis is slowed down or even inhibited in iCM-p38 KO mice when injected with α-Ly6G.

4.5 Interorgan communication between the failing heart and skeletal muscle in the iCM-p38 KO mouse model

Heart failure is, in general, not an isolated disease of the heart but rather must be considered as systemic disease. Therefore, another focus of this work was the investigation of the interorgan communication between the failing heart and peripheral organs. The establishment of the long-term iCM-p38 KO model was of great importance in this context since it enables the analysis of the long-term effect of heart failure on skeletal muscle without pharmacological intervention through AngII. To perform additional analyses of interorgan communication, the iCM-p38 KO mouse model was appropriate since it developed persistent heart failure after 7 days of AngII treatment. Therefore, the skeletal muscle of the hind limb was used, and programs of skeletal muscle atrophy were examined.

4.5.1 Induction of cardiac dysfunction through pressure overload led to a short-term decrease in body weight in iCM-p38 KO mice, but had no effect on skeletal muscle weight

The weights of the individual muscles of the hind limb were determined as the first parameter. Therefore, *Musculus soleus* (*M. soleus*), *Musculus plantaris* (*M. plantaris*), and *Musculus gastrocnemius* (*M. gastrocnemius*) were analyzed. To find a suitable normalization for the weight of each muscle, the body weight and heart weight of all iCM-p38 KO and control mice were measured at different time points of AngII treatment as well as after an additional recovery time of 14d. It was observed that the body weight was greatly reduced after 48h, especially in iCM-p38 KO mice. Over time, however, the animals recovered from the loss and almost returned to their baseline weight (Figure 40a). Since heart weight was the same between iCM-p38 KO and control mice at all time points (Figure 40b), this value was used to normalize the muscle weights of *M. soleus*, *M. plantaris,* and *M. gastrocnemius* individually. In addition, total muscle weight was determined. Analysis of muscle weight showed that neither there were differences between control mice and iCM-p38 KO animals nor changes could be determined at the

different time points that were examined. This applies to all three muscles analyzed (Figure 40c–f).

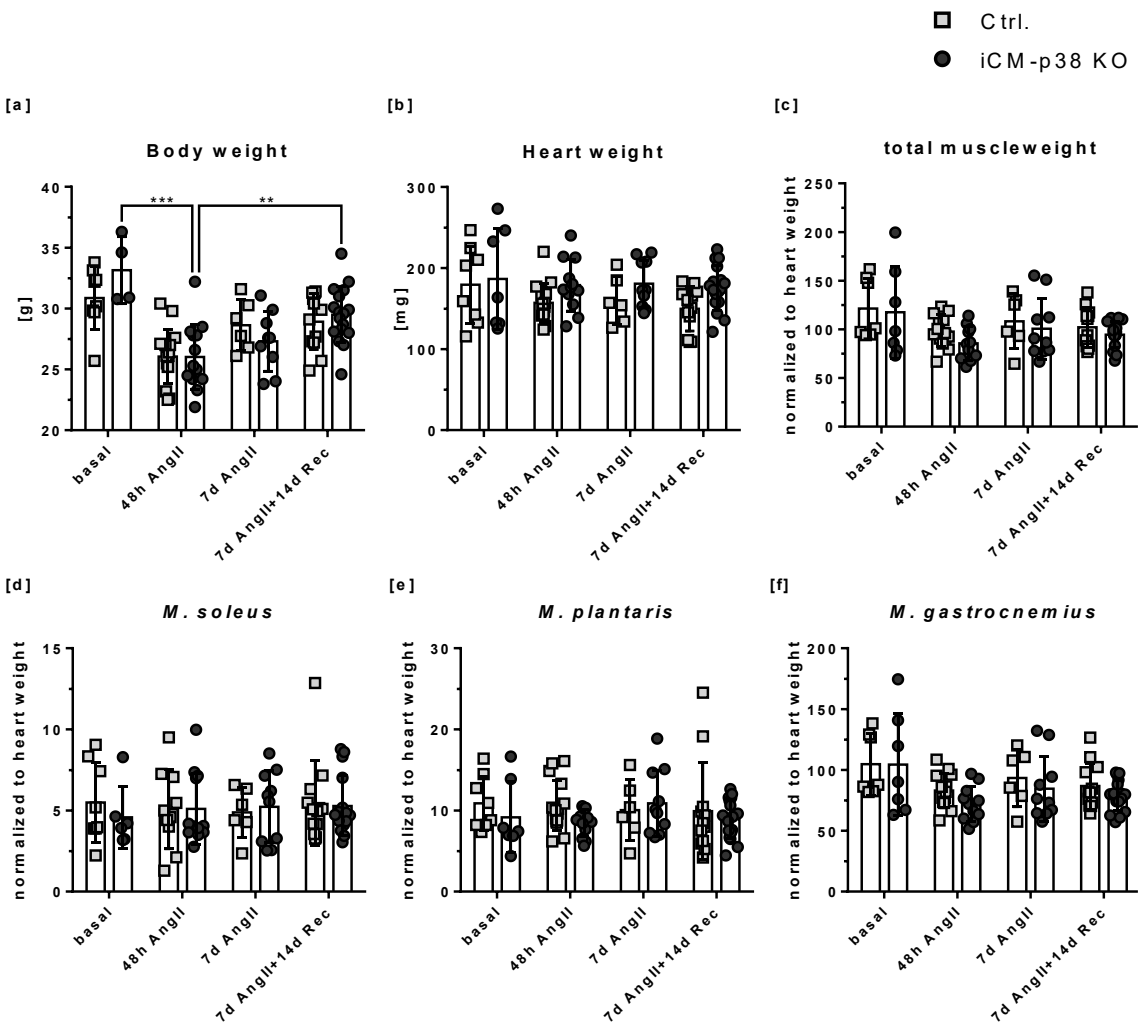

Figure 40: Body-, heart-, and hind limb muscle weight of iCM-p38 KO (round) and control (square) animals after 48h and 7d of AngII treatment, as well as an additional recovery of 14d. [a] The mean body weight of mice is reduced after 48h of AngII administration but increases over time in both groups, while **[b]** heart weight remains mainly unchanged. **[c]** The total muscle weight (normalized to heart weight) did not alter over time and was comparable between the two genotypes. **[d-f]** No differences between iCM-p38 KO and control mice were observed in *M. soleus*, *M. plantaris,* or *M. gastrocnemius* (all normalized to total heart weight) over time. Data are presented as mean ±SD, n = 6-17. Statistical significance was calculated by using Two-way ANOVA with with Bonferroni's multiple comparisons test (** p <0.01; *** p <0.001).

4.5.2 Chronic heart failure has no effect on the composition or size of skeletal muscle fibers in iCM-p38 KO mice

In further histological analysis, the hind limb skeletal muscles of iCM-p38 KO and control mice were examined regarding changes in muscle fiber type composition within the individual muscles. Hind limb skeletal muscles *M. soleus, M. plantaris,* and *M. gastrocnemius* of iCM-p38 KO and control mice were therefore analyzed after 7d of AngII treatment, as well as after 7d of AngII followed by a 14d recovery period. Figure 41 shows representative, microscopic images of the fiber distribution in the different

muscles. Type I fibers are shown in red. Type IIa fibers are green, and type IIb/x fibers remain unstained.

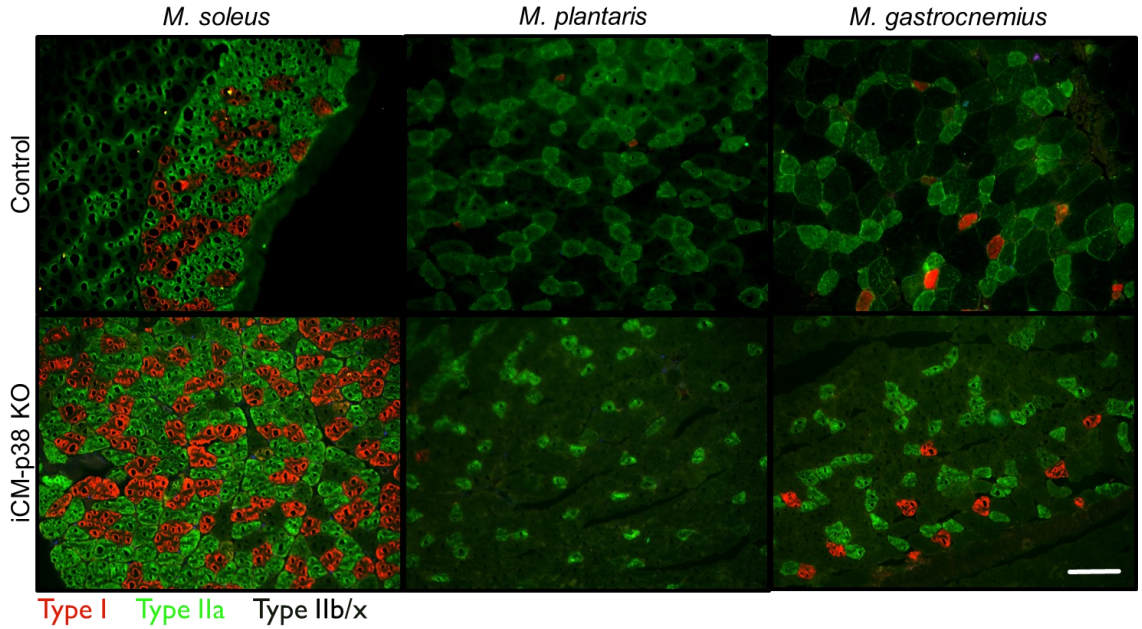

Figure 41: Representative pictures of fiber type composition in hind limb skeletal muscles *M. soleus, M. plantaris,* and *M. gastrocnemius* of iCM-p38 control and KO mice after 7d AngII + 14d recovery. Type I fibers are shown in red. Type IIa fibers are green, and type IIb/x fibers remain unstained. Magnification: 20x. Exposure time: red (1.3 sec) green (1.0 sec). Scale bar: 100 µm.

Quantification of histological images was performed regarding the distribution of fiber types within the different muscles as well as the size of the individual fibers.

Quantification of histological images was performed by counting the fiber types, respectively. Therefore, three images of a muscle were evaluated, and mean values were used to calculate the percentage of fiber types within the three investigated muscles. Analysis of the hind limb skeletal muscle of iCM-p38 control and KO mice over time revealed no differences in the fiber type composition of both genotypes in any of the investigated muscles. Furthermore, no alterations over time occurred in *M. soleus*. The *M. soleus* comprised mainly type I (35-40%) and type IIa (~ 50%) fibers. Less than 15% of all fibers were type IIb/x fibers (Figure 42a+b). The fiber type distribution in *M. plantaris*, on the other hand, looked different. No type I fibers were detected. After 7d AngII treatment, the muscle consisted of 25% type IIa and 75% type IIb/x fibers. After a recovery time of 14d after the end of AngII administration, a slight shift towards type IIb/x fibers was recognized. 80% of all fibers were type IIb/x fibers, whereas type IIa fibers make up about 20% of muscle. However, there were no differences between the two examined genotypes, meaning that the observed shift in fiber type distribution cannot have occurred due to the present cardiac dysfunction in iCM-p38 KO mice (Figure 42c+d). Similar conclusions could be drawn for *M. gastrocnemius,* although unlike *M. plantaris*, about 2-4% of the muscle consisted of type I fibers. After 7d of AngII treatment, the

distribution between type IIa and type IIb/x fibers is approximately the same as in *M. plantaris* at the same time point (type IIa: 20% and type IIb: 75%). This distribution was not changed, even after a recovery period of 14d (Figure 42e+f).

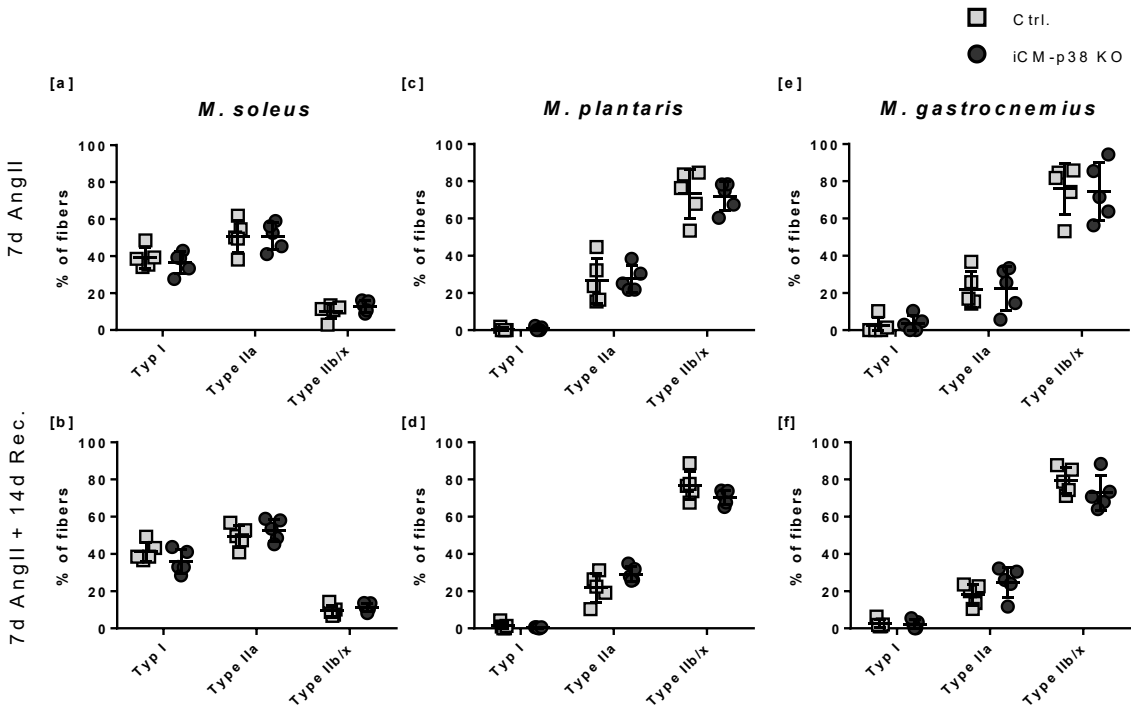

Figure 42: Quantification of fiber type distribution in *M. soleus, M. plantaris,* and *M. gastrocnemius* with 7d AngII treatment and 7d AngII + 14d of recovery in iCM-p38 KO (round) and control (square) mice. [a,b] *M. soleus* is composed mainly of type I and IIa fibers, although type IIb/x fibers were present as well. No changes in fiber type composition over time could be observed. **[c,d]** *M. plantaris* did not contain type I fibers but mainly type IIb/x fibers and, to a lesser extent, type IIa fibers. The shift towards type IIb/x fibers even expanded over time. **[e,f]** Analysis of fiber type composition in *M. gastrocnemius* showed the same results. Between the two genotypes, no differences were observed. Data are presented as mean ±SD, n = 5. Statistical significance was calculated by using One-way ANOVA with Tukey's multiple comparisons test.

The evaluation of the fiber type distribution within the three muscles examined did not show any differences between iCM-p38 KO and control mice. However, the microscopic images suggested that the cross-sectional area of the fiber types in iCM-p38 KO mice was reduced compared to the respective controls (Figure 41). A reduction in cross-sectional area is characteristic of skeletal muscle atrophy and can therefore be used as an additional marker [176]. The fibers of *M. soleus*, *M. plantaris,* and *M. gastrocnemius* were therefore analyzed after 7d of AngII treatment and additionally after 7d AngII treatment + 14d of recovery. In the *M. soleus,* type I, type IIa, and type IIb/x fibers were found. All fibers had an area of around 1500 µm^2 and no differences were observed between the two time points examined (Figure 43a+b). In the *M. plantaris*, only type IIa and IIb/x fibers were evaluated since there were too few type I fibers to analyze them meaningfully. The same applied to the evaluation of the *M. gastrocnemius*. In general,

the area of type IIa and type IIb/x fibers was 1000-1500 µm^2 (Figure 43c–f). No changes over time were observed in these muscles either.

Additionally, the fiber type size was comparable between the muscles of the iCM-p38 KO mice and the controls at all time points and in all analyzed muscles. Hence, no alterations in fiber type size due to the existing heart failure were measured in the iCM-p38 KO mice.

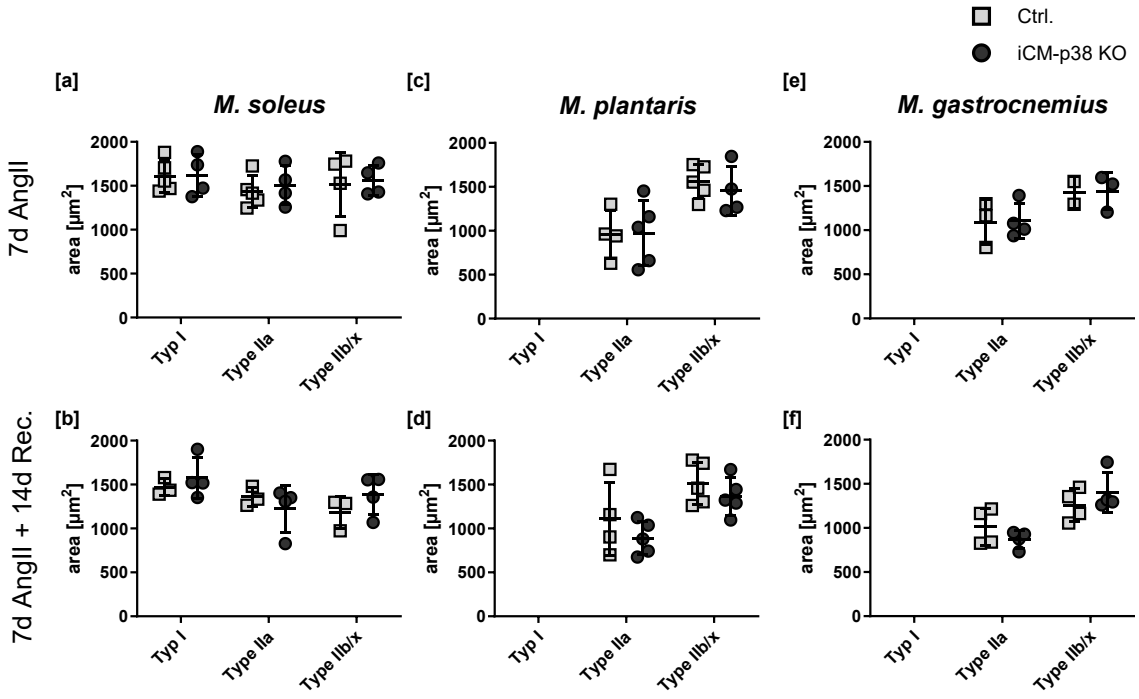

Figure 43: Quantification of fiber type size cross-section in *M. soleus, M. plantaris,* and *M. gastrocnemius* with 7d AngII treatment and 7d AngII + 14d of recovery in iCM-p38 KO (round) and control (square) mice. [a,b] In the *M. soleus,* all fibers had an area of around 1500 µm^2. **[c,d]** In the *M. plantaris,* the number of Type I fibers was minor, therefore, the area could not be determined. Type I fibers had an average area of 1000 µm^2 and Type IIa fibers of 1500 µm^2. **[e,f]** The same applied for analysis of the *M. gastrocnemius*. No differences were measured between the time points or the genotypes. Data are presented as mean ±SD, n = 3-5. Statistical significance was calculated by using One-way ANOVA with Tukey's multiple comparisons test.

4.5.3 Cardiac dysfunction in iCM-p38 KO mice transiently increased expression of atrophy-related genes in *Musculus plantaris*

In order to examine the early onset of muscle atrophy, the skeletal muscle was analyzed on the expressional level. Because fast-twitch glycolytic fibers were shown to be more vulnerable to the processes of atrophy than slow-twitch oxidative fibers, and *M. plantaris* shows the highest content of glycolytic fibers, this muscle was used for these investigations. To explore the beginning of a skeletal muscle wasting program, expression of atrophy-related genes (also called atrogenes) was measured at various time points.

The *Fbxo32* gene encodes for the F-box-only protein 32. This protein functions in phosphorylation-dependent ubiquitination and is overly expressed during muscle atrophy [177]. *Fbxo32* expression in iCM-p38 control mice's muscles was generally low and did not change over time, while in iCM-p38 KO mice, an 8-fold increase was measured after 48h of AngII treatment. This increase diminished after 7d AngII treatment, and the expression stayed low after the recovery phase (Figure 44a).

E3 ubiquitin-protein ligase (*Trim63*, also known as *Murf1*) is an enzyme that is highly expressed during skeletal muscle atrophy, which causes myosin heavy chain degradation, causing loss of muscle mass [177, 178]. Control mice almost do not express *Trim63* at any time in *M. plantaris,* while iCM-p38 KO mice showed an increase of more than 5-fold in *Trim63* levels after 48h of AngII treatment. Again, the increased expression disappeared over time (Figure 44b).

Interestingly, the same results were observed for *Gabarapl1* expression in *M. plantaris*. GABA type A receptor-associated protein like 1 (*Gabarapl1*) causes the formation of phagophores and ultimately leads to autophagy [179, 180]. Here, an increase in expression by 3.2-fold in iCM-p38 KO mice was observed after 48h of AngII treatment compared to baseline conditions, while this increase turned back to baseline levels at later time points. In control hearts, an increase in *Gabarapl1* expression was not observed (Figure 44c).

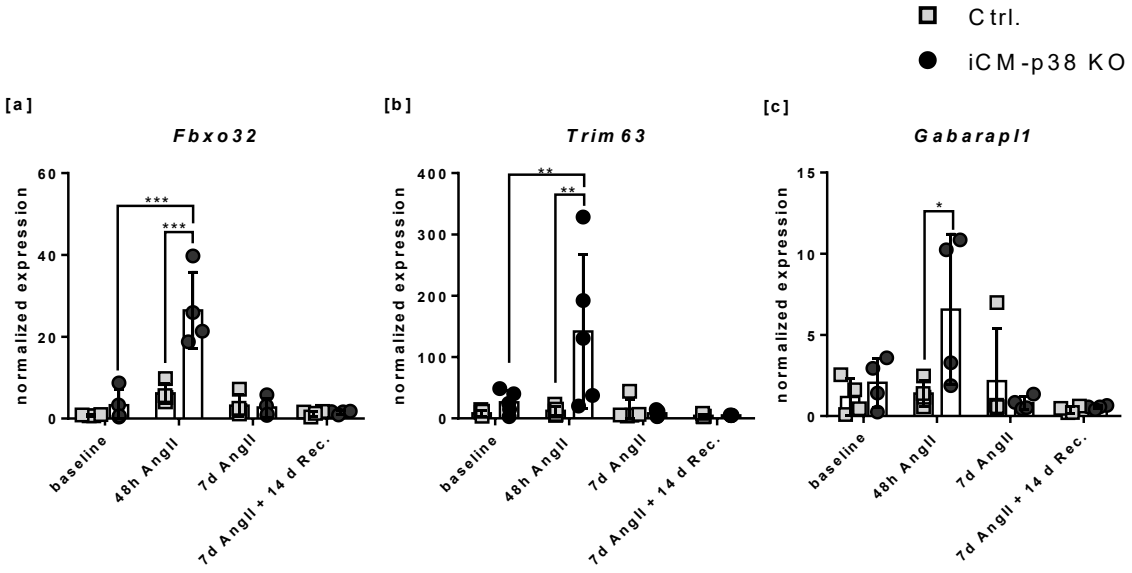

Figure 44: Expression of atrogenes over time in *M. plantaris* of iCM-p38 KO (round) and control (square) mice. [a] Elevation of *Fbxo32* (F-box-only protein 32) expression in iCM-p38 KO mice was observed after 48h of AngII treatment. At later time points, the change was reversed, and the expression returned to the baseline level. In control mice, no changes were observed for all measured time points. The same applies for expression measurements of **[b]** *Trim63* (E3 ubiquitin-protein ligase *Trim63*, also known as *MuRF1* (Muscle Ring-Finger Protein-1)) and **[c]** *Gaparapl1* (GABA type A receptor-associated protein like 1). Data are normalized to *Nudc* expression. Data are presented as mean ±SD, n = 4-5. Statistical significance was calculated by using Two-way ANOVA with Bonferroni's multiple comparisons test (*p<0.05; **p<0.01; *** p<0.001).

The analysis of skeletal muscle tissue in the iCM-p38 mouse model did indeed show the first signs of heart failure-associated muscle wasting. But interestingly, this effect was only detected at the onset of insufficient cardiac function after 48h of AngII treatment. Over time, the expression levels of the atrogenes normalized again and returned to baseline levels, although cardiac dysfunction was still present, as described in 4.3.1.

4.6 The iCM-AKT1/2 KO mouse model with cardiac atrophy to study the interorgan communication between the deficient heart and skeletal muscle

The iCM-AKT1/2 mouse model differs in some respects from the iCM-p38 mouse model. In iCM-AKT1/2 KO mice, no additional pharmacological treatment is required to induce cardiac dysfunction; solely the elimination of the two AKT isoforms is sufficient. Furthermore, mice do not develop dilation but rather show a severe form of cardiac atrophy associated with substantial functional depression. To analyze the interorgan communication between the failing heart and the skeletal muscle, the initial weights of the individual muscles were measured before a closer look was drawn to the fiber type composition via immunohistochemistry.

4.6.1 Cardiac atrophy in iCM-AKT1/2 KO mice has no effect on body weight or skeletal muscle weight

Even though iCM-AKT1/2 KO mice develop severe cardiac dysfunction 14 days after the start of the KO induction, no significant reduction in body weight or total hind limb muscle weight was measured in the course of the 21-day experiment (Figure 45a). Since the body weight did not change over time, it was used to normalize the weight of the skeletal muscle to the body weight. The weight of the hind limb skeletal muscle (*M. soleus*, *M. plantaris* and *M. gastrocnemius* together) did not show any differences between the two genotypes or alterations over time (Figure 45b).

Despite this, the individual muscles were also examined separately to see whether specific muscles were affected. The results also showed that the weight of the individual muscles was the same between iCM-AKT1/2 KO mice and respective controls and also did not change over time (Figure 45c-e). Based on the muscle weights, no effect of heart failure on the skeletal muscle could be determined. However, modifications of the muscle could still be present. Therefore, fiber type composition was investigated in further experiments.

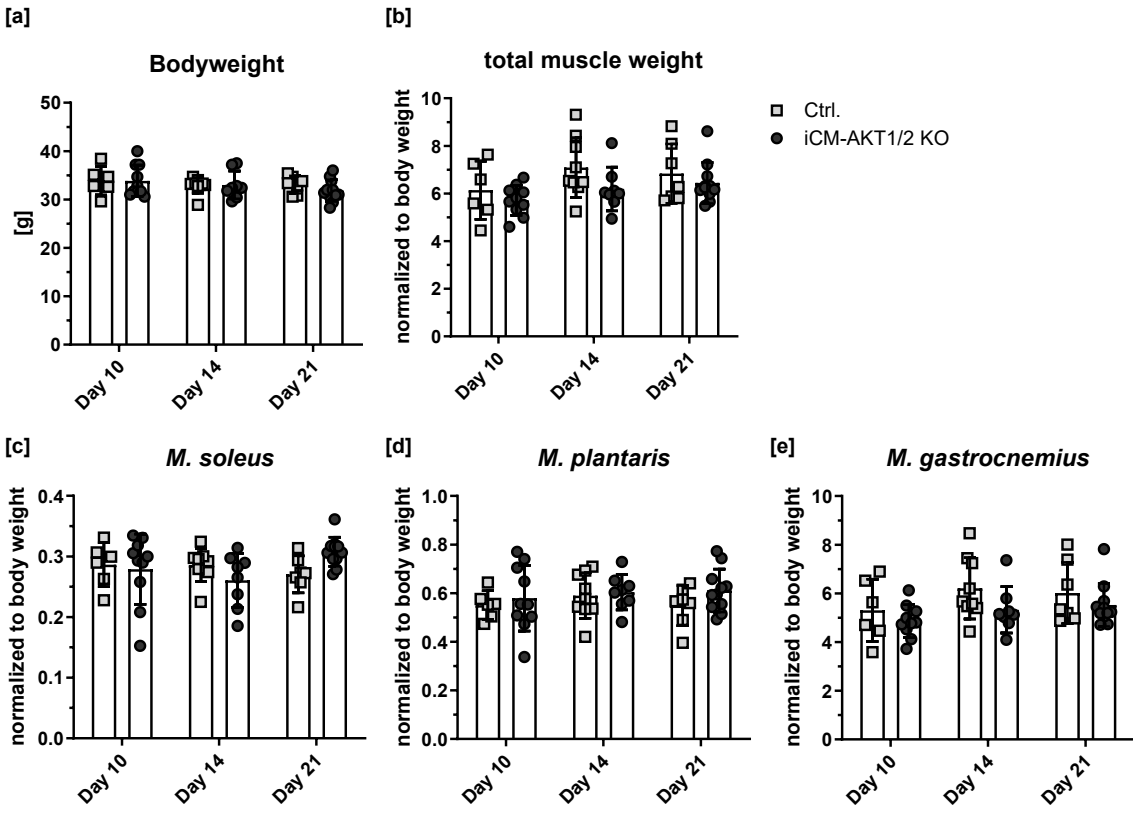

Figure 45: Body- and hind limb muscle weights of iCM-AKT1/2 KO (round) and control (square) animals 10, 14 and 21 days after the start of tamoxifen injection. [a] The mean body weight of mice was marginally decreasing over time in both groups, **[b]** while total muscle weight (normalized to body weight) slightly increased. No differences between iCM-AKT1/2 KO and control mice were observed in **[c]** *M. soleus*, **[d]** *M. plantaris* or **[e]** *M. gastrocnemius* (all normalized to body weight) over time. Data are presented as mean ±SD, n = 6-10. Statistical significance was calculated by using Two-way ANOVA with Bonferroni's multiple comparisons test.

4.6.2 Fiber type distribution in the skeletal muscle of iCM-AKT1/2 mice is unaltered despite heart failure

Histological analysis of the hind limb skeletal muscles of iCM-AKT1/2 KO and control mice were examined regarding the fiber type composition within the individual muscles. Hind limb skeletal muscles (*M. soleus, M. plantaris,* and *M. gastrocnemius*) of iCM-AKT1/2 KO and control mice were therefore analyzed at three time points after the start of the tamoxifen injection. Figure 46 shows representative, microscopic images of the fiber distribution in the different muscles. Type I fibers are shown in red. Type IIa fibers are green, and type IIb/x fibers remain unstained or blue.

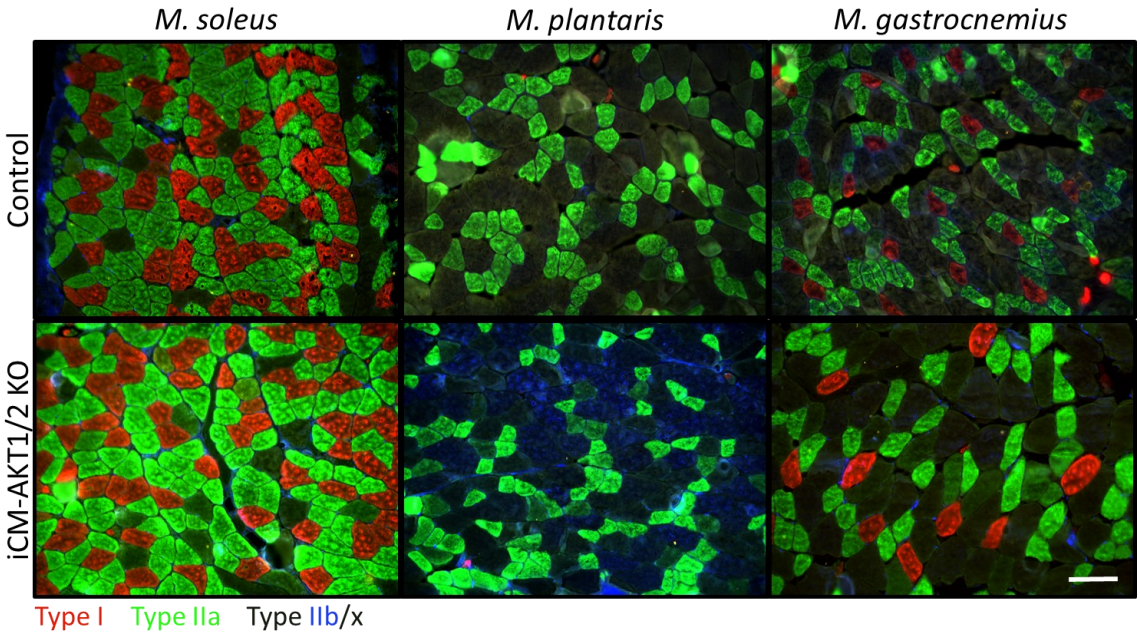

Figure 46: Representative pictures of the fiber type composition in the hind limb skeletal muscles *M. soleus, M. plantaris,* and *M. gastrocnemius* of iCM-KT1/2 control and KO mice 10 days after the start of tamoxifen injection. Type I fibers are shown in red. Type IIa fibers are green, and type IIb/x fibers were stained blue or remained unstained. Magnification: 20x. Exposure time: red (1.3 sec) green (1.0 sec). Scale bar: 100 µm.

Quantification of histological analysis of hind limb skeletal muscles of iCM-AKT1/2 control and KO mice was performed as described in 4.5.2. Over time, no differences in fiber type composition between control and KO animals in any of the investigated muscles were observed. *M. soleus* comprised mainly type I (37%) and type IIa (47%) fibers. Less than 20% of all fibers were type IIb/x fibers (Figure 47a-c). The fiber type distribution in *M. plantaris*, on the other hand, looked different. No type I fibers were detected. On day 10, after the start of tamoxifen treatment, the muscle consisted of 40% type IIa and 60% type IIb/x fibers. Over time, a slight shift towards type IIb/x fibers could be recognized. 77% of all fibers were type IIb/x fibers, whereas type IIa fibers make up about 23% of muscle. Despite this, there were still no differences between the two examined genotypes (Figure 47d-f). Similar conclusions could be drawn for *M. gastrocnemius,* although unlike *M. plantaris*, about 10% of the muscle consisted of type I fibers. At the first time point examined, at day 10 after the start of tamoxifen injection, the distribution between type IIa and type IIb/x fibers was approximately the same. At day 14 and 21, the amount of type IIa fiber lessened to 30% and more type IIb/x fibers were counted (65%) (Figure 47g-i). When comparing the fiber type composition of hind limb skeletal muscle from iCM-AKT1/2 KO and control mice to iCM-p38 KO and control mice, the results were very similar. This relates to the distribution of fibers within the individual muscles on the one hand, and the lack of alteration between the two genotypes on the other.

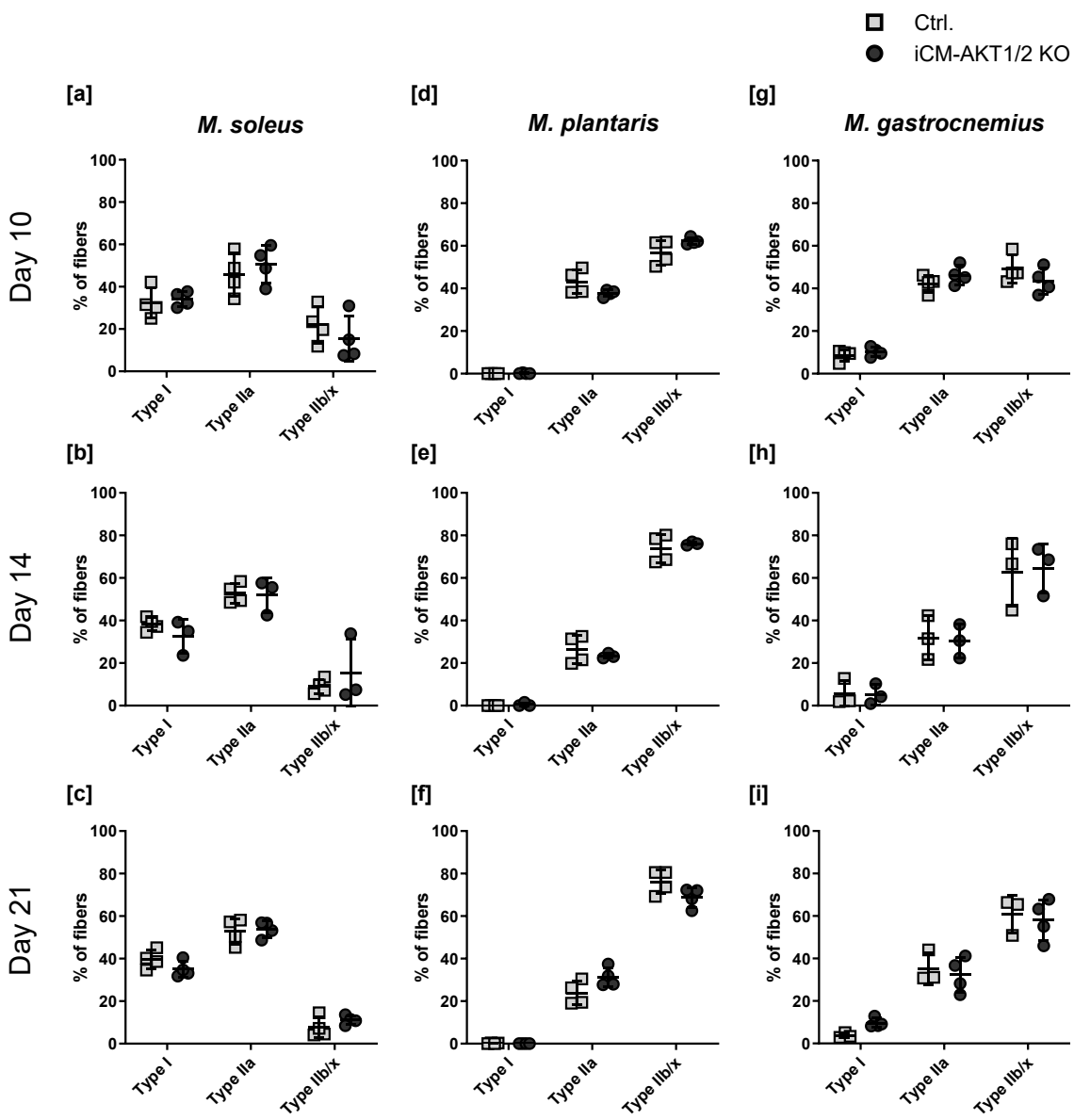

Figure 47: Quantification of histological analysis of fiber type composition in *M. soleus, M. plantaris,* and *M. gastrocnemius* at day 10, 14 and 21 after the start of tamoxifen injection in iCM-AKT1/2 KO (round) and control (square) mice. [a-c] *M. soleus* consists mainly of type I and IIa fibers, although type IIb/x fibers were present as well. No changes in fiber type composition over time were observed. **[d-f]** *M. plantaris* does not have type I fibers; therefore, it has mainly type IIb/x fibers and, to a lesser extent, type IIa fibers. Over time, the shift towards type IIb/x fibers even expanded. **[g-i]** The same applies for the fiber type composition in *M. gastrocnemius*. Between the two genotypes, no differences were observed. Data are presented as mean ± SD, n = 5. Statistical significance was calculated by using One-way ANOVA with Tukey's multiple comparisons test.

4.6.3 Atrophy-related genes are elevated in *Musculus plantaris* of iCM-AKT1/2 KO mice near the end of the animal's lifespan

Although histological studies gave no evidence of changes in the fiber-type composition of skeletal muscle from iCM-AKT1/2, further analysis was performed regarding the expression of atrogenes in the muscle. In further experiments, gene expression data from hind limb skeletal muscle *M. plantaris* intended to indicate whether the start of a

skeletal muscle wasting program is taking place. Five genes known to be upregulated in skeletal muscle atrophy were analyzed on an expressional level using quantitative PCR.

The *Mstn* gene encodes for the myostatin protein and belongs to the TGF beta family [181, 182]. Elevated levels of myostatin cause substantial loss of skeletal muscle and body fat [183, 184]. *Mstn* expression of *M. plantaris* in control mice did not change over time, while in iCM-AKT1/2 KO, expression increased by 2.5-fold 21 days after the start of tamoxifen injection (Figure 48a).

An increased expression of the IL-6 receptor (*IL-6ra*) indicates an imbalance of growth factor-related signaling favoring catabolic pathways via STAT3 and STAT5 signaling [185]. *IL-6ra* expression was exclusively elevated in iCM-AKT1/2 KO mice 21 days after start of tamoxifen in injection. An increase of around 16-fold compared to 10 days could be measured, while in control mice the expression stayed at a low level (Figure 48b).

Fbxo32 expression in *M. plantaris* of iCM-AKT1/2 control mice was inferior and did not change over time, while again in iCM-AKT1/2 KO mice, a 6.5-fold increase was measured at day 21 after KO induction compared to day 10 (Figure 48c).

Further, iCM-AKT1/2 control mice did not express *Trim63* at any time in *M. plantaris,* while iCM-AKT1/2 KO mice showed a 10-times elevation of *Trim63* levels 21 days after KO induction (Figure 48d).

Foxo3 proteins belong to the O subclass of the forkhead family of transcription factors and function as triggers for apoptosis while upregulating genes involved in cell death and downregulating the expression of anti-apoptotic genes [186-188]. Expression of *Foxo3* did not differ in *M. plantaris* of iCM-AKT1/2 control mice between the three time points. On the other hand, an increase in *Foxo3* expression by 2.7-fold could be observed in iCM-AKT1/2 KO mice at day 21 compared to day 10 (Figure 48e).

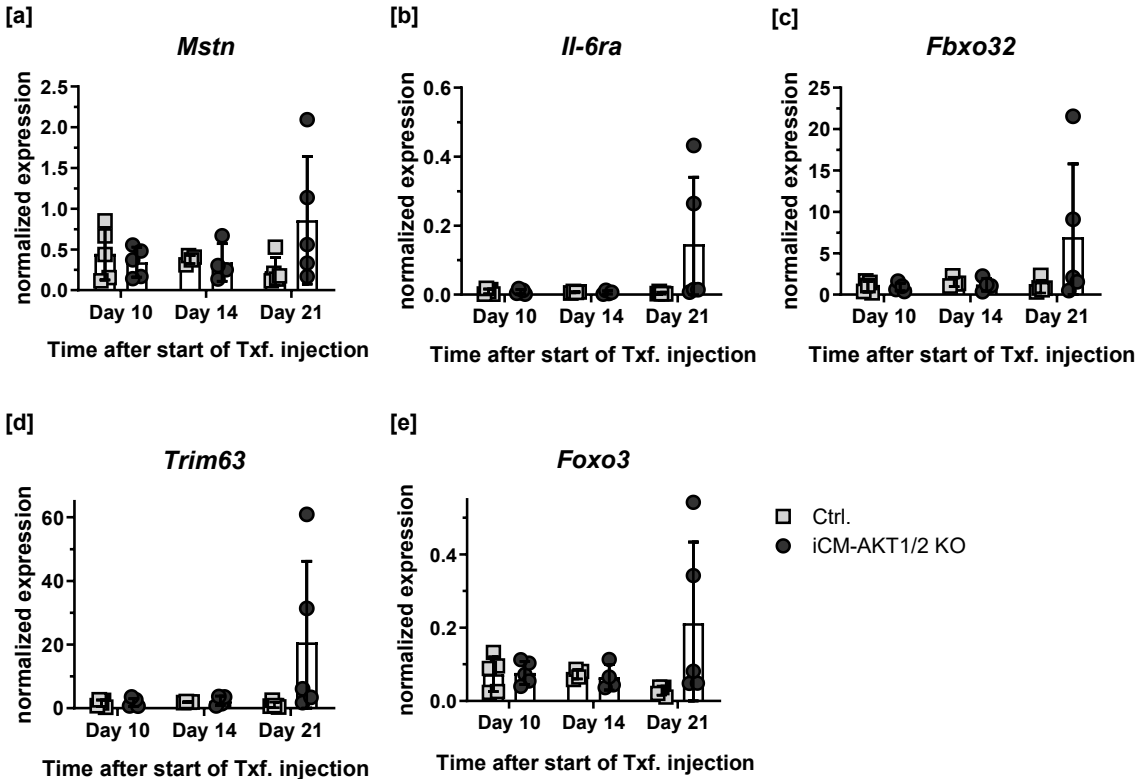

Figure 48: Expression of atrogenes over time in *M. plantaris* of iCM-AKT1/2 KO (round) and control (square) mice. [a] *Mstn* (Myostatin), **[b]** *IL-6ra* (Interleukin-6 receptor), **[c]** *Trim63* (E3 ubiquitin-protein ligase TRIM63, also known as MuRF1 (Muscle Ring-Finger Protein-1)), **[d]** *Fbxo32* (F-box-only protein 32), and **[e]** *Foxo3* (Forkhead-Box-Protein O3) were tested in both groups 10, 14 and 21 days after the start of tamoxifen injection. All expression profiles revealed an increased expression in iCM-Akt1/2 KO mice at day 21 after the start of tamoxifen injection, while this increase was not seen in the respective control mice. Data are normalized to *Hprt1* expression. Data are presented as mean ±SD, n = 4-5. Statistical significance was calculated by using Two-way ANOVA with Bonferroni's multiple comparisons test.

Interestingly, the expression of all investigated genes varies greatly at day 21 between the individual animals of the iCM-AKT1/2 KO group (Figure 48a-e). Since the lifespan of these animals shows that the KO animals die more frequently from day 21 on (Figure 7f), it can be hypothesized that the increased expression of atrogenes is present in the animals that would soon have died, while atrogenes are expressed at lower levels in animals with a longer survival time. This hypothesis is supported by the fact that the expression of the examined genes is always increased in the same animals. Since it cannot be predicted exactly when an animal will die, a study to confirm this hypothesis poses difficulties.

5. Discussion

With 2.4% of the adult population, heart failure is one of the most common diseases in western countries. Globally, around 64 million people are affected. Thanks to improved treatment options, the incidence rates are stable and no longer increase in industrialized countries for the first time however, further research is still essential for the development of treatments for CVD [1, 2]. Therefore, understanding how CVD evolves, how it can be treated effectively, and, at best, how it can be prevented, is of utmost importance. This work contributes to understanding the mechanisms involved in the development of persistent cardiac insufficiency. Therefore, a heart failure mouse model was used. In this model, the cardiomyocyte-specific deletion of p38 MAPKα results in reduced LV pump function and the infiltration of lipids and immune cells into cardiac tissue after 48h of pressure overload via AngII.

Through this thesis, the following new perspectives about the iCM-p38 KO mouse model were obtained:

1. Based on transcriptional analysis (12h after start of AngII treatment), genes assembled under the pathway of “oxidative phosphorylation” were already downregulated, suggesting that metabolic depression is one of the earliest pathomechanisms leading to heart failure in iCM-p38 KO mice.
2. Excessive sympathetic tone is not the main trigger of HF.
3. A short-term PO of 48h did not cause persistent cardiac insufficiency; however, a prolongation of the PO to 7d induced chronic HF.
4. Early infiltrating neutrophils are largely responsible for the development of HF, as depletion of these leads to a significant improvement in cardiac function.

5. In the short term, increased skeletal muscle wasting can be observed in HF-affected iCM-p38 KO mice. However, this effect disappears over time, although cardiac function remains impaired.

The results of all performed experiments are discussed below and classified according to the current state of the art.

5.1 Induction of pressure overload rapidly triggers metabolic dysfunction in iCM-p38 KO hearts

The iCM-p38 KO mouse model used in this study was described before by Bottermann et al. [41] and gives evidence that deletion of cardiomyocyte p38 MAPKα contributes to metabolic and functional depression of the heart in response to PO. The deletion of the p38 MAPKα stress kinase alone had no effect on cardiac function as determined by echocardiography, although the hearts had already established an insulin resistance [103]. Treatment with AngII, which causes pressure overload, triggered a severe dilation of the left ventricle, resulting in reduced cardiac function already 48h after the start of the AngII treatment. Above all, the EDV and the ESV increased, which led to a strong reduction of the EF (see 4.1). At this time, Bottermann et al. also found mitochondrial dysfunction and reduced β-oxidation in the affected hearts. Based on these results, the cardioprotective role of p38 MAPKα in mice facing PO was demonstrated. Interestingly, during the development of heart failure in iCM-p38 KO mice, no hypertrophy of the LV was observed, which normally occurs during the establishment of the disease. This course of heart failure is unusual, as hypertrophy is typically considered a compensatory mechanism for maintaining the pumping function of the LV. Hypertrophy is characterized by the enlargement of cardiomyocyte mass without an increase in cell number, which ultimately leads to an increase in ventricle mass. p38 MAPKα activation, therefore, must be crucial for the development of hypertrophy of cardiomyocytes. This finding obtained in *in vivo* experiments is in line with work by Zechner et al., who showed that pharmacological inhibition of p38 MAPKα/β through SB203580 prevents hypertrophic growth in cardiomyocytes *in vitro* [189].

Up to this point, the changes in iCM-p38 KO hearts were mainly examined after 48h of AngII treatment. Earlier changes that may cause the distinct cardiac phenotype have not been addressed yet. Therefore, in this work, a focus was placed on the early changes. Hence, RNA sequencing analysis of the heart was performed after just 12h of AngII treatment. Despite the short time of AngII treatment, already two pathways were found that were differently expressed (absolute Z-score >2) in iCM-p38 KO hearts compared to the respective controls. These were “Oxidative Phosphorylation” and “Superpathway

of Inositol Phosphate Compounds"/"3-phosphoinositide Biosynthesis". Whereas a reduction of the "Oxidative Phosphorylation" pathway was observed in iCM-p38 KO hearts, an activation of the other pathway was detected. Reduced gene expression of genes belonging to the "Oxidative Phosphorylation" pathway potentially indicates early depression of mitochondrial function in iCM-p38 KO hearts. Interestingly, the "Oxidative Phosphorylation" pathway was also one of the most altered signaling pathways after 48h of AngII treatment. This result shows that fatty acid oxidation, which is the main source of energy in a healthy heart [8-10], is severely restricted right from the beginning of the AngII administration. In such a case, glucose normally becomes the main energy source [11-13]. However, since the iCM-p38 KO hearts already suffer from insulin resistance under basal conditions [103], glucose utilization may also be limited, and energy depletion occurs.

Members of the "Superpathway of Inositol Phosphate Compounds" and "3-phosphoinositide Biosynthesis" pathways are involved in processes like DNA metabolism, mRNA export, and regulation of gene expression. Phosphoinositides are phosphatidic acids that are integrated into the cell membrane. They play a key role in signal transduction and act as secondary messengers to transmit signals within a cell [190]. *Ip6k3*, for example, is one of the genes that was found to be upregulated in the hearts of iCM-p38 KO mice already after 12h of AngII treatment. Diabetes, fasting, and muscle disuse conditions all cause upregulation of this gene in the skeletal muscle and heart of mice. *Ip6k3*$^{-/-}$ mice have lower blood glucose levels, enhanced glucose tolerance, reduced plasma insulin level, and lower body weight due to decreased fat mass. Additionally, *Ip6k3*$^{-/-}$ mice have a prolonged lifespan, proving the importance of *Ip6k3* in cellular regulation and its metabolic impact [191]. Increased expression of this gene is therefore likely to have the opposite effect and negatively impact substrate metabolism in iCM-p38 KO mice, thus contributing to the severe phenotype of these mice.

5.2 Elevated sympathetic activity is not the main cause for cardiac dysfunction in iCM-p38 MAPKα KO mice

Cardiac functional depression is usually associated with elevated sympathetic stimulation, which is a typical response to a drop in contractive function and blood pressure. Elevation of heart rate and inotropy, together with increased total peripheral resistance, are suitable mechanisms to normalize blood pressure. However, in cases of heart failure, β-adrenergic stimulation may exacerbate heart failure condition because it elevates oxygen demand of the heart. Another effect of elevated sympathetic tone would be an enhanced lipolysis in white adipose tissue. Interestingly, we have shown before

that iCM-p38 KO mice have elevated lipolysis and increased lipid deposition in cardiomyocytes [41, 102], which is most likely the consequence of increased β-adrenergic activity due to AngII-induced heart failure [192].

One attempt to rescue the strongly deteriorated cardiac function in iCM-p38 KO mice after AngII administration was therefore an additional treatment with propranolol (PR). PR is a non-selective β-adrenoceptor antagonist that blocks β_1- and β_2-receptors. Initial attempts to establish the combined treatment of AngII and PR using osmotic mini pumps were successful. Invasive blood pressure measurements revealed that mice treated with PR no longer responded to s.c. administration of the β_1- and β_2-agonist dobutamine, which is usually known to increase heart rate [193, 194]. Although Calligaris et al. [194] additionally reported a dobutamine-induced increase in systolic and diastolic blood pressure, these effects could not be confirmed by this work. It must be noted that in Calligaris work, dobutamine was provided intravenously over a longer period of time (20 minutes) and was steadily increased from 0-14 ng/g/min. In this thesis, however, dobutamine was given s.c. in a single injection of 1 µg/g. The different types of applications could explain the different results.

In addition, PR treatment inhibited an AngII-induced increase in non-esterified fatty acid (NEFA) levels in iCM-p38 KO mice. Sympathetic stimulation results in an increased release of catecholamines by postganglionic fibers and the adrenal medulla, which in turn enhances lipolysis in adipose tissue [195-197]. This can be measured in blood plasma as NEFA levels. By inhibiting $\beta_{1/2}$-receptors through PR, the effects of catecholamines are attenuated, and lipolysis is not activated, resulting in reduced circulating NEFA levels. In this work, a slight decrease in NEFA levels was observed in mice treated with PR. The lack of full inhibition of lipolysis could be due to β_3-receptors [198], which are largely responsible for the activation of lipolysis in rodents but are not targeted by PR. Therefore, lipolysis may only be restricted partially, and NEFA levels were less reduced than expected.

Besides lipolysis, the effect of PR treatment on cardiac function of iCM-p38 KO and control mice was analyzed 48h after the start of AngII/(+PR) treatment. In all PR-treated mice, a reduction in heart rate was measured, but overall, only minor improvements in heart function due to PR treatment were measured in iCM-p38 KO mice. The ESV was slightly reduced, resulting in a small elevation of the EF. Additionally, the SV was significantly increased. The analysis of immune cell infiltration in cardiac tissue of AngII/(+PR)-treated iCM-p38 KO and control mice revealed reduced numbers of monocytes ($Ly6C^{high}$) and neutrophils in PR-treated iCM-p38 KO mice compared to only AngII-treated iCM-p38 KO mice. On the other hand, the number of dendritic cells (DCs)

was significantly increased and reached the same level as AngII/(+PR)-treated control mice.

Figure 49 summarizes the processes in HF conditions and the differences due to additional PR treatment in iCM-p38 KO mice. HF, induced by pressure overload via AngII, causes most likely sympathetic overstimulation. Therefore, catecholamines, e.g., norepinephrine, are increasingly released by the adrenal medulla and the postganglionic fibers of the sympathetic nervous system [195, 196]. Thus, lipolysis in adipose tissue is activated, and circulating NEFA levels rise [197]. This causes an accumulation of lipids in cardiac tissue. The damage to cardiomyocytes and the release of DAMPs in turn attract immune cells, particularly neutrophils, to infiltrate the heart. This results in a worsening of cardiac function. Inhibition of sympathetic overstimulation through β-blockers, e.g., propranolol, reduces catecholamine release. Lipolysis is therefore not activated, and NEFA levels are reduced. Additionally, PR treatment directly blocks β-receptors in adipose tissue, preventing lipolysis even stronger. Thus, lipid accumulation and immune cell infiltration in heart tissue should be reduced and cardiac function preserved. Although the effectiveness of the PR treatment was demonstrated (heart rate and NEFA level were decreased), the effect on immune cell infiltration and preservation of cardiac function was less than expected.

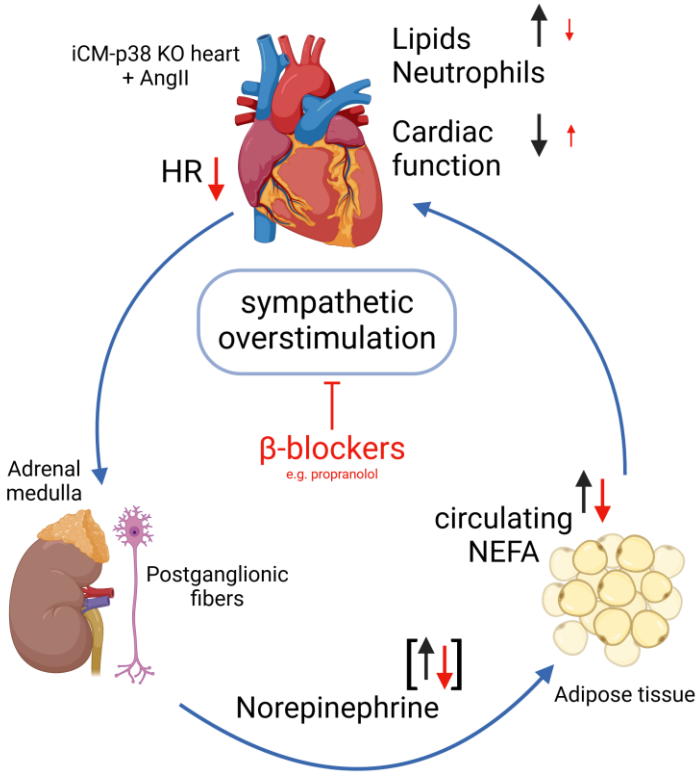

Figure 49: Effects of β-blocker (propranolol) treatment in iCM-p38 KO mice. Black arrows indicate processes of AngII-induced HF in iCM-p38 KO mice. Red arrows show changes due to additional PR administration in those mice. The size of the arrows indicates the magnitude of the impact. When arrows are in brackets, values were not measured but anticipated. ⊣ indicates inhibition. HR: heart rate; NEFA: non-esterified fatty acid. Created with BioRender.com.

Since cardiac function was not significantly improved in PR-treated iCM-p386 KO mice, it is demonstrated that excessive activation of the SNS is not the main cause of cardiac dysfunction in iCM-p38 KO mice. It can be concluded that either the selected β-blocker is not fully restricting lipolysis or that the elevated lipolysis is not the cause of heart failure. However, earlier work showed that direct inhibition of lipolysis via atglistatin treatment leads to a significant reduction of lipid droplet accumulation in cardiac tissue, accompanied by partially restored cardiac function in iCM-p38 KO mice. Additionally, the number of infiltrating neutrophils was reduced, suggesting that these are attracted due to the lipid droplet accumulation in the myocardium [41, 102]. Based on these previous findings in the iCM-p38 KO mouse model, it can be assumed that restriction of SNS stimulation via β-blocker did not inhibit lipolysis sufficiently. As already described, lipolysis in adipose tissue depends to a large extent on β_3-receptors, which are not targeted by the used β-blocker propranolol. This would explain the minor influence of PR treatment on the cardiac function of iCM-p38 KO mice. For selective β_3-receptor inhibition, SR59230A and L748337 are most commonly used [199]. However, these are not effective for β_1- and β_2-receptor inhibition; thus, two different β-receptor antagonists need to be administered to effectively inhibit all three subtypes of β-receptors.

5.3 Establishment of a mouse model with persistent cardiac insufficiency without pharmacological intervention

The iCM-p38 KO mouse model is characterized by a rapid and impressive HF condition just within 48h of AngII administration. However, up to this point, functional and metabolic changes in the hearts of iCM-p38 KO mice were only examined at early time points (up to 48h of AngII treatment). The analysis of the cardiac function beyond the AngII administration should reveal if the short-term AngII treatment is sufficient to trigger persistent chronic heart failure. A recovery time of 14d after the end of AngII administration showed a return to almost normal heart function in iCM-p38 KO mice (see 4.3). Although severe heart failure rapidly develops in these animals just within 48 hours, the effect is not sustained, indicating that the process of cardiac remodeling is still in its early stages.

5.3.1 Long-term AngII treatment causes cardiac remodeling of iCM-p38 KO hearts characterized by dilation and fibrosis

Since 48h of AngII treatment did not cause persistent HF in iCM-p38 KO mice, the AngII treatment was prolonged to 7d. Body weight and cardiac function were analyzed

regularly, even 14d beyond the AngII administration, to investigate if the cardiac dysfunction remained even without the influence of AngII.

Regular measurements of body weight initially showed a reduction in iCM-p38 KO and control mice. However, after 48h of AngII, control mice gained weight again, even though the AngII treatment remained. In iCM-p38 KO mice, a decrease in body weight was observed until the end of AngII treatment. Weight gain only occurred again during the 14d recovery period. The initial loss of body weight may have occurred as a result of the surgery to implant the osmotic mini pumps. Mice probably consumed less food and water, which explains the weight loss.

During the time of PO, cardiac function was reduced in iCM-p38 KO mice but only slightly decreased in controls. However, prolonged AngII treatment in iCM-p38 KO mice resulted in sustained HF, and cardiac function could no longer recover even after the end of AngII administration (see 4.3.1).

Even though it is already known that prolonged PO causes hypertrophy of the cardiac muscle, no change in ventricular thickness was found, even in control animals. Although AngII is known to be a potent modulator of blood pressure and effectively induces cardiac hypertrophy, the 7d treatment is not sufficient to clearly see these results. To induce cardiac hypertrophy, AngII treatments mostly last 4 weeks, as described by various studies [200-202]. A publication by Diaz et al. also suggests that 7d AngII treatment may be too short to induce hypertrophy. Although they found a slight increase in the expression of marker genes related to fibrosis and hypertrophy in the cardiac tissue of control mice, there were no changes in the hypertrophic index (heart weight/tibia length). The same group prolonged AngII administration to 14d and then found cardiac hypertrophy [203].

5.3.2 Neutrophil infiltration is largely responsible for cardiac insufficiency of iCM-p38 KO mice

Because our earlier work has shown that immune cell infiltration is an important pathogenic factor in heart failure development of iCM-p38 KO mice, the time course of immune cell infiltration was analyzed [41].

The course of immune cell infiltration into cardiac tissue of iCM-p38 KO and control mice is summarized graphically in Figure 50. Under baseline conditions, the number of immune cells in the hearts of iCM-p38 KO and control mice was very low and did not differ between the two groups. The number of infiltrating immune cells peaked 48h after the start of AngII treatment. In hearts of control mice, a strong infiltration of dendritic cells (DCs) was observed, while this was absent in iCM-p38 KO hearts. Especially remarkable

was the massive infiltration of neutrophils and pro-inflammatory monocytes in the cardiac tissue of iCM-p38 KO mice, which was not observed in the respective controls. Although the AngII administration continued for 5 more days, the number of infiltrating immune cells decreased in both groups over time. Only the number of macrophages reached its peak after 7 days of AngII. However, differences between iCM-p38 KO and controls were not measured. 14 days after the end of AngII treatment, most of the immune cells had disappeared in both groups.

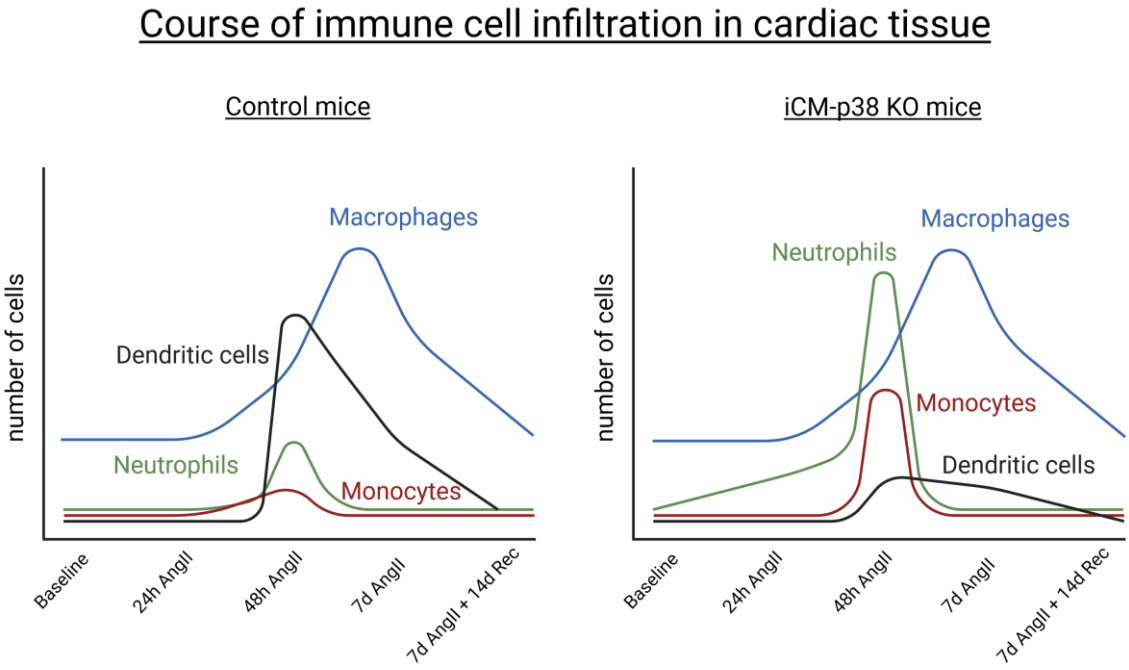

Figure 50: Schematic representation of the course of immune cell infiltration in cardiac tissue after AngII administration and additional recovery in iCM-p38 KO mice and controls. To simplify the presentation, not all immune cell types that were measured are shown. The left side represents the immune infiltration in the hearts of control mice in response to AngII treatment. A strong infiltration of dendritic cells was measured after 48h. Monocyte and neutrophil infiltration were minor. After 7d of AngII, macrophage infiltration peaked. The right side represents the immune cell infiltration in iCM-p38 KO hearts. After 48h AngII administration, a massive infiltration of neutrophils and monocytes was observed. Dendritic cells, on the other hand, were almost absent in these hearts. Macrophage infiltration peaked as well at day 7 of AngII treatment, but no differences were measured compared to control hearts. Created with BioRender.com.

Immune cells are involved in various processes in cardiac diseases, as described before in 1.2.1. They may have a positive impact by, for instance, breaking down dead cells or assisting in the resolution of inflammation, but they may also contribute to the decline of cardiac function.

Neutrophils are known to be among the first cells to infiltrate the myocardium after the induction of pressure overload [39, 204]. They are responsible for clearance of cell debris by phagocytosis while also releasing ROS, proteolytic enzymes, and cytokines [205-207]. In a TAC model of pressure overload, neutrophil depletion significantly reduced the hypertrophic response. Additionally, levels of infiltrating pro-inflammatory monocytes,

analyzed using flow cytometry, were reduced in these mice. These findings support the detrimental impacts of neutrophil infiltration while also suggesting that the recruitment of monocytes into the myocardium is neutrophil-dependent. Monocyte recruitment happens mainly as a result of cytokine release by neutrophils, including CCL2, CCL3, and CCL5. In iCM-p38 KO hearts, RNA sequencing data revealed that *CCL3* expression levels were significantly increased compared to controls after 48h of AngII treatment, supporting the hypothesis.

Monocytes infiltrate cardiac tissue early in the process of PO-induced heart failure [37], which was also confirmed in this thesis as, after 48h of AngII treatment, particularly pro-inflammatory monocytes (Ly6C^{high}) were detected in the heart of iCM-p38 KO mice. The primary function of these cells is to remove damaged tissue through phagocytosis and the release of proteolytic enzymes. Additionally, Ly6C^{high} monocytes' cytokine profile showed that high amounts of TNF-α and IL-1β were released at the site of inflammation early on [208, 209]. This cytokine release can then cause the attraction of even more neutrophils to the inflammatory site, starting a self-reinforcing cycle.

Surprisingly, DCs were strongly infiltrating the cardiac tissue of control mice and were missing in the hearts of iCM-p38 KO mice, suggesting a cardioprotective role of those cells. Guimarães-Costa et al. showed in *in vitro* experiments that neutrophil extracellular traps inhibit monocytes ability to differentiate into DCs [210]. This effect of neutrophils on monocytes could explain the high number of monocytes and the low number of DCs in the cardiac tissue of iCM-p38 KO mice. However, DCs do not exclusively originate from monocytes, they also develop directly from myeloid stem cells. Therefore, the source of the high number of DCs in iCM-p38 control mice remains ambiguous. According to a recent publication by Pistulli and colleagues [211], cardiac DCs are less common in heart biopsies taken from patients with symptomatic dilated cardiomyopathy (DCM). This decrease, which is associated with an unfavorable short-term prognosis of patients, may be the consequence of cellular death, myocardial tissue damage, or inadequate vascularization in chronic heart failure. Therefore, the lack of DCs appears to be crucial in the development of DCM. Another study demonstrated that a depletion of DCs following MI resulted in deteriorated cardiac remodeling and a worsening of cardiac function compared to controls [212]. These observations from Pistulli and Anzai, together with the findings of this thesis, demonstrate the importance of infiltrating DCs to protect from cardiac disease; however, the role of DCs is by far not completely understood, and more research is required before considering DCs as a potential target for therapies.

Later, Ly6C^{low} monocytes infiltrate the injured tissue. These cells may promote fibrotic processes and angiogenesis, as they also express *TGF-β* and *VEGF* (vascular endothelial growth factor).

Macrophages and B-/T-lymphocytes also infiltrate the heart in the iCM-p38 mouse model. It was observed that pro-inflammatory macrophages are first found in the myocardium and are later replaced by anti-inflammatory macrophages. T-lymphocytes are particularly important in the progression of fibrosis [59, 213]. Chapter 5.3.3 provides a more thorough explanation of the underlying processes. However, differences in macrophage and lymphocyte infiltration between control and iCM-p38 KO mice were minor, suggesting that these immune cell types are not major contributors to the development of cardiac dysfunction in iCM-p38 KO mice. Figure 51 illustrates the hypothetical processes in the hearts of iCMp38-KO mice.

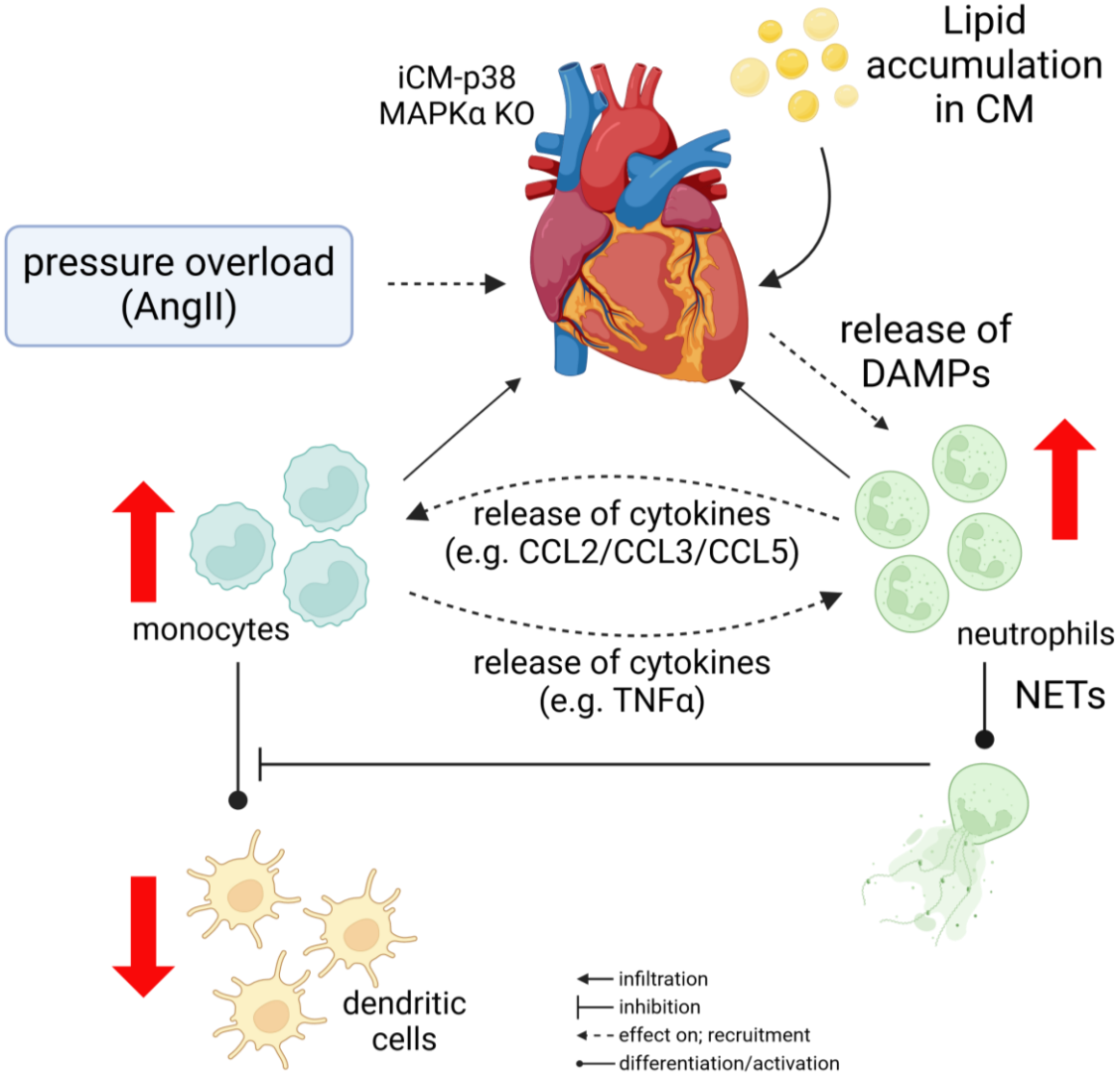

Figure 51: Hypothetical mechanisms causing heart failure in iCM-p38 KO mice. Induction of pressure overload via AngII promotes lipid accumulation in cardiomyocytes (CM). Thus, stressed cardiomyocytes start to release DAMPs (damage-associated molecular patterns), which in turn attract neutrophils. The release of cytokines, e.g., CCL2/3/5, by neutrophils recruits pro-inflammatory monocytes into the cardiac tissue. Monocytes release cytokines as well, like TNF-α, which further enhances neutrophil infiltration in the myocardium. Additionally, neutrophil extracellular traps (NETs) inhibit monocyte differentiation into dendritic cells (DCs). Red arrows indicate changes in cell number within the myocardium. Created with BioRender.com.

Next, a more detailed analysis of the impact of neutrophil infiltration on the severity of HF in iCM-p38 KO mice was performed. Therefore, neutrophils were depleted by a

specific α-Ly6G antibody. This was done once before the AngII-filled osmotic mini pumps were implanted. Since the antibody only has a short half-life (it could be shown that antibodies from xenogenic sources have a half-life time of about 18 hours [214]), only early infiltrating neutrophils were actually removed. Olofsen et al. showed in a study from 2022 that an effective, long-term depletion of neutrophils requires α-Ly6G antibody injection three times a week [215]. Maturation of neutrophils in bone marrow is estimated to take around 2.3 days, and the average half-life time of circulating neutrophils is considered to be 12.5 h [216]. This demonstrates that a single injection only leads to a short-term depletion of neutrophils. The results of the experiments can therefore be attributed exclusively to the reduction of the first infiltrating neutrophils.

Neutrophil depletion prevented body weight loss and sustainably improved the cardiac function of iCM-p38 KO mice. These results prove that the early infiltration of neutrophils into the heart tissue significantly contributes to the HF phenotype and is one of the main triggers for the disease. These findings are in line with our earlier work (Bottermann et al. [41]), where neutrophil depletion significantly improved cardiac function after 48h of AngII treatment. Furthermore, Wang et al. demonstrated that TAC-induced cardiac dysfunction in mice was significantly attenuated after neutrophil depletion [40].

Based on the hypothesis of how heart failure manifests in iCM-p38 KO mice (described in Figure 51), the following results after neutrophil depletion: The induction of PO causes lipid accumulation in the cardiac tissue of iCM-p38 KO mice [41, 102]. Cardiomyocytes release DAMPs, which in turn would cause an infiltration of neutrophils; however, these are depleted and therefore not able to reach the cardiac tissue. Pro-inflammatory monocyte recruitment via cytokine release of neutrophils does not take place, and there is no cycle of declining heart function caused by the attraction of pro-inflammatory immune cells. On the other hand, the differentiation of monocytes into DCs is not inhibited by NETs. Therefore, DCs differentiate within the myocardium and support maintaining cardiac function.

5.3.3 iCM-p38 KO mice suffer from increasing cardiac fibrosis after AngII treatment

In diseased hearts, uncontrolled extracellular matrix (ECM) deposition and cardiac fibrosis are frequent end-organ features that cause tissue stiffness and decreased myocardial function, thus contributing to the progression of heart failure. Even though it is now widely accepted that fibrosis accompanies and exacerbates a variety of CVDs [217], the underlying mechanisms that cause and control the progression of fibrosis are still not fully understood. Additionally, there are currently no clinical therapies that target

cardiac fibrosis specifically; consequently, there is an urgent need for research in this field.

In the iCM-p38 KO mouse model, cardiac fibrosis was analyzed using FACS analysis, gene expression, and immunohistological staining of tissue sections. All three methods revealed progressive fibrosis over time in iCM-p38 KO hearts, whereas this phenotype was found less in control mice (see 4.3.3).

Cardiac fibroblasts make up about two-thirds of the total number of cells in the healthy heart [218] and therefore form the largest cell population in the heart. Under pathological conditions, the number of fibroblasts in the heart tissue even increases, not only through the proliferation of resident fibroblasts but also due to the differentiation of endothelial cells transitioning into cardiac fibroblasts [219]. Pro-inflammatory and pro-fibrotic cytokines, such as transforming growth factor-β1 (TGF-β1), IL-1, and IL-18, activate fibroblasts. TGF-β1 has been identified as the primary inducer and regulator of fibrosis in CVDs and is mainly produced by macrophages and T-lymphocytes [220]. However, it has also been demonstrated that TGF-β1 can be released by cardiomyocytes in response to AngII. In the iCM-p38 KO mouse model, it was observed that macrophages and T-lymphocytes infiltrate into the cardiac tissue, thus mainly contributing to the activation of fibroblasts [77-79].

Activated fibroblasts, also called myofibroblasts, are characterized, i.e., by the expression of αSMA [217] and high proliferation rates. Following MI, αSMA expression is highest between day 4 and day 7. Between day 7 and day 10 fibroblasts proliferate less, and αSMA expression is massively reduced. Similar results were obtained in the iCM-p38 KO mouse model. The behavior of fibroblasts over time in the iCM-p38 KO mouse model is therefore comparable to the behavior of fibroblasts after MI, even though chronic heart failure is present.

With the expression and release of ECM proteins such as fibronectins, periostin, and collagen I and III [221], myofibroblasts stiffen surrounding tissue, and remodel the ECM scaffold, and therefore prevent the tissue from rupture. Following acute activation of fibroblasts, myofibroblasts undergo different fates. They either remain in a resting/senescent state or undergo apoptosis. Additionally, it has been reported recently that myofibroblasts transform into a novel differentiated state known as a matrifibrocyte [72]. In iCM-p38 KO hearts, an increased expression of *Tnsf11b* and *Comp* was measured after 7d of AngII + 14d of recovery time. These genes are usually expressed in bones and cartilage and are marker genes for matrifibrocytes. Thus, matrifibrocytes are more specialized cells that support damaged cardiac tissue [72]. After myocardial infarction, this effect is beneficial to prevent the heart from rupture [222]. However, in

chronic heart failure, a stiff myocardium is associated with a poor prognosis for heart failure patients [223].

Neutrophil depletion reduces fibrosis in iCM-p38 hearts

Interestingly, not only cardiac function was improved after neutrophil depletion in iCM-p38 KO mice, but also cardiac fibrosis was reduced (see 4.4.1). Histological staining of cardiac tissue indicated a distinct reduction of fibrotic area in the hearts of neutrophil-depleted mice compared to IT-injected mice. Moreover, the depletion of neutrophils markedly decreased the expression of fibrosis-associated genes. However, the effect was not only found in iCM-p38 KO mice; also in controls, these results were observed, although differences were less severe. Hence, improved cardiac function in neutrophil-depleted mice is accompanied by a reduction of fibrosis in the cardiac tissue. Similar results were also obtained in a MI-mouse model, were a reduction in neutrophil count improved cardiac function and reduced scar formation [224].

Neutrophils accumulate primarily in the early phase (48h) of AngII treatment in iCM-p38 KO hearts, whereas fibrotic processes develop at later times. Thus, one could conclude that neutrophils have a minimal impact on the progression of fibrosis. Remarkably, this is not necessarily the case. It has been demonstrated that neutrophil extracellular traps (NETs) promote fibroblasts' migration and proliferation while upregulating TGF-β1 expression and collagen synthesis [75, 76]. Thus, the reduction of neutrophils and, therefore, the minimization of NETs may have a direct influence on fibroblast function, which potentially prevents extensive fibrosis.

5.4 Interorgan communication of the failing heart and skeletal muscle

It has long been known that chronic diseases occur with a wide variety of comorbidities. These may include renal dysfunction, respiratory disease, or affect pancreatic tissue, leading to diabetes mellitus. Comorbidities of chronic diseases lead to further deterioration of patient health and are often the ultimate cause of death. One comorbidity of HF affects the skeletal muscle and is called cachexia. Cachexia is defined as a complex metabolic syndrome causing the loss of skeletal muscle and fat mass. The prevalence of cardiac cachexia is hard to determine precisely but is in a range between 10-40% of all patients with heart failure [225]. Mechanisms of heart failure-induced cachexia are already described in detail in section 1.4. Since heart failure does not necessarily lead to cachexia, it is difficult to generate a reliable animal model to study the underlying processes comprehensively. In this work, two mouse models with different

types of heart failures were examined in more detail to find out whether these models are suitable to analyze cardiac cachexia. The iCM-p38 KO mouse model suffers from dilative cardiomyopathy after induction of pressure overload, while in the iCM-AKT1/2 KO mouse model, deletion of the *Akt1* and *Akt2* genes is sufficient to induce cardiac atrophy.

5.4.1 The iCM-p38-MAPKα KO mouse model: rapid development of cardiac dilation does not cause sustained skeletal muscle atrophy

The analysis of skeletal muscle weight, fiber type composition, and fiber type size in *M. soleus*, *M. plantaris,* and *M. gastrocnemius* did not show differences between iCM-p38 KO and control mice at all measured time points.

Additionally, *M. plantaris* was further investigated on an expression level. In 2013, Wang et al. demonstrated that fast-twitch glycolytic (Type IIb/x) fibers are more prone to atrophy than slow-twitch oxidative (Type I) fibers [226]. Type IIb/x fibers show high myosin ATPase activity and therefore have high glycolytic but, in return, low oxidative capacities. *M. plantaris* mainly consists of Type II fibers, which is why this muscle was chosen to study the expression of atrophy-related genes in more detail.

Interestingly, an increase in expression of atrophy-related genes was measured in iCM-p38 KO mice after 48h AngII treatment. At later time points (7d AngII / 7d AngII + 14d Rec) this increase in expression had disappeared. Likewise, no elevated expression was seen in control mice at all times. Since the AngII treatment lasted for 7 days and control mice also received AngII, it can be ruled out that the AngII treatment was the cause of the increased expression of atrogenes.

A possible explanation for the increased expression of atrogenes in iCM-p38 KO muscles could be high levels of circulating cytokines released by the failing heart. Pro-inflammatory cytokines are suggested to be involved in inducing and mediating catabolic processes in various organs. Cytokines that are associated with skeletal muscle atrophy are, for example, IL-6 and TNF-α. Haddad et al. demonstrated that IL-6 infusion in rats results in skeletal muscle atrophy [185]. Additionally, TNF-α was shown to be elevated in cachectic CHF patients [227-229]. TNF-α is one of the key molecules in catabolism. In animal studies, it was shown that TNF-α–producing tumor cells induce skeletal muscle wasting, indicating that TNF-α plays a critical role in the progression of cachexia. The heart also directly releases TNF-α in the event of failure [230]. But IL-6 and TNF-α are also produced by immune cells like neutrophils and monocytes [231, 232]. Since the number of infiltrating immune cells in iCM-p38 KO hearts is highest after 48h of AngII treatment and then declines, it can be speculated that the cytokines are produced by

these cells and then proceed via the blood to the skeletal muscle, where they induce catabolic mechanisms.

Another explanation for the short-term effect on the skeletal muscle may be related to an insufficient supply of nutrients through food. Especially in the first 48 hours after starting AngII treatment, iCM-p38 KO mice lose significant body weight (Figure 24). The main reason for this is probably the insufficient intake of food, as the animals are physically restricted due to the impaired heart function. Over time, animals recovered physically; thus, they were able to consume enough food again and therefore gain body weight. However, their heart function continued to be poor. The skeletal muscle serves as a major source for amino acids stored in form of proteins. As a last option in starvation and severe energy shortages, those proteins are broken down and serve as energy sources to maintain vital functions [233]. In the short period of starvation, the skeletal muscle of iCM-p38 KO mice probably serves as an energy source, explaining why the expression of atrophy-related genes could be increased in the short term. The subsequent physical recovery and the associated increased food intake may explain why the effects are no longer present at later time points. Hence, the skeletal muscle is no longer needed as an energy source, and the expression of atrophy-related genes is decreased again.

The iCM-AKT1/2 mouse model as a second model for studying cardiac cachexia

In contrast to the iCM-p38 KO mouse model, the iCM-AKT1/2 KO mouse model does not suffer from dilative cardiomyopathy but from massive atrophy of cardiac tissue, resulting in heart failure. In these animals, it was as well examined how cardiac dysfunction affects the hind limb skeletal muscle in the context of cardiac cachexia. While measurements of muscle weight and fiber type distribution did not reveal signs of muscle wasting, the expression of atrophy-related genes was increased in iCM-AKT1/2 KO mice 21 days after induction of the KO. However, only some animals were affected; in others, the expression was not higher than in the controls, and the standard deviation was particularly high. This can be due to the following reasons:

1. Survival curves of the iCM-AKT1/2 KO animals elucidate that from day 21 on (post-KO induction), the animals die more frequently. In general, life expectancy does not exceed 28 days. The increased expression of the examined genes could occur in those animals that would die soon. A lower expression would therefore be present in animals whose lifespan is longer.
2. Further, cachexia does not occur in all patients with cardiac dysfunction. As previously discussed, the prevalence of cardiac cachexia ranges between 10-40% of all patients [225]. Expressional analysis of atrophy-related genes in iCM-AKT1/2 KO mice showed a particularly strong increase in 2 of the 5 animals examined. In

the other animals, the expression did not differ from the controls. These results also represent a 40% incidence.

Overall, it can be concluded that neither the iCM-p38 KO nor the iCM-AKT1/2 KO mouse model is a suitable animal model to study cardiac cachexia. Although there are signs of atrophy in *M. plantaris* on an expressional level in both mouse models, the variability between the individual animals examined is excessive. Finding a suitable model to study cachexia is challenging, as all available models have limitations. In 2016, Molinari et al. [234] summarized several animal models proposed to be suitable to study cardiac cachexia. In these models, cardiac dysfunction is triggered genetically or pharmacologically. However, it cannot be ruled out that the triggering mechanism does not only affect the skeletal muscle itself, since molecular and physiological mechanisms between myocardium and skeletal muscle are extremely similar. In these cases, it cannot be determined whether changes in skeletal muscle tissue are due to the deterioration in heart function or solely to the treatment, which is intended to restrict heart function.

6. Open questions

Figure 52 summarizes the molecular mechanism contributing to the development of chronic heart failure in iCM-p38 KO hearts. Under baseline conditions, cardiac tissue is already insulin resistant, which results in a reduced glucose uptake [103]. However, functional changes are not detected at this stage. Only after induction of pressure overload via AngII a reduced LV pump function is measured. This is accompanied by LV dilation and, after around 4h of AngII application, reduced blood pressure (Bottermann, unpublished). RNA sequencing revealed reduced mitochondrial function and impaired β-oxidation early on, resulting in energy depletion of the myocardium. Consequently, increased SNS activity leads to activation of lipolysis in adipose tissue. As a result, glycerol and free fatty acid levels in the blood rise, and lipids are stored in cardiomyocytes. When these factors come together, the cardiac tissue is subjected to progressive stress, which damages the cells and causes DAMPs to be released. The heart is then infiltrated by immune cells like neutrophils and monocytes. Eventually, the damage to the heart becomes so severe that cardiac fibrosis develops, contributing to irreversible chronic heart failure.

Although the iCM-p38 KO mouse model has already been examined in detail, some questions remain unanswered, and more questions continue to arise after new findings have been collected. Some of these will be discussed in the following.

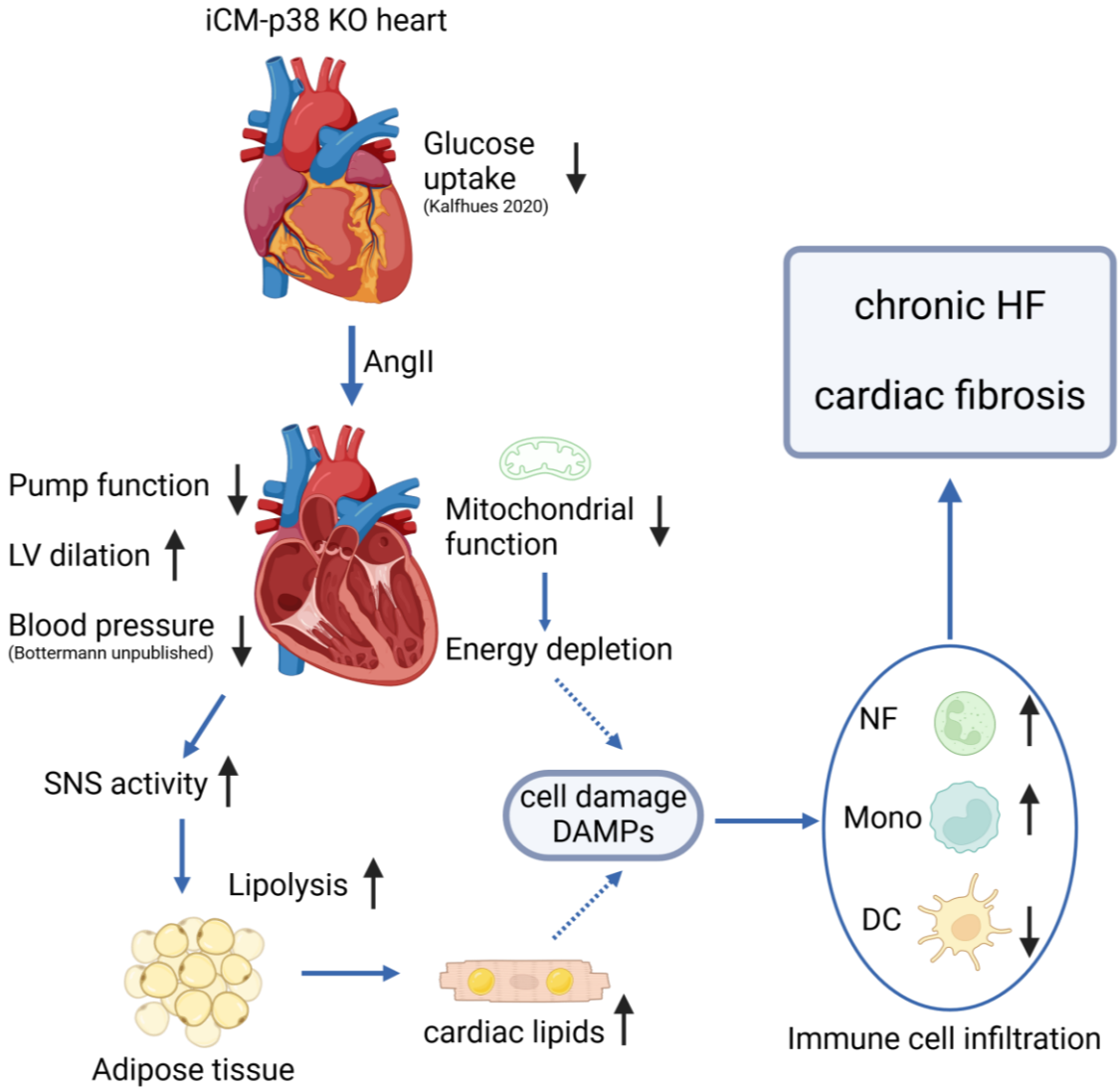

Figure 52: Mechanisms causing chronic heart failure in iCM-p38 KO mice after AngII treatment. Black arrows indicate either increase (↑) or decrease (↓) of the respective effect. NF: Neutrophil, Mono: Monocyte, DC: dendritic cell, HF: heart failure, DAMPs: damage-associated molecular patterns. SNS: sympathetic nervous system, LV: left ventricle. Created with BioRender.com.

6.1 Analysis of neutrophil subtypes infiltrating cardiac tissue of iCM-p38 KO mice after induction of PO

Neutrophil infiltration in the hearts of iCM-p38 KO mice was shown to be one of the major players in the progression of cardiac dysfunction in these mice. Therefore, it would be interesting to determine which subtype of neutrophils is involved in the progression of HF. One attempt to investigate neutrophils in more detail would be the isolation of infiltrating neutrophils from cardiac tissue and subsequent analysis of gene expression via qPCR, RNA sequencing, or single cell sequencing. Thus, genes that are known to be expressed in the neutrophil subtypes N1 and N2 could be the focus. These genes are for the N1 phenotype *TNF-α*, *IL-12a*, and *NOS2,* and for the N2 phenotype *Arginase 1,*

Retnla, and *Chi3l3*. Using this kind of analysis, neutrophils could be categorized into pro- and anti-inflammatory phenotypes, which in turn gives information about the cytokines and chemokines that neutrophils may release and the immune cells that are subsequently attracted.

6.2 Additional research on immune cell interactions in the hearts of iCM-p38 KO mice after PO induction

A single depletion of neutrophils in iCM-p38 KO mice resulted in significantly improved cardiac function and reduced fibrosis after AngII treatment. However, the amount of monocytes and DCs also significantly differs between iCM-p38 KO and control hearts.

Therefore, it would be interesting to further analyze the impact of monocytes and dendritic cells on the progression of heart failure. The depletion of Ly6C^{high} monocytes, for example, would reveal if neutrophils are drawn into cardiac tissue due to previous monocyte infiltration. The depletion of Ly6C^{high} monocytes is principally possible, as various studies have already successfully demonstrated [235, 236].

Since the number of DCs is reduced in iCM-p38 KO hearts compared to controls, a cardioprotective role of those cells can be anticipated. This positive effect of infiltrating DCs was also demonstrated in DCM patients [211] and following MI [212], supporting the findings from the iCM-p38 KO model. However, a more detailed analysis of infiltrating DCs is needed to get new insights into the exact function of these cells. It would be conceivable to analyze which DC subtype is present in the heart of iCM-p38 control hearts to determine the specific function. Interestingly, in a mouse model of Chronic Chagas disease cardiomyopathy (CCC), Santos et al. demonstrated that a treatment with tolerogenic DCs, a subclass of DCs with immuno-suppressive properties, was able to reduce cardiac inflammation as well as fibrosis [237]. However, it must be noted that CCC is a parasite-induced disease, so the results are unlikely to be accurately applicable to heart failure with sterile inflammation. However, an attempt to rescue the phenotype of iCM-p38 KO mice can be made by directly injecting DCs into those mice. An improvement in cardiac function as a result of DC injection would prove the protective effect of the cells.

Furthermore, the interaction between neutrophil and DCs infiltration could be investigated to analyze if infiltrating DCs prevent the accumulation of neutrophils and whether a depletion of DCs would consequently lead to an accumulation of neutrophils and therefore reduce cardiac function also in control mice. Future treatments that target DCs may be based on the findings of this study, which could help improve the cardiac function of heart failure patients.

6.3 Analysis of circulating cytokines and chemokines

As already briefly discussed, circulating cytokines and chemokines can affect organs in various ways. Immune cells, which strongly infiltrate iCM-p38 KO hearts after induction of PO, are a known source of cytokines and chemokines. The release of those mediators causes, on the one hand, the attraction of more immune cells to the site of injury; on the other hand, they are delivered to all other body organs through the bloodstream. This can then have a variety of effects on the organs that have been reached. In the iCM-p38 KO mouse model, for example, after the induction of cardiac dysfunction, an elevation of atrophy-related gene expression was measured in *M. plantaris*. Since this elevation was not present in the respective control animals, the AngII treatment to induce cardiac dysfunction cannot be the reason for the observed changes. Additional factors must therefore play a role, and the heart, as a compromised organ, seems to be a potential trigger. Measurements of relevant cytokines and chemokines, such as TNF-α, IL-6, CCL2, CCL3, and CCL5, in the blood of the affected animals would give insights into the communication between the failing heart and the skeletal muscle. Nevertheless, it also needs to be confirmed which organ is the source of the released cytokines and chemokines. However, the analysis of secreted cytokines and chemokines can make an important contribution to the development of new therapies that aim to reduce or even prevent comorbidities in heart failure patients. The improvement of comorbidities should not be underestimated, as these significantly limit the quality of life and are often the ultimate cause of death in heat failure patients. Further investigations of comorbidities and their interaction with the primary disease are therefore essential and require even more attention.

References

1. Shahim, B., C.J. Kapelios, G. Savarese, and L.H. Lund, *Global Public Health Burden of Heart Failure: An Updated Review.* Card Fail Rev, 2023. **9**: p. e11.

2. Tsao, C.W., A.W. Aday, Z.I. Almarzooq, C.A.M. Anderson, et al., *Heart Disease and Stroke Statistics-2023 Update: A Report From the American Heart Association.* Circulation, 2023. **147**(8): p. e93-e621.

3. Jones, N.R., A.K. Roalfe, I. Adoki, F.D.R. Hobbs, et al., *Survival of patients with chronic heart failure in the community: a systematic review and meta-analysis.* Eur J Heart Fail, 2019. **21**(11): p. 1306-1325.

4. Yancy, C.W., M. Jessup, B. Bozkurt, J. Butler, et al., *2013 ACCF/AHA guideline for the management of heart failure: a report of the American College of Cardiology Foundation/American Heart Association Task Force on Practice Guidelines.* J Am Coll Cardiol, 2013. **62**(16): p. e147-239.

5. van der Vusse, G.J., J.F. Glatz, H.C. Stam, and R.S. Reneman, *Fatty acid homeostasis in the normoxic and ischemic heart.* Physiol Rev, 1992. **72**(4): p. 881-940.

6. van Bilsen, M., F.A. van Nieuwenhoven, and G.J. van der Vusse, *Metabolic remodelling of the failing heart: beneficial or detrimental?* Cardiovasc Res, 2009. **81**(3): p. 420-8.

7. Stanley, W.C., F.A. Recchia, and G.D. Lopaschuk, *Myocardial substrate metabolism in the normal and failing heart.* Physiol Rev, 2005. **85**(3): p. 1093-129.

8. Sochor, H., H.R. Schelbert, M. Schwaiger, E. Henze, et al., *Studies of fatty acid metabolism with positron emission tomography in patients with cardiomyopathy.* Eur J Nucl Med, 1986. **12 Suppl**: p. S66-9.

9. de las Fuentes, L., P. Herrero, L.R. Peterson, D.P. Kelly, et al., *Myocardial fatty acid metabolism: independent predictor of left ventricular mass in hypertensive heart disease.* Hypertension, 2003. **41**(1): p. 83-7.

10. Bedi, K.C., Jr., N.W. Snyder, J. Brandimarto, M. Aziz, et al., *Evidence for Intramyocardial Disruption of Lipid Metabolism and Increased Myocardial Ketone Utilization in Advanced Human Heart Failure.* Circulation, 2016. **133**(8): p. 706-16.

11. Tadamura, E., T. Kudoh, N. Hattori, M. Inubushi, et al., *Impairment of BMIPP uptake precedes abnormalities in oxygen and glucose metabolism in hypertrophic cardiomyopathy.* J Nucl Med, 1998. **39**(3): p. 390-6.

12. Davila-Roman, V.G., G. Vedala, P. Herrero, L. de las Fuentes, et al., *Altered myocardial fatty acid and glucose metabolism in idiopathic dilated cardiomyopathy.* J Am Coll Cardiol, 2002. **40**(2): p. 271-7.

13. Christe, M.E. and R.L. Rodgers, *Altered glucose and fatty acid oxidation in hearts of the spontaneously hypertensive rat.* J Mol Cell Cardiol, 1994. **26**(10): p. 1371-5.

14. Neubauer, S., *The failing heart--an engine out of fuel.* N Engl J Med, 2007. **356**(11): p. 1140-51.

15. Kishi, T., *Heart failure as an autonomic nervous system dysfunction.* J Cardiol, 2012. **59**(2): p. 117-22.

16. Zhan, D.Y., S. Morimoto, C.K. Du, Y.Y. Wang, et al., *Therapeutic effect of beta-adrenoceptor blockers using a mouse model of dilated cardiomyopathy with a troponin mutation.* Cardiovasc Res, 2009. **84**(1): p. 64-71.

17. *Effect of metoprolol CR/XL in chronic heart failure: Metoprolol CR/XL Randomised Intervention Trial in Congestive Heart Failure (MERIT-HF).* Lancet, 1999. **353**(9169): p. 2001-7.

18. Packer, M., M.R. Bristow, J.N. Cohn, W.S. Colucci, et al., *The effect of carvedilol on morbidity and mortality in patients with chronic heart failure. U.S. Carvedilol Heart Failure Study Group.* N Engl J Med, 1996. **334**(21): p. 1349-55.

19. Sompayrac, L.M., *How the immune system works*. 2019: Wiley-Blackwell.

20. Litman, G.W., J.P. Cannon, and L.J. Dishaw, *Reconstructing immune phylogeny: new perspectives.* Nat Rev Immunol, 2005. **5**(11): p. 866-79.

21. Netea, M.G., J. Quintin, and J.W. van der Meer, *Trained immunity: a memory for innate host defense.* Cell Host Microbe, 2011. **9**(5): p. 355-61.

22. Sherwood, E.R., K.R. Burelbach, M.A. McBride, C.L. Stothers, et al., *Innate Immune Memory and the Host Response to Infection.* J Immunol, 2022. **208**(4): p. 785-792.

23. Janeway, C., Paul, C., Travers, M., Walport, M., Shlomchik, M., *Immunobiology*. 2001: New York and London: Garland Science.

24. Restifo, N.P. and L. Gattinoni, *Lineage relationship of effector and memory T cells.* Curr Opin Immunol, 2013. **25**(5): p. 556-63.

25. Kurosaki, T., K. Kometani, and W. Ise, *Memory B cells.* Nat Rev Immunol, 2015. **15**(3): p. 149-59.

26. Alberts, B., Johnson, A., Lewis, J., Raff, M., Roberts, K., Walters, P., *Molecular Biology of the Cell*. 2002: New York and London: Garland Science.

27. Al-Shura, A.N., *"Lymphocytes". Advanced Hematology in Integrated Cardiovascular Chinese Medicine*. 2020: Elsevier.

28. Luckheeram, R.V., R. Zhou, A.D. Verma, and B. Xia, *CD4(+)T cells: differentiation and functions.* Clin Dev Immunol, 2012. **2012**: p. 925135.

29. Dick, S.A. and S. Epelman, *Chronic Heart Failure and Inflammation: What Do We Really Know?* Circ Res, 2016. **119**(1): p. 159-76.

30. Liu, T., L. Zhang, D. Joo, and S.C. Sun, *NF-κB signaling in inflammation.* Signal Transduct Target Ther, 2017. **2**: p. 17023-.

31. Panizzi, P., F.K. Swirski, J.L. Figueiredo, P. Waterman, et al., *Impaired infarct healing in atherosclerotic mice with Ly-6C(hi) monocytosis.* J Am Coll Cardiol, 2010. **55**(15): p. 1629-38.

32. Meyer, I.S., A. Jungmann, C. Dieterich, M. Zhang, et al., *The cardiac microenvironment uses non-canonical WNT signaling to activate monocytes after myocardial infarction.* EMBO Mol Med, 2017. **9**(9): p. 1279-1293.

33. Swirski, F.K., P. Libby, E. Aikawa, P. Alcaide, et al., *Ly-6Chi monocytes dominate hypercholesterolemia-associated monocytosis and give rise to macrophages in atheromata.* J Clin Invest, 2007. **117**(1): p. 195-205.

34. Sunderkotter, C., T. Nikolic, M.J. Dillon, N. Van Rooijen, et al., *Subpopulations of mouse blood monocytes differ in maturation stage and inflammatory response.* J Immunol, 2004. **172**(7): p. 4410-7.

35. Auffray, C., D. Fogg, M. Garfa, G. Elain, et al., *Monitoring of blood vessels and tissues by a population of monocytes with patrolling behavior.* Science, 2007. **317**(5838): p. 666-70.

36. Frantz, S., U. Hofmann, D. Fraccarollo, A. Schafer, et al., *Monocytes/macrophages prevent healing defects and left ventricular thrombus formation after myocardial infarction.* FASEB J, 2013. **27**(3): p. 871-81.

37. Brenes-Castro, D., E.C. Castillo, E. Vazquez-Garza, G. Torre-Amione, et al., *Temporal Frame of Immune Cell Infiltration during Heart Failure Establishment: Lessons from Animal Models.* Int J Mol Sci, 2018. **19**(12).

38. Horckmans, M., L. Ring, J. Duchene, D. Santovito, et al., *Neutrophils orchestrate post-myocardial infarction healing by polarizing macrophages towards a reparative phenotype.* Eur Heart J, 2017. **38**(3): p. 187-197.

39. Xia, Y., K. Lee, N. Li, D. Corbett, et al., *Characterization of the inflammatory and fibrotic response in a mouse model of cardiac pressure overload.* Histochem Cell Biol, 2009. **131**(4): p. 471-81.

40. Wang, Y., S. Sano, K. Oshima, M. Sano, et al., *Wnt5a-Mediated Neutrophil Recruitment Has an Obligatory Role in Pressure Overload-Induced Cardiac Dysfunction.* Circulation, 2019. **140**(6): p. 487-499.

41. Bottermann, K., L. Kalfhues, R. Nederlof, A. Hemmers, et al., *Cardiomyocyte p38 MAPKalpha suppresses a heart-adipose tissue-neutrophil crosstalk in heart failure development.* Basic Res Cardiol, 2022. **117**(1): p. 48.

42. Hart, D.N. and J.W. Fabre, *Demonstration and characterization of Ia-positive dendritic cells in the interstitial connective tissues of rat heart and other tissues, but not brain.* J Exp Med, 1981. **154**(2): p. 347-61.

43. Choi, J.H., Y. Do, C. Cheong, H. Koh, et al., *Identification of antigen-presenting dendritic cells in mouse aorta and cardiac valves.* J Exp Med, 2009. **206**(3): p. 497-505.

44. Zhang, J., Z.X. Yu, S. Fujita, M.L. Yamaguchi, et al., *Interstitial dendritic cells of the rat heart. Quantitative and ultrastructural changes in experimental myocardial infarction.* Circulation, 1993. **87**(3): p. 909-20.

45. Wang, L., D. Li, K. Yang, Y. Hu, et al., *Toll-like receptor-4 and mitogen-activated protein kinase signal system are involved in activation of dendritic cells in patients with acute coronary syndrome.* Immunology, 2008. **125**(1): p. 122-30.

46. Maekawa, Y., N. Mizue, A. Chan, Y. Shi, et al., *Survival and cardiac remodeling after myocardial infarction are critically dependent on the host innate immune interleukin-1 receptor-associated kinase-4 signaling: a regulator of bone marrow-derived dendritic cells.* Circulation, 2009. **120**(14): p. 1401-14.

47. Swirski, F.K. and M. Nahrendorf, *Cardioimmunology: the immune system in cardiac homeostasis and disease.* Nat Rev Immunol, 2018. **18**(12): p. 733-744.

48. Testa, M., M. Yeh, P. Lee, R. Fanelli, et al., *Circulating levels of cytokines and their endogenous modulators in patients with mild to severe congestive heart failure due to coronary artery disease or hypertension.* J Am Coll Cardiol, 1996. **28**(4): p. 964-71.

49. Deswal, A., N.J. Petersen, A.M. Feldman, J.B. Young, et al., *Cytokines and cytokine receptors in advanced heart failure: an analysis of the cytokine database from the Vesnarinone trial (VEST).* Circulation, 2001. **103**(16): p. 2055-9.

50. Ramanujam, D., A.P. Schön, C. Beck, P. Vaccarello, et al., *MicroRNA-21-Dependent Macrophage-to-Fibroblast Signaling Determines the Cardiac Response to Pressure Overload.* Circulation, 2021. **143**(15): p. 1513-1525.

51. Falkenham, A., R. de Antueno, N. Rosin, D. Betsch, et al., *Nonclassical resident macrophages are important determinants in the development of myocardial fibrosis.* Am J Pathol, 2015. **185**(4): p. 927-42.

52. Yunna, C., H. Mengru, W. Lei, and C. Weidong, *Macrophage M1/M2 polarization.* Eur J Pharmacol, 2020. **877**: p. 173090.

53. O'Brien, M., C.F. Baicu, A.O. Van Laer, Y. Zhang, et al., *Pressure overload generates a cardiac-specific profile of inflammatory mediators.* Am J Physiol Heart Circ Physiol, 2020. **319**(2): p. H331-h340.

54. Ngwenyama, N., A.M. Salvador, F. Velázquez, T. Nevers, et al., *CXCR3 regulates CD4+ T cell cardiotropism in pressure overload-induced cardiac dysfunction.* JCI Insight, 2019. **4**(7).

55. Vdovenko, D. and U. Eriksson, *Regulatory Role of CD4(+) T Cells in Myocarditis.* J Immunol Res, 2018. **2018**: p. 4396351.

56. Yasuda, M., K. Takeuchi, M. Hiruma, H. Iida, et al., *The complement system in ischemic heart disease.* Circulation, 1990. **81**(1): p. 156-63.

57. Rock, K.L., J.J. Lai, and H. Kono, *Innate and adaptive immune responses to cell death.* Immunol Rev, 2011. **243**(1): p. 191-205.

58. Yan, W., Y. Song, L. Zhou, J. Jiang, et al., *Immune Cell Repertoire and Their Mediators in Patients with Acute Myocardial Infarction or Stable Angina Pectoris.* Int J Med Sci, 2017. **14**(2): p. 181-190.

59. Groschel, C., A. Sasse, S. Monecke, C. Rohrborn, et al., *CD8(+)-T Cells With Specificity for a Model Antigen in Cardiomyocytes Can Become Activated After Transverse Aortic Constriction but Do Not Accelerate Progression to Heart Failure.* Front Immunol, 2018. **9**: p. 2665.

60. Nevers, T., A.M. Salvador, A. Grodecki-Pena, A. Knapp, et al., *Left Ventricular T-Cell Recruitment Contributes to the Pathogenesis of Heart Failure.* Circ Heart Fail, 2015. **8**(4): p. 776-87.

61. Curato, C., S. Slavic, J. Dong, A. Skorska, et al., *Identification of noncytotoxic and IL-10-producing CD8+AT2R+ T cell population in response to ischemic heart injury.* J Immunol, 2010. **185**(10): p. 6286-93.

62. Varda-Bloom, N., J. Leor, D.G. Ohad, Y. Hasin, et al., *Cytotoxic T lymphocytes are activated following myocardial infarction and can recognize and kill healthy myocytes in vitro.* J Mol Cell Cardiol, 2000. **32**(12): p. 2141-9.

63. Chute, M., P. Aujla, S. Jana, and Z. Kassiri, *The Non-Fibrillar Side of Fibrosis: Contribution of the Basement Membrane, Proteoglycans, and Glycoproteins to Myocardial Fibrosis.* J Cardiovasc Dev Dis, 2019. **6**(4).

64. Brower, G.L., J.D. Gardner, M.F. Forman, D.B. Murray, et al., *The relationship between myocardial extracellular matrix remodeling and ventricular function.* Eur J Cardiothorac Surg, 2006. **30**(4): p. 604-10.

65. Eckhouse, S.R. and F.G. Spinale, *Changes in the myocardial interstitium and contribution to the progression of heart failure.* Heart Fail Clin, 2012. **8**(1): p. 7-20.

66. Ju, H., S. Zhao, D.S. Jassal, and I.M. Dixon, *Effect of AT1 receptor blockade on cardiac collagen remodeling after myocardial infarction.* Cardiovasc Res, 1997. **35**(2): p. 223-32.

67. van den Borne, S.W., S. Isobe, H.R. Zandbergen, P. Li, et al., *Molecular imaging for efficacy of pharmacologic intervention in myocardial remodeling.* JACC Cardiovasc Imaging, 2009. **2**(2): p. 187-98.

68. Ciulla, M.M., R. Paliotti, A. Esposito, J. Diez, et al., *Different effects of antihypertensive therapies based on losartan or atenolol on ultrasound and biochemical markers of myocardial fibrosis: results of a randomized trial.* Circulation, 2004. **110**(5): p. 552-7.

69. Hayashi, M., *[Immediate administration of mineralocorticoid receptor antagonist spironolactone prevents post-infarct left ventricular remodeling associated with suppression of a marker of myocardial collagen synthesis in patients with first anterior acute myocardial infarction].* J Cardiol, 2004. **43**(2): p. 88-91.

70. Pandey, A., S. Garg, S.A. Matulevicius, A.M. Shah, et al., *Effect of Mineralocorticoid Receptor Antagonists on Cardiac Structure and Function in Patients With Diastolic Dysfunction and Heart Failure With Preserved Ejection Fraction: A Meta-Analysis and Systematic Review.* J Am Heart Assoc, 2015. **4**(10): p. e002137.

71. Zannad, F., F. Alla, B. Dousset, A. Perez, et al., *Limitation of excessive extracellular matrix turnover may contribute to survival benefit of spironolactone therapy in patients with congestive heart failure: Insights from the Randomized Aldactone Evaluation Study (RALES).* Circulation, 2000. **102**(22): p. 2700-2706.

72. Fu, X., H. Khalil, O. Kanisicak, J.G. Boyer, et al., *Specialized fibroblast differentiated states underlie scar formation in the infarcted mouse heart.* J Clin Invest, 2018. **128**(5): p. 2127-2143.

73. Kurose, H., *Cardiac Fibrosis and Fibroblasts.* Cells, 2021. **10**(7): p. 1716.

74. Martinod, K., T. Witsch, L. Erpenbeck, A. Savchenko, et al., *Peptidylarginine deiminase 4 promotes age-related organ fibrosis.* Journal of Experimental Medicine, 2016. **214**(2): p. 439-458.

75. Eghbalzadeh, K., L. Georgi, T. Louis, H. Zhao, et al., *Compromised Anti-inflammatory Action of Neutrophil Extracellular Traps in PAD4-Deficient Mice Contributes to Aggravated Acute Inflammation After Myocardial Infarction.* Front Immunol, 2019. **10**: p. 2313.

76. Chrysanthopoulou, A., I. Mitroulis, E. Apostolidou, S. Arelaki, et al., *Neutrophil extracellular traps promote differentiation and function of fibroblasts.* J Pathol, 2014. **233**(3): p. 294-307.

77. Peng, H., Z. Sarwar, X.P. Yang, E.L. Peterson, et al., *Profibrotic Role for Interleukin-4 in Cardiac Remodeling and Dysfunction.* Hypertension, 2015. **66**(3): p. 582-9.

78. Kanellakis, P., M. Ditiatkovski, G. Kostolias, and A. Bobik, *A pro-fibrotic role for interleukin-4 in cardiac pressure overload.* Cardiovasc Res, 2012. **95**(1): p. 77-85.

79. Cieslik, K.A., G.E. Taffet, S. Carlson, J. Hermosillo, et al., *Immune-inflammatory dysregulation modulates the incidence of progressive fibrosis and diastolic stiffness in the aging heart.* J Mol Cell Cardiol, 2011. **50**(1): p. 248-56.

80. Hulsmans, M., H.B. Sager, J.D. Roh, M. Valero-Muñoz, et al., *Cardiac macrophages promote diastolic dysfunction.* J Exp Med, 2018. **215**(2): p. 423-440.

81. Ueshima, E., M. Fujimori, H. Kodama, D. Felsen, et al., *Macrophage-secreted TGF-β(1) contributes to fibroblast activation and ureteral stricture after ablation injury.* Am J Physiol Renal Physiol, 2019. **317**(7): p. F52-f64.

82. Bryant, D., L. Becker, J. Richardson, J. Shelton, et al., *Cardiac failure in transgenic mice with myocardial expression of tumor necrosis factor-alpha.* Circulation, 1998. **97**(14): p. 1375-81.

83. Ramachandran, P., A. Pellicoro, M.A. Vernon, L. Boulter, et al., *Differential Ly-6C expression identifies the recruited macrophage phenotype, which orchestrates the*

regression of murine liver fibrosis. Proc Natl Acad Sci U S A, 2012. **109**(46): p. E3186-95.

84. Fallowfield, J.A., M. Mizuno, T.J. Kendall, C.M. Constandinou, et al., *Scar-associated macrophages are a major source of hepatic matrix metalloproteinase-13 and facilitate the resolution of murine hepatic fibrosis.* J Immunol, 2007. **178**(8): p. 5288-95.

85. Leitner, L.M., R.J. Wilson, Z. Yan, and A. Godecke, *Reactive Oxygen Species/Nitric Oxide Mediated Inter-Organ Communication in Skeletal Muscle Wasting Diseases.* Antioxid Redox Signal, 2017. **26**(13): p. 700-717.

86. von Haehling, S. and S.D. Anker, *Cachexia as a major underestimated and unmet medical need: facts and numbers.* J Cachexia Sarcopenia Muscle, 2010. **1**(1): p. 1-5.

87. Morley, J.E., D.R. Thomas, and M.M. Wilson, *Cachexia: pathophysiology and clinical relevance.* Am J Clin Nutr, 2006. **83**(4): p. 735-43.

88. Pende, A., N.R. Musso, C. Vergassola, F. Puppo, et al., *Neuroendocrine effects of interferon alpha 2-a in healthy human subjects.* J Biol Regul Homeost Agents, 1990. **4**(2): p. 67-72.

89. Shintani, F., T. Nakaki, S. Kanba, R. Kato, et al., *Role of interleukin-1 in stress responses. A putative neurotransmitter.* Mol Neurobiol, 1995. **10**(1): p. 47-71.

90. Rydén, M., E. Arvidsson, L. Blomqvist, L. Perbeck, et al., *Targets for TNF-alpha-induced lipolysis in human adipocytes.* Biochem Biophys Res Commun, 2004. **318**(1): p. 168-75.

91. Guttridge, D.C., M.W. Mayo, L.V. Madrid, C.Y. Wang, et al., *NF-kappaB-induced loss of MyoD messenger RNA: possible role in muscle decay and cachexia.* Science, 2000. **289**(5488): p. 2363-6.

92. Roth, S.M. and S. Walsh, *Myostatin: a therapeutic target for skeletal muscle wasting.* Curr Opin Clin Nutr Metab Care, 2004. **7**(3): p. 259-63.

93. Baumgartner, R.N., D.L. Waters, J.E. Morley, P. Patrick, et al., *Age-related changes in sex hormones affect the sex difference in serum leptin independently of changes in body fat.* Metabolism, 1999. **48**(3): p. 378-84.

94. Caregaro, L., A. Favaro, P. Santonastaso, F. Alberino, et al., *Insulin-like growth factor 1 (IGF-1), a nutritional marker in patients with eating disorders.* Clin Nutr, 2001. **20**(3): p. 251-7.

95. Mendell, J.R. and W.K. Engel, *The fine structure of type II muscle fiber atrophy.* Neurology, 1971. **21**(4): p. 358-65.

96. Tiao, G., M. Lieberman, J.E. Fischer, and P.O. Hasselgren, *Intracellular regulation of protein degradation during sepsis is different in fast- and slow-twitch muscle.* Am J Physiol, 1997. **272**(3 Pt 2): p. R849-56.

97. Acharyya, S., M.E. Butchbach, Z. Sahenk, H. Wang, et al., *Dystrophin glycoprotein complex dysfunction: a regulatory link between muscular dystrophy and cancer cachexia.* Cancer Cell, 2005. **8**(5): p. 421-32.

98. Li, P., R.E. Waters, S.I. Redfern, M. Zhang, et al., *Oxidative phenotype protects myofibers from pathological insults induced by chronic heart failure in mice.* Am J Pathol, 2007. **170**(2): p. 599-608.

99. Drexler, H., U. Riede, T. Münzel, H. König, et al., *Alterations of skeletal muscle in chronic heart failure.* Circulation, 1992. **85**(5): p. 1751-9.

100. Rockman, H.A., R.S. Ross, A.N. Harris, K.U. Knowlton, et al., *Segregation of atrial-specific and inducible expression of an atrial natriuretic factor transgene in an in vivo murine model of cardiac hypertrophy.* Proc Natl Acad Sci U S A, 1991. **88**(18): p. 8277-81.

101. Leitner, L.M., *Heart Failure Rapidly Induces Wasting-related Program in Skeletal Muscle.* 2018.

102. Oenarto, V., *Interorgan Crosstalk between the Heart and Adipose Tissue during Heart Failure Establishment.* 2020.

103. Kalfhues, L., *p38 MAPKα is a Key Regulator of Cardiac Metabolism*. 2020.

104. Martin, E.D., R. Bassi, and M.S. Marber, *p38 MAPK in cardioprotection - are we there yet?* Br J Pharmacol, 2015. **172**(8): p. 2101-13.

105. Ono, K. and J. Han, *The p38 signal transduction pathway: activation and function.* Cell Signal, 2000. **12**(1): p. 1-13.

106. Han, J., J.D. Lee, L. Bibbs, and R.J. Ulevitch, *A MAP kinase targeted by endotoxin and hyperosmolarity in mammalian cells.* Science, 1994. **265**(5173): p. 808-11.

107. Zarubin, T. and J. Han, *Activation and signaling of the p38 MAP kinase pathway.* Cell Res, 2005. **15**(1): p. 11-8.

108. Han, J., J.D. Lee, P.S. Tobias, and R.J. Ulevitch, *Endotoxin induces rapid protein tyrosine phosphorylation in 70Z/3 cells expressing CD14.* J Biol Chem, 1993. **268**(33): p. 25009-14.

109. Rouse, J., P. Cohen, S. Trigon, M. Morange, et al., *A novel kinase cascade triggered by stress and heat shock that stimulates MAPKAP kinase-2 and phosphorylation of the small heat shock proteins.* Cell, 1994. **78**(6): p. 1027-37.

110. Han, S.J., K.Y. Choi, P.T. Brey, and W.J. Lee, *Molecular cloning and characterization of a Drosophila p38 mitogen-activated protein kinase.* J Biol Chem, 1998. **273**(1): p. 369-74.

111. Brewster, J.L., T. de Valoir, N.D. Dwyer, E. Winter, et al., *An osmosensing signal transduction pathway in yeast.* Science, 1993. **259**(5102): p. 1760-3.

112. Shiozaki, K. and P. Russell, *Cell-cycle control linked to extracellular environment by MAP kinase pathway in fission yeast.* Nature, 1995. **378**(6558): p. 739-43.

113. Derijard, B., J. Raingeaud, T. Barrett, I.H. Wu, et al., *Independent human MAP-kinase signal transduction pathways defined by MEK and MKK isoforms.* Science, 1995. **267**(5198): p. 682-5.

114. Raingeaud, J., A.J. Whitmarsh, T. Barrett, B. Derijard, et al., *MKK3- and MKK6-regulated gene expression is mediated by the p38 mitogen-activated protein kinase signal transduction pathway.* Mol Cell Biol, 1996. **16**(3): p. 1247-55.

115. Remy, G., A.M. Risco, F.A. Inesta-Vaquera, B. Gonzalez-Teran, et al., *Differential activation of p38MAPK isoforms by MKK6 and MKK3.* Cell Signal, 2010. **22**(4): p. 660-7.

116. Stokoe, D., K. Engel, D.G. Campbell, P. Cohen, et al., *Identification of MAPKAP kinase 2 as a major enzyme responsible for the phosphorylation of the small mammalian heat shock proteins.* FEBS Lett, 1992. **313**(3): p. 307-13.

117. Huang, C.K., L. Zhan, Y. Ai, and J. Jongstra, *LSP1 is the major substrate for mitogen-activated protein kinase-activated protein kinase 2 in human neutrophils.* J Biol Chem, 1997. **272**(1): p. 17-9.

118. Tan, Y., J. Rouse, A. Zhang, S. Cariati, et al., *FGF and stress regulate CREB and ATF-1 via a pathway involving p38 MAP kinase and MAPKAP kinase-2.* EMBO J, 1996. **15**(17): p. 4629-42.

119. Heidenreich, O., A. Neininger, G. Schratt, R. Zinck, et al., *MAPKAP kinase 2 phosphorylates serum response factor in vitro and in vivo.* J Biol Chem, 1999. **274**(20): p. 14434-43.

120. Mahtani, K.R., M. Brook, J.L. Dean, G. Sully, et al., *Mitogen-activated protein kinase p38 controls the expression and posttranslational modification of tristetraprolin, a regulator of tumor necrosis factor alpha mRNA stability.* Mol Cell Biol, 2001. **21**(19): p. 6461-9.

121. Johnson, G.V. and C.D. Bailey, *The p38 MAP kinase signaling pathway in Alzheimer's disease.* Exp Neurol, 2003. **183**(2): p. 263-8.

122. Hollenbach, E., M. Neumann, M. Vieth, A. Roessner, et al., *Inhibition of p38 MAP kinase- and RICK/NF-kappaB-signaling suppresses inflammatory bowel disease.* FASEB J, 2004. **18**(13): p. 1550-2.

123. Perregaux, D.G., D. Dean, M. Cronan, P. Connelly, et al., *Inhibition of interleukin-1 beta production by SKF86002: evidence of two sites of in vitro activity and of a time and system dependence.* Mol Pharmacol, 1995. **48**(3): p. 433-42.

124. Guan, Z., S.Y. Buckman, A.P. Pentland, D.J. Templeton, et al., *Induction of cyclooxygenase-2 by the activated MEKK1 --> SEK1/MKK4 --> p38 mitogen-activated protein kinase pathway.* J Biol Chem, 1998. **273**(21): p. 12901-8.

125. Li, M., D. Georgakopoulos, G. Lu, L. Hester, et al., *p38 MAP kinase mediates inflammatory cytokine induction in cardiomyocytes and extracellular matrix remodeling in heart.* Circulation, 2005. **111**(19): p. 2494-502.

126. Kyoi, S., H. Otani, S. Matsuhisa, Y. Akita, et al., *Opposing effect of p38 MAP kinase and JNK inhibitors on the development of heart failure in the cardiomyopathic hamster.* Cardiovasc Res, 2006. **69**(4): p. 888-98.

127. Adams, R.H., A. Porras, G. Alonso, M. Jones, et al., *Essential role of p38alpha MAP kinase in placental but not embryonic cardiovascular development.* Mol Cell, 2000. **6**(1): p. 109-16.

128. Allen, M., L. Svensson, M. Roach, J. Hambor, et al., *Deficiency of the stress kinase p38alpha results in embryonic lethality: characterization of the kinase dependence of stress responses of enzyme-deficient embryonic stem cells.* J Exp Med, 2000. **191**(5): p. 859-70.

129. Schneider, S., W. Chen, J. Hou, C. Steenbergen, et al., *Inhibition of p38 MAPK alpha/beta reduces ischemic injury and does not block protective effects of preconditioning.* Am J Physiol Heart Circ Physiol, 2001. **280**(2): p. H499-508.

130. Barancik, M., P. Htun, C. Strohm, S. Kilian, et al., *Inhibition of the cardiac p38-MAPK pathway by SB203580 delays ischemic cell death.* J Cardiovasc Pharmacol, 2000. **35**(3): p. 474-83.

131. Nemoto, S., Z. Sheng, and A. Lin, *Opposing effects of Jun kinase and p38 mitogen-activated protein kinases on cardiomyocyte hypertrophy.* Mol Cell Biol, 1998. **18**(6): p. 3518-26.

132. Goedecke, S., A. Heinen, F. Moeller, R. Deenen, et al., *AKT signaling is essential for functional and structural integrity of the heart.* The FASEB Journal, 2017. **31**(S1): p. lb149-lb149.

133. Sohal, D.S., M. Nghiem, M.A. Crackower, S.A. Witt, et al., *Temporally regulated and tissue-specific gene manipulations in the adult and embryonic heart using a tamoxifen-inducible Cre protein.* Circ Res, 2001. **89**(1): p. 20-5.

134. Verrou, C., Y. Zhang, C. Zurn, W.W. Schamel, et al., *Comparison of the tamoxifen regulated chimeric Cre recombinases MerCreMer and CreMer.* Biol Chem, 1999. **380**(12): p. 1435-8.

135. Feil, R., J. Brocard, B. Mascrez, M. LeMeur, et al., *Ligand-activated site-specific recombination in mice.* Proc Natl Acad Sci U S A, 1996. **93**(20): p. 10887-90.

136. Feil, R., J. Wagner, D. Metzger, and P. Chambon, *Regulation of Cre recombinase activity by mutated estrogen receptor ligand-binding domains.* Biochem Biophys Res Commun, 1997. **237**(3): p. 752-7.

137. Orban, P.C., D. Chui, and J.D. Marth, *Tissue- and site-specific DNA recombination in transgenic mice.* Proc Natl Acad Sci U S A, 1992. **89**(15): p. 6861-5.

138. Lakso, M., B. Sauer, B. Mosinger, Jr., E.J. Lee, et al., *Targeted oncogene activation by site-specific recombination in transgenic mice.* Proc Natl Acad Sci U S A, 1992. **89**(14): p. 6232-6.

139. King, V.L., V.L. English, K. Bharadwaj, and L.A. Cassis, *Angiotensin II Stimulates Sympathetic Neurotransmission to Adipose Tissue.* Physiol Rep, 2013. **1**(2).

140. Smith, P.K., R.I. Krohn, G.T. Hermanson, A.K. Mallia, et al., *Measurement of protein using bicinchoninic acid.* Anal Biochem, 1985. **150**(1): p. 76-85.

141. Laemmli, U.K., *Cleavage of structural proteins during the assembly of the head of bacteriophage T4.* Nature, 1970. **227**(5259): p. 680-5.

142. Schroeder, A., O. Mueller, S. Stocker, R. Salowsky, et al., *The RIN: an RNA integrity number for assigning integrity values to RNA measurements.* Bmc Molecular Biology, 2006. **7**.

143. Sasse, A., M. Wallich, Z. Ding, A. Goedecke, et al., *Coxsackie-and-adenovirus receptor mRNA expression in human heart failure.* J Gene Med, 2003. **5**(10): p. 876-882.

144. Borrione, A.C., A.M. Zanellato, L. Saggin, M. Mazzoli, et al., *Neonatal myosin heavy chains are not expressed in Ni-induced rat rhabdomyosarcoma.* Differentiation, 1988. **38**(1): p. 49-59.

145. Schiaffino, S., L. Gorza, S. Sartore, L. Saggin, et al., *Three myosin heavy chain isoforms in type 2 skeletal muscle fibres.* J Muscle Res Cell Motil, 1989. **10**(3): p. 197-205.

146. Emde, B., A. Heinen, A. Godecke, and K. Bottermann, *Wheat germ agglutinin staining as a suitable method for detection and quantification of fibrosis in cardiac tissue after myocardial infarction.* Eur J Histochem, 2014. **58**(4): p. 2448.

147. Bhavanandan, V.P. and A.W. Katlic, *The interaction of wheat germ agglutinin with sialoglycoproteins. The role of sialic acid.* J Biol Chem, 1979. **254**(10): p. 4000-8.

148. Monsigny, M., A.C. Roche, C. Sene, R. Maget-Dana, et al., *Sugar-lectin interactions: how does wheat-germ agglutinin bind sialoglycoconjugates?* Eur J Biochem, 1980. **104**(1): p. 147-53.

149. Gonatas, N.K. and S. Avrameas, *Detection of plasma membrane carbohydrates with lectin peroxidase conjugates.* J Cell Biol, 1973. **59**(2 Pt 1): p. 436-43.

150. Huet, C. and J. Garrido, *Ultrastructural visualization of cell-coat components by means of wheat germ agglutinin.* Exp Cell Res, 1972. **75**(2): p. 523-7.

151. Pena, S.D., B.B. Gordon, G. Karpati, and S. Carpenter, *Lectin histochemistry of human skeletal muscle.* J Histochem Cytochem, 1981. **29**(4): p. 542-6.

152. Ohno, J., Y. Tajima, and N. Utsumi, *Binding of wheat germ agglutinin in the matrix of rat tracheal cartilage.* Histochem J, 1986. **18**(10): p. 537-40.

153. Soderstrom, K.O., *Lectin binding to collagen strands in histologic tissue sections.* Histochemistry, 1987. **87**(6): p. 557-60.

154. Kostrominova, T.Y., *Application of WGA lectin staining for visualization of the connective tissue in skeletal muscle, bone, and ligament/tendon studies.* Microsc Res Tech, 2011. **74**(1): p. 18-22.

155. Eckes, B. and S.A. Eming, *Tissue fibrosis: a pathomechanistically unresolved challenge and scary clinical problem.* Exp Dermatol, 2017. **26**(2): p. 135-136.

156. Heinen, A., R. Nederlof, P. Panjwani, A. Spychala, et al., *IGF1 Treatment Improves Cardiac Remodeling after Infarction by Targeting Myeloid Cells.* Mol Ther, 2019. **27**(1): p. 46-58.

157. Pinto, A.R., A. Ilinykh, M.J. Ivey, J.T. Kuwabara, et al., *Revisiting Cardiac Cellular Composition.* Circ Res, 2016. **118**(3): p. 400-9.

158. Nakano, A., T. Harada, S. Morikawa, and Y. Kato, *Expression of leukocyte common antigen (CD45) on various human leukemia/lymphoma cell lines.* Acta Pathol Jpn, 1990. **40**(2): p. 107-15.

159. Nadler, L.M., S.J. Korsmeyer, K.C. Anderson, A.W. Boyd, et al., *B cell origin of non-T cell acute lymphoblastic leukemia. A model for discrete stages of neoplastic and normal pre-B cell differentiation.* J Clin Invest, 1984. **74**(2): p. 332-40.

160. Feller, A.C., M.R. Parwaresch, H. Stein, A. Ziegler, et al., *Immunophenotyping of T-lymphoblastic lymphoma/leukemia: correlation with normal T-cell maturation.* Leuk Res, 1986. **10**(8): p. 1025-31.

161. Chan, J.K., C.S. Ng, and P.K. Hui, *A simple guide to the terminology and application of leucocyte monoclonal antibodies.* Histopathology, 1988. **12**(5): p. 461-80.

162. Fagerholm, S.C., M. Varis, M. Stefanidakis, T.J. Hilden, et al., *alpha-Chain phosphorylation of the human leukocyte CD11b/CD18 (Mac-1) integrin is pivotal for integrin activation to bind ICAMs and leukocyte extravasation.* Blood, 2006. **108**(10): p. 3379-86.

163. Liesveld, J.L., J.M. Winslow, K.E. Frediani, D.H. Ryan, et al., *Expression of integrins and examination of their adhesive function in normal and leukemic hematopoietic cells.* Blood, 1993. **81**(1): p. 112-21.

164. Orr, Y., J.M. Taylor, S. Cartland, P.G. Bannon, et al., *Conformational activation of CD11b without shedding of L-selectin on circulating human neutrophils.* J Leukoc Biol, 2007. **82**(5): p. 1115-25.

165. Lee, P.Y., J.X. Wang, E. Parisini, C.C. Dascher, et al., *Ly6 family proteins in neutrophil biology.* J Leukoc Biol, 2013. **94**(4): p. 585-94.

166. Langlet, C., S. Tamoutounour, S. Henri, H. Luche, et al., *CD64 expression distinguishes monocyte-derived and conventional dendritic cells and reveals their distinct role during intramuscular immunization.* J Immunol, 2012. **188**(4): p. 1751-60.

167. Patente, T.A., M.P. Pinho, A.A. Oliveira, G.C.M. Evangelista, et al., *Human Dendritic Cells: Their Heterogeneity and Clinical Application Potential in Cancer Immunotherapy.* Frontiers in Immunology, 2019. **9**.

168. Desmoulière, A., A. Geinoz, F. Gabbiani, and G. Gabbiani, *Transforming growth factor-beta 1 induces alpha-smooth muscle actin expression in granulation tissue myofibroblasts and in quiescent and growing cultured fibroblasts.* J Cell Biol, 1993. **122**(1): p. 103-11.

169. Bartness, T.J., Y. Liu, Y.B. Shrestha, and V. Ryu, *Neural innervation of white adipose tissue and the control of lipolysis.* Front Neuroendocrinol, 2014. **35**(4): p. 473-93.

170. Saqib, U., S. Sarkar, K. Suk, O. Mohammad, et al., *Phytochemicals as modulators of M1-M2 macrophages in inflammation.* Oncotarget, 2018. **9**(25): p. 17937-17950.

171. Giannakis, N., B.E. Sansbury, A. Patsalos, T.T. Hays, et al., *Dynamic changes to lipid mediators support transitions among macrophage subtypes during muscle regeneration.* Nat Immunol, 2019. **20**(5): p. 626-636.

172. DeSandro, A., U.M. Nagarajan, and J.M. Boss, *The bare lymphocyte syndrome: molecular clues to the transcriptional regulation of major histocompatibility complex class II genes.* Am J Hum Genet, 1999. **65**(2): p. 279-86.

173. Reith, W. and B. Mach, *The bare lymphocyte syndrome and the regulation of MHC expression.* Annu Rev Immunol, 2001. **19**: p. 331-73.

174. Rao, K.B., N. Malathi, S. Narashiman, and S.T. Rajan, *Evaluation of myofibroblasts by expression of alpha smooth muscle actin: a marker in fibrosis, dysplasia and carcinoma.* J Clin Diagn Res, 2014. **8**(4): p. ZC14-7.

175. Ma, Y., *Role of Neutrophils in Cardiac Injury and Repair Following Myocardial Infarction.* Cells, 2021. **10**(7).

176. Yin, L., N. Li, W. Jia, N. Wang, et al., *Skeletal muscle atrophy: From mechanisms to treatments.* Pharmacological Research, 2021. **172**: p. 105807.

177. Bodine, S.C. and L.M. Baehr, *Skeletal muscle atrophy and the E3 ubiquitin ligases MuRF1 and MAFbx/atrogin-1.* Am J Physiol Endocrinol Metab, 2014. **307**(6): p. E469-84.

178. Peris-Moreno, D., D. Taillandier, and C. Polge, *MuRF1/TRIM63, Master Regulator of Muscle Mass.* Int J Mol Sci, 2020. **21**(18).

179. Mercer, T.J., A. Gubas, and S.A. Tooze, *A molecular perspective of mammalian autophagosome biogenesis.* J Biol Chem, 2018. **293**(15): p. 5386-5395.

180. Jacquet, M., M. Guittaut, A. Fraichard, and G. Despouy, *The functions of Atg8-family proteins in autophagy and cancer: linked or unrelated?* Autophagy, 2021. **17**(3): p. 599-611.

181. Carnac, G., S. Ricaud, B. Vernus, and A. Bonnieu, *Myostatin: biology and clinical relevance.* Mini Rev Med Chem, 2006. **6**(7): p. 765-70.

182. Joulia-Ekaza, D. and G. Cabello, *The myostatin gene: physiology and pharmacological relevance.* Curr Opin Pharmacol, 2007. **7**(3): p. 310-5.

183. Catalán, V., G. Frühbeck, and J. Gómez-Ambrosi, *Chapter 8 - Inflammatory and Oxidative Stress Markers in Skeletal Muscle of Obese Subjects*, in *Obesity*, A.M. del Moral and C.M. Aguilera García, Editors. 2018, Academic Press. p. 163-189.

184. Saunders, M.A., J.M. Good, E.C. Lawrence, R.E. Ferrell, et al., *Human adaptive evolution at Myostatin (GDF8), a regulator of muscle growth.* Am J Hum Genet, 2006. **79**(6): p. 1089-97.

185. Haddad, F., F. Zaldivar, D.M. Cooper, and G.R. Adams, *IL-6-induced skeletal muscle atrophy.* J Appl Physiol (1985), 2005. **98**(3): p. 911-7.

186. Yu, H., A. Fellows, K. Foote, Z. Yang, et al., *FOXO3a (Forkhead Transcription Factor O Subfamily Member 3a) Links Vascular Smooth Muscle Cell Apoptosis, Matrix Breakdown, Atherosclerosis, and Vascular Remodeling Through a Novel Pathway Involving MMP13 (Matrix Metalloproteinase 13).* Arterioscler Thromb Vasc Biol, 2018. **38**(3): p. 555-565.

187. Ekoff, M., T. Kaufmann, M. Engström, N. Motoyama, et al., *The BH3-only protein Puma plays an essential role in cytokine deprivation induced apoptosis of mast cells.* Blood, 2007. **110**(9): p. 3209-17.

188. Skurk, C., H. Maatz, H.S. Kim, J. Yang, et al., *The Akt-regulated forkhead transcription factor FOXO3a controls endothelial cell viability through modulation of the caspase-8 inhibitor FLIP.* J Biol Chem, 2004. **279**(2): p. 1513-25.

189. Zechner, D., D.J. Thuerauf, D.S. Hanford, P.M. McDonough, et al., *A role for the p38 mitogen-activated protein kinase pathway in myocardial cell growth, sarcomeric organization, and cardiac-specific gene expression.* J Cell Biol, 1997. **139**(1): p. 115-27.

190. Posor, Y., M. Eichhorn-Gruenig, D. Puchkov, J. Schöneberg, et al., *Spatiotemporal control of endocytosis by phosphatidylinositol-3,4-bisphosphate.* Nature, 2013. **499**(7457): p. 233-237.

191. Moritoh, Y., M. Oka, Y. Yasuhara, H. Hozumi, et al., *Inositol Hexakisphosphate Kinase 3 Regulates Metabolism and Lifespan in Mice.* Scientific Reports, 2016. **6**(1): p. 32072.

192. Engelhardt, S., L. Hein, F. Wiesmann, and M.J. Lohse, *Progressive hypertrophy and heart failure in beta1-adrenergic receptor transgenic mice.* Proc Natl Acad Sci U S A, 1999. **96**(12): p. 7059-64.

193. Dubin, A., B. Lattanzio, and L. Gatti, *The spectrum of cardiovascular effects of dobutamine - from healthy subjects to septic shock patients.* Rev Bras Ter Intensiva, 2017. **29**(4): p. 490-498.

194. Calligaris, S.D., M. Ricca, and P. Conget, *Cardiac stress test induced by dobutamine and monitored by cardiac catheterization in mice.* J Vis Exp, 2013(72).

195. Perlman, R.L. and M. Chalfie, *Catecholamine release from the adrenal medulla.* Clin Endocrinol Metab, 1977. **6**(3): p. 551-76.

196. Dendorfer, A., A. Thornagel, W. Raasch, O. Grisk, et al., *Angiotensin II induces catecholamine release by direct ganglionic excitation.* Hypertension, 2002. **40**(3): p. 348-54.

197. Bahnsen, M., J.M. Burrin, D.G. Johnston, A. Pernet, et al., *Mechanisms of catecholamine effects on ketogenesis.* Am J Physiol, 1984. **247**(2 Pt 1): p. E173-80.

198. Tavernier, G., M. Jimenez, J.P. Giacobino, N. Hulo, et al., *Norepinephrine induces lipolysis in beta1/beta2/beta3-adrenoceptor knockout mice.* Mol Pharmacol, 2005. **68**(3): p. 793-9.

199. Schena, G. and M.J. Caplan, *Everything You Always Wanted to Know about β(3)-AR * (* But Were Afraid to Ask).* Cells, 2019. **8**(4).

200. Guo, L., A. Yin, Q. Zhang, T. Zhong, et al., *Angiotensin-(1–7) attenuates angiotensin II-induced cardiac hypertrophy via a Sirt3-dependent mechanism.* American Journal of Physiology-Heart and Circulatory Physiology, 2017. **312**(5): p. H980-H991.

201. Ma, E., C. Wu, J. Chen, D. Wo, et al., *Resveratrol prevents Ang II-induced cardiac hypertrophy by inhibition of NF-κB signaling.* Biomed Pharmacother, 2023. **165**: p. 115275.

202. Li, J.C., J. Jia, L. Dong, Z.J. Hu, et al., *Angiotensin II mediates hypertensive cardiac fibrosis via an Erbb4-IR-dependent mechanism.* Mol Ther Nucleic Acids, 2023. **33**: p. 180-190.

203. Peres Diaz, L.S., M.L. Schuman, M. Aisicovich, J.E. Toblli, et al., *Angiotensin II requires an intact cardiac thyrotropin-releasing hormone (TRH) system to induce cardiac hypertrophy in mouse.* J Mol Cell Cardiol, 2018. **124**: p. 1-11.

204. Weisheit, C., Y. Zhang, A. Faron, O. Köpke, et al., *Ly6C(low) and not Ly6C(high) macrophages accumulate first in the heart in a model of murine pressure-overload.* PLoS One, 2014. **9**(11): p. e112710.

205. Daseke, M.J., 2nd, U. Chalise, M. Becirovic-Agic, J.D. Salomon, et al., *Neutrophil signaling during myocardial infarction wound repair.* Cell Signal, 2021. **77**: p. 109816.

206. Frangogiannis, N.G., *The inflammatory response in myocardial injury, repair, and remodelling.* Nature Reviews Cardiology, 2014. **11**(5): p. 255-265.

207. Banerjee, D., R. Tian, and S. Cai, *The Role of Innate Immune Cells in Cardiac Injury and Repair: A Metabolic Perspective.* Current Cardiology Reports, 2023. **25**(7): p. 631-640.

208. Libby, P., M. Nahrendorf, and F.K. Swirski, *Monocyte heterogeneity in cardiovascular disease.* Semin Immunopathol, 2013. **35**(5): p. 553-62.

209. Stansfield, B.K. and D.A. Ingram, *Clinical significance of monocyte heterogeneity.* Clin Transl Med, 2015. **4**: p. 5.

210. Guimarães-Costa, A.B., N.C. Rochael, F. Oliveira, J. Echevarria-Lima, et al., *Neutrophil Extracellular Traps Reprogram IL-4/GM-CSF-Induced Monocyte Differentiation to Anti-inflammatory Macrophages.* Frontiers in Immunology, 2017. **8**.

211. Pistulli, R., S. König, S. Drobnik, D. Kretzschmar, et al., *Decrease in dendritic cells in endomyocardial biopsies of human dilated cardiomyopathy.* Eur J Heart Fail, 2013. **15**(9): p. 974-85.

212. Anzai, A., T. Anzai, S. Nagai, Y. Maekawa, et al., *Regulatory role of dendritic cells in postinfarction healing and left ventricular remodeling.* Circulation, 2012. **125**(10): p. 1234-45.

213. Ramos, G., U. Hofmann, and S. Frantz, *Myocardial fibrosis seen through the lenses of T-cell biology.* J Mol Cell Cardiol, 2016. **92**: p. 41-5.

214. Hooks, M.A., C.S. Wade, and W.J. Millikan, Jr., *Muromonab CD-3: a review of its pharmacology, pharmacokinetics, and clinical use in transplantation.* Pharmacotherapy, 1991. **11**(1): p. 26-37.

215. Olofsen, P.A., M.C. Stip, J.H.M. Jansen, C. Chan, et al., *Effective, Long-Term, Neutrophil Depletion Using a Murinized Anti-Ly-6G 1A8 Antibody.* Cells, 2022. **11**(21).

216. Pillay, J., I. den Braber, N. Vrisekoop, L.M. Kwast, et al., *In vivo labeling with 2H2O reveals a human neutrophil lifespan of 5.4 days.* Blood, 2010. **116**(4): p. 625-7.

217. Frangogiannis, N.G., *Cardiac fibrosis: Cell biological mechanisms, molecular pathways and therapeutic opportunities.* Mol Aspects Med, 2019. **65**: p. 70-99.

218. Vliegen, H.W., A. van der Laarse, C.J. Cornelisse, and F. Eulderink, *Myocardial changes in pressure overload-induced left ventricular hypertrophy. A study on tissue composition, polyploidization and multinucleation.* Eur Heart J, 1991. **12**(4): p. 488-94.

219. Zeisberg, E.M., O. Tarnavski, M. Zeisberg, A.L. Dorfman, et al., *Endothelial-to-mesenchymal transition contributes to cardiac fibrosis.* Nature Medicine, 2007. **13**(8): p. 952-961.

220. Frangogiannis, N.G., *The role of transforming growth factor (TGF)-beta in the infarcted myocardium.* J Thorac Dis, 2017. **9**(Suppl 1): p. S52-S63.

221. Ignotz, R.A. and J. Massagué, *Transforming growth factor-beta stimulates the expression of fibronectin and collagen and their incorporation into the extracellular matrix.* J Biol Chem, 1986. **261**(9): p. 4337-45.

222. Talman, V. and H. Ruskoaho, *Cardiac fibrosis in myocardial infarction-from repair and remodeling to regeneration.* Cell Tissue Res, 2016. **365**(3): p. 563-81.

223. Regitz-Zagrosek, V., S. Brokat, and C. Tschope, *Role of gender in heart failure with normal left ventricular ejection fraction.* Prog Cardiovasc Dis, 2007. **49**(4): p. 241-51.

224. Guthoff, H., A. Hof, A. Klinke, M. Maaß, et al., *Protective Effects of Therapeutic Neutrophil Depletion and Myeloperoxidase Inhibition on Left Ventricular Function and Remodeling in Myocardial Infarction.* Antioxidants (Basel), 2022. **12**(1).

225. Carson, M.A., J. Reid, L. Hill, L. Dixon, et al., *Exploring the prevalence, impact and experience of cardiac cachexia in patients with advanced heart failure and their caregivers: A sequential phased study.* Palliat Med, 2022. **36**(7): p. 1118-1128.

226. Wang, Y. and J.E. Pessin, *Mechanisms for fiber-type specificity of skeletal muscle atrophy.* Current Opinion in Clinical Nutrition & Metabolic Care, 2013. **16**(3): p. 243-250.

227. Levine, B., J. Kalman, L. Mayer, H.M. Fillit, et al., *Elevated Circulating Levels of Tumor Necrosis Factor in Severe Chronic Heart Failure.* New England Journal of Medicine, 1990. **323**(4): p. 236-241.

228. McMurray, J., I. Abdullah, H.J. Dargie, and D. Shapiro, *Increased concentrations of tumour necrosis factor in "cachectic" patients with severe chronic heart failure.* Br Heart J, 1991. **66**(5): p. 356-8.

229. Anker, S.D., T.P. Chua, P. Ponikowski, D. Harrington, et al., *Hormonal Changes and Catabolic/Anabolic Imbalance in Chronic Heart Failure and Their Importance for Cardiac Cachexia.* Circulation, 1997. **96**(2): p. 526-534.

230. Torre-Amione, G., S. Kapadia, J. Lee, J.-B. Durand, et al., *Tumor Necrosis Factor-α and Tumor Necrosis Factor Receptors in the Failing Human Heart.* Circulation, 1996. **93**(4): p. 704-711.

231. Agarwal, S., N.P. Piesco, L.P. Johns, and A.E. Riccelli, *Differential expression of IL-1 beta, TNF-alpha, IL-6, and IL-8 in human monocytes in response to lipopolysaccharides from different microbes.* J Dent Res, 1995. **74**(4): p. 1057-65.

232. Jablonska, E., J. Jablonski, and A. Holownia, *Role of neutrophils in release of some cytokines and their soluble receptors.* Immunol Lett, 1999. **70**(3): p. 191-7.

233. Argiles, J.M., N. Campos, J.M. Lopez-Pedrosa, R. Rueda, et al., *Skeletal Muscle Regulates Metabolism via Interorgan Crosstalk: Roles in Health and Disease.* J Am Med Dir Assoc, 2016. **17**(9): p. 789-96.

234. Molinari, F., N. Malara, V. Mollace, G. Rosano, et al., *Animal models of cardiac cachexia.* Int J Cardiol, 2016. **219**: p. 105-10.

235. Schumak, B., K. Klocke, J.M. Kuepper, A. Biswas, et al., *Specific depletion of Ly6C(hi) inflammatory monocytes prevents immunopathology in experimental cerebral malaria.* PLoS One, 2015. **10**(4): p. e0124080.

236. Gibbons, M.A., A.C. MacKinnon, P. Ramachandran, K. Dhaliwal, et al., *Ly6Chi monocytes direct alternatively activated profibrotic macrophage regulation of lung fibrosis.* Am J Respir Crit Care Med, 2011. **184**(5): p. 569-81.

237. Santos, E.S., L.S. de Aragão-França, C.S. Meira, J.V. Cerqueira, et al., *Tolerogenic Dendritic Cells Reduce Cardiac Inflammation and Fibrosis in Chronic Chagas Disease.* Front Immunol, 2020. **11**: p. 488.

List of Abbreviations

ACE	Angiotensin-converting enzyme
Acta2	Actin alpha 2
AIDS	Acquired immunodeficiency syndrome
AKT	Protein kinase B
AngII	Angiotensin II
ANS	Autonomic nervous system
APS	Ammonium persulfate
ATP	Adenosine triphosphate
BPM	Beats per minute
BSA	Bovine serum albumin
CCR	C-C chemokine receptor
CD	Cluster of differentiation
CF	Cardiac fibroblasts
CHF	Chronic heart failure
Cilp2	Cartilage intermediate layer protein 2
CKD	Chronic kidney disease
CM	Cardiomyocyte
CO	Cardiac output
CO_2	Carbon dioxide
Col1a1	Collagen 1A1
Col3a1	Collagen 3A1
COMP	Cartilage oligomeric matrix protein
COPD	Chronic obstructive pulmonary disease
Cre	Causes recombination
Csnk2b	Beta subunit of casein kinase II
Ctrl.	Control
CVD	Cardiovascular diseases
d	Day
DAMPS	Damage-associated molecular patterns
DAPI	4‘,6-Diamidin-2-phenylindol
DC	Dendritic cells
DNA	Deoxyribonucleic acid
DTT	Dithiothreitol
ECM	Extracellular matrix
EDTA	Ethylendiamintetraacetate
EDV	End-diastolic volume
EF	Ejection Fraction
ESV	End-systolic volume
FA	Fatty acids
FACS	Fluorescence activated cell sorting
FBS	Fetal bovine serum
Fbxo32	F-box protein 32
FS	Fractional shortening
Fwd	forward

Gabarapl1	GABA type A receptor-associated protein
gDNA	Genomic DNA
g	Gram
h	Hour
H_2O	Water
Has1	Hyaluronan Synthase 1
Has2	Hyaluronan Synthase 2
HBSS	Hank's Balanced Salt Solution
HF	Heart failure
HFpEF	Heart failure with preserved ejection fraction
HFrEF	Heart failure with reduced ejection fraction
Hprt1	Hypoxanthine-guanine phosphoribosyltransferase
HS	Horse serum
HSP	Heat shock protein
i.p.	intraperitoneal
IGF-1	Insulin-like growth factor 1
IgG	Immunoglobulin G
IgM	Immunoglobulin M
IL	Interleukin
INF-γ	Interferon-γ
kDa	Kilo Dalton
$KHCO_3$	Potassium bicarbonate
KO	Knock out
l	Liter
L/D	Live/Dead
LV	Left ventricle
LVAW	Left ventricular anterior wall
M	Molar
m	Milli
M. gastrocnemius	*Musculus Gastrocnmeius*
M. plantaris	*Musculus Plantaris*
M. soleus	*Musculus Soleus*
mA	Milliampere
MAPK	Mitogen-activated protein kinase
mg	Milligramm
MHC	Myosin heavy chain
mHz	Megahertz
MI	Myocardial infarction
MIF	Myocardial interstitial fibrosis
min	Minute
MK2	MAP kinase-activated protein kinase 2
MKK	MAPK kinase
MKKK	MAPK kinase kinase
mRNA	Messenger-RNA
NaCl	Sodium chloride
NEFA	Non-esterified fatty acid
NF-κB	Nuclear factor-κB

n	Nano
NGS	Normal goat serum
NH_4Cl	Ammonium chloride
nm	Nanometer
nM	Nanomolar
Nudc	Nuclear migration protein nudC
OH-Tx	Hydroxytamoxifen
PBS	Phosphate-buffered saline
PCR	Polymerase chain reaction
PD-1	Programmed cell death protein 1
PEB	Protein extraction buffer
PFA	Perfluoroalkoxy polymers
PNS	Parasympathetic nervous system
PO	Pressure overload
Postn	Periostin
PR	Propranolol
PRRs	Pattern-recognition receptors
qPCR	Quantitative real-time PCR
RAAS	Renin-angiotensin-aldosterone system
Rev	reverse
RNA	Ribonucleic acid
ROS	Reactive oxygen species
rpm	Rounds per minute
RQN	RNA quality number
s.c.	Subcutaneous injection
SD	Standard deviation
SDS	Sodium-Dodecyl-Sulfate
SNS	Sympathetic nervous system
SV	Stroke volume
TAC	Transverse aortic constriction
TBS	Tris-buffered saline
TEMED	Tetramethylethylendiamin
TGF-β	Transforming Growth Factor β
TLRs	Toll-like receptors
Tnfrsf11b	TNF Receptor Superfamily Member 11b
TNF-α	Tumor necrosis factor-alpha
Trim63	E3 ubiquitin-protein ligase TRIM63
UV	Ultraviolet
V	Volt
v/w	Volume/weight
WGA	Wheat germ agglutinin
αSMA	Alpha smooth muscle actin

%	Percentage
°C	Degrees Celsius
µ	Micro

Statutory Declaration

Statutory declaration

I declare under oath that I have produced my thesis independently and without any undue assistance by third parties under consideration of the ‘Principles for the Safeguarding of Good Scientific Practice’ at Heinrich Heine University Düsseldorf. Furthermore, I assure that I did not submit this dissertation, either in full or in part, to any other faculty and did not absolve any promotion trials before.

Düsseldorf,

_____

Anne Hemmers

Eidesstattliche Erklärung

Ich versichere an Eides Statt, dass die Dissertation von mir selbstständig und ohne unzulässige fremde Hilfe unter Beachtung der "Grundsätze zur Sicherung guter wissenschaftlicher Praxis an der Heinrich-Heine Universität Düsseldorf" erstellt worden ist. Darüber hinaus versichere ich, dass ich die Dissertation weder in der hier vorgelegten noch in einer ähnlichen Form bei einem anderen Institut eingereicht habe und bisher keine Promotionsversuche unternommen habe.

Düsseldorf, den

_____

Anne Hemmers

Danksagung

Axel – Danke, dass du mich in dein Team aufgenommen hast und ich damit Teil der HKP und des IRTG1902 werden konnte. Danke für deine Unterstützung und dass du mich gefördert und gefordert hast, sodass ich mich fachlich aber auch persönlich weiterentwickeln konnte. Ich bin jeden Tag gerne ins Institut gekommen und kann mir nicht vorstellen, dass dieser Abschnitt bald vorbei sein wird.

Prof. Dr. rer. nat. Joachim Altschmied – Vielen Dank für die Übernahme des Zweitgutachtens.

Sophia, Kathi & Olesia – Danke für jedes Gespräch und jede Aufmunterung, auch wenn es mal nicht so lief, wie ich es gehofft habe. Danke, dass ihr immer da wart, um mich aufzubauen, aber auch für die vielen schönen Stunden, die wir im Labor und außerhalb miteinander verbracht haben.

Lisa, Rianne und André - Danke für jede Art der Unterstützung, die ich von euch bekommen habe, sei es wissenschaftlich oder emotional. Danke, dass ihr immer ein offenes Ohr hattet, auch in Zeiten, in denen ich gezweifelt habe und dass ihr immer an mich geglaubt habt.

Das ganze Team der HKP – Vielen Dank, dass ihr mich von Beginn an offen und herzlich bei euch aufgenommen habt und ich jederzeit Unterstützung und Hilfe von jedem einzelnen von euch bekommen habe.

Sandra, Janett & Kathryn und das gesamte IRTG1902 – Danke, für die Planung aller Events und die vielfältigen Möglichkeiten, die ihr uns gegeben habt, um uns fachlich und persönlich weiterzuentwickeln.

Jule & Jasmin – Vielen Dank für die unvergessliche Zeit in Charlottesville. Ich bin unglaublich dankbar, dass ich diese Erinnerungen mit euch teilen darf. Ich hätte mir keine besseren Mitbewohnerinnen wünschen können.

Mama, Papa, Maik und Lukas und allen meinen Freunden – Danke für eure bedingungslose Liebe, Unterstützung und euer Verständnis - nicht nur während der Zeit meiner Promotion, sondern immer.